Improved Quantification of Viscoelastic Effects during Polymer flooding using Extensional Rheology

by

Madhar Sahib Azad

A thesis submitted in partial fulfilment for the degree of

Doctor of Philosophy

in

Petroleum Engineering

Department of Civil and Environmental Engineering

University of Alberta

Abstract

Polymer flooding is one of the traditional chemical enhanced oil recovery (EOR) methods with a high rate of success. Synthetic polymer such as hydrolyzed polyacrylamide (HPAM) characterized by flexible chain exhibits viscoelastic characteristics in porous media. Some of the implications of the polymer viscoelastic effects are reduced injectivity, enhanced residual oil saturation *(S_{or})* reduction, and enhanced permeability reduction. Conventional shear rheology has been used for decades to screen the optimal polymers and simulate the in-situ rheological behaviour. Oscillatory shear rheology has also been used to characterize the viscoelastic properties of EOR polymers. Several research problems exist in the literature because of the existing characterization techniques.

The research problems include the inability of the shear rheology to explain the different pressure behavior of HPAM and its similar shear associative polymer. Shear rheology fails to explain the typical flow behavior of associative polymer triggered by intermolecular hydrophobic association. Also, the inability of oscillatory rheology to honour the polymers' viscoelastic effect on pressure drop and residual oil recovery is a limitation. The hypothesis regarding the polymer's extensional rheological role on the permeability reduction remains unanswered. While the role of polymer's viscoelastic effect on S_{or} reduction has been studied in detail, the extensional rheological role on the sweep efficiency and injectivity for heavy oil recovery conditions is unexplored. Viscoelastic polymers that show thinning in the shear field thickens in porous media after a critical onset rate. Existing viscoelastic models rely on the core flood data to predict viscoelastic behavior such as onset and shear thickening of synthetic polymers in porous media. Performing core flooding with respect to many pertinent EOR variables is a cumbersome process. Other limitations include the inability of the conventional capillary number calculated using apparent viscosity to explain the

different residual oil recovery potential of viscoelastic polymers with varying level of elasticity. The rapid residual oil mobilization shown by viscoelastic polymers at the capillary number calculated using the shear/apparent viscosity well below the critical capillary number means that classical capillary theory becomes invalidated in the case of viscoelastic polymers. Also, contrasting opinion exists among leading EOR researchers about the polymer's linear oscillatory viscoelastic effect on S_{or} reduction.

Displacing polymer solutions propagating in porous reservoirs are subjected to both shear and elongational forces. Rotational rheometer has been used successfully to characterize the shear rheological properties of the EOR polymers. Characterizing the extensional properties of low viscous EOR polymer has been the challenge. In this thesis, capillary breakup extensional rheometer (CaBER) is used for the extensional characterization of EOR polymers. The special features of extensional rheology is its ability to distinguish the similar shear polymers based on elasticity. The higher pressure drop, due to higher permeability and mobility reduction and slightly higher recovery exhibited by the associative polymer over its similar shear HPAM, is due to its higher extensional resistance. Extensional rheology with its unique capability to probe the polymer's structure clearly explains the typical behavior, triggered by different hydrophobic associations of associative polymer in porous media. Higher S_{or} reduction, shown by a higher saline polymer solution with a lower oscillatory Deborah number over the low saline polymer solutions with higher oscillatory Deborah numbers, is due to its higher extensional parameters indicative of higher stretch ability. Even though extensional rheology does not play a significant role in the sweep efficiency of heavy oil recovery, its role on injectivity cannot be overlooked. A novel viscoelastic model named Azad Trivedi (AT-VEM) is developed using the concept that viscoelastic polymer that thins in shear field will strain harden in the extensional field. The

developed model could predict the viscoelastic onset and shear thickening regime, without any core flooding using direct extensional measurements. Extensional viscosity of viscoelastic polymers are significantly higher than shear viscosity during extensional flow. Modified capillary number developed using extensional viscosity validates the capillary theory and distinguishes the highly elastic polymer (with higher S_{or} reduction) from less elastic polymer. The correlation named the Azad Trivedi correlation (AT-C) is developed which predicts the S_{or} of various viscoelastic polymers.

This dissertation emphasizes the need for incorporating extensional over shear/oscillatory parameters into polymer screening criteria. Furthermore, AT-VEM and AT-C can be incorporated into the commercial simulators for predicting injectivity and residual oil recovery during polymer flooding.

Preface

A version of chapter 2 submitted as Azad, M.S. and Trivedi, J.J. 2018 "Quantification of viscoelastic effects during polymer flooding: A critical review" was accepted for publication in SPE Journal with revision. I collated the different literature to provide a critical review. I wrote the manuscript, addressed the reviewer questions. Dr. Japan Trivedi was responsible for overall supervision, project design and manuscript write up.

A version of chapter 3 of this dissertation was published as Azad, M.S., Dalsania, Y.K., and Trivedi, J.J. 2018 "Capillary breakup extensional rheometry of associative and hydrolyzed polyacrylamide polymers for oil recovery applications", *Journal of applied polymer science*, volume 135, issue 22, 46253- 46264. I was responsible for conceptualization, performing extensional rheological experiments, and analysis. Yokesh Dalsania and I performed core flooding together. Yokesh Dalsania performed shear rheological experiments. I wrote the manuscript and answered the reviewer's questions. Dr. Japan Trivedi was responsible for overall supervision, project design and manuscript write up.

A version of chapter 4 of this dissertation was published as Azad, M.S., Dalsania, Y.K., and Trivedi, J.J. 2018 "Understanding the flow behavior of copolymer and associative polymers in porous media using extensional viscosity characterization: Effect of hydrophobic association" , *Canadian Journal of Chemical Engineering*, volume 96, issue 11, 2498-2508. I was responsible for conceptualization, extensional rheological experiments, results analysis, manuscript write up and addressing the reviewer's question. Yokesh Dalsania performed shear rheological and core flooding experiments. Dr. Japan Trivedi was responsible for overall supervision, project design and manuscript write up.

A version of chapter 5 of this dissertation will be submitted as Azad, M.S. and Trivedi, J.J. 2018 "Extensional rheological role to viscoelastic polymer flooding: Unanswered Questions – Myth or Reality? to SPE Journal. I was responsible for conceptualization, extensional rheological experiments, results analysis, and manuscript write up. Dr. Japan Trivedi was responsible for overall supervision, project design and manuscript write up.

A version of chapter 6 of this dissertation submitted as Azad, M.S. and Trivedi, J.J. 2018 "Does polymer viscoelasticity influence the heavy oil sweep efficiency and injectivity at 1ft/day? Is

accepted for publications in SPE reservoir evaluation and engineering journal with revisions. I was responsible for conceptualization, extensional rheological experiments, results analysis, and manuscript write up. Dr. Japan Trivedi was responsible for overall supervision, project design and manuscript write up.

A version of chapter 7 of this dissertation was published as Azad, M.S and Trivedi, J.J. 2019 "Novel viscoelastic model for predicting the synthetic polymer's viscoelastic behavior in porous media using direct extensional rheological measurements", *Fuel,* vol 235, 218-226. A version of this chapter was also published as Azad, M.S and Trivedi, J.J. 2018 "Extensional rheological data from ex-situ measurements for predicting the porous media behavior of the viscoelastic EOR polymers", *Data in Brief,* vol 20, 293-305. A version of this chapter was also filed for a patent as Trivedi, J.J and Azad, M.S. 2017 "An Improved Method of Recovering Oil from A Depleted Oil Reservoir", US Patent Applications Serial No: 62/559, 086. I was responsible for conceptualization, data collections, extensional rheological experiments, results in analysis, writing manuscript, answering the reviewer's comments. Dr. Japan Trivedi provided data sets. Dr. Japan Trivedi was responsible for overall supervision, project design and manuscript write up.

I was responsible for conceptualization of content of chapter-8. I also performed the extensional rheological experiments, analyzed the results analysis, and wrote the manuscript. Dr. Japan Trivedi was responsible for overall supervision, project design and manuscript write up.

Appendix of this dissertation contains the step needed for predicting the onset and shear thickening of EOR polymers. Appendix also contains the supplementary figures, used in the development of development of Azad Trivedi Viscoelastic Model.

Acknowledgements

Firstly, I thank and praise ALLAH (swt) for all His blessings which enabled me to attain the PhD degree by completing this research. I am acknowledging my beloved father M.S. Azad (late) who selflessly sent me for my higher studies.

I would like to convey my special appreciation to my thesis advisor Dr. Japan Trivedi for appointing me as his PhD student. I am also acknowledging him for his motivation, supervision, encouragement and patience throughout the research. He spent a lot of time with me even during the weekend. His advises on professional and redundant-free write up, carrier, and work-life balance are to be thanked. He is such a wonderful person and teacher and I may not have got a better professor than him. EOR was my passion and I became more passionate about EOR after working with him. I am also thanking Dr. Randy Seright, Dr. Joao Soares, Dr. Hassan Dehghanpour, and Dr. Sina Ghaemi for serving as the member of the examination committee. I am thanking Mr. Todd Kinnee for his assistance in the experimental set-ups.

Thanks to my beloved mother mainly for her patience, sacrifice and duas. My dear wife and my cute son Azad Mathar deserves a special thanks and appreciation for their patience and support during my PhD. My sister and brother-in-law (Moosa machan) who gifted me a dictionary of petroleum exploration, drilling and production back in 2005 deserves a special mentioning and thanks. My beloved maternal uncles (L.S Mohammed Abdul Kader (late) and L.S Segu Maricar (late)) who loved me so much and desired a success in my life deserves a special acknowledgement. Thanks also to my father-in-law (Rasool Mama), other in-laws, my nieces, my paternal uncle (Meera Sahib Periappa), other maternal uncles (Akbar Sha mama, Naser mama, and Anwar mama), cousin brothers (especially A.R. Mathar Sahib) and all the family members. Special thanks to Dr. Mohammed Idhress, Ali appa (Colombo), my childhood friends (Mansor, Kasim, P.P Ibrahim, Salih), Rizvi mama and Salih kaka for their moral support during my graduate studies. Thanks to my dear brothers Khaleel Hussein, Mohammed, Farhan and Hashim for their support, friendship during my stay in Edmonton. Thanks also to Abdul Mannan, Abdul Aziz, Irfan, Abdul Kabir and Gabriel. Thanks to all the past and present members of JT- lab especially Rajan, Ali, Yogesh, and Tarang. I am also acknowledging the scholarship received from Gerald J Maier Nova chemicals corporations and University of Alberta.

Table of Contents

List of Figures

List of tables

Chapter 1: Introduction

1.1 Background of oil recovery

Oil recovery from reservoirs can be categorized into primary, secondary, and tertiary stages. In the primary recovery stage, the natural energy of the reservoirs pushes the oil towards the producing well. Water drive, gas cap drive, and solution gas drive are the typical examples of primary recovery mechanisms. The primary recovery factor is generally less than 30% (Azad 2014). Once 1the natural energy in the reservoir is exhausted, secondary recovery techniques such as water flooding are implemented to supplement the pressure that is required to the push the oil towards the producing wells. However, water flooding efficiency is also low, with the recovery factor ranging from only 30% to 50% (Azad 2014). The reasons for the low recovery factor of water flooding are poor sweep and displacement efficiency. Sweep efficiency is defined as the fraction of the reservoir pore volume invaded by the injected fluid (Green and Willhite 1998). Sweep efficiency is lower in heterogeneous reservoirs and heavy oil reservoirs during water flood. Channeling becomes an issue in the heterogeneous characterized by the high permeable streaks. Viscous fingering becomes more pronounced in heavy oil reservoirs. More than 8 trillion barrels of resources are in the form of heavy oil worldwide (Alboudwarej et al. 2006). The average water flooding recovery factor in the heavy oil reservoir is less than 10% (Delamaide et al. 2014). The oil that is not swept by the displacing slugs are called bypassed oil. Displacement efficiency is defined as the fraction of residual oil that has been recovered from a well swept zone by water flooding or other EOR processes. High interfacial tension (IFT) and capillarity are the major causes for the poor displacement efficiency of water flood. The oil that is swept but cannot be displaced is called residual oil. Both displacement and sweep efficiency are vital for an efficient oil recovery process. Enhanced oil recovery (EOR) techniques are employed to recover the additional oil that cannot be recovered by water flooding.

1.1.1 EOR concepts

The efficiency of an EOR process can be quantified through capillary number (N_c) and mobility ratio (M). The efficiency of an EOR slugs to recover the residual oil and bypassed oil is quantified through N_c (Eq. 1.1) and M (Eq. 1.2) respectively.

$$N_c = \frac{\mu * \upsilon}{\sigma} \quad (1.1)$$

where

μ is the viscosity of displacing fluid, cP

υ is the velocity of displacing fluid, $m.s^{-1}$

σ is the interfacial tension between displacing and displaced fluids, $mN.m^{-1}$

The N_c of the typical water flooding (with μ = 1 cP, υ = 1 ft/day, and σ = 30 $mN.m^{-1}$) is in the range of 10^{-7}.When N_c exceeds the critical value (10^{-5}- 10^{-4}), rapid oil mobilization begins to occur (Chatzis and Morrow 1982; Qi et al. 2017). The higher the N_c, the higher the residual oil recovery. N_c can be increased by increasing the viscosity of the displacing slugs, increasing the injection velocity, and/or by reducing the interfacial tension between the water and oil.

Sweep efficiency is quantified through *M* (Eq. 1.2).

$$M = \frac{\frac{k_{rw}}{\mu_d}}{\frac{k_{ro}}{\mu_o}} \quad (1.2)$$

where

k_{rw} is the relative permeability to displacing water phase

μ_w is the viscosity of displacing water phase, cP

k_{ro} is the relative permeability to displaced oil phase

μ_o is the viscosity of displaced oil phase, cP

When the *M* is less than 1, piston-like sweep occurs, causing the higher bypassed oil recovery. Lesser *M* can be obtained by either increasing the viscosity of displacing fluid or decreasing the permeability of reservoirs. EOR polymer solutions has the ability to reduce the permeability of the reservoir (Green and Willhite 1998; Sheng 2010). It can also be obtained by decreasing the viscosity of displaceable oil.

Increasing the N_c and/or reducing the M is the aim of any EOR method. Thermal EOR methods such as steam flooding, which is widely applied in heavy oil reservoirs, reduce the viscosity of oil. Reducing the viscosity of oil creates a favourable M. However, heavy oil reservoirs characterized by low thickness are not the ideal candidate for thermal methods (Azad et al. 2014). 80% of Western Canadian heavy oil reservoirs that have a thickness of less than 16 feet account for 1.3 trillion barrels of heavy oil (Adams 1982). Miscible methods that provide complete miscibility and zero capillarity suffer from poor sweep. Surfactant flooding that increases the N_c by IFT reduction is also prone to poor sweep. Surfactant and polymers can be used to provide favorable N_c and M. Floods involving such multiple slugs are prone to chromatographic separation (Lyons & Plisga 2011).Sweep efficiency is more important in oil recovery processes than displacement efficiency, as the injected slugs need to contact oil first before displacing it from capillary pores.

1.1.2 Polymer flooding

Polymer flooding is the main variant of chemical EOR methods used to alter the M. Xanthan gum and hydrolyzed polyacrylamide (HPAM) are two commonly used EOR polymers. Xanthan gum is a purely viscous polymer and HPAM is a viscoelastic polymer. In polymer flooding, dry polymer powder is added to the displacing brine for retarding its adverse mobility. Thin heavy oil reservoirs in Western Canada are targeted using polymer flooding (Wassmuth et al. 2009; Wassmuth et al. 2012; Delamaide et al. 2014). Polymer flooding is also employed in light oil reservoirs to provide sweep efficiency (Sheng 2015). Polymer flooding has been a successful EOR method and researchers formerly attributed the success of the polymer flood only to the enhanced sweep. To recover significant amount of residual oil, N_c has to exceed the critical value. Critical value of N_c for sandstone reservoir is in the range of 10^{-5} to 10^{-4} (Foster 1972; Taber et al. 1973; Abrahms 1975; Chatzis and Morrow 1984; Sheng 2010). The N_c of water flood is in the range of 10^{-7}. EOR polymer solutions that can generate an in-situ viscosity of 10-100 cP cannot increase the N_c beyond its critical value. Therefore polymer flooding is not expected to reduce S_{or} values beyond the water flooded residual oil values. Contrarily, recent studies have asserted the viscoelastic polymer's role on the S_{or} reduction even at the N_c of 10^{-5} (Ehrenfried 2013; Qi et al. 2017). The mechanism causing the additional S_{or} reduction by viscoelastic polymer is not properly understood (Seright 2017).

Polymer solutions propagating in the reservoirs are subjected to various shear rates. The non-Newtonian nature of the polymer solutions result in different viscosity at various shear rates. Rheology is the study of flow and the subsequent deformation of matter as a result of flow.

Rheology is an important aspect of polymer flooding as the EOR polymers are non-Newtonian in nature. Despite being one of the most successful EOR method, proper rheological characterization of EOR polymers is lacking. Until now, shear rheology has been used widely by the chemical EOR researchers (Hirasaki and Pope 1974; Masuda et al. 1992; Delshad et al. 2008; Seright et al. 2011a). Pressure drop and residual oil recovery shown by the viscoelastic polymers is more than expected from the polymer's shear rheological forces (Delshad et al. 2008; Clarke et al. 2016). Steady shear rheology gives a good measure of polymer's viscosity (Sheng 2010). Shear-based oscillatory rheology is used to characterize the viscoelastic behaviour of EOR polymers. Oscillatory rheology can characterize the linear viscoelastic behavior of polymer solutions (Macosko 1994). Figure 1.1 clearly shows that when viscoelastic polymer solution propagates from pore body to pore-throat, the polymer chain stretches (Jouenne and Heurteux 2017). This result in the generated of elongational resistance to flow (Haas and Durst 1982). However, EOR researchers overlooked the extensional aspect of viscoelastic polymer flow in the reservoir. Several problems exists in the literature because of persistence usage of shear based rheology by EOR researchers.

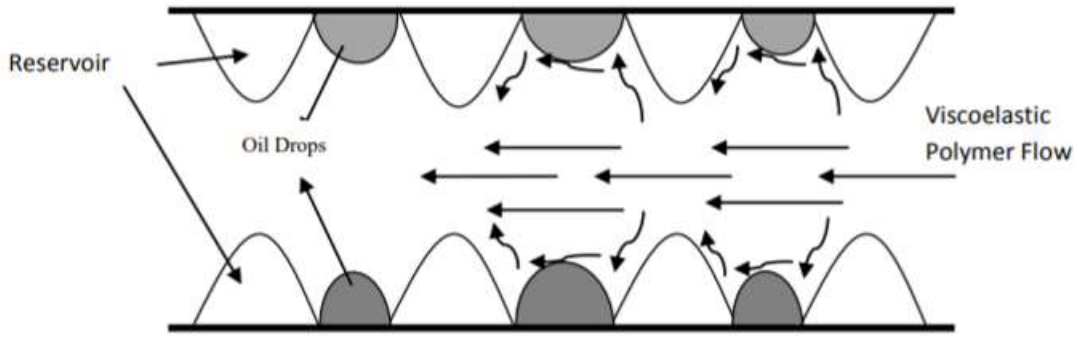

Figure 1.1: *General schematic of typical polymer flow in the porous media test (reprinted from Doda 2014)*

1.1.3 Extensional rheology and its special features

Until the mid-1960s, the field of rheology was dominated by shear flows and only scant attention was given to the extensional flow (Barnes et al. 1989). There has been a significant appreciation for the importance of extensional flow in many practical situations over the last 40 years. Extensional flow occurs in orifices, fibers, pipe constriction, and in porous media (Odell and Carrington 1999). Completely different extensional behavior shown by elastic liquids when compared to Newtonian fluids (Barnes 2010) urged the rheologist to pay more attention to the extensional rheology. The key difference between the shear and extensional flow is that during the

shear flow, the liquid elements flow over or past each other, creating a two-dimensional flow. However, in the extensional flow, the adjacent elements flow towards and away from each other, creating a uniaxial flow. In the extensional flow, the elements of the fluid are stretched out rather than being sheared. During stretching, the particles that are aligned in the flow direction create a strong interactive network. Coil stretch transition gives very long aligned particles. This makes the elongational flow a strong one that possess several unique features that are listed below

a. Viscoelastic systems that show thinning in the shear field exhibit strain hardening behavior in the extensional field (Barnes 2010; Taha 2010; Boni et al. 2016).
b. The structure and morphology of the polymer or any elastic system can be probed effectively using the extensional rheology (Ares et al. 1993; Silva et al. 2007; Bharadwaj et al. 2007; Silva et al. 2010; Boni et al. 2016).
c. Extensional viscosity that measures the polymer's resistance during stretching is orders of magnitude higher than the shear viscosity (Barnes 2010).
d. Furthermore, the polymer solutions that behaved similarly in the shear field were reported to behave differently in the extensional field (Macosko 1994; Barnes 2010; Taha 2010).

Extensional flow becomes dominant when there is abrupt change in the geometry of flow field (Barnes 2010). Oil reservoirs are highly tortuous with converging-diverging geometry and stagnation points (Sorbie 1991; Chauveteau et al. 2002). Polymer solutions flowing in the porous media are subjected to elongational flow (Figure 1.1) (Haas and Durst 1982; Nguyen 1982; Vorwerk and Brunn 1991; Afsharpoor et al. 2012). However, extensional rheology has been overlooked by EOR researchers.

1.2 Problem statements

Several problems, hypotheses, and complexities exists in the usage of viscoelastic polymer flooding because of scant importance given to the extensional rheology. They are listed below.

1. Polymer solutions employed as the displacing phase during EOR applications provide favorable *M.* through both enhanced flow resistance and permeability reduction. Viscoelastic polymer solutions were reported to exhibit shear thickening in the porous media after a critical viscoelastic onset rate. These viscoelastic characteristics cause the overall resistance exhibited by the polymer solutions to be higher than expected from its shear forces. Several researchers have hypothetically attributed these effects to extensional

viscosity (Hirasaki and Pope 1974; Masuda et al. 1992; Ranjbar et al. 1992; Delshad et al. 2008; Stavland et al. 2010). Permeability reduction shown by the polymer solutions is also empirically attributed to its elongational characteristics (Besio et al. 1999; Han et al. 1995). However, there is no experimental proof to these claims.

2. EOR polymers behaving similarly in the steady shear field were reported to behave differently in porous media (Seright et al. 2011b). Oscillatory rheology also fails to explain the behavior of similar shear polymers that showed different flow behavior in porous media. (Garrouch and Gharbi 2006; Seright et al. 2011b). Oscillatory rheology represents the weak linear viscoelastic effects (Macosko 1994). Polymer solutions flowing in porous media are subjected to strong elongational deformation. Extensional rheology represents the non-linear viscoelastic effects (Macosko 1994). However, no efforts were made to study the extensional behavior of the similar shear polymers that showed vastly different behavior in porous media.
3. The Deborah number is usually calculated using the oscillatory relaxation time. Low saline viscoelastic polymer solutions possessing a higher oscillatory Deborah number were reported to contribute to lower residual oil recovery than the high saline viscoelastic polymer solutions possessing a lower oscillatory Deborah number. The number and intensity of inter-chain interactions that the fluid undergoes during the extensional flow is higher and stronger than that of the oscillatory flow (Ferguson et al. 1990; Kennedy et al. 1995; Stolz et al. 2006; Sharma et al. 2015). Extensional relaxation time is higher than the oscillatory relaxation time (Clasen et al. 2010). Magbagbeolo (2008) reported that high saline polymer solutions with lower oscillatory relaxation time resulted in the higher strain hardening index than the low saline viscoelastic polymer solutions with the higher oscillatory relaxation time. Extensional rheology can classify the set of polymers that behaved differently in the shear field (Barnes 2010). A Deborah number calculated using the extensional relaxation time may explain the higher S_{or} reduction shown by the high saline viscoelastic polymer solutions.
4. Most of the unrecovered oil is located in the farthest part of wellbore where the flood front get exposed to the larger area. Several studies reported that the elasticity of viscoelastic polymer solutions can increase the residual oil recovery at flux rate of 1ft/day. (Ehrenfried 2013; Cottin et al. 2014; Clarke et al. 2015; Koh 2015). Sweep efficiency is also an

important aspect of the recovery process. To history match the overall oil recovery shown by the viscoelastic polymer solutions, Chen et al.'s (2011) assumed that the viscosity of the viscoelastic polymer contributes to the sweep efficiency. However, the relative role of viscosity and elasticity of viscoelastic polymer on the sweep efficiency at the flux rate of 1ft/day has not been studied experimentally.

5. Viscous polymer solutions showed thinning (drop in viscosity) in both the bulk shear field and in the porous media (Seright et al. 2009). Therefore, the shear-based Carreau model predicts the viscous polymer behavior in porous media without any core flood experiments (Cannella et al. 1988). Viscoelastic polymer solutions that shows thinning in the shear field exhibit thickening (increase in viscosity) after a critical flow rate in the porous media (Delshad et al. 2008). Therefore, shear-based Carreau model under predicts the apparent viscosity of EOR polymers by significant margin at higher fluxes (Delshad est al. 2008). All the previous viscoelastic models relied on core flooding experiments to model the thickening phenomenon shown by the viscoelastic polymer solutions (Masuda et al. 1992; Delshad et al. 2008; Stavland et al. 2010). Performing core flood experiments with respect to many variables pertinent to EOR is a cumbersome process. Strain hardening index, attained in the extensional field can quantify the thickening ability of the polymer solutions (Barnes 2010). Employing the measured strain hardening index and the extensional viscosity may get rid of the core flooding experiments.
6. N_c has been used for decades to study the efficiency of chemical EOR slugs in reducing the S_{or}. N_c that is calculated using the apparent viscosity fails to explain the residual oil recovery and honours the capillary theory (Clarke et al. 2016; Qi et al. 2017).As per the capillary theory, residual oil cannot be mobilized unless the N_c exceeds the critical N_c (Peter 2002). Qi et al. (2017) reported that viscoelastic polymer flooding reduce the S_{or} at values of the N_c, lower than the critical N_c. Residual oil recovery is a pore-scale phenomenon. EOR researchers targeted the residual oil recovery through IFT reduction. IFT is a microscopic property. Representing the balance between the driving viscous force and trapping capillary force at the pore-scale is crucial. Apparent viscosity used in the viscous force term of the N_c represents the driving viscous force on the core-scale. At the pore-scale, 75% of resistance is due to polymer's elongational deformation (Haas and Durst 1982). Extensional viscosity is significantly higher than shear viscosity and/or apparent

viscosity (Barnes 2010; Azad et al. 2018a). N_c calculated using the extensional viscosity could represent the interplay between the driving viscoelastic forces and trapping capillary force at the pore-scale. Pore-scale N_c calculated using the extensional viscosity may be higher than the critical N_c. N_c calculated using the extensional viscosity may be a better method than existing methods such as conventional N_c.

Polymer flooding is a widely used EOR method. Any improvement that could reduce the expense and/or increase profitability is highly desired. Improving the rheological characterization through extensional rheology could answer the existing hypothesis and resolve the existing limitations that surround viscoelastic polymer flooding. This research is undertaken to gain a better understanding about the viscoelastic effects during polymer flooding. This research may help EOR researchers and the operating companies working on the viscoelastic polymer flooding.

Shear rheological characterization of EOR polymers has been carried out successfully using bulk shear rheometer (Heemskerk et al. 1984; Azad 2014; Delshad et al. 2008; Seright et al. 2009; Clarke et al. 2015). Extensional characterization of low viscous EOR polymers remains the challenge. Conventional extensional characterization techniques such as tubeless siphon, spinning flow, and bubble collapse can measure rheological properties for the polymer solutions possessing a zero shear viscosity of 0.1, 0.35, and 60 Pa.s, respectively. However, EOR polymer solutions possess a zero shear viscosity of around 0.04 Pa.s (Seright et al. 2009). A capillary breakup extensional rheometer is reported to handle the low viscosity fluid with zero shear viscosity between 0.002 and 0.01 Pa.s (Clasen et al. 2006). CaBER is used in this research for the extensional characterization of EOR polymers. The picture of CaBER is shown in Figure 1.2.

Figure 1.2: *Picture of CaBER used in this research*

1.3 Objective

To address the above problems, this thesis is divided into seven different tasks. The research objectives and related problem statements that will be answered are also listed below:

a. Compiling a critical review on the existing techniques for quantifying the polymer's viscoelastic effects
   - ✓ to identify the deficiencies or shortcomings with the existing methods,
   - ✓ to compile the misconceptions existing among the scientific community,
   - ✓ to provide better rheological insights for the existing deficiencies, and
   - ✓ to investigate the potential of a commercial simulator to honor the residual oil recovery potential of viscoelastic polymers.

b. Providing extensional insights into the different behavior of the similar shear polymers during oil recovery applications
   - ✓ to investigate the role of the extensional rheology on oil recovery, pressure profile, propagation shown by the similar shear polymers, and
   - ✓ to investigate the role of extensional rheology on the permeability reduction by performing chase water flooding.

c. Examining the effect of hydrophobic association on the flow behavior of associative polymer
   - ✓ to investigate if the typical behavior of associative polymer triggered by different hydrophobic associations can be decoded through the extensional rheology,
   - ✓ to identify the relation between permeability reduction at various hydrophobic associations and extensional rheology,
   - ✓ to ascertain if the critical association concentration will be different at shear field, extensional field and in the porous media, and
   - ✓ to verify if Deborah number is an appropriate method to correlate the behavior of associative polymer and HPAM.

d. Examining the extensional rheological role on viscoelastic polymer's S_{or} reduction
   - ✓ to investigate if there is any extensional rheological influence on S_{or} reduction,
   - ✓ to identify the appropriate rheological method among the oscillatory and extensional rheology in representing the viscoelastic effects during polymer flooding.

- ✓ to verify if the capillary theory that becomes invalidated with the usage of apparent viscosity as driving viscous force, can be validated through extensional viscosity.

e. Examining the role of polymer's viscoelasticity on the sweep efficiency and injectivity
   - ✓ to verify if the hypothetical claim that viscosity of viscoelastic polymer increases sweep efficiency is valid by comparing the role of viscosity and elasticity on the sweep efficiency, and
   - ✓ to ascertain if the existing screening criteria for heavy oil polymer selection is deficient.

f. Developing a core flooding independent viscoelastic model using measured extensional parameters to predict the apparent viscosity of EOR polymer
   - ✓ to determine the onsets, and shear thickening regime of viscoelastic polymers using the developed model.
   - ✓ to compare the developed model with existing models in predicting the onset, shear thickening regime.

g. Modifying the capillary number using extensional rheological parameters to account the viscoelastic polymer's S_{or} reduction potential
   - ✓ to compare the modified N_c with conventional N_c and Deborah number,
   - ✓ to develop a correlation between modified N_c and S_{or} reduction, and
   - ✓ to compare the developed correlation with the existing correlation in predicting the S_{or} reduction.

1.4 Thesis organization

In this dissertation, Chapter 1 provides a brief review about basic oil recovery mechanisms, EOR methods and concepts, polymer flooding, key features of extensional rheology, and the related problem statements. Quantification of polymer's viscoelastic effect during EOR has been a challenge among the chemical EOR researchers. Viscoelastic polymer flooding causes reduced injectivity and enhanced residual oil recovery. Several attempts were made to quantify the altered response in the injectivity and recovery due to polymer's viscoelastic effects. Chapter 2 of this dissertation provides a comprehensive critical review of the existing quantification techniques. Several core-scale models and pore-scale models developed by various researchers were summarized and critiqued. The limitation of CMG in honouring polymer's viscoelastic effect on residual oil saturation reduction is emphasized through a simulation study. Chapter 3 provides

extensional rheological insights into the different responses in the recovery and pressure behavior, shown by the similar shear polymers (associative polymer and [HPAM]), during heavy oil recovery applications. Chapter 4 highlights the direct link that the intermolecular hydrophobic association has on the resistance and residual resistance factor of associative polymers. The chapter also illustrates the typical flow behavior of associative polymer at various hydrophobic associations over the non-associating HPAM, and an improved understanding is made through extensional viscosity characterization. Chapter 5 answers the research questions posed by prominent researchers on the viscoelastic polymer flooding through extensional rheology measurements. Negative claims about the polymer's extensional rheological role on residual oil recovery is refuted for the first time through direct extensional measurements in this chapter. Classical capillary theory, which remained invalidated in the case of viscoelastic polymers, is validated through direct extensional rheological measurements. The advantage of extensional rheology over oscillatory rheology in the quantifying for the residual oil recovery is emphasized. This chapter clearly signifies the extensional role on microscopic residual oil recovery, viscoelastic onset, and shear thickening and urges the need to incorporate extensional rheological parameters in the polymer screening criteria. Chapter 6 investigates the shear and extensional rheological role of viscoelastic polymers on the sweep efficiency and injectivity during heavy oil recovery applications. In Chapter 7, the novel viscoelastic model named the Azad Trivedi viscoelastic model (AT-VEM), developed to predict the viscoelastic behavior of synthetic EOR polymers through direct extensional rheological measurements, is presented. In Chapter 8, N_c modified to account for the polymer's viscoelastic effect on S_{or} through extensional rheological parameters is presented. The correlation named the Azad Trivedi correlation (AT-C) is developed which can predict the S_{or} of various viscoelastic polymer solutions. All the chapters have their own literature review and conclusions. Also, the symbols used in different equations are explained within the text in all chapters. The extensional rheological parameters (extensional relaxation time, maximum extensional viscosity at the critical Deborah number, and strain hardening index) attained through CaBER theories are used throughout the thesis. To avoid redundancy, CaBER theories are detailed only in Chapter 3 and cross-referenced in the other chapters. Each chapter of this thesis (from Chapter 2 to Chapter 8) has been/will be submitted for publication in the journal. The conclusion pertinent to each chapter as well as overall conclusions and recommendations are provided in Chapter 9

Chapter 2: Quantification of the Viscoelastic Effects during Polymer Flooding: A Critical Review[1]

2.1 Introduction

Polymer flooding is a mature enhanced oil recovery (EOR) method with a high success rate for developing depleted oil reservoirs. Biopolymer and synthetic polymers are widely used in polymer flooding. Conventional shear rheological methods are sufficient to characterize the porous media behavior of viscous biopolymer. However, synthetic EOR polymers exhibit complex viscoelastic phenomena in porous media that causes an additional flow resistance more than expected from their shear forces. From the application point of view, it is believed that the polymer's viscoelasticity may lead to a reduced injectivity and an enhanced residual oil recovery. Polymer's viscoelastic effect on residual oil recovery is not universally agreed (Seright 2017).

Several researchers have provided a comprehensive review on polymer flooding for oil displacement. Chang (1978) reviewed the past polymer floods, appraised the then present technology and defined the guidelines for the future. Needham and Doe (1987) reviewed the usage of different polymers, mechanism associated with polymer flooding and polymer flood case histories. Kamal et al. (2015) provided information about the novel EOR polymers suited for harsh conditions. Sheng (2015) provided an update about the status of the polymer flooding on the field scale. The author also discussed the lesson learnt from the past projects and gave a brief description about the polymers' viscoelastic properties. Seright (2017) discussed the amount of polymer that needs to be injected at various scenarios. Wei et al. (2014) reviewed the mechanism associated with the residual oil recovery of viscoelastic polymers.

Viscoelastic polymers are widely used in EOR; however, quantification of polymers' viscoelastic effect is one of the major challenges among the chemical EOR researchers. Several attempts were made in this regard through Deborah number, continuum viscoelastic models and pore scale studies. Nevertheless, efforts are made to provide a comprehensive critical review on the existing methods or models that are available for quantifying the altered response in the injectivity and recovery caused by polymer's viscoelastic effects. This motivated us to provide a detailed review

[1] A version of this chapter has been accepted for publication in SPE Journal with revision

on this topic which will enable the readers to understand the deficiency of existing methods and their potential consequences.

In the initial part of the study, the general details about the residual/ bypassed oil, viscoelastic polymer flow in the porous media, shear and extensional viscosity, polymer's viscoelastic influence on injectivity and residual oil recovery are discussed. Existing methodologies used for quantifying the altered response in the injectivity and oil recovery caused by viscoelastic polymers are detailed in this paper. The deficiency of existing methods of viscoelastic quantification are illustrated through the contradicting literature and rheological concepts. The inability of the Deborah number to explain the pressure drop behavior in porous media, mechanical degradation and residual oil recovery potential of viscoelastic polymers are discussed. Practical difficulties that exist because of the unawareness about the certain important concepts are highlighted. For example, viscoelastic polymers that show thinning (drop in the viscosity with respect to shear rate) behavior in the shear field, exhibit hardening (increase in the viscosity with respect to strain) behavior in the extensional field. Other terminologies such as dilatant, pseudo-dilatant, shear thickening, viscoelastic behavior has also been used to describe the increase in the apparent viscosity with respect to flux (Seright et al. 2011a). Since the thickening that occurs during the extensional flow is not aided by any shear forces, we have used the term 'strain hardening' to differentiate it from thickening under shear flow. The extent of strain hardening during the extensional flow can be quantified through strain hardening index. Strain hardening index along with the downscaling factor can be used to estimate the intensity of shear thickening in the porous media (Azad and Trivedi 2019). Failure to appreciate the viscoelastic polymer's hardening phenomenon in the extensional field, resulted in the requirement of extensive core flooding experiments to predict the polymer's shear thickening behavior in the porous media. Some common misconceptions that exist among the researchers because of the existing deficiency are also discussed. While the polymer's viscoelastic effect on injectivity is agreed universally, few controversial opinions still exist among the EOR researchers regarding its effect on residual oil recovery. Capillary theory conventionally used to explain the residual oil recovery fails to explain the reduction caused by the polymer's viscoelastic effects. Extensional rheological and petro physical insights are provided to clarify the existing misconception regarding the polymer's viscoelastic influence on residual oil recovery. Several research gaps are identified that if addressed may lead to the optimal implementation of viscoelastic polymer flooding.

2.2 Background

2.2.1 Residual and bypassed oil.

Water flooding is the most commonly used improved oil recovery (IOR) method. Water flooding results in the lots of oil unswept and immobilized. The amount of oil unswept after water flooding is high in the reservoirs characterized by high oil viscosity and heterogeneity. Unswept oil is called the bypassed or the remaining oil. The low viscous, Newtonian nature of the water is the reason for low sweep efficiency of water flooding. The amount of oil immobilized after water flooding is high in the reservoir where there is high capillary pressure. Capillary pressure is a strong function of interfacial tension (IFT) between water and oil. Immobilized oil that is swept by the displacing slugs but could not be displaced is called as a residual oil (Lake 1989; Green and Wilhite 1998; Peter 2002). The minimal interfacial activity of water results in the higher residual oil saturation (S_{or}). Recovery factor can be decomposed into the displacement efficiency and sweep efficiency and an optimal EOR method should contribute to both displacement and sweep efficiency.

2.2.2 Conventional recovery mechanism in polymer flooding

Chemical EOR methods use different chemicals that provide surface activity and flow resistance needed for enhanced mobilization and sweep. Polymer flooding is one of the main variants of the chemical EOR method. In polymer flooding, the added polymer imparts viscosity to the displacing water, which in turn reduces its mobility during its propagation in the porous media. The displacing polymer solutions with reduced mobility contact more oil and increase the sweep efficiency (Taber 1969; Chang 1978; Lake 1989; Green and Willhite 1998; Sheng 2010).

2.2.3 Viscoelastic polymer flow through porous media

Two commonly used EOR polymers are biopolymers such as xanthan gum (Chiou and Kellerhals 1981), schizophyllum (Beeder et al. 2018), Sceluroglucan (Rivenq et al. 2015) and synthetic polymers such as HPAM (Delshad et al. 2008), associative polymer (Azad et al. 2018a), living polymers (Azad and Sultan 2014), sulfonated polyacrylamide (Han et al. 2012), ter polymer (Vermolen et al. 2011), copolymer (Levitt and Pope 2008). Biopolymer has a rigid rod-like structure (Moorhouse et al. 1977; Tyseer and Vetter 1981). Synthetic polymers have a flexible chain (Jones 1976; Sheng 2010). The rheological difference between these two polymers is the viscoelastic properties offered by the flexible chains in the synthetic polymers (Gennes 1974; Sorbie 1991; Wang et al. 2006).

Polymer solutions injected into porous oil reservoirs are subjected to various shear rates during the course of propagation. Different flow regimes are shown by the viscoelastic polymer solutions at different shear rates (Sheng 2010). The generic plot depicting the different flow regimes of a synthetic polymer is shown in Figure 2.1.

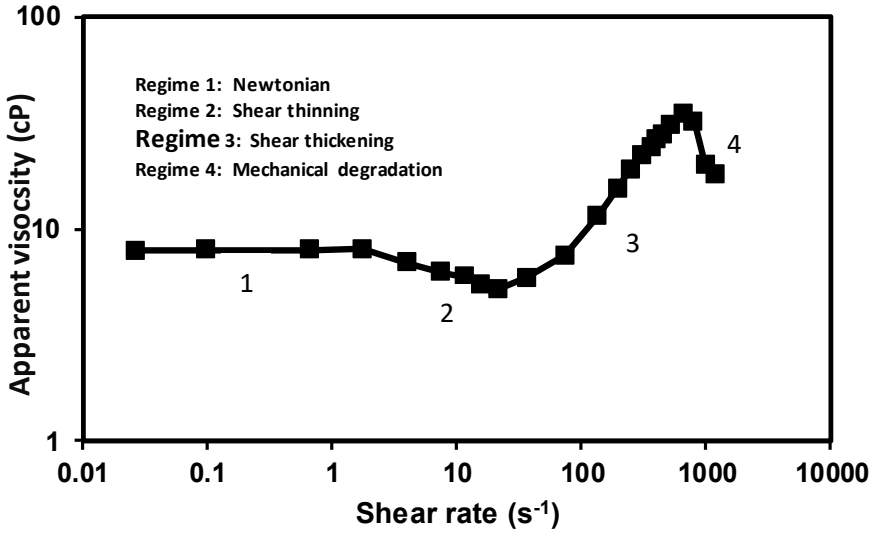

Figure 2.1*: Generic plot showing the typical porous media behavior of synthetic polymer*

Newtonian flow dominates at very low flux rates (regime 1). In this regime, apparent viscosity remains unaffected with the change in the shear rate. After a critical rate, the rheology of the synthetic polymer is dominated by the non-Newtonian, slight shear thinning behavior (regime 2). The apparent viscosity of the polymer solutions begins to decrease in this shear dominated regime. After a second critical rate also known as onset rate, shear thickening behavior is evident (regime 3). This behavior is the specific characteristic of viscoelastic polymers characterized by the presence of flexible chains. Onset rate decreases with decreasing permeability and increasing molecular weight (Mw), concentration (Heemskerk et al. 1984). Contrary to the observations by Heemskerk et al (1984), several authors have reported that polymer concentration doesn't play a significant role on the viscoelastic onset (Kulicke and Haas 1984; Seright et al. 2011a; Howe et al. 2014). Extensional flow dominates in this regime and the apparent viscosity increases with respect to shear rate for synthetic polymers (Hirasaki and Pope 1974; Delshad et al. 2008; Sheng 2010; Zamani et al. 2015). Both, coil-stretch phenomenon (Gennes 1974) and intermolecular network formation of stretched molecules are the attributed reasons for shear thickening phenomenon

(Choplin and Sabatie 1986; Muller et al. 1988; Rodriguez et al. 1993). Onset and shear thickening are not observed during the flow of viscous biopolymer due to the absence of flexible, stretchable chains (Seright et al. 2009). Once the shear thickening viscoelastic polymer becomes fully stretched at high rates, it accumulates excessive stresses that result in the eventual mechanical breakup of the polymer chain resulting in the decrease of apparent viscosity with respect to shear rate (Martin 1974; Seright 1983; Sorbie and Roberts 1984; Southwick and Manke 1988; Seright et al. 2009; Stavland et al. 2010; Manichand et al. 2013; Zechner et al. 2015; Puls et al. 2016). Odell (1986) reported that degradation occurs when the extensional stresses overcome the macromolecular covalent bonding forces. Regime 4 in Figure 2.1 represents this phenomenon. Vorwerk and Brunn (1991) reported that extensional viscosity decreases with respect to strain rate, after exhibiting a maximum. The higher the molecular weight of the polymer, the more easily it is degraded (Martin 1986; Taylor and Nasr-el-Din 1995). Low permeability results in earlier degradation (Gumpenger et al. 2015). Hill et al. (1974) observed the mechanical degradation effects with viscoelastic polymer but not with the viscous biopolymer. During mechanical degradation, high Mw components break into to low Mw components.

2.2.4 Shear and extensional viscosity

Shear viscosity is the measurement of resistance to the shear flow. It can be defined as the ratio between the shear stress to shear rate (Eq. 2.1). Extensional viscosity is the measurement of resistance to the extensional flow. It can be defined as the ratio between the normal stress differences to the elongation rate (Eq. 2.2). During the shear flow, stress acts in the direction perpendicular to its flow direction. Extensional flow is the flow in which the particles are stretched and aligned in the direction of flow, causing the stresses to act in the direction of flow (Barnes 2010). As can be seen from the Eq. 2.2, the higher the stresses in the direction of flow, the higher the extensional viscosity. In the porous media, extensional flow occurs when the displacing polymer solutions flow from pore throat to pore body and around the stagnation points (Chauveteau 1986). Extensional viscosity can also occur during a shear flow but at a relatively higher speed.

$$\mu_{shear} = \frac{\tau_{12}}{\dot{\gamma}} \tag{2.1}$$

where

μ_{shear} is the shear viscosity, Pa.s

τ_{12} is the shear stress, Pa

$\dot{\gamma}$ is the shear rate, s^{-1}

$$\mu_{extensional} = \frac{\tau_{11} - \tau_{22}}{\dot{\varepsilon}} \quad (2.2)$$

where

$\mu_{extensional}$ is the extensional viscosity, Pa.s

τ_{11} is the normal stress in the x-direction

τ_{22} is the normal stress in the y-direction

$\dot{\varepsilon}$ is the strain rate, s^{-1}

2.2.5 Shear and extensional rheological characterization

Steady rheological measurement of low viscous EOR polymers have been carried out successfully using rotational rheometer (Heemskerk et al. 1982; Cannella et al. 1988; Masuda et al. 1992; Delshad et al. 2008; Magbagbeola 2008; Azad and Sultan 2014; Kamal et al. 2015; Qi et al. 2017; Erinick et al. 2018). Tubeless siphon, spinning flow, and bubble collapse, the conventional extensional characterization methods can measure the extensional properties of the polymer solutions only when the zero shear viscosities are above 0.1 Pa.s, 0.35 Pa.s, and 60 Pa.s, respectively (Schummer and Tebel 1983). However, EOR polymers have been reported to exhibit zero shear viscosity of less than 0.04 Pa.s **(**Seright et al. 2009). Other extensional characterization methods such as the opposed jet rheometer (Fuller et al. 1987), optimal detection of birefringence through four roller apparatus (Harrison et al. 1999), and uniaxial systems replicating the porous media (Maguer et al. 1984) are time-consuming and relatively complex (Plog et al. 2005). Generating the pure elongational flow is not possible with any of these methods (Schummer and Tebel 1982; Martischius 1982; Bhardwaj et al. 2007). Strain hardening index that gives an estimate on the polymer thickening capability is difficult to quantify with the above methods that fail to produce the pure elongational flow. Shear thinning index that gives an estimate on polymer thinning capability in pure shear field is determined by fitting the power law to the decreasing shear viscosity values with respect to shear rate. Similarly, strain hardening index can only be determined in the pure extensional field by fitting the power law to the increasing value of

etensional viscosity with respect to strain. Since all the aforementioned method fails to produce the pure elongational flow, quantifying the strain hardening index is difficult. Relaxation time is the time taken by the polymeric solutions to return to its original shape after being disturbed. Measuring the relaxation time of low viscous fluids is also not possible with the aforementioned characterization methods. Rayleigh Ohnesorge Jet Elongational rheometer (Sharma 2015; Keshavarz et al. 2015), optically detected elastocapillary self-thinning dripping-onto-substract extensional rheometer (Dinic et al. 2015), the capillary break up extensional rheometer (CaBER) (Azad et al. 2018 a, b), miniaturized filament breakup device combining the slow retraction and high speed imaging (Sousa et al. 2017) are reported to give a good measure of extensional relaxation time of low viscous polymers. Screen factor, which gives an estimate of polymer's viscoelastic characteristics to elongational deformation has been measured using screen viscometer (Jennings et al. 1971; Lim et al. 1986). Castor et al. (1981) reported that screen factor measurements are polymer specific and cannot be used to compare different polymers. It is suggested that screen factor measurements can be used for qualitative characterization of EOR polymers (Sheng 2010).

2.2.6 Polymer's viscoelastic influence on injectivity

Shear thickening phenomenon exhibited by the viscoelastic polymers (Figure 2.1) has a negative influence on the injectivity. Around the wellbore, the velocity and shear rates experienced by the displacing slugs are high. Injectivity, the measurement of the ease with which the fluid can be injected into the reservoir (Hyne 1994) can be defined as the ratio between the injection rate to the generated injection pressure. Injecting at a high rate may cause the injection pressure to exceed the formation parting pressure. It will lead to the creation of fractures (Seright et al. 2009; Seright 2010; Seright et al. 2011a; Seright 2017). High permeable fractures will cause the injection fluid to get exposed to the relatively larger area and therefore velocity/shear rate will be reduced for the same injection rate. It could reduce the magnitude of the shear thickening and therefore the viscoelastic effects will be of diminished relevance and possibility of S_{or} reduction around the wellbore will be negligible. However, injectivity loss can be avoided with the creation of fractures. Properly controlled fractures were reported to increase the injectivity, sweep efficiency (Crawford and Collins 1954; Dyes et al. 1958; Wang et al. 2008; Seright 2017). The improperly induced fracture might affect the sweep efficiency of the process as the created high permeable streak could cause channelling (Crawford and Collins 1954; Dyes et al. 1958; Bargas and Yanosik 1988;

Seright et al. 2009; Seright 2017). Bargas and Yanosik (1988) reported the vertical fractures will not affect the sweep efficiency considerably at the mobility ratio of 1. However, the authors reported that at the mobility ratio of 10, the sweep efficiency was impaired significantly. Whether the operators decide to go for careful fracturing or not, it is imperative to predict the apparent viscosity and injection pressure of different polymer slugs. Displacing viscoelastic polymer solutions capable of generating high viscosity/resistance factor at high shear rate necessitate high injection pressure which may exceed the threshold pressure for fracturing and/or mechanical degradation. The injection rate needs to be reduced in order to avoid the fracturing. Consequently, injectivity becomes low with viscoelastic polymers (Milton et al. 1982; Seright 1983; Zaitoun and Kohler 1987; Weiss 1992; Wang et al. 2008; Seright et al. 2009; Han et al. 2012; Glasbergen et al. 2015; Sheng 2015; Lotfollahi et al. 2016a). Pure viscous polymers solutions also have relatively higher injectivity than viscoelastic polymeric solutions due to its complete shear thinning nature in porous media (Burnett 1975; Seright et al. 2009). Low injectivity causes the flood front delay, voidage problems and affects the economics of the EOR projects (Wang et al. 2008; Seright et al. 2009; Han et al. 2012; Clemens et al. 2013; Sheng 2015; Glasbergen et al. 2015). Seright (2010) made a cost analysis and reported the low injectivity has a more pronounced effect on the economics of heavy oil project than the cost of the polymer itself.

2.2.7 Polymer's viscoelastic influence on residual oil recovery

Capillary number (N_c), the ratio between the viscous and capillary force is used to represent the microscopic displacement process. Most of the numerical reservoir simulators use N_c to simulate the microscopic displacement recovery. N_c is used in the chemical EOR process to relate the balance between viscous and interfacial force with S_{or} (Wu et al. 2007; Wang et al. 2010; Tavasoli et al. 2014a; Tavasoli et al. 2014b). Several expressions of N_c have been reported in the literature (Taber 1981). Most commonly used expression is represented by the Eq.2.3

$$N_c = \frac{\mu * \upsilon}{\sigma} \tag{2.3}$$

where

μ is the viscosity, cP

υ is the velocity, $m.s^{-1}$

σ is the interfacial tension, $mN.m^{-1}$

The N_c of the typical water flooding (with μ = 1 cP, υ = 1 ft/day and σ = 30 mN.m^{-1}) is in the range of 10^{-7}. Capillary desaturation curve (CDC) describes the relation between the N_c and S_{or} **(**Chatzis and Morrow, 1984; Jr et al. 1985; Chatzis et al. 1988; Garnes and Mathisen, 1990; Tang 1992; Chukwudeme et al. 2011**).** Critical capillary number ($N_{c,\,crit}$) is the number above which, the oil mobilization begins to occur. $N_{c,\,crit}$ for most of the sandstone reservoirs are in the range of 10^{-4} to 10^{-5} (Foster 1972; Taber et al. 1973; Abrahms 1975; Chatzis and Morrow 1984; Sheng 2010). Surfactant flooding increases the N_c by more than three orders by decreasing the IFT between the water and oil to the range of 10^{-3} to 10^{-4} mN.m^{-1}. Polymers used in cEOR do not have a significant effect on IFT reduction. The shear/apparent viscosity shown by the polymer solutions at the typical flux rate of 1ft/day is in the range of 10-100 cP. With these values, N_c of the polymer solutions does not exceed the critical N_c and polymer solutions are not expected to reduce the S_{or} beyond that of water flood (Taber 1969; Lake 1989). Earlier results were consistent with this view, at least in water-wet reservoirs (Schneider and Owens 1982; Pusch et al. 1987; Wreath 1989). Research articles published by the Daqing researchers indicate that viscoelastic polymer can reduce the S_{or} reduction beyond that of water flood and more than expected from N_c (Wu al. 2007).

Viscoelastic properties of polymer were reported to cause an additional oil recovery (Han et al. 1995; Urbissinova et al. 2010; Azad et al. 2018 a). To confirm, whether viscoelasticity has an effect on S_{or} specifically, sweep effect need to be isolated so that capillary trapped residual oil is distinguished from the bypassed oil. This can be achieved by flooding enough water to ensure that the water-cut is closer to 100% and the left over oil is the capillary trapped residual oil, by ensuring the mobility ratio is less than 1, by injecting a purely viscous slug with a viscosity higher than the viscoelastic slugs, or by performing microscopic studies which confirm that the oil is recovered from the well-swept region. Several studies asserted the polymer's viscoelastic influence on S_{or} by complying to at least one of aforementioned conditions (Wang et al. 2000; Wang et al. 2001a; Wang et al 2001b; Xia et al. 2004; Wang et al. 2007; Wu et al. 2007; Xia et al. 2008; Jiang et al. 2008; Wang et al. 2010; Wang et al. 2011; Seright 2011; Ehrenfried 2013; Vermolen et al. 2014; Koh 2015; Clarke et al. 2016; Qi et al. 2017). Pulling effect, stripping effect, oil thread stabilization and shear thickening effect are the four different types of oil mobilization mechanisms caused by viscoelastic polymers solutions (Sheng 2010; Wei et al. 2014; Sheng 2015). All these mechanisms emphasize the influence of normal stresses.

Conventionally, it is believed that normal stresses or shear thickening viscoelastic effects become dominant at high shear/flux rates (Yuan 1981; Masuda et al, 1992; Delshad et al. 2008; Magbagbeolo 2008; Seright 2017). It is important to point out that significant difference between the apparent viscosity and shear viscosity is seen only at the very high shear rate of 500-1000s^{-1} by these researchers. However, several researchers have also reported that injecting viscoelastic polymer solutions can recover residual oil even at the flux of 1 ft/day (Ehrenfried 2013; Cottin et al. 2014; Koh et al. 2015; Clarke et al. 2016; Qi et al. 2017; Erinick et al. 2018).

On contrary to viscoelastic effects, some researchers also believe that the reported that S_{or} reduction could be due to other mechanisms. Wettability influence is suggested to be a possible mechanism for S_{or} reduction by the viscoelastic polymers (Seright 2017; Morejon et al. 2018). Qi et al. (2018) reported that the core-scale shear thickening concepts cannot explain the S_{or} reduction. They explained the additional S_{or} reduction using Deborah number. HPAM 6040 possessing low core-scale apparent viscosity and shear viscosity were reported to contribute to higher S_{or} reduction than the HPAM 3130 that core high core-scale apparent viscosity and shear viscosity (Clarke et al. 2016). Elastic turbulence has been considered as the mechanism for residual oil recovery by viscoelastic polymers (Clarke et al. 2016; De et al. 2018). Zaitoun and Kohler (1987) reported adsorption of polyacrylamide reduced the S_{or} by ~3% in the water-wet Berea and voges sandstone. There are also reported studies that did not observed S_{or} reduction and have argued against the polymer's viscoelastic effect on the residual oil recovery under certain conditions. Vermolen et al. (2014) observed the S_{or} reduction with 9 cP light oil but not with the viscous oil of 300 cP. Seright (2011) observed the S_{or} reduction during the recovery of 190 cP viscous oil from hydrophobic core. Seright et al. (2018) performed the series of polymer flooding at various concentration in the Cactus lake core saturated with 1610 cP heavy oil. The authors didn't report a significant residual heavy oil recovery with the high concentrated polymer flooding that is understood to possess higher elasticity. Azad and Trivedi (2018a) reported that the viscoelastic polymer solutions with higher elasticity do not influence the residual heavy oil recovery significantly in sand pack when compared to the less elastic polymer solutions. Vik et al. (2018) did not observe S_{or} reduction during the recovery of 500 cP oil from Bentheimer core samples. Similarly, Huh and Pope (2008) and Sandengen et al. (2017) also did not observe S_{or} reduction during tertiary polymer flooding in water-wet Berea core saturated with 26-28 cP oil and Bentheimer core samples saturated with 135.7 cP oil, respectively.

Cottin et al. (2014) and Morejon et al. (2018) reported that performing the viscoelastic polymer flooding in the secondary mode resulted in higher S_{or} reduction when compared to the tertiary mode. Morejon et al. (2018) reported that polymer flooding provided higher recovery during intermediate wettability conditions when compared to the water-wet conditions. Vermolen et al. (2014) showed that viscoelastic polymer can contribute to higher S_{or} reduction at higher fluxes, when compared to the low flux in Bentheimer sandstone. Qi et al. (2017) observed the S_{or} reduction with viscoelastic HPAM when compared to viscous glycerin. Schnedier and Owens (1982) reported that viscoelastic polymer flooding resulted in the rapid S_{or} reduction with low permeable oil-wet formation when compared to the relatively high permeable water-wet formation. During the experiments conducted by (Al-Qattan et al. 2018), low salinity viscoelastic polymer injection resulted in the additional 4% S_{or} reduction in water-wet cores compared to the low salinity water flood. Erinick et al. (2018) and Ehrenfried (2013) reported high saline viscoelastic polymer solutions with lower elasticity causes the higher S_{or} reduction in Bentheimer sandstone than the low saline viscoelastic polymers solutions with higher elasticity. From these studies, it can be seen that S_{or} reduction not only depends on flux rates but also oil viscosity, mode of polymer flooding, polymer elasticity, reservoir permeability, brine salinity, and reservoir wettability.

2.3 Critical discussions on viscoelastic quantification

2.3.1 Deborah number

Deborah number is defined as the ratio between the characteristic relaxation time of the material to its characteristic flow time (Macosko 1994; Barnes 2010). In EOR perspective, Deborah number can be defined as the ratio between the relaxation time of polymer slugs to its residential time in the porous media. Residential time can be defined as the time, the polymer solutions reside in the pore. Deborah number is used to represent the viscoelastic effects in the porous media. Weissenberg number (White 1964; Dealy 2010; Tiu et al. 2012; Wilton and Torabi 2013; Sobti and Wachoo 2014) also carrying a similar definition, is used to describe the viscoelastic effects. Marshall and Metzener (1966) used the Deborah number to explain the viscoelastic effects in porous media. They reported that a measurable increase in pressure drop due to viscoelastic effects begins to occur at a Deborah number of around 0.05. However, at the Deborah number of 1, significant viscoelastic effects were observed. The usage of Deborah number for describing the polymer's viscoelastic effects in porous media can be found in more literature (Sadowski and Bird 1965; Savins 1969; Choplin and Sabatie 1986; Vorverk and Brunn 1991; Kozicki 2002). Several

chemical EOR researchers have used the Deborah number for describing the viscoelastic effects during polymer flooding (Marshall and Metzener 1967: Heemskerk et al. 1984; Ehrenfried 2013; Koh 2015; Qi et al. 2017; Azad and Trivedi 2017; Azad et al. 2018a; Azad et al. 2018 b; Erinick et al. 2018; Qi et al. 2018). Deborah number may vary depending on the usage of relaxation time and residential time.

2.3.1.1 Relaxation time

Various approaches are reported for calculating the relaxation time. The relaxation time can be calculated using normal stresses and shear rate through contra variant convected Maxwell model (Marshall and Metzener 1967; Fred et al. 1979; Deiber and Schowalter 1981; Wissler 1971; Vossoughi and Seyer 1974; Kemblowski and Dziubinski 1978; Machac and Dolejs 1982; Dehghanpour et al. 2008). Relaxation time was expressed as a decreasing function of the shear rate through the Maxwell model. It is important to point out that relaxation time calculated as a decreasing function of the shear rate through Maxwell model cannot be used to predict the viscoelastic polymer behavior in porous media. Cakl and Machac (1995) reported that expressing relaxation time as a function of the shear rate will have limitations, especially for Boger (elastic) fluids as it will lead to the continual decrease in the Deborah number with respect to flow rate. Expressing the relaxation time as a continuous decreasing function of the increasing flux/shear rate will underestimate the elastic effects caused by the shear thickening phenomenon. In another approach, the Rouse model has been used to determine the relaxation time. In the Rouse model, the flexible polymer molecule is represented by the chains of N beads which are interconnected by N-1 elastic springs. The molecule immersed in the solvent would have relaxation times that is 1 less than the number of the chain beads. The longest relaxation time is the one that encompasses all the resistance (Rouse 1953). The critical Deborah number, corresponding to the viscoelastic onset in porous media was first reached for the longest relaxation time (Heemskerk et al. 1984). The Rouse model was used for determining the longest relaxation time through oscillatory rheology (Heemskerk et al. 1984 and Garrouch and Gharbi 2006). Zimm extended the Rouse model by incorporating the hydrodynamic interaction between the chains (Zimm 1956). Zimm relaxation time can be higher or lower, depending on the degree of coordination between the solvent and beads. Warner (1972) proposed the finite extensible non-linear elastic dumbbell model (FENE) for describing the non-linear flow behavior of dilute polymer solutions. FENE dumbell model was also used to determine the relaxation time (Haas and Durst 1982; Hester 1994). The

dumbell relaxation time attained in the extensional mode is 0.42 times higher than the relaxation time attained using the Zimm model (Haas and Durst 1982; Delshad et al. 2008). According to the cross over point method, the longest relaxation time can be found by reciprocating the frequency value, at which storage modulus and elastic modulus intersects (Doughty and Bogue 1967; Macosko 1994; Volpert et al.1998; Munoz 2003; Rubenstein and Colby 2003; Castelletto et al. 2004; Barnes 2010).

For weakly entangled polymer solutions in the strong flow, characteristic relaxation time associated with the transition to elastic turbulence is not the linear viscoelastic time that is measured in oscillatory rheology (Howe et al. 2015) but rather evolves as a single Rouse relaxation time. Two relaxation times namely, reptation relaxation time and Rouse relaxation time were associated with the polymer solutions that flows through constricted media (Reis and Wilson 2013). Reptation relaxation time associated with deformation of entangled polymer solutions occurs during shear flow. Rouse relaxation time associated with the straigtened polymer backbone occurs during the extensional dominated flow. Howe et al. (2015) have shown that oscillatory linear viscoelastic time is dependent on concentration and Mw. They also showed that characteristic time derived from the core is independent of the concentration and scales as Rouse relaxation time. Both Rouse relaxation time and characteristic time scales as the square of Mw. (Howe et al. 2015). Therefore, the onset rate that characterizing the transition from shear thinning to shear thickening is independent of the concentration (Seright et al. 2011a). It is important to note that extensive core flood experiments are required to determine the core relaxation time used by Howe et al. (2015). Qi et al. (2017) reported that the characteristic time determined from the cross-over point method is similar to the rouse relaxation time (within 20% to 30% experimental error) and have used the crossover relaxation time in the Deborah number calculation. Crossover method is considered by EOR researchers to be the most efficient and simple method to determine the longest relaxation time (Magbagbeola 2008; Delshad et al. 2008; Ehrenfried 2013; Vermolen et al. 2014; Koh 2015; Hincapie and Gazner 2015; Qi et al. 2017; Erinick et al. 2018; Qi et al. 2018)

2.3.1.2 Residential time

Residential time, which is the inverse of velocity gradient is the time that the fluid resides in the pore. Vast difference exists in the range of the Deborah number that corresponds to the viscoelastic onset and residual oil recovery because both the strain rate (Hirasaki and Pope 1974; Haas and

Durst 1982; Heemskerk et al. 1984; Durst et al. 1987; Delshad et al. 2008; Azad and Trivedi 2017; Azad et al. 2018 a, b) and shear rates (Masuda et al. 1992; Koh 2015; Lotfollahi et al. 2016b; Qi et al. 2017) are used for the calculation of Deborah number. Several researchers have used different formulas for the shear rate calculations (Christoper and Middleman 1965; Gogarty 1967; Hirasakhi and Pope 1974; Masuda et al. 1992; Magbagbeolo 2008; Seright et al. 2011a; Sun and Li 2014). Shear rate and strain rate, in general represented by the Eqs. 2.4 and 2.5, indicates that the rate is proportional to the interstitial velocity divided by the pore size.

$$\dot{\gamma} = C\left[\left[\frac{3n+1}{4n}\right]^{n/(n-1)}\left[\frac{u_w}{\sqrt{S_w \phi k k_{rw}}}\right]\right] \tag{2.4}$$

where

$\dot{\gamma}$ is the shear rate, s^{-1}

C is the shear correction factor

n is the shear thinning index

u_w is the interstitial velocity, $m.s^{-1}$

S_w is the water saturation

ϕ is the porosity

k is the permeability, D

k_{rw} is the relative permeability.

$$\dot{\varepsilon} = \left[\frac{u_w}{(1-\phi S_w)\sqrt{150 k k_{rw} / \phi S_w}}\right] \tag{2.5}$$

where

$\dot{\varepsilon}$ is the strain rate, s^{-1}

Deborah number calculated using strain rate will be lower than the one calculated with shear rate (Ehrenfried 2013; Qi et al. 2017) because the coefficient used in the denominator of strain rate calculation is higher than the one used in the denominator of shear rate calculation (Eq. 2.4 and Eq.2.5). For example, Deborah numbers (calculated using shear rate) reported by Qi et al. (2017) are very high in the range 10-25. Significant differences in the residual oil recovery are reported

by the authors to occur only at such high Deborah number. However, the viscoelastic effects were reported to be observed in the porous media when the Deborah number was much lower. Marshall and Metzener (1967) reported that the onset of viscoelastic effects corresponded to the Deborah number (calculated using the strain rate) of around 0.05 to 0.06. Several other researchers also reported, that viscoelastic onset corresponds to the similar value of lower Deborah number calculated using the strain rate (Vossoughi and seyer 1974; Kemblowski and Dziubinski 1978; Kemblowski and Michniewicz 1979; Skartsis 1992). Siskovic et al. (1971) reported that the critical Deborah number corresponding to the viscoelastic onset is 0.19. Heemskerk et al. (1984) and Stavland et al. (2010) reported that viscoelastic onsets correspond to 0.1 and 0.22 respectively. Since there is a vast difference in magnitude of Deborah number, it is difficult to have a quick reference that indicates at what range of Deborah number the viscoelastic effects begins to occur as well as at what range of Deborah number significant S_{or} reduction occurs.

2.3.2 Deborah number and S_{or}

Qi et al. (2017) converted the Deborah number reported by Ehrenfried (2013) to account for the differences arising due to the difference in the residential time. Ehrenfried (2013) used the strain rate for residential time calculation. Qi et al. (2017) developed the correlation between the Deborah number and S_{or} by using the data from Qi et al. (2017), Koh et al. (2015), and Ehrenfried (2013). Koh (2015) and Qi et al. (2017) used the shear rate for residential time calculation. Deborah number incorporating oscillatory relaxation time is then used in the developed correlation (Eq.2.6).

$$S_{or} = -0.0034 * N_{De} + 0.2747 \tag{2.6}$$

where

N_{De} is the Deborah number calculated using the oscillatory relaxation time.

Recently, Erinrick et al. (2018) performed series of core flood experiments with water, glycerin, low salinity polymer solutions at 1400 ppm salinity with higher oscillatory Deborah number and high salinity polymer solutions at 24300 ppm salinity with low oscillatory Deborah number (Figure 2.2).

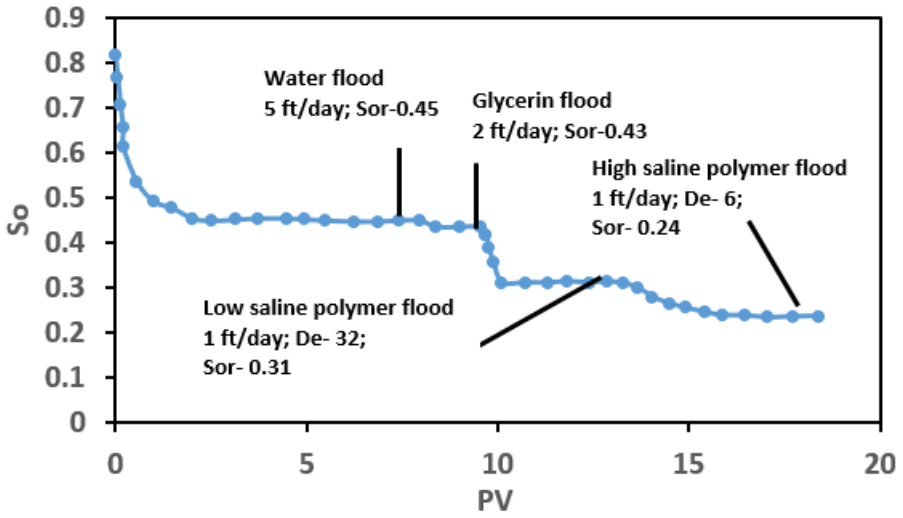

Figure 2.2*: Residual oil recovery potential and Deborah number of high salinity polymer flood compared with low salinity polymer flood (reproduced from Erinick et al. 2018)*

The authors reported low salinity polymer solutions with high oscillatory Deborah number recovers more residual oil than glycerin (with similar viscosity but negligible Deborah number). Authors attributed the viscoelastic effect to additional residual oil recovery caused by the polymer solutions with higher oscillatory Deborah number. However, the authors also reported that high salinity polymer solutions with lower Deborah number results in the further additional residual oil recovery than the low salinity polymer solutions with high Deborah number. Erinick et al. (2018) claimed that viscoelasticity is not a factor for the additional recovery caused by high saline solutions. Similarly, Ehrenfried (2013) reported that higher saline polymer solutions at higher concentration corresponded to a lower S_{or} reduction than the lower saline polymer solutions at the lower concentration. The polymer solutions at lower salinity corresponded to the oscillatory Deborah number of around 364, whereas the high saline polymer solutions correspond to the oscillatory Deborah number of around 4 (Figure 2.3a and Figure 2.3b).

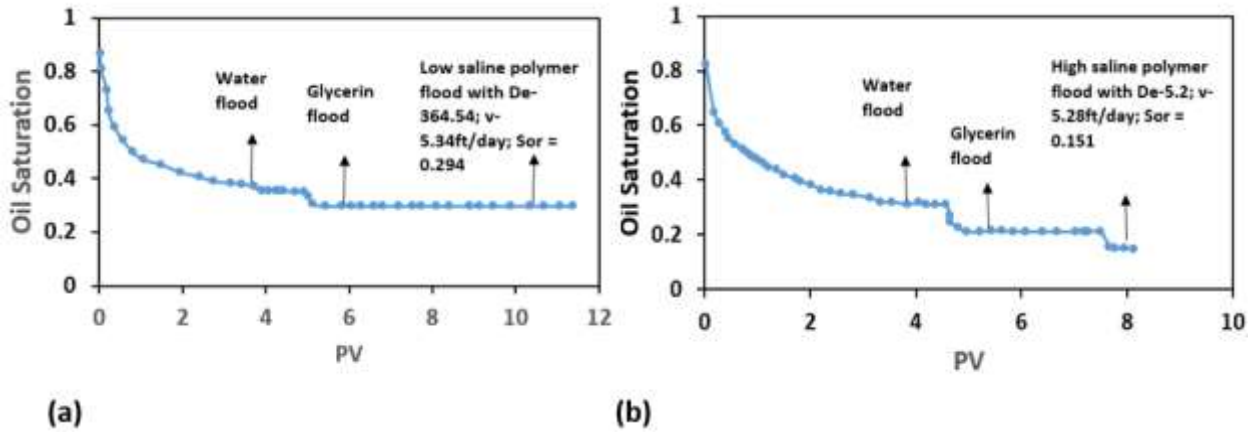

Figure 2.3: *a) Residual oil recovery potential and Deborah number of low salinity polymer flood compared with (reproduced from Ehrenfried 2013) b) residual oil recovery potential and Deborah number of high salinity polymer flood (reproduced from Ehrenfried 2013)*

Employing these values of Deborah number reported by Erinick et al. (2018) and Ehrenfried (2013) in the correlation (Eq. 2.6) developed by Qi et al. (2017) will give an incorrect estimation of S_{or}. Therefore, the authors concluded saying polymer's viscoelastic influence on S_{or} appears elusive.

Observations from Magbagbeola (2008) and Seright et al. (2011a) provide better insight to the core flood results observed by Ehrenfried (2013) and Erinick et al. (2018). Magbagbeola (2008) reported that 10,000 ppm salinity viscoelastic polymer solutions and 1000 ppm salinity viscoelastic polymer solutions possess oscillatory relaxation time of 0.035 s and 0.066 s, respectively at the same concentration of 1000 ppm. However, the strain hardening index for high saline polymer solutions and low saline polymer solutions are 2.3 and 1.65, respectively suggesting higher extensional characteristics of the high salinity polymer solution. Seright at al. (2011a) discussed that at high salinity, the polymer solutions exist in the coiled state due to the electrostatic repulsion. However, at the low salinity, the polymer solutions exist in the elongated form because of unshielded electrostatic repulsion between the anionic groups along the polymer chains. More energy needs to be expended to uncoil the chains so that the polymer molecules can flow through the pore constriction. Contrarily, the energy needed to stretch the uncoiled polymer chains is relatively lesser. This could be the reason for the lower strain hardening index value of low saline polymer solutions reported by Magbagbeolo (2008), even though it possesses higher oscillatory relaxation time than the high saline polymer solutions. The results and discussion of Magbagbeolo (2008) and Seright et al. (2011a) highlight the deficiency of oscillatory relaxation time for

quantifying the viscoelastic effects for saline polymer solutions. Therefore, the extensional rheological measurements are essential to obtain strain hardening index when dealing with saline polymer solutions.

The possible rheological reasons for these discrepancies are that the oscillatory shear is a weak field where the deformation experienced by the polymer solution is small. Since the deformation is small, it represents the linear viscoelasticity (Macosko 1994). However, porous media has strong extensional flow component in the pore throat region of the reservoir (Nguyen 1999; Afsharpoor et al. 2012) as the normal stresses become higher around the pore constrictions. The polymer solutions tend to get stretched that result in the generation of stress parallel to the flow. The generated stresses in the stretched state results in the stronger extensional flow. When the polymer gets stretched in extensional flow, the diameter of the polymer chain gets reduced. As a result, the force acts on the area that is shrinking (Liu et al. 2013). Therefore, the generated extensional stresses become highly potent. However, in the shear flow, the force is generated from the constant area (Liu et al. 2013). The deformation experienced by the polymer solutions in the extensional field is higher than the deformation experienced by the polymer solutions in the oscillatory field (Clasen et al. 2006). Therefore, the use of oscillatory rheological parameters for quantifying the viscoelastic effects on S_{or} reduction needs a revisit.

2.3.3 Oscillatory Rheology and Porous Media Behavior

Garrouch and Gharbi (2006) reported that viscous xanthan gum resulted in a comparable Deborah number with viscoelastic HPAM at high salinity (Figure 2.4a).

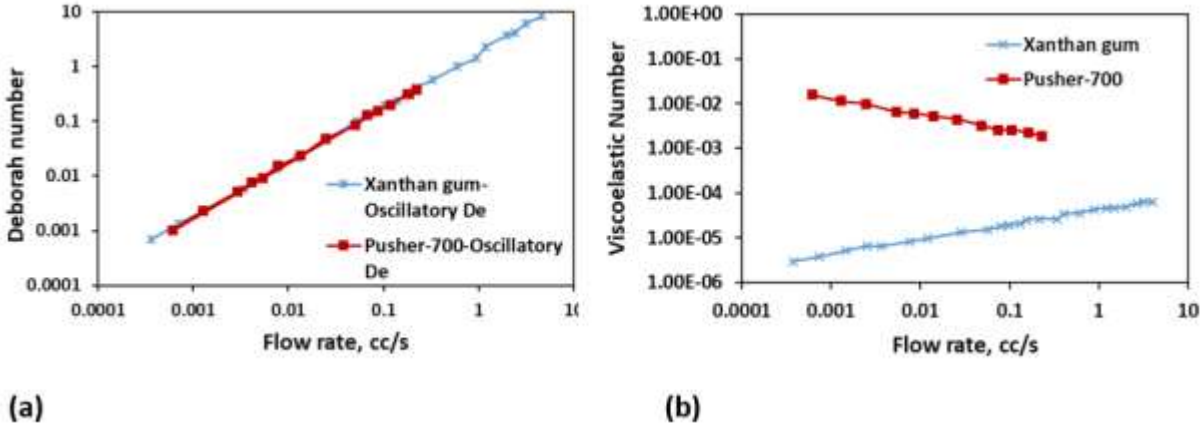

Figure 2.4: *a) Deborah number vs flow rate for Xanthan gum and Pusher-700 (reproduced from Garrouch and Gharbi 2006) b) Viscoelastic number vs flow rate for Xanthan gum and Pusher-700 (reproduced from Garrouch and Gharbi 2006)*

Oscillatory relaxation time, used in the Deborah number calculation was similar for both the viscous and viscoelastic polymers. However, in porous media, a different but an expected response was shown by these polymer solutions with viscoelastic HPAM exhibiting higher pressure drop and resistance factor over viscous xanthan gum. The authors highlighted the deficiency of oscillatory Deborah number and explained this discrepancy by proposing a new viscoelastic number that incorporates the empirical parameter reflecting their elastic behavior in porous media (Figure 2.4b). Porous media characterized by the shear and extensional components gives rise to non-linear viscoelastic effects and the proposed viscoelastic number appeared to encompass it. In the extensional flow, when the conditions required for the coil-stretch transitions are met, the polymer coils become extended and it leads to an increased interaction volume (Dunlap and Leal 1987) and a longer extensional relaxation time. Extensional relaxation time is higher than the oscillatory relaxation time (Clasen et al 2006). Seright et al. (2011b) reported a similar behavior of HPAM and associative polymer in a steady shear field (Figure 2.5a).

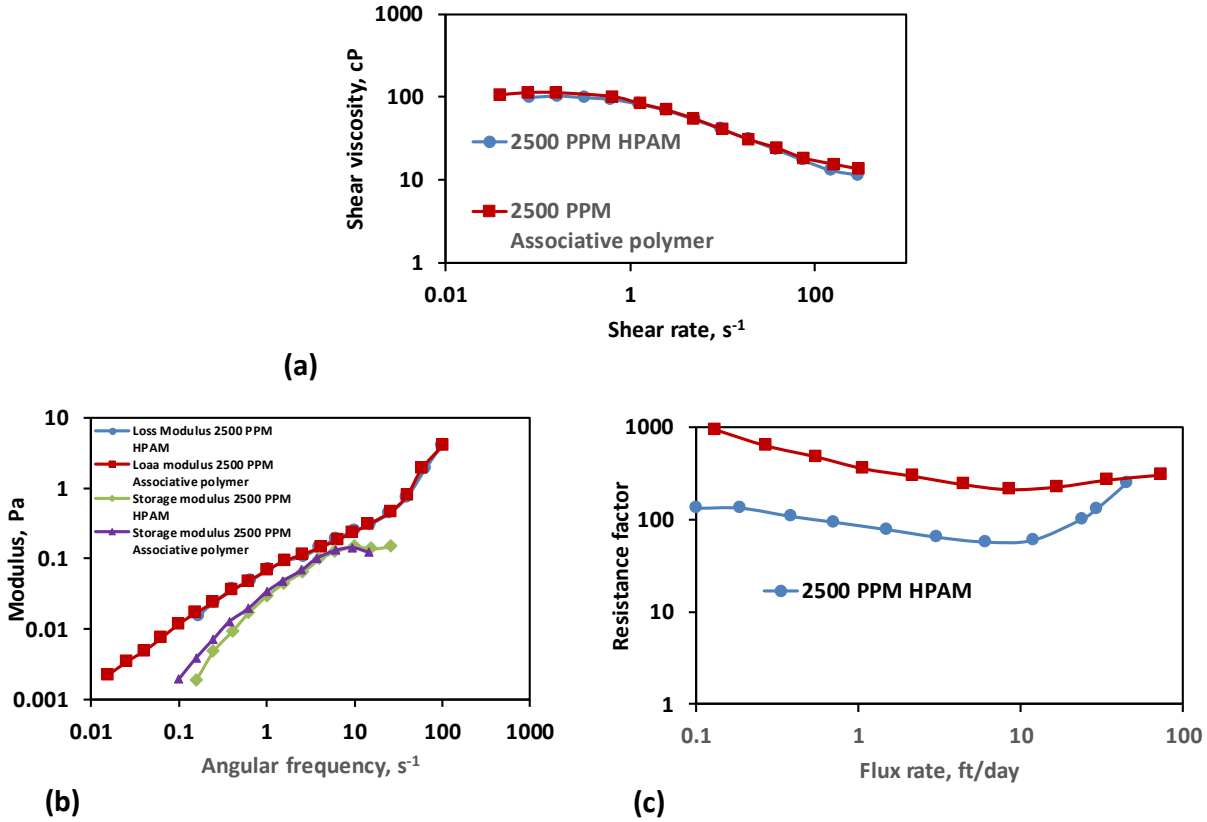

Figure 2.5: *a) Steady shear rheology of associative polymer and HPAM (reproduced from Seright et al. 2011b) b) Oscillatory shear rheology of associative polymer and HPAM (reproduced from Seright et al. 2011b) c) Porous media behavior of associative polymer and HPAM (reproduced from Seright et al. 2011b).*

The oscillatory shear behavior for both the polymer solutions was also reported to be the same by Seright et al. (2011b) (Figure 2.5b). However, the flow behavior differs vastly in the porous media with associative polymer exhibiting higher resistance factor than HPAM (Seright et al. 2011b) (Figure 2.5c). Azad et al. (2018 b) observed the similar shear behavior between HPAM and associative polymer and explained their different porous media behavior through extensional rheology (Figures 2.6 a-c).

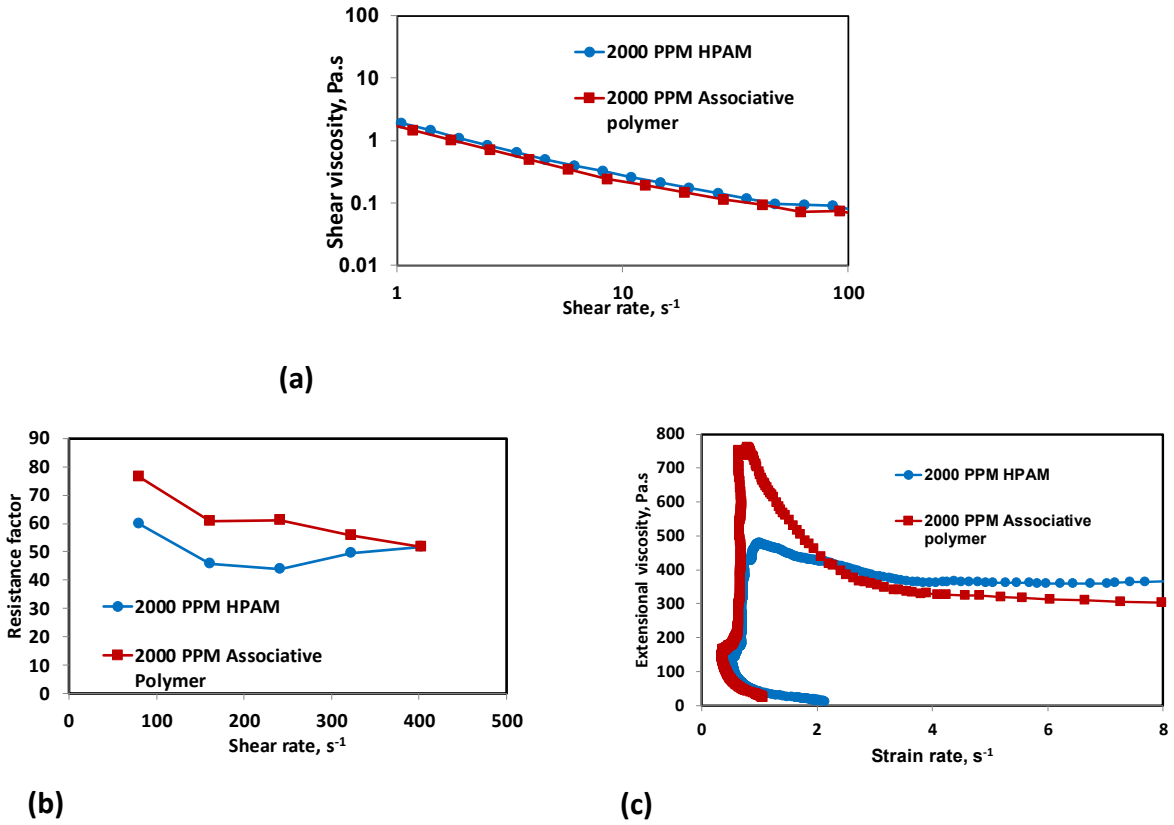

Figure 2.6: *a) Steady shear rheology of associative polymer and HPAM (reproduced from Azad et al. 2018b) b) Porous media behavior of associative polymer and HPAM (reproduced from Azad et al. 2018b) c) Extensional rheological behavior of associative polymer and HPAM (reproduced from Azad et al. 2018b)*

The presence of hydrophobic groups was reported to induce the higher extensional resistance in guar gum (Young et al. 1998; Taylor and Nasr-el-din 2007). However, no attempts were made to compare the extensional and oscillatory relaxation time of purely viscous and viscoelastic polymers.

2.3.4 Limitation of Deborah number calculated using fixed relaxation time

Using Deborah number (calculated using the single relaxation time) as such can explain the viscoelastic phenomenon at fairly low rates/intermediate rates (Azad et al. 2018 b). However, it will overlook the drop in the apparent viscosity caused by mechanical degradation. The associative polymer exhibits a higher resistance factor than HPAM at low rates. At higher rates, resistance factor of associative polymer drops to a level that has a comparable resistance factor to HPAM (Azad et al. 2018 b) (Figure 2.6b). However the Deborah number of the associative polymer was higher than the Deborah number of HPAM throughout the range of flux rates (Figure 2.7).

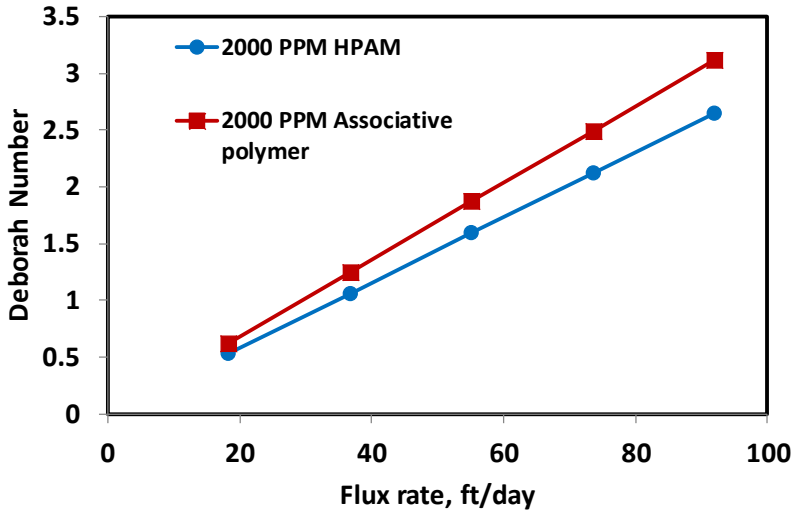

Figure 2.7: *Deborah number of associative polymer and HPAM (reproduced from Azad et al. 2018b)*

Azad et al. (2018b) reported the limitation of Deborah number calculated using the fixed extensional relaxation time. It is to be noted that the relaxation time determined from the most commonly used cross-over point method will suffer from the same limitation. Few attempts were made to address these limitations.

Azad et al. (2018 b) explained the typical porous media behavior of associative polymer through extensional viscosity vs strain rate trend (Figure 2.6c). Unified apparent viscosity (UVM) model developed by Delshad et al. (2008) seems to be based on the concept that mechanical degradation of polymer is due to the excessive buildup of elongational stresses (Culter et al. 1972; Culter et al. 1975; Maerker 1975; Farinato and Yen 1987; Moreno et al. 1996; Martin 1986; Dupas et al. 2013). So there has to be a maximum elongational viscosity that the polymer solutions should possess, above which the polymer will degrade and show a drop in the apparent viscosity due to chain scission. The maximum elongational viscosity was placed empirically in the UVM model along with the Deborah number (Delshad et al. 2008). Stavland et al. (2010) also followed a similar approach and added terms such as mechanical shear thinning exponent, the time constant and shear rate to represent the loss of apparent viscosity with respect to velocity due to mechanical degradation. Another possible way that could have resolved these issue is to express the relaxation time as an increasing/decreasing function of shear rate. Wilton and Torabi (2013) used the specialized oscillatory V-E rheometer with inbuilt capillary plug and expressed relaxation time as an increasing and decreasing function of shear rate. Using the relaxation time as a function of

increasing/decreasing shear rates may enable the Deborah number to explain the mechanical degradation effects caused by excessive buildup of extensional stresses. However, no efforts were made in this regard.

2.4 Viscoelastic models for quantifying the apparent viscosity

The Deborah number that has been used to describe the polymer's viscoelastic effect in the porous media cannot be used to quantify the apparent viscosity because it is dimensionless quantity. Deborah number has to be combined with appropriate viscosity terms to represent the apparent viscosity at various flow rates in the porous media. The continuum viscoelastic models were developed based on the core scale permeability where all the localized effects are included. Continuum viscoelastic models give the measure of polymer's apparent viscosity for various ranges of shear rates. The models can give an estimation of the polymer's injectivity at higher shear rates, encountered around the wellbore. Several viscoelastic models were developed in this regard.

Wissler (1971) used the third order perturbation analysis for studying the excess resistance caused by the viscoelastic fluids over viscous fluids in the converging-diverging section (Eq. 2.7).

$$\Delta P_{viscoelastic} = \Delta P_{viscous}\left[1 + A\left(\frac{\lambda v}{D_p}\right)^2\right] \tag{2.7}$$

where

A is a constant.

λ is the characteristic relaxation time, s

v is the interstitial velocity, micron.s^{-1}

D_p is the pore size, microns

$\Delta P_{viscous}$ is the viscous pressure drop

$\Delta P_{viscoelastic}$ is the viscoelastic pressure drop

Weisler further used the data of Marshall and Metzener (1967) and proposed a model that expressed the excess resistance in terms of frictional factor (f) and Reynolds number (Re) (Eq. 2.8). A in Eq.2.7 is scaled to be 10 in Eq.2.8

$$f\,\mathrm{Re} = 1 + 10\left[\frac{\lambda v}{D_p}\right]^2 \tag{2.8}$$

where

$$\left[\frac{\lambda v}{D_p}\right] = D_e$$

However, the flow resistance increases indefinitely with respect to D_e. Moreover the apparent viscosity was not expressed with D_e or flow resistance. Further, only three data sets reported by Marshall and Metzener (1967) were used for validation.

Hirasaki and Pope (1974) developed the apparent viscoelastic model in early 70s. Modelling was done based on the postulation that flow through varying cross-sectional pores is simply elongational. Apparent viscosity is related to Deborah number and shear viscosity by the Eq. 2.9.

$$\mu_{app} = \frac{\mu_{shear}}{1 - N_{Deb}} \tag{2.9}$$

where

μ_{app} is the apparent viscosity, cP;

μ_{shear} is the shear viscosity, cP;

N_{Deb} is the Deborah number

The physical meaning of the model (Eq. 2.9) is lost for the values of Deborah number above **one**. Commonly used high molecular weight polymers exhibit Deborah number much higher than **one** (Magbagbeola 2008; Qi et al. 2017; Azad et al. 2018 a; Azad et al. 2018 b).

Heemskerk et al. (1984) performed a detailed core flood experiments to study the viscoelastic onset. The authors quantified the viscoelastic effects through the critical flow rate causing the viscoelastic onsets and two power-law coefficients (n_1 and n_2) representing thinning and thickening effects. The apparent viscosity and power-law coefficients are related by Eq.2.10.

$$\mu_{app}(\dot{\gamma}) = \begin{cases} K_1(\dot{\gamma})^{n_1-1} \left(\dot{\gamma} \le \dot{\gamma}_{crit}, n_1 < 1\right) \\ K_2(\dot{\gamma})^{n_2-1} \left(\dot{\gamma} \ge \dot{\gamma}_{crit}, n_2 > 1\right) \end{cases} \tag{2.10}$$

where

K_1 and K_2 are the consistency factors.

n_1 and n_2 are the shear thinning and shear thickening coefficient.

$\dot{\gamma}_{crit}$ is the critical shear rate, s^{-1}

$\mu_{app}(\dot{\gamma})$ is the apparent viscosity, cP

As per Heemskerk et al. (1984), viscoelastic onsets decrease with increasing temperature, permeability and salinity and increases with increasing molecular weight, concentration. Parameters such as salinity and temperature degrade the polymer and thereby making it less elastic, needing a higher flow rate to induce the viscoelastic effects. For high permeability reservoirs, the injected polymers are subjected to less deformation as the polymers are flowing through the pore spaces with less resistance and therefore high flow rate is required to induce the deformation that can lead to coil-stretch transition and viscoelastic effects. At higher concentration, polymer's elastic nature increased for high Mw polymer and thereby viscoelastic onset was lower. However, Kulicke and Hass (1984) and Seright et al. (2011a) reported that the concentration doesn't influence the viscoelastic onset rate. The conducted studies by Heemskerk et al. (1984) provided a detailed sensitivity analysis of polymer and porous media properties on the viscoelastic effects. However, it cannot be used for quick screening of the polymers as the extensive core flooding experiments are needed to determine the n_1 and n_2.

Sorbie and Robert (1984) proposed a kinetic model for calculating the injectivity of the polymer solutions along with the mechanical degradation effects. Sorbie and Robert's model is developed based on the notion that the molecular weight distribution (MWD) changes due to the mechanical degradation of the high molecular component into the lower molecular weight components. The corrected viscosity is then expressed as a function of Darcy velocity for the specific component (Eqs.2.11 and 2.12)

If v is $> v_{ci}$

$$\eta_i(v, c_i) = \eta_s + \eta_{oi}\left(1 + D\left(v - v_{ci}\right)\right)^x \tag{2.11}$$

If $v < v_{ci}$

$$\eta_i(\bar{v}, c_i) = \eta_s + \eta_{oi} \tag{2.12}$$

where

η_i is the corrected shear viscosity, cP

$\bar{v}$ is the Darcy velocity, ms^{-1}

v_{ci} is the critical onset darcy velocity, ms^{-1}

η_{oi} is the zero-shear viscosity, cP

η_s is the solvent viscosity, cP

c_i is the concentration of an i_{th} component of the polymer, ppm

D and *x* are the positive constants, used to determine the polymer rheology in the porous media through core flood experiments

The total fluid viscosity in the porous medium is expressed by Eq. 2.13.

$$\eta_T(\bar{v},\underline{c}) = \eta_s + \sum_{i=1}^{J}(\eta_i - \eta_s) \tag{2.13}$$

where

η_T is the total viscosity, cP

$\underline{c}$ is the vector of *J* concentration representing the polymer

Using the Mark Howink relation, critical velocity is related to molecular weight as per the Eq.2.14

$$v_{ci} = FM_i^{-f} \tag{2.14}$$

where v_{ci} is the critical velocity for the onset of shear thickening, ms^{-1}; M_i is the molecular weight of the particular component, gm/cc; *F* and *f* are positive constants determined through core flooding.

The authors have observed that critical velocity varies with respect to porosity and permeability and expressing them in the Deborah number is more accurate. Eq. 2.15 relating MW and critical velocity, is specific to a particular reservoir core. Therefore, this relation is not universal.

Sorbie and Robert (1984) represent the degradation using the Eq.2.15

$$\left[\frac{dC_i}{dr}\right]_{\text{deg}} = -k(\tau_{pm} - \tau_{ci})^m C_i^{\infty} \tag{2.15}$$

where

$\frac{dC_i}{dr}$ is the concentration degradation term

k is the degradation rate constant

τ_{pm} is the porous media stress, Pa

τ_{ci} is the critical stress for the onset of degradation, Pa.

If the porous media stress is greater than the critical stress for the onset, concentration degradation becomes zero (Eq.2.16).

$$\left[\frac{dC_i}{dr}\right]_{\deg} = 0 \tag{2.16}$$

If the porous media stress is less than or equal to the critical stress for the viscoelastic onset, the critical shear stress of particular component is related to the midpoint MW of the ith component (Abdelhalim 1973). Sorbie and Robert (1984) expressed it by the Eq.2.17.

$$\tau_{ci} = gM_i^{-e} \tag{2.17}$$

where,

g and e are the constants determined from core flood

M_i the molecular weight of individual component

Extensive core flood experiments are required to determine the parameters needed for calculating the critical onset velocity for shear thickening. Also core flood experiments are required to determine the critical shear stress for mechanical degradation calculations. Further, this model is not universal as it is also developed based on the specific reservoir core.

Masuda et al. (1992) provided an improved version of the viscoelastic model. The authors accounted for the additional pressure drop through the shear viscosity, Deborah number and empirical constants. Deborah number was represented as the ratio of elastic force to viscous force. The authors proposed the viscoelastic model of the form, represented by Eq.2.18.

$$\mu_{ext} = \mu_{shear} * (C * N_{Deb}^{m_c}) \tag{2.18}$$

where

μ_{ext} is the extensional viscosity, Pa.s

μ_{shear} is the shear viscosity, Pa.s

N_{Deb} is Deborah number

C and m_c are the empirical constants

Two limitations in the Masuda's model are that it relied completely on core flooding to determine the *C*, m_c and the relaxation time used in Deborah number calculation. Another limitation is that the elastic force in the elongational part increases indefinitely when Deborah number increases. Ranjbar et al. (1992) developed a model for accounting the additional apparent viscosity caused by the strain flow of viscoelastic polymer solutions in the porous media. Apparent viscosity was treated as the sum of shear and strain (elongational) viscosity. The model is based on Maxwell-Fluid relation and it was found that the model index is an important parameter for viscoelastic quantification. The model index is determined by changes induced to the polymer molecules before and after the reduction of injection rate and injection pressure. Model index increases with decreasing permeability and increasing storage modulus and concentration. The relation between the model indexes, original viscosity, altered viscosity during shear and elongational flow is represented by the Eq. 2.19 and Eq. 2.20.

$$\eta'(t) = \eta\left(1 - e^{-\frac{t}{\tau}}\right) \text{ (During shear flow)} \tag{2.19}$$

$$\eta'(t) = \eta \bullet e^{-\frac{t}{\tau}} \text{ (During elongational flow)} \tag{2.20}$$

where

$\eta'(t)$ is viscosity at time t, cP

η is original viscosity, cP

t is time, s

τ is a model index, determined through extensive core flood experiments.

Han et al. (1995) calculated two critical velocities between which the elongational flow occurs. However, strong dilatant behavior was observed only after the second critical velocity. First critical velocity was calculated using the notion that if the ratio between the permeability caused by the chase water injection at a high rate to low rate is greater than 1, then it is due to the stretching of retained polymer molecules and polymer exhibits viscoelastic effects at that high rate which is

called the first critical velocity. However, in porous media, strong dilatant is not observed until the certain rate, that is second critical velocity. The authors investigated these observations by comparing the bulk rheological and porous media behavior of viscoelastic polymer (Figure 2.8) and reported that there is a first critical velocity at which the curve representing the porous media behavior of the polymers begins to deviate from the curve representing the bulk rheological behavior of the polymer. However, even after the critical velocity the polymer solutions exhibit shear thinning for a while before it starts to exhibit dilatant effects at the second critical velocity (Figure 2.8)

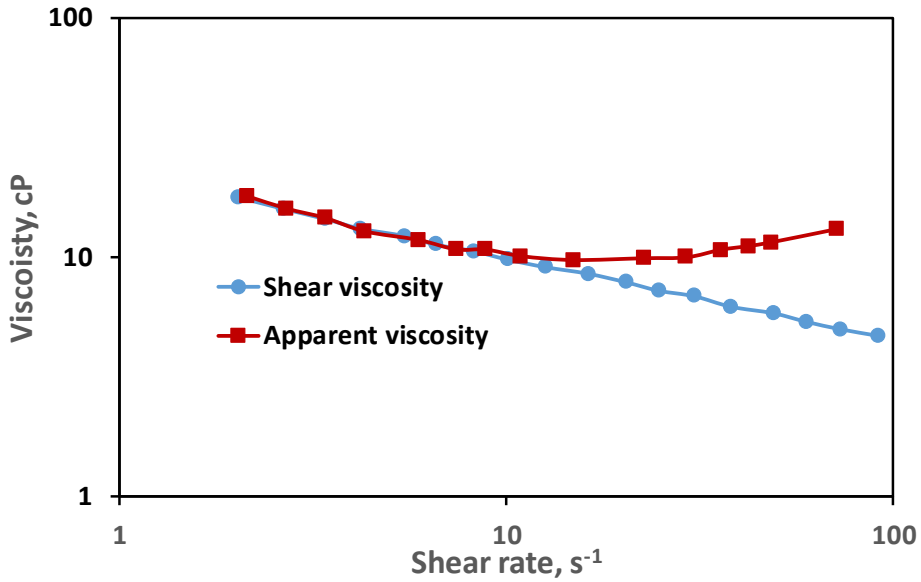

Figure 2.8: *Porous media behavior of viscoelastic polymer begins to deviate from bulk shear behavior even before the onset (Reproduced from Han et al. 1995)*

Since the porous media behavior starts to deviate from the rheological behavior even before the onsets of dilatant effects, the authors concluded that the viscoelastic effects are experienced in the porous media even before the onset of the strong dilatant effects and the flow in the porous media is both elongational and shear. This comparison appears to indicate that the flow becomes elongational immediately after the first critical flow rate. However, the extensional flow is not strong at the low rate until the second critical velocity. Both the flow rate shifted towards high value when the permeability is increased. The authors also developed Han's Index (H) for describing the viscoelastic effects of polymer solutions in the porous media. Han's Index is nothing but the relaxation time. Oil recovery experiments conducted by the authors revealed that recovery efficiency increases from first critical velocity and attains the maximum around the second critical

velocity suggesting that the elongational flow has a pronounced effect on the oil recovery. These observations also suggest that recovery due to the viscoelastic (extensional) effects happen even before the onset rate corresponding to the shear thickening**.** 1-D numerical simulation of polymer flood was performed to validate their calculated results with experimental data. Extensive core flood is required to calculate the Han-index and to determine two critical velocities.

Garrouch and Gharbi (2006) reported the inadequacy of Deborah number (calculated using oscillatory relaxation time) to distinguish the behavior of xanthan gum and HPAM (Figure 2.4a). The authors introduced a new viscoelastic number that could distinguish viscous xanthan gum and viscoelastic HPAM (Figure 2.4b). The viscoelastic number represented by Eq. 2.21 incorporates bulk oscillatory relaxation time and power law exponent. The direct relation between the viscoelastic number and the pressure drop is represented by Eq. 2.22.

$$N_v = \frac{\sqrt{k * \phi}}{\theta_{f_1} * u^{\bar{n}-1}} \tag{2.21}$$

where

k is the permeability, Darcy

ϕ is the porosity

u is the velocity, m.s^{-1}

$\bar{n}$ is the power law exponent in the porous media, determined through core flood experiments

θ_{f_1} is the relaxation time, s

$$N_v = \alpha\left(\frac{\Delta p}{L}\right)^{\beta} \tag{2.22}$$

where

Δp is the pressure gradient, psi/ft

L is the length, ft

α and β are the intercepts determined from the core flood experiment, between N_v and Δp

The authors reported the $\bar{n}$ values to be above 1 for the viscoelastic HPAM flooding and less than 1 for the viscous xanthan gum flooding. As per Eq.2.21, the authors have reported that the viscoelastic number is higher for viscoelastic HPAM (with $\bar{n}$ higher than 1) than viscous xanthan gum (with $\bar{n}$ less than 1), despite both having the same oscillatory relaxation time. The higher the

viscoelastic number, the higher the pressure drop (Eq. 2.22). Extensive core flood experiments are required to determine the power law exponent.

Delshad et al. (2008) developed the Unified apparent viscosity model (UVM) based on the postulation that the apparent viscosity of polymer solutions is the sum of shear and elongational viscosity. UVM model accounts for the viscoelastic thickening in the extensional part through relaxation time, strain hardening index and maximum elongational viscosity. The model is represented by Eq. 2.23

$$\mu_{app} = \mu_{\infty} + \left(\mu_p^o - \mu_{\infty}\right)\left[1 + \left(\lambda * \gamma\right)^{\alpha}\right]^{\frac{(n-1)}{\alpha}} + \mu_{\max} * \left[1 - \exp\left(-\left(\beta * N_{Deb}\right)\right)\right]^{n_2 - 1} \quad (2.23)$$

where

μ_{∞} is the infinite shear viscosity, Pa.s

μ_p^o is the zero shear viscosity, Pa.s

λ is the shear characteristic time, s

γ is the shear rate, s^{-1}

α is the correction factor, 2

n is the shear thinning index

$\mu_{\max}$ is the maximum elongational viscosity, cP

β is the universal constant, 0.01

N_{Deb} is the Deborah number

n_2 is the strain hardening index

Shear parameters μ_{∞}, μ_p^o, λ, α and n are determined through bulk shear rheology using a Carreau model. Extensional parameters such as $\mu_{\max}$ and n_2 are determined through core flooding. Relaxation time used for Deborah number calculation is determined through oscillatory rheology. UVM model addressed the limitation of previous viscoelastic models by not letting the indefinite rise of apparent viscosity with respect to Deborah number. This is based on the concept (Odell 1986; Vorwerk and Brunn 1991) that there exists a maximum elongational viscosity in the porous media, after which the mechanical degradation occurs. UVM model has been successfully used in the injectivity models (Li and Delshad 2014; Lotfollahi et al. 2016a). However it is dependent on

the core flood data to predict the extensional parameters such as maximum elongational viscosity and strain hardening index.

Kim et al. (2010b) developed an empirical correlation using the generalized Maxwell model to determine relaxation time for various conditions of salinity and temperature. The developed correlation is shown in Eq.2.24.

$$\tau_t = A_1 C_p^2 + A_2 C_p + \tau_0 \tag{2.24}$$

where

τ_t is the relaxation time, s

C_p is the polymer concentration (%)

A_1 and A_2 are the empirical constants related salinity and hardness

τ_0 is the empirical constant related to temperature.

The relaxation time is used successfully in elongational dominated part of the UVM to predict the shear thickening. However, other extensional parameters such as maximum elongational viscosity and strain hardening index are obtained through core flood experiments.

Stavland et al. (2010) developed an extended viscoelastic model that could predict the four different viscosity regimes exhibited by viscoelastic polymers in porous media. These regimes are Newtonian, shear thinning, shear thickening and shear degradation. The model developed by Stavland et al. (2010) is given by the Eq. 2.25.

$$\eta_{app} = \eta_\infty + \left[(\eta_0 - \eta_\infty).(1 + \lambda_1\gamma)^n + (\lambda_2\gamma)^m\right]\left[1 + (\lambda_3\gamma)^x\right]^{j/x} \tag{2.25}$$

where

n_o is the zero shear viscosity, cP

n_∞ is the infinite shear viscosity, cP

n_{app} is the apparent viscosity, cP

λ_1 is the characteristic time determined from the shear rheology, s

n is the shear thinning index determined from the shear rheology

λ_2 is the relaxation time determined from the oscillatory rheology, s

m is the elongational exponent determined from the core flood data

x is the mechanical shear thinning exponent

λ_3 is the time constant determined through the effluent sample, s

γ is the shear rate, s^{-1}

j is the tuning parameter for accounting the degradation

Stavland's model also requires core flood experiments to predict the shear thickening regime and mechanical degradation behavior of polymer solutions

Wang et al. (2013) proposed a new method where effective viscosity is represented as the summation of shear and elastic viscosity (Eq. 2.26). The authors emphasize that their proposed model can account for the sweep efficiency.

$$\mu_{eff} = \mu_v + \mu_e = \mu_v + BD(\mu_v - \mu_w) \tag{2.26}$$

where

μ_{eff} is the effective viscosity, cP

B is the coefficient related to the pore structure

μ_v is the shear viscosity, cP

μ_e is the elastic viscosity, cP

μ_w is the water viscosity, cP

D is the dimensionless number, represented by Eq. 2.27

$$D = \frac{\theta_f \times V}{R} \tag{2.27}$$

where

θ_f is the relaxation time, s

V is the Darcy velocity, m/s

R is the pore radius, micron.

The viscoelastic models, available so far correlated the additional pressure drop caused by the shear thickening viscoelastic effects to the extensional viscosity empirically. This results in the requirement of core flooding experiments for the existing viscoelastic models to predict the shear thickening in porous media of synthetic polymers solution. Chemical EOR is an extensive and

complex process. Connate water salinity and the injection fluid's salinity usually differ and this could lead to the salinity variances in the reservoir. Depending on the oil viscosity, reservoir heterogeneity and capillarity, the chemical slugs would be designed. Accordingly, a different combination of surfactant, polymer, and alkali could be considered. Based on economics, the concentration of these slugs has to be chosen. Performing core flooding with respect to these many variables is a daunting task. Further, cores for representative reservoirs are not available in most of the cases, or obtaining the cores is an expensive process. An ideal rheological model is the one that can predict the polymer behavior in the porous media without core flood experiments.

Carreau model, (Carreau 1997) is represented by Eq.2.28.

$$\mu_{app} = \mu_{\infty} + \left(\mu_p^0 - \mu_{\infty}\right)\left[1 + \left(\lambda\gamma\right)^{\alpha}\right]^{(n-1)/\alpha} \tag{2.28}$$

Carreau model links the bulk shear properties to the porous media. Carreau model was successful in matching the viscous polymer's shear thinning behavior in porous media (Canella et al. 1988) through bulk shear rheological data (Figure 2.9).

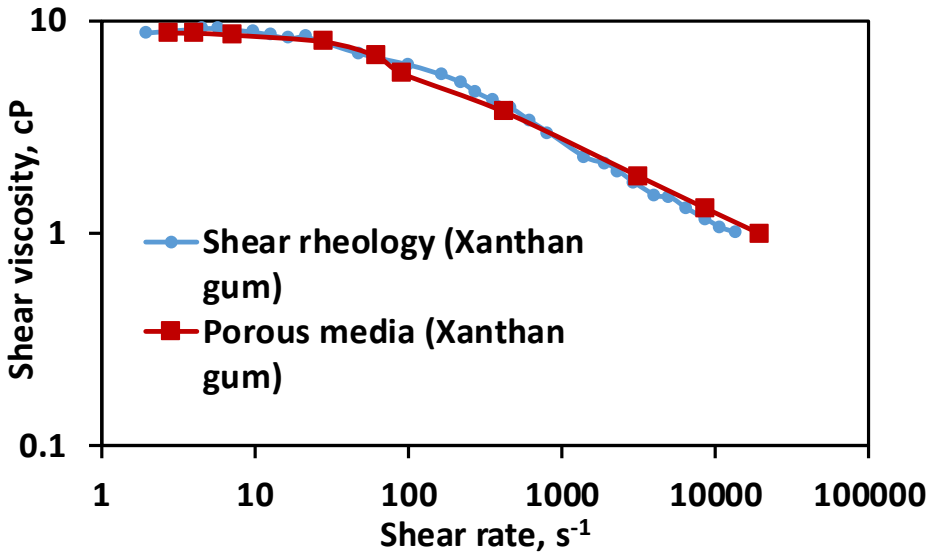

Figure 2.9: *Similar behavior shown by viscous xanthan gum in the shear field and in the porous media (Reproduced from Cannella et al. 1988)*

Shear thinning index (n) employed in the Carreau model scales the decrease of apparent viscosity with respect to shear rate fairly well. The shear based Carreau model was successful in predicting the behavior of purely viscous polymer solutions without core flood experiments (Canella et al.

1988; Seright et al. 2009). However, the Carreau model underpredicts the apparent viscosity of viscoelastic polymers by a significant margin (Delshad et al. 2008) (Figure 2.10). UVM model proposed by Delshad et al. (2008) relied on the core flood experiments to predict the apparent viscosity of viscoelastic polymers (Figure 2.10).

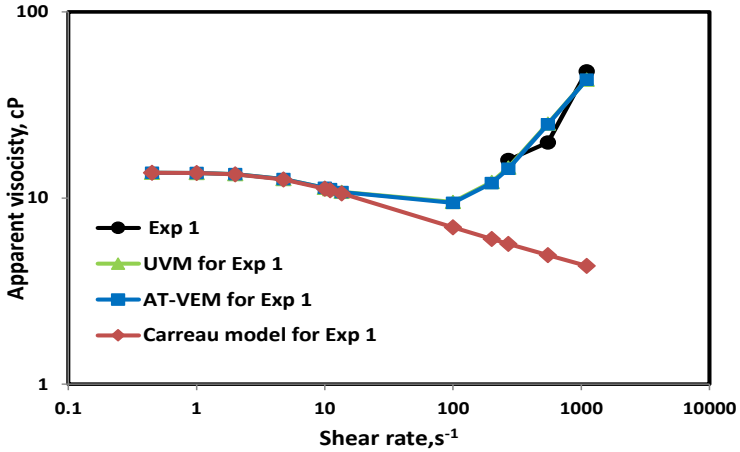

Figure 2.10: *Porous media behavior of viscoelastic EOR polymer predicted by the Carreau model, UVM and AT-VEM (Reproduced from Magbagbeolo 2008 & Azad and Trivedi 2019)*

Viscoelastic polymer solutions exhibit shear thickening phenomena after a critical onset rate in the porous media. Both viscous and viscoelastic polymer solutions exhibit thinning phenomenon in bulk shear field (Seright et al. 2009; Clarke et al. 2016). The viscoelastic polymer that thins in the shear field, thickens in the extensional field (James and Saringer 1980; Keller et al. 1987; Ferguson et al. 1990; Kennedy et al. 1995; Moreno et al. 1996; Barnes 2010; Sochi 2010; Azad and Trivedi 2017; Azad et al. 2018a; Azad et al. 2018 b). Strain hardening index is a parameter that quantifies the increase in the viscosity with respect to the strain. Strain hardening index is needed for modeling the shear thickening effects (Delshad et al. 2008). Direct measurement of strain hardening index may get rid of the core flood dependency. However, no significant efforts were made in this regard to develop a core flood independent viscoelastic model. One notable exception is the Azad Trivedi Viscoelastic Model (AT-VEM) (Eq. 2.29) developed using direct extensional rheological measurements (Azad and Trivedi 2018a; Azad and Trivedi 2019). AT-VEM can predict the apparent viscosity of viscoelastic polymers fairly well without core flood experiments (Figure 2.10).

$$\mu_{app} = \mu_{\infty} + \left(\mu_p^o - \mu_{\infty}\right)\left[1 + \left(\lambda * \gamma\right)^{\alpha}\right]^{\frac{(n-1)}{\alpha}} + \mu^{0.35}_{\max@De_{cr-0.66}}\left[1 - \exp\left(-\left(\beta * \tau_{ext} * \gamma\right)^{n_2 - 1.2 - 1}\right)\right] \quad (2.29)$$

where

μ_{∞} is the infinite shear viscosity, Pa.s

μ_p^o is the zero shear viscosity, Pa.s

λ is the shear characteristic time, s

γ is the shear rate, s^{-1}

α is the correction factor,

n is the shear thinning index

$\mu^{0.35}_{\max@De_{cr-0.66}}$ is the measured maximum elongational viscosity at the critical De, Pa.s

β is the universal constant, 0.01

τ_{ext} is the extensional relaxation time, s

n_2 is the measured strain hardening index.

2.5 Viscoelastic effects on S_{or} and N_c

N_c has been used for decades in EOR applications to relate the viscous/interfacial force balance to S_{or} reduction. To recover the trapped residual oil, the IFT between the oil and water has to be reduced by three orders by surfactant flooding. Polymer flooding, without interfacial activity was reported to cause additional S_{or} reduction, which is more than expected from the capillary number. Wang et al. (2001b) reported that flooding with viscoelastic fluid resulted in an increased displacement efficiency by more than 7% of OOIP over that of water flooding. The authors found that forces parallel to the oil-water interface are dominating over a perpendicular force that increased mobilization of residual oil. However, the N_c increase corresponding to the increase in displacement efficiency was only marginal (< 100). This contradicts the conventional belief that the N_c needs to increase by more than 1000 to mobilize the residual oil. Unless the N_c increases by more than 3 orders, the pressure gradient generated by EOR polymers with the viscosity of around 10-100 cP would not be sufficient to mobilize the trapped residual oil. Capillary pressure trapping the residual oil is around few thousands psi/ft (Stegemeier 1977; Peter 2002).

Xia et al. (2004) studied the rheological and displacement efficiency of viscoelastic HPAM and viscous glycerin. The studies are conducted using a glass model and artificial cores. The authors

concluded that HPAM (with higher normal stress) always results in higher recovery than glycerin at the same viscosity and N_c.

Wu et al. (2007) highlighted the limitation of N_c in explaining the different level of residual oil saturation reduction caused by viscoelastic polymer solutions having differing elasticity. They are represented by normal stress and polymer solutions with high normal stress corresponded to higher S_{or} reduction at the same N_c. The relationship that is well established between the N_c and residual oil recovery for Newtonian fluids fails for viscoelastic fluids (Wang et al. 2000).

Wang et al. (2007) also reported that the macro pressure gradient generated by the polymer solution cannot explain the drastic increase in displacement efficiency. The authors reported that the mobilization of residual oil occurs `at the low N_c. The authors observed the presence of a micro force causing oil mobilization in viscoelastic polymers. They attributed these micro forces, representing elasticity, as the reasons for the high displacement efficiency. The authors represent the elasticity through micro force. Micro force occurs when the residual oil blob obstructs the flow of driving fluid. This in turn results in the change of flow velocity in magnitude and direction. The magnitude of the resulting micro force is given by Eq. 2.30.

$$F = m\,{}^{dV}\!/_{t} \tag{2.30}$$

For Newtonian fluids, there is no micro force. The authors also reported that micro force will not affect the macro pressure gradient as the micro-forces acting on the certain region cancel each other out.

Xia et al. (2008) concluded the micro force as an additional driving force for oil mobilization. The authors used upper convected Maxwell in the flow equation. Micro-force that is bound to occur due to the localized velocity changes in the protruding portion of oil blob will not affect the macro pressure gradient. However, it should account for the micro pressure gradient which in turn might affect the N_c on a localized scale. The conventional belief N_c doesn't have an influence on the S_{or} needs to be reanalyzed on a localized scale. Any changes in localized velocity should be reflected as the changes in the stress or viscosity on the local scale. So the claims by the authors that the velocity changes are independent of viscosity need to be reassessed. Normal stress or extensional viscosity becomes dominant locally around the pore throat (Afsharpoor et al. 2010).

Huh and Pope (2008) studied the laboratorial and theoretical aspect of S_{or} in both secondary and tertiary mode. The authors claim the viscoelasticity of polymer solutions reduces S_{or} only in the

secondary mode of flooding. The authors claimed that the elasticity of polymer solutions delays the breakage of the oil column and therefore snap off is minimized. The interfacial tension between oil and polymer solutions results in the deformation of the interface which is resisted by the viscosity and elasticity of the polymer solutions. This results in a lower S_{or} for viscoelastic polymer flood than water flood. The authors explain this phenomenon through a pore scale model using stability analysis. The relation between the dimensionless growth rate of interface and other associated properties are given by Eq.2.31

$$G = \frac{\gamma \times \mu_p \times R}{\sigma} \tag{2.31}$$

where

G is the dimensionless growth rate

γ is the time constant for stability, s^{-1}

μ_p is the Maxwell model polymer viscosity, cP

R is the tube radius, m

σ is the interfacial tension, mN/m

From their studies, the authors interpreted that the high elasticity resists the growth rate of interface deformation. They proposed a pore scale model to explain one kind of S_{or} reduction through oil thread stabilization. Recently, Delamaide (2016) compared the recovery potential of polymer flood on the field scale during the primary, secondary and tertiary mode. Secondary polymer injection achieved higher recovery than the tertiary injection. However, the authors were unsure about the mechanism. Oil thread stabilization and snap off prevention might be the reason for higher recovery achieved in the secondary mode than the tertiary mode in agreement with the explanation by the Huh and Pope (2008).

Jiang et al. (2008**)** conducted core scale studies to understand the influence of viscoelasticity on S_{or} reduction and displacement efficiency. The deficiency of N_c was again highlighted. The authors varied the flux rate from 1.45 m/s to 2.68 m/s and observed that displacement efficiency increases by more than 10%. Since the shear viscosity of the polymer solutions decreases with rate, the increase in displacement efficiency cannot be explained by the conventional capillary theory. It is to be noted, that viscoelastic polymers that thin in the shear field, thicken after a critical rate in the porous media (Delshad et al. 2008; Azad et al. 2018 b) and in the extensional field (Barnes 2010;

Azad et al. 2018 b). Therefore, use of shear viscosity as the viscous force in the N_c calculation needs a reassessment.

Vermolen et al. (2014) reported that N_c calculated using the shear viscosity is lower than the N_c calculated using the apparent viscosity. At the same value of N_c, the authors observed that the polymer solution with high elasticity resulted in a higher displacement efficiency of light oil only.

Sochi (2009) developed a simulation code using Bautista-Manero model for describing the viscoelastic effects at the pore scale. The applicability of the model was tested using a sand pack and a Berea sand network. The authors identified the importance of extensional flow and converging-diverging geometry. However, the authors didn't attempt to explain the microscopic displacement potential of viscoelastic fluids using the developed model.

Chen et al. (2011) proposed Eq. 2.32 and Eq.2.33 that related S_{or} with first normal stress difference and N_c.

$$[S_{or} = S_{or}(N_1, N_c)] \tag{2.32}$$

where

N_1 is the normal stress difference, Pa

$$S_{or} = S_{or}^{h} + \frac{S_{or}^{w} - S_{or}^{h}}{1 + T_1 N_1 + T_2 N_{co}} \tag{2.33}$$

where

N_{co} is the capillary number for the oil

S_{or}^{w} is the residual oil saturation under water flood conditions

S_{or}^{h} is the residual oil saturation at ultra-high polymer elasticity and ultra high capillary number

T_1 and T_2 are the input parameters

N_1 and N_c are calculated using the Eq. 2.34 and 2.35

$$N_1 = C_{n1}(M_r).C_{pw} + C_{n2}(M_r).C_{PW}^2 \tag{2.34}$$

where

C_{pw} is the polymer concentration in the aqueous phase

$C_{n1}(M_r)$ and $C_{n2}(M_r)$ are the input parameter, depending on Mw

$$N_{cl} = \frac{K.grad\phi_l}{\sigma_{ll}} \tag{2.35}$$

where

N_{cl} is the capillary number

K is the permeability tensor

σ_{ll} is interfacial tension between the displaced and displacing phase

ϕ_l is the potential of displacing phase

The authors used the above elasticity model and history matched the oil recovery in the Daqing field. Since there any many fitting parameters involved in the model, it cannot be used to have a prediction about the polymer flood performance

Yin *et al.* (2012) used the Upper-Convected Maxwell equation to model viscoelastic polymer solution flowing in expansion, contraction, and expansion contraction channels. Their results showed that the viscoelasticity of polymer solution is proportional to the polymer velocity at pores. With the increase in elasticity, the solution velocity increases at the point where the diameter changes that causes the reduction in S_{or}.

Afsharpoor et al. (2012) performed computational fluid dynamics simulations of viscoelastic flow around the static oil droplets in the geometries representative of pore throat and concluded that the normal force of viscoelastic fluids becomes higher with increasing Deborah number. Normal stress results in a total imposed force, much higher than of the Newtonian fluid with the same viscosity. The authors also reported that the overall pressure drop for the viscoelastic fluids with higher Deborah number is lower than the pressure drop around the pore throat while for Newtonian fluids, the overall pressure drop is higher than the pressure drop around pore throat. The normal stress influences the residual oil recovery on the pore scale was the key conclusion.

Chen (2006) expressed the first normal stress difference as the function of concentration and molecular weight (Eq. 2.36).

$$N_{pl} = N_{pl}(C_p, M_r) \tag{2.36}$$

Where

N_{pi} is the first normal stress difference

C_p is the polymer concentration

M_r is the relative molecular weight

S_{or} is considered as the function of first normal stress difference and N_c (Eq. 2.37)

$$S_{or} = S_{or}^h + \frac{S_{or}^w - S_{or}^h}{1 + T_1 N_{pl} + T_2 N_c} \tag{2.37}$$

where

S_{or}^h is the residual oil saturation limit after polymer flooding with high elasticity and high N_c ideally

S_{or}^w is the residual oil saturation after water flooding

T_1 and T_2 are the parameters determined from the experiment data

Wang et al. (2013) proposed the model that accounted for the sweep (Eq.2.26). The authors also used the model to account for the displacement through the first normal stress difference. However, first normal stress difference is attained from the parameters used for the calculation of effective viscosity (apparent viscosity) that accounted for the sweep. Elongation rate can be calculated by Eq. 2.38.

$$\varepsilon = \frac{1}{2}\left(\frac{4n}{3n+1}\right)^{0.5} \gamma \left(\frac{2\mu_v}{\mu_e}\right)^{0.5} \tag{2.38}$$

where

n is the power law index

ε is the elongation rate, s^{-1}

The relationship between the elongation rate and first normal stress difference is given by Eq.2.39.

$$\tau_{22} - \tau_{11} = -\mu_e \varepsilon \tag{2.39}$$

where

τ_{11} is the normal stress in the x-direction

τ_{22} is the normal stress in the y-direction

Extensional viscosity is represented by Eq.2.40.

$$\mu_e = 2\gamma\theta_f \mu_v \tag{2.40}$$

Shear rate (γ) in Eq. 2.40 is represented by Eq. 2.41.

$$\gamma = \alpha \frac{4v}{\sqrt{k\phi}} \tag{2.41}$$

where

K is the permeability D

ϕ is the porosity

α is the function of pore size distribution

Upon substitution and rearrangement of Eq. 2.39 to 2.41, the first normal stress difference can be represented by Eq. 2.42.

$$\tau_{22} - \tau_{11} = -\mu_e \varepsilon = -\mu_e \cdot \frac{1}{2}\left(\frac{4n}{3n+1}\right)^{0.5} \gamma \left(\frac{2\mu_v}{\mu_e}\right)^{0.5} \tag{2.42}$$

The N_c is considered to have less contribution to residual oil saturation and can be neglected (Wang et al. 2000). Hence, Eq. 2.36 was represented, without N_c by the Eq. 2.43.

$$S_{or} = S_{or}^{h} + \frac{S_{or}^{w} - S_{or}^{h}}{1 + T_1 N_{pl}} \tag{2.43}$$

Limitation of this work is the shear dependence for calculating the extensional viscosity that is used for the calculation of normal stress difference. Determination of extensional viscosity empirically through shear parameters is not appropriate for oil recovery applications as the EOR polymers reported to behave similarly in a shear field behaved differently in an extensional field as well as in porous media (Garrouch and Gharbi 2006; Seright et al. 2011b; Azad et al. 2018a; Azad et al. 2018b). First normal stress difference depends on the rate and goes to zero at zero rate. Therefore, this would not allow the Eq.2.43 to predict the behavior reported by Xia et al. (2007).

Lotfollahi et al. (2016b) proposed a new mechanistic model for accounting the S_{or} through trapping number and Deborah number (Eqs. 2.44 to 2.47).

$$S_{or_1} = S_{or_1}^{high} + \frac{S_{or_1}^{low} - S_{or_1}^{high}}{1 + T_1 \times N_T} \tag{2.44}$$

where

S_{or_1} is the residual oil saturation from the capillary desaturation curve

S_{or_1} and S_{or_2} are residual oil saturations at low and high trapping numbers

T_1 is the model parameter.

N_T is the trapping number, defined by Eq.2.45

$$N_T = \frac{\left|\bar{\bar{k}} \bullet \nabla\phi + \bar{\bar{k}} \bullet \left[g(\rho_w - \rho_o)\nabla D\right]\right|}{\sigma_{ow}} \tag{2.45}$$

where

$\bar{\bar{k}}$ is the permeability tensor

g is the gravitational constant

$\nabla\phi$ is the potential gradient

$\rho_w - \rho_o$ is the density difference between water and oil

σ is the interfacial tension

∇D is the depth gradient

$$S_{or_2} = S_{or_2}^{high} + \frac{S_{or_2}^{low} - S_{or_2}^{high}}{1 + T_2 \times N_{De}} \tag{2.46}$$

where

S_{or_2} is the residual oil saturation from the viscoelastic desaturation curve

$S_{or_2}^{low}$ and $S_{or_2}^{high}$ are residual oil saturations at low and high Deborah numbers

T_2 is the model parameter

N_{De} is the Deborah number

$$S_{or} = \min\left(S_{or_1}, S_{or_2}\right) \tag{2.47}$$

The authors reported that mobilization occurs at a trapping number much lower than the critical trapping number. The authors attributed the S_{or} reduction through Deborah number. Trapping number is the generalization of N_c (Pope et al. 2000). This again highlights the limitation of N_c

Clarke et al. (2016) reported that HPAM 6040 recovered higher residual oil than HPAM 3130 at the flux rate of 1ft/day, despite the latter being characterized by the higher shear and apparent viscosity at the equivalent shear rate of $2s^{-1}$ (Figures 2.11 a- c).

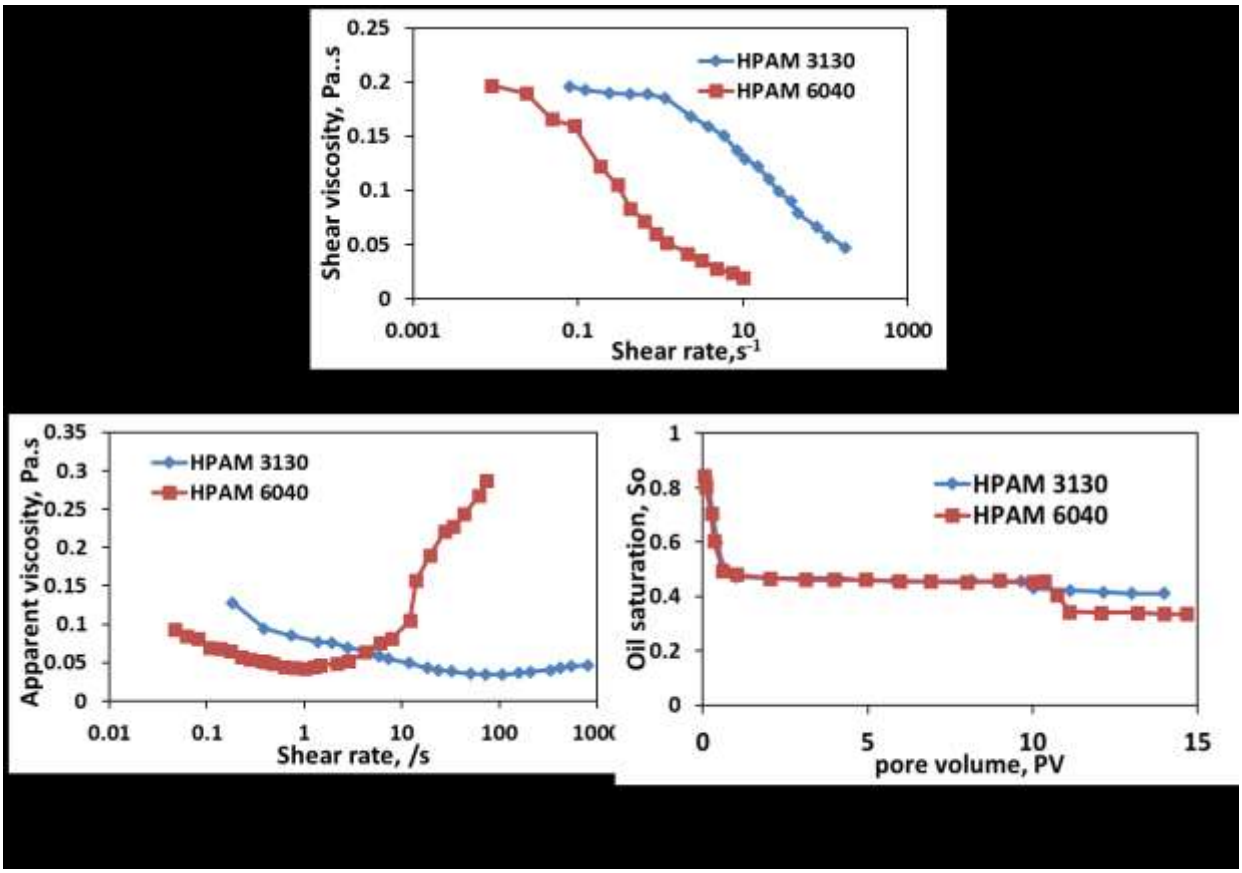

Figure 2.11: *a) The Shear rheological plot of HPAM 3130 and HPAM 6040 reproduced from Clarke et al. (2016) b) Apparent viscosity data for HPAM 3130 and HPAM 6040 reproduced from Clarke et al (2016) c) Oil Recovery plot of HPAM 3130 and HPAM 6040 reproduced from Clarke et al. (2016)*

Therefore, the authors concluded saying that the polymer's viscoelasticity can contribute to S_{or} reduction, more than expected from the apparent viscosity and shear viscosity. Clarke et al. (2016) discounted the role of extensional viscosity as the recovery mechanism based on the N_c calculated in psi/ft. They reported elastic turbulence as the cause for oil mobilization. As per the capillary theory, rapid oil mobilization begins to occur after the $N_{c,\,crit}$. However, in the case of viscoelastic polymers, rapid oil mobilization was reported to begin before the $N_{c,\,crit}$ (Lotfollahi et al. 2016b; Qi et al. 2017). This invalidates the capillary theory for viscoelastic polymers (Guo et al. 2014).

Qi et al. (2017) reported that viscoelastic HPAM causes an additional residual oil recovery than viscous glycerin, at the same N_c (Figure 2.12). All these suggest that the conventional N_c is not a proper method for correlating the polymer's viscoelastic effects with S_{or} reduction.

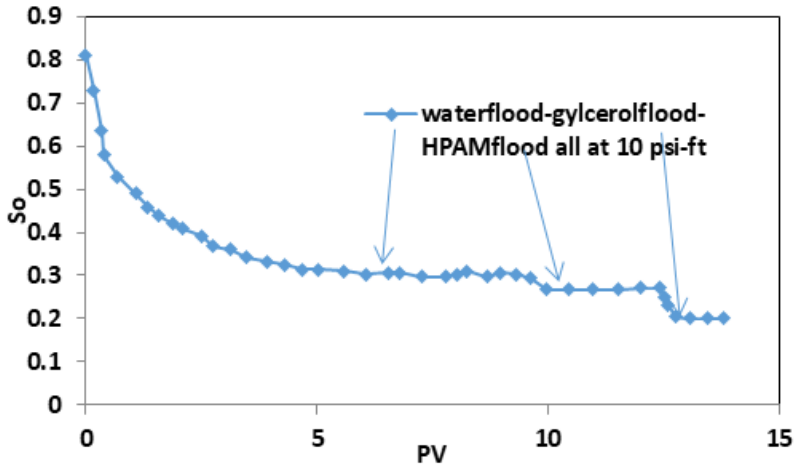

Figure 2.12: *Oil recovery plot showing the residual oil recovery potential of HPAM 3630 and Glycerin at the same core scale pressure and capillary number of 10^{-5} (reproduced from Qi et al. 2017).*

The authors developed a correlation between the oscillatory Deborah number and S_{or} (Eq. 2.6). Recently, Qi et al. (2018) simulated the viscoelastic polymer performance in the field. The authors pointed out the work of Ma and McClure (2017) to show that conventional shear thickening will not be observed in the reservoir conditions and therefore authors refrained from using core-scale viscoelastic models such as UVM model (Delshad et al. 2008) for predicting the S_{or} reduction. Extensive data sets to develop the correlation between the oscillatory Deborah number and S_{or} was used. The generated curve was referred as the elastic desaturation curve (EDC) which is similar to capillary desaturation curve. Two sets of correlations were developed based on the value of Deborah number (Eq. 48 and 49). The authors used the EDC curve in the UT-CHEM and predicted the additional 12% field-scale recovery for elastic polymer flooding over the inelastic polymer flooding. They reported that no differences in the recovery were seen between elastic and inelastic polymer flooding by using viscosity data alone. However, correlation developed by Qi et al. (2018) relied on the oscillatory Deborah number which has its own drawbacks. Moreover, proper laboratory test needed for upscaling the results from lab to field is lacking in the current literature.

For Deborah number less than 1,

$$\frac{S_{orp}}{S_{orw}} = 1 \tag{2.48}$$

For Deborah number greater than 1,

$$\frac{S_{orp}}{S_{orw}} = 1 - 0.133 * \log(D_e) \tag{2.49}$$

where

S_{orp} is the residual oil saturation to polymer flood

S_{orw} is the residual oil saturation to water flood

D_e is the Deborah number

2.5.1 Misconceptions in S_{or} quantification

Polymer flooding causes a significant S_{or} reduction to occur at flux of 1ft/day and at the values of N_c lesser than the critical N_c (Lotfollahi et al. 2016b; Qi et al. 2017). The experiments reported by Lotfollahi et al. (2016) were performed at the N_c of 10^{-7} which is less than the critical N_c. Qi et al. (2017) conducted the experiments at the N_c of 10^{-5} which is lower than the reported critical N_c of 10^{-4}. Vermolen et al. (2014) reported that during the experiment 2 and 4 conducted using highly elastic polymer solutions, oil mobilization begins to occur at the capillary number value of 10^{-6} which is less than the critical capillary number value of 10^{-5}. Research studies, till date, attributed it to the role of polymer's normal stresses to residual oil recovery (Wang et al. 2001a; Wang et al. 2001 b; Hueifen et al. 2004; Afsharpoor et al. 2012; Wang et al. 2013; Lotfollahi et al. 2016b). Generally, it is believed that normal stress or viscoelastic effects tend to occur only at the high shear rates (Figure 2.10). Therefore, it is expected that only at high fluxes viscoelastic effects influence the residual oil recovery. However, several studies have also showed that the viscoelastic polymer solutions can recover the residual oil at the flux of 1 ft/day (Ehrenfried 2013; Vermolen et al. 2014; Cottin et al. 2014; Koh et al. 2015; Clarke et al. 2016; Qi et al. 2017; Erinick et al. 2018). Clarke et al. (2016) reported that HPAM 3130 polymer solution resulted in the S_{or} reduction at the shear rate of around 2 s^{-1} (corresponding to the flux rate of 1ft/day) while the shear rate corresponding to the viscoelastic onset was around 100 s^{-1} (Figure 2.11 b, c). HPAM 6040 polymer solution corresponded to higher S_{or} reduction than HPAM 3130 at the shear rate of around 2 s^{-1}

(flux rate of 1ft/day), despite possessing the lower shear, apparent viscosity and N_c than HPAM 3130 (Figure 2.11 a, b, c). N_c calculated using the apparent viscosity for HPAM 3130 and HPAM 6040 are $9*10^{-5}$ and $7*10^{-5}$ respectively. The authors reported that HPAM 6040 possess more elastic turbulence than HPAM 3130. These results by Clarke et al. (2016) imply that viscoelastic effects in porous media can influence residual oil saturation at lower flux shear where shear viscosity or apparent viscosity doesn't show viscoelastic onset. Similarly, Qi et al. (2017) also reported that elastic HPAM 3630 with the N_c *of* $1*10^{-5}$ contributed to higher S_{or} reduction than viscous Glycerin with the N_c of $4*10^{-5}$ at the flux of ~1ft/day (Figure 2.12). The higher the elasticity, the higher the extensional viscosity (Azad and Trivedi 2017; Azad et al. 2018a; Azad et al. 2018b; Azad and Trivedi 2018a; Azad and Trivedi 2018b; Azad and Trivedi 2019) suggesting that extensional effects may have a role on the S_{or} reduction even at the flux of 1 ft/day. The mechanisms by which extensional effects contribute to S_{or} reduction at this flux can be understood by appreciating the dominance of extensional flow around the pore scale and by understanding the rheological difference between the shear thickening and strain hardening. Despite of these studies, quantification of S_{or} reduction due to viscoelastic effects has been an unresolved challenge. Investigating the S_{or} reduction potential of viscoelastic polymer at less than 1ft/day is necessary since the propagation rate is expected to be much lower far away from the wellbore, especially where inter-well distances are higher.

2.5.1.1 *Dominance of extensional flow at the pore scale*

Many researchers observed that there is an additional micro force associated with viscoelastic polymers that act on the pore scale and contributes to the S_{or} reduction (Xia et al. 2004; Wang et al. 2007; Jiang et al. 2008; Afsharpoor et al. 2012). Normal stress is a part of this micro-force (Wang et al. 2010; Afsharpoor et al et al. 2012). Shear viscosity is related to shear stress and extensional viscosity is directly related to normal stress (Eq.2.1 and Eq.2.2; Barnes 2010). At the pore scale, 75% of resistance is due to elongation (Durst et al. 1987). Sylvester and Rosen (1970) attributed 80% of the total entrance pressure drop exhibited by dilute polymer solutions in the cylindrical tube to the elastic forces. Chauveteau (1986) reported that elongational forces around the stagnation points are ten times stronger than the elongational forces experienced by the polymer solutions while flowing through the converging diverging section of the sand grains. Stretching occurs only when the polymer solutions characterized by the flexible coils are propagating in the constricted region between pore bodies and pore throat (Marshall and Metzener

1966; Marshall and Metzener 1967; Haas and Durst 1982; Maguer et al. 1983; Vorverk and Brunn 1991; Nyugen 1999). All these literature affirms the dominance of extensional flow at the pore scale.

2.5.1.2 *Early onset during the extensional flow*

The thickening shown by the polymer solutions during the bulk extensional flow can be called strain hardening or extensional thickening. Thickening shown by the polymer solutions during bulk shear flow or mixed core scale flow is called shear thickening. Ferguson et al. (1990) reported strain hardening occurring at a critical strain rate of around $200s^{-1}$ for 5 ppm concentration polyacrylamide (PAM) solutions in the extensional field (Figure 2.13a).

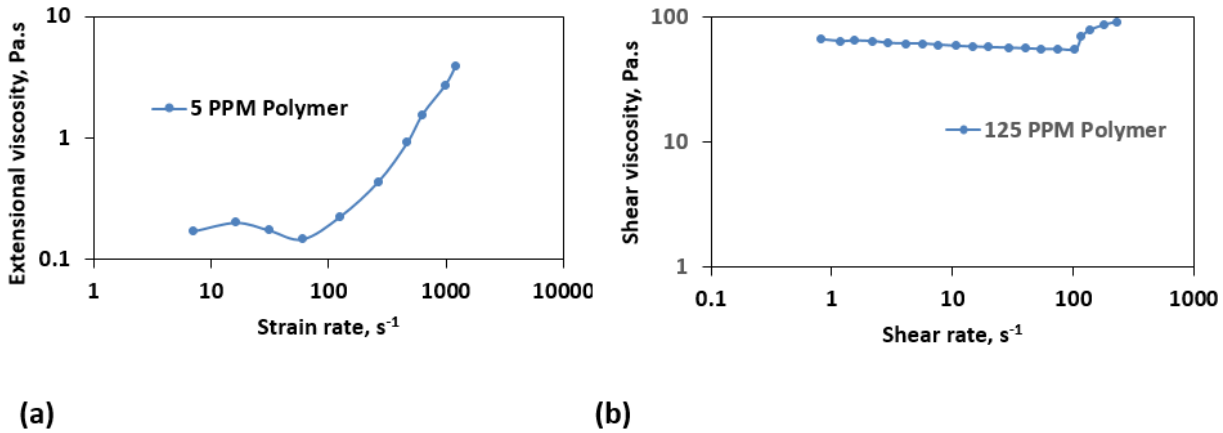

Figure 2.13: *a) Onset shown by 5 ppm polymer solutions in the extensional field (Reproduced from Ferguson et al. 1990) b) Onset shown by the 125 ppm solutions in the shear field (Reproduced from Ferguson et al. 1990)*

However, at a shear rate of $200s^{-1}$, the concentration needs to be 125 ppm for exhibiting shear thickening in a shear field (Figure 2.13b). Azad et al. (2018 b) reported that HPAM 2000 ppm begins to show thickening at a shear and strain rate of around $250s^{-1}$ and $1s^{-1}$ in the porous media and in the extensional field, respectively (Figure 6b and Figure 6c). The authors didn't observe any shear thickening in a shear field (Figure 6a). Kennedy et al. (1995) reported that the onset corresponds to a strain rate of $3s^{-1}$ in the extensional field for 0.75% and 1% concentration of associative polymer (Figure 2.14a).

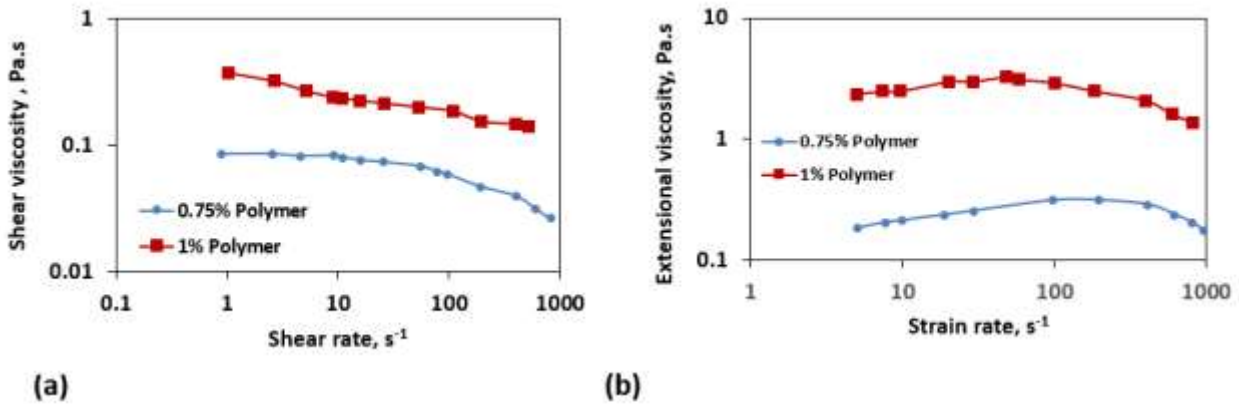

Figure 2.14: *a) Onset shown by 0.75% and 1% polymer solutions at the strain rate of 3s-1 in the extensional field (Reproduced from Kennedy et al. 1995) b) Complete thinning shown by the 0.75% and 1% polymer solutions in the shear field up to the shear rate of 1000s^{-1} (Reproduced from Kennedy et al. 1995)*

However, no thickening is shown by both polymers in the shear field even up to the shear rate of 1000s^{-1} (Figure 2.14b). Similar behavior is consistently reported in other documents (Jones and Walter 1989; Schunk and Scriven 1990; Barnes 2010; Sochi 2010). It can be summarized that the onset rate causing the thickening phenomenon is significantly lower in the extensional field, when compared to the core scale porous media and shear field. This implies that extensional flow itself is a strong flow even at low flux, while shear flow can be considered as a strong flow, only at high fluxes (Doshy and Dealy 1987). Therefore, low flux is sufficient to stretch the polymer chains to cause extensional thickening around the pore scale. This could be a possible reason for the higher residual oil recovery shown by the viscoelastic polymers at low rates (Xia et al. 2004; Wang et al. 2007; Clarke et al. 2016; Qi et al. 2017). It is be noted that, most of the chemical EOR researchers who have put forth their opinion that viscoelastic effects occur at high flux rate are based on the shear thickening concept observed on the core scale.

2.5.1.3 *Subsidence of extensional flow at the core scale*

Flew and Sellin (1993) reported that strain rate experienced by the polymer solutions during the converging flow around the pore scale is higher when compared to the strain rate experienced by the polymer solutions during the expansion flow around the diverging part. The strain rates vary around the pore scale. Wang et al. (2007) reported that the micro-force representative of viscoelastic effects gets nullified for viscoelastic polymers on the core scale and the pressure gradient is represented by the macro-force or the shear force. The stretching length of the polymer chain between the pore body and pore throat is of the order of a few microns (Maerker 1975).

Therefore on the core scale, shear force dominate (Zamani et al. 2015). Afsharpoor et al. (2012) reported that overall pressure drop exhibited by the viscoelastic polymer solutions is lower than the pressure drop exhibited around the pore throat. It is understood that extensional stresses which becomes dominant around the stagnation point/ converging part pores at a low rate will vanish, when fluids flow through expansion channels and pore bodies. Therefore core scale viscous force will be dominated by fluid's shear resistance, which causes the N_c of viscous polymers (with higher shear resistance) to be comparable with viscoelastic polymers despite the higher S_{or} reduction shown by the latter.

2.5.2 Possible extensional rheological role on S_{or} reduction

Residual oil recovery is a microscopic phenomenon and $N_{c,\ crit}$ that gives an estimate on the viscous force required to mobilize the trapped residual oil, is estimated based on the pore dimensions (Melrose and Brander 1974; Peter 2002). This implies that N_c needs to incorporate extensional rheological parameters, for accounting for the microscopic residual oil recovery that occurs on the pore scale.

Clarke et al. (2016) reported that the value of N_c that corresponds to the onset of rapid oil mobilization is significantly lower for viscoelastic HPAM 3630 than viscous xanthan gum (Figure 2.15b). Since the N_c was calculated using the core-scale pressure gradients (in psi/ft), the authors claimed that extensional viscosity is encompassed into the N_c. Authors also discounted extensional viscosity as the mechanism for additional S_{or} reduction shown by viscoelastic HPAM 3630. However, residual oil recovery is a pore-scale phenomenon and the critical N_c that gives an estimate on the driving viscous force required to mobilize the residual oil is calculated based on the pore-scale parameters (Melrose and Brander 1974; Peter 2002). Moreover, viscoelastic polymers show transient extensional/ normal stress resistance only at the pore-scale (Wang et al. 2007; Afsharpoor et al. 2012). Therefore, using the conventional N_c that is calculated based on the core-scale pressure measurements (in psi/ft) for representing the viscoelastic polymer's residual oil recovery potential may not be ideal. This could be the reason that N_c corresponding to the onset of rapid oil mobilization is significantly lower for viscoelastic HPAM 3630 than viscous xanthan gum. One of ways to rectify and represent CDC curve for polymer enhanced oil recovery processes can be by incorporating extensional viscosity in N_c calculation. Since the extensional viscosity is a better representative of polymer' elasticity (Azad and Trivedi 2017; Azad et al. 2018a; Azad et al. 2018b; Azad and Trivedi 2018a; Azad and Trivedi 2018b; Azad and Trivedi 2019), it is

expected that elastic HPAM 3630 may possess higher extensional viscosity than the purely viscous xanthan gum. Therefore, extensional \viscosity has a role on the residual oil recovery

Figure 2.15 reproduced from Qi et al. (2017) reveals that viscoelastic HPAM 3630 causes the higher residual oil recovery than viscous glycerin, despite possessing the similar core scale pressure, IFT, and N_c. The authors also reported that HPAM 3630 polymer contributed to residual oil recovery even before the critical N_c (0.0001). As per the capillary theory, residual oil mobilization will not occur until the capillary number exceeds the critical capillary number (Peter 2002). Therefore, the capillary theory is invalid for explaining the S_{or} reduction during viscoelastic polymer flooding with conventional N_c defination (Guo et al. 2014). Conventional N_c requires a modification to honor S_{or} reduction, if any.

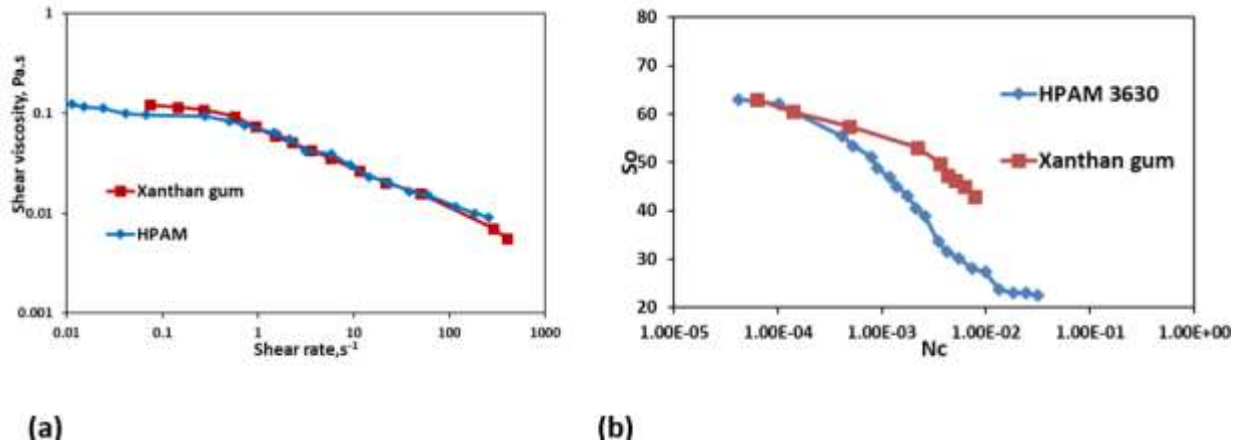

Figure 2.15: *a) Similar shear behavior between viscoelastic HPAM 3630 and viscous xanthan gum (Reproduced from Clarke et al. 2016) b) Capillary desaturation curve for HPAM 3630 and xanthan gum (Reproduced from Clarke et al. 2016)*

2.6 Numerical simulation of viscoelastic polymer flooding

The ability of a numerical simulator, with its current features to honor the viscoelastic polymer's microscopic displacement recovery and injectivity is analyzed by performing polymer flood simulation experiments. Two 1-D reservoir model discretized into 11*1*1 grid blocks with an injector and producer is used for simulating the performance of polymer flood carried out using two different polymers (HPAM 3130 and HPAM 6040) having different rheological behavior Two runs were made in each of the models at two different velocities. In the first two runs, the shear rate of $2s^{-1}$ is chosen to compare the S_{or} reduction potential of HPAM 3130 and HPAM 6040 at the typical low flux recovery conditions. In the last two runs, the high shear rate of 100 s^{-1} is chosen to investigate the viscoelastic effects on the injectivity. Different researchers have attributed

normal stresses, elastic turbulences, Deborah number as the mechanism for additional S_{or} reduction (Wang et al. 2007; Clarke et al. 2016; Qi et al. 2017). However, the existing numerical simulator doesn't have the features to incorporate these mechanisms. The simulator has the option to take the viscosity vs shear rate value. Masuda et al. (1992) and Delshad et al. (2008) explained the oil recovery is more than expected from the shear forces and explained through apparent viscosity data. The apparent viscosity data used by Clarke et al. (2016) are used as the rheological inputs in the model.

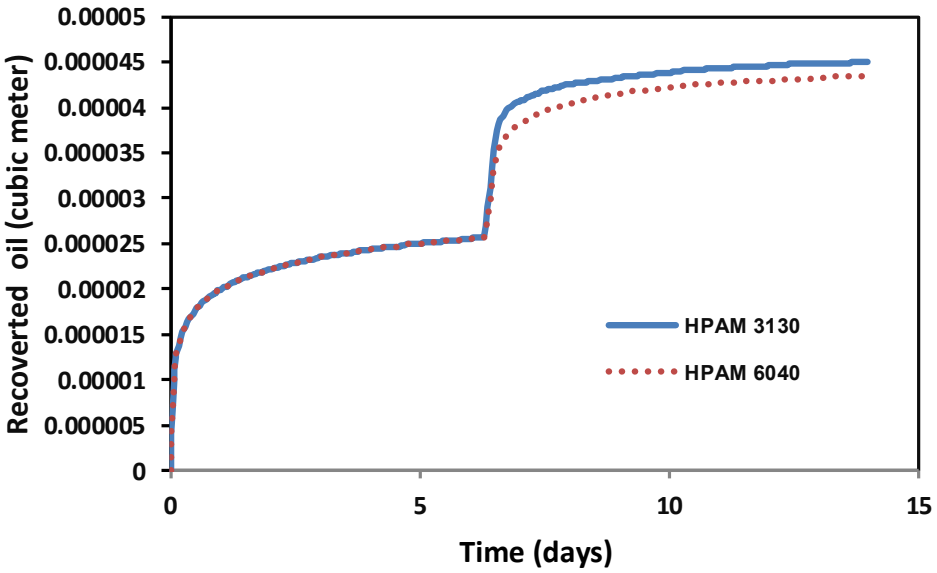

Figure 2.16: *a) Simulation of recovery potential of HPAM 3130 and 6040 at the shear rate of $2s^{-1}$ (using apparent viscosity data from Clark et al. (2016))*

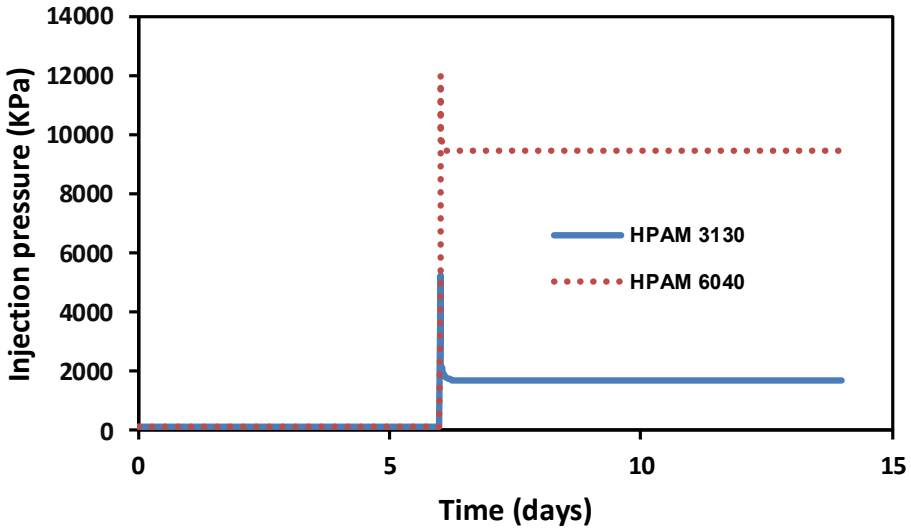

Figure 2.17: *Injection pressure of HPAM 3130 and 6040 at around the shear rate of 100s^{-1} (using the apparent viscosity Data from Clarke et al. (2016))*

Oil recovery predicted by the simulator is higher for HPAM 3130 (Figure 2.16) which contradicting the actual oil recovery, reported by Clarke et al. (2016). At the flood rate of 1ft/day, the actual oil recovery by HPAM 6040 is higher than HPAM 3130 despite the latter being characterized by high shear and high apparent viscosity (Clarke et al. 2016). Apparent viscosity is calculated on the core scale and the inadequacy of the existing simulator to honor the displacement recovery on the pore scale is evident. It is to be noted these core scale apparent viscosity data can be used for determining macroscopic properties such as sweep recovery (Wang et al. 2013; Azad and Trivedi 2018 b) but not the microscopic displacement efficiency. The core apparent viscosity data can also honor the injectivity decline caused by polymer's viscoelastic effects at higher shear rates (Figure 2.17).

Commercial simulators rely on the conventional N_c concept to predict the microscopic displacement recovery. Further, N_c has been conventionally used to study the residual oil recovery potential of chemical slugs from the reservoir (Stegemeier 1977; Green and willhite 1998). However, no efforts were made to modify the N_c to incorporate the elastic phenomenon.

2.7 Synopsis of the existing core-scale and pore-scale models

Among the existing viscoelastic models that can predict the core-scale apparent viscosity, viscoelastic onsets, and injectivity UVM (Delshad et al. 2008), Stavland's model (Stavland et al. 2010) and AT-VEM (Azad and Trivedi 2019) stands out. Other viscoelastic models showed an

indefinite increase in the apparent viscosity with respect to the flux rates. However, these three models a maximum extensional viscosity to negate the indefinite increase in the apparent viscosity with respect to the flux rates. UVM and Stavland's model can be only be used if the parameter from extensive core flood experiments are available whereas AT-VEM rely only on bulk ex-situ rheology measurements and not on core flood experiments. Both UVM and AT-VEM cannot honor the mechanical degradation regime. Stavland's model can be used if the mechanical degradation regime needs to be predicted.

Pore-scale viscoelastic models proposed by Lotfallahi et al. (2016), Qi et al. (2017), and Qi et al. (2018) predicted the residual oil mobilization at a flux of 1ft/day. The model by Lotfallahi et al. (2016) requires fitting parameters obtained by core flood experiments and hence one cannot use it to have a quick prediction of S_{or}. The correlations developed by Qi et al. (2017, 2018) are independent of core flooding experiments. However, both the models relied on the conventional oscillatory Deborah number, which has its own drawbacks. Employing them for saline polymer solutions may give an incorrect prediction of S_{or}. The simulation study conducted by Qi et al (2018) using UTCHEM showed that 12% additional oil can be recovered using the elastic polymer flooding when compared to the inelastic polymer flooding. However, both inelastic and elastic polymers were reported to exhibit the same oscillatory Deborah number (Garrouch and Gharbi 2006).

Most of the pore scale studies explain the S_{or} reduction phenomenon through normal stress (Wang et al. 2001a; Wang et al. 2001 b; Xia et al. 2004; Afsharpoor et al. 2012; Wang et al. 2013; Lotfallahi et al. 2016). Normal stress is related to the extensional viscosity (Barnes 2010) and therefore we strongly believe that extensional viscosity is the prime reason for S_{or} reduction. Adsorption (Zaitoun and Kohler 1987), elastic turbulence (Clarke et al. 2016) and wettability alteration (Seright 2017) are also considered as other mechanisms associated with additional S_{or} reduction

2.8 Recommendations

- Once the shear thickening viscoelastic polymer becomes fully stretched at high rates, it accumulates excessive stresses that result in the eventual mechanical breakup of the polymer chain resulting in the decrease of apparent viscosity with respect to shear rate. Using Deborah number calculated using the single relaxation time explain the shear

thickening effects but overlook the drop in the apparent viscosity caused by mechanical degradation. Using the relaxation time as a function of increasing/decreasing shear rates may enable the Deborah number to explain the mechanical degradation effects caused by excessive buildup of extensional stresses. Wilton and Thorabi (2013) expressed relaxation time as an increasing/decreasing function of shear rate and their approach could be expanded for explaining both shear thickening and mechanical degradation regime through Deborah number.

- Either the shear rate or the strain rate has been used by Polymer EOR researchers for residential time calculation to be used in Deborah number. Vast difference exists in the range of the Deborah number that corresponds to the viscoelastic onset and residual oil recovery because of not sticking with the particular rate. Qi et al. (2017) made a good attempt to unify the shear rate and strain rate calculations by combining their own data sets with Ehrenfried (2013) and Koh (2015).
- Garrouch and Gharbi (2006) reported that oscillatory relaxation time used for calculating Deborah number of xanthan gum and pusher-700 polymers was similar. However, in porous media, viscoelastic pusher-700 exhibited higher pressure drop and resistance factor over viscous xanthan gum. Polymer solutions flowing in the porous media are subjected to the elongational deformation. Therefore, comparison should be made between the extensional and oscillatory relaxation time of purely viscous and viscoelastic polymers. Using extensional relaxation time for calculating Deborah number can explain pressure drop and resistance factor of viscoelastic polymer in porous media.
- Garrouch and Gharbi (2006) calculated the Rouse relaxation time using the oscillatory rheology and claimed it to be the longest relaxation time for viscoelastic polymer. However, the extensional relaxation time is claimed to be higher than the oscillatory relaxation time for viscoelastic polymers (Clasen et al 2006). Measuring the extensional relaxation time on the viscoelastic polymers used by Garrouch and Gharbi (2006) may clarify this discrepancy.
- The steady shear and oscillatory shear behavior for HPAM and associative polymer were reported to be similar by Seright et al. (2011b). However, their flow behavior differed vastly in the porous media with associative polymer exhibiting higher resistance factor than HPAM (Seright et al. 2011b). Azad et al. (2018b) explained the higher pressure drop shown

by associative polymer over similar shear HPAM polymer using extensional rheology. Therefore, extensional rheological experiments are suggested to understand injectivity performance of HPAM and associative polymers.

- The shear based Carreau model was successful in predicting the behavior of purely viscous polymer solutions without core flood experiments (Canella et al. 1988). The viscoelastic models correlated the additional pressure drop caused by the shear thickening viscoelastic effects to the extensional viscosity empirically. This results in the requirement of core flooding experiments for the existing viscoelastic models to predict the shear thickening in porous media during the flow of synthetic polymers solutions**.** The viscoelastic polymer that thins in the shear field, thickens in the extensional field (James and Saringer 1980; Keller et al. 1987; Ferguson et al. 1990; Kennedy et al. 1995; Moreno et al. 1996; Barnes 2010; Sochi 2010; Azad and Trivedi 2017; Azad et al. 2018a; Azad et al. 2018 b). Direct measurement of strain hardening index may get rid of the core flood dependency. Recently developed AT-VEM uses strain hardening index measured from bulk ex-situ extensional rheology and has shown good predictability without parameters obtained from core flood experiments. (Azad and Trivedi 2018; Azad and Trivedi 2019).
- Clarke et al. (2016) reported that the value of N_c that corresponds to the onset of rapid oil mobilization is significantly lower for viscoelastic HPAM 3630 than viscous xanthan gum (Fig. 15b). Since the N_c was calculated using the core-scale pressure gradients (in psi/ft), the authors claimed that extensional viscosity is encompassed into the N_c. Authors also discounted extensional viscosity as the mechanism for additional S_{or} reduction shown by viscoelastic HPAM 3630. Measurements of the extensional viscosity of HPAM 3630 and Xanthan gum used by Clarke et al. (2016) may answer whether there is any extensional rheological influence on the S_{or} reduction or not.
- Ehrenfried (2013) and Erinick et al. (2018) reported that high salinity polymer solutions with lower Deborah number results in the higher residual oil recovery than the low salinity polymer solutions with high Deborah number. The authors claimed that viscoelasticity is not a factor for the additional recovery caused by high saline solutions. Magbagbeola (2008) reported that high saline viscoelastic polymer solutions and low saline viscoelastic polymer solutions possess oscillatory relaxation time of 0.035 s and 0.066 s, respectively. However, the strain hardening index for high saline polymer solutions and low saline

polymer solutions are 2.3 and 1.65, respectively suggesting higher extensional characteristics of the high salinity polymer solution. Therefore, the extensional rheological measurements are essential to obtain strain hardening index when dealing with saline polymer solutions

- Among the existing viscoelastic models that can predict the core-scale apparent viscosity, viscoelastic onsets, and injectivity UVM (Delshad et al. 2008), Stavland's model (Stavland et al. 2010) and AT-VEM (Azad and Trivedi 2019) stands out. UVM and Stavland's model can be only be used if the parameter from extensive core flood experiments are available whereas AT-VEM rely only on bulk ex-situ rheology measurements and not on core flood experiments. Both UVM and AT-VEM cannot honor the mechanical degradation regime. Stavland's model can be used if the mechanical degradation regime needs to be predicted.
- Models proposed by Lotfallahi et al. (2016), Qi et al. (2017), and Qi et al. (2018) can predict the residual oil mobilization at a flux of 1ft/day. Lotfallahi et al.'s model (2016) requires fitting parameters obtained by core flood experiments and hence one cannot use it to have a quick prediction of S_{or}. The correlations developed by Qi et al. (2017, 2018) are independent of core flooding experiments. However, both the models relied on the conventional oscillatory Deborah number, which has its own drawbacks. Employing these models for saline polymer solutions may give an incorrect prediction of S_{or}. A new correlation if developed using the extensional rheological parameters may provide better predictability for wide range of conditions.
- Qi et al. (2017) reported that viscoelastic HPAM 3630 causes the higher residual oil recovery than viscous glycerin, despite possessing the similar core scale pressure, IFT, and conventional N_c. Therefore, conventional definition of N_c needs a revisit. Since these polymers have different extensional viscosity, N_c for polymer flooding should include extensional viscosity term. They reported that HPAM 3630 polymer solutions contributed to residual oil recovery even before the critical N_c (0.0001). As per the capillary theory, residual oil mobilization will not occur until the capillary number exceeds the critical capillary number (Peter 2002). Therefore, the capillary theory is invalid for explaining the S_{or} reduction during viscoelastic polymer flooding with conventional N_c defination (Guo et al. 2014). Conventional N_c requires a modification to honor S_{or} reduction.

2.9 Conclusion

This review paper highlight the deficiency of the existing methodologies used for quantifying the viscoelastic effects exhibited by the EOR polymers. Three common methodologies are Deborah number, continuum viscoelastic models and pore scale models

1. Deborah number as such has been successfully used to represent the polymer's viscoelastic effect in the porous media. However for polymer flooding applications, one cannot use Deborah number for quantifying the viscoelastic effects because of the following deficiencies.
    a. Conventional Deborah number calculated using oscillatory relaxation time fails to explain the porous media behavior of the similar shear polymers. Two polymer solutions behaving similarly in the shear field were reported to behave differently in the extensional field.
    b. Conventional Deborah number fails to explain the higher S_{or} reduction shown by the highly saline viscoelastic polymer solutions over the lower saline polymer solutions. Highly saline polymer solutions were reported to exhibit higher strain hardening index, despite possessing a lower oscillatory relaxation time than the lower saline polymer solutions.
    c. Deborah number that is usually calculated with the single longest relaxation time will overlook the mechanical degradation effects.
    d. Another limitation of Deborah number usage is that, the residential time calculation is not universal. Authors invariably used both shear and strain rate for residential time calculation. However, Qi et al. (2017) made a good attempt to unify the shear rate and strain rate calculation and proposed the correlation between Deborah number and S_{or}.
2. Several continuum viscoelastic models were developed to predict the apparent viscosity, corresponding to the viscoelastic onset and shear thickening regime. UVM model that addresses the limitations of previous viscoelastic models relies on the core flooding experiments for modelling the shear thickening regime. Carreau model that can predict the viscous polymer porous media behavior, cannot be used to predict the shear thickening behavior of the viscoelastic polymers in the porous media. Both viscous and viscoelastic polymers were reported to exhibit shear thinning in ***a*** shear field. Viscoelastic polymers were reported to exhibit strain hardening behavior in the extensional field. Direct

measurements of the strain hardening index through bulk extensional rheometer may get rid of core flooding experiments.

3. All the pore scale models explain the S_{or} reduction phenomenon through normal stress.
    a. The claim that normal stress becomes dominant only at high shear rate needs to be reassessed. Elongational flow becomes dominant at the pore scale and the onset rate for strain hardening during extensional flow is reported to be much lower than the onset rate corresponding to the core scale flow. This could be the possible reason for higher S_{or} reduction shown by the viscoelastic polymers at low fluxes.
    b. Discounting the extensional rheological role on S_{or} reduction based on the N_c calculated in psi/ft need to be reassessed. The claim that viscoelastic polymer contributes to higher S_{or} reduction than viscous polymer at the same N_c need to be investigated. N_c calculated using the extensional viscosity might be differing for the viscous and viscoelastic polymers.
4. The simulation studies conducted using the apparent viscosity vs velocity data revealed that numerical simulators (CMG STARS used in this study) cannot honor the microscopic displacement. But the injectivity decline can be honored. Apparent viscosity and injectivity is a macroscopic property. Residual oil recovery is the microscopic property.

Chapter 3: Capillary Breakup Extensional Rheometry of Associative and HPAM Polymers for Oil Recovery Applications[2]

3.1 Introduction

Heavy oil reservoirs that cannot be developed by thermal enhanced oil recovery (EOR) methods are targeted using polymer flooding (Delamaide et al. 2014). To combat the high viscosity of the oil and to attain a favorable mobility ratio the polymers employed are usually high in molecular weight (MW), which could give higher viscosity to the displacing slugs. The polymer solutions that show complete shear thinning behavior in shear field exhibit shear thinning behavior in the porous media only up to the critical rate. Above the critical rate, a dilatant behavior is observed for the viscoelastic polymer in the porous media. This strain hardening behavior, also called as shear thickening, above critical flux rate causes increased apparent viscosity in porous media. Critical flux rate that characterizes the onset of shear thickening in porous media is lower for polymer solutions with high molecular weight and high concentration. Low salinity and low temperature also result in the early onset of shear thickening effects (Heemskerk et al. 1984; Clarke et al. 2016). Shear thickening can be attributed to the memory of polymer solution or extensional viscosity (Masuda et al. 1992; Delshad et al. 2008; Sheng 2010; Seright et al. 2011a). Purely viscous polymer solutions such as xanthan gum exhibit thinning phenomenon both in the shear field and in porous media (Seright et al. 2009). Viscoelastic polymers solutions thin in bulk shear field, thickens in the bulk extensional field (Barnes 2010) and in porous media (Jones 1980; Heemskerk et al. 1984; Masuda et al. 1992; Delshad et al. 2008; Seright et al. 2011a). As the flow rate increases, the dominance of extensional viscosity or extensional flow will increase over the shear (Taha 2010; Clarke et al. 2015). Extensional viscosity is the ratio of normal stress to the strain rate (Barnes 2010). Normal stress represents the viscoelastic effects in porous media better than the shear stress (Xia et al. 2007).

Among the high MW polymers, HPAM and its associative polymers that exhibited identical shear rheology behaved differently in porous media (Seright et al. 2011b). During rotational shearing, polymer molecules are rolled such that directional stresses are averaged out resulting in its cancellation (Zell et al. 2010). While traversing through the constricted pore throat region of the reservoir, the injected slug would generate extensional, viscoelastic stress that led to the difference

[2] A version of this chapter has been published in journal of applied polymer science

in their behavior. Several types of research were carried out to investigate the role of viscoelasticity on additional recovery during chemical flooding (Wang et al. 2000; Wang et al. 2001; Wang et al. 2007; Xia et al. 2007; Wang et al. 2010). It was concluded that viscoelasticity is an additional recovery mechanism that could mobilize some of the residual oil. Apart from its contribution to micro-displacement, viscoelasticity can provide stable sweep (Veerabhadrappa et al. 2013). However, viscoelasticity can also detrimentally cause the injectivity issues (Seright 2010; Sheng 2015; Lotfollahi et al. 2016a) that would result in the flood front delay, voidage problems.

Mobility control and conformance control are the two different phenomena that improve the sweep efficiency during polymer flooding. Mobility control process requires high injectivity and relatively lower viscosity from the displacing slugs sufficient enough to displace the oil without fingering through it. Conformance control process requires very high elastic properties from the displacing slugs so that the channeling of the injected slugs through high permeable streaks can be controlled. Thus while characterizing polymers for specific EOR applications, importance should be given to their viscoelastic properties. Prior characterization of the elongational properties of the polymers exhibiting identical shear behavior would help to screen them based on their elasticity.

Characterization of EOR polymer solutions in bulk shear field has been carried out using shear rheometer with ease and precision (Heemskerk et al. 1984; Cannella et al. 1988; Azad 2014; Clarke et al. 2015; Delshad et al. 2008; Seright et al. 2009; Urbissinova et al. 2010; Seright et al. 2011a; Han et al. 2012). However, bulk extensional characterization of EOR slugs remains the challenge. The challenges involved in the bulk extensional characterization of EOR polymer was reported in the chapter 2 and our publications (Azad and Trivedi 2017; Azad et al. 2018a; Azad et al. 2018b; Azad and Trivedi 2018a; Azad and Trivedi 2018b; Azad and Trivedi 2018c; Azad and Trivedi 2018d; Azad and Trivedi 2019). Capillary and breakup extensional rheometry (CaBER) and filament stretching extensional rheometry (FISER) were considered as the fastest, simplest, and efficient methods to determine the extensional elastic nature of polymer solutions (Bhardwaj et al. 2007b).CaBER and FISER methods can characterize the properties of the polymeric fluids in the uniaxial elongational flow. (Plog et al. 2004; Bhardwaj et al. 2007b; Anna and McKinley 2001; Clasen et al. 2006). Bhardwaj et al. (2007b) conducted CaBER and FISER experiments to study the effect of branching on the extensional rheology of wormlike micelles (WLM) solutions and revealed that the additional branching at higher concentration resulted in an additional stress relief mechanism, which was captured efficiently in extensional flows. It is understood that both CaBER

and FISER could characterize the extensional properties in the complex fluid. Similarly, it is essential to characterize polymers of different natures that exhibit similar shear behavior for EOR applications. However, FISER methods are not capable of characterizing polymer solutions possessing zero shear viscosity above 0.5 Pa.s (McKinley and Sridhar 2002; Clasen et al. 2006). CaBER on the other hand was reported to handle much low viscous fluid with zero shear viscosity between 0.002 Pa.s and 0.01 Pa.s. (Rodd et al. 2005). CaBER is used to characterize the extensional properties of EOR polymers.

HPAM and its associative polymer with similar MW were tested in shear and extensional fields, and the results were compared with their behavior in porous media to identify the suitable polymer for specific cEOR applications. The comparison was made between two polymers based on extensional properties such as extensional viscosity, extensional relaxation time that could classify the polymers based on the elasticity. In this chapter, the Deborah number of the polymers in porous media (De_p) was calculated using the residential time of the fluid in the pore and the relaxation time of the polymer samples. Relaxation time can be obtained by oscillatory rheology through storage modulus (G') and storage modulus (G") cross over point model. During the frequency sweep, G' and G" intersects at the certain frequency. The inverse of frequency at which G' and G" intersects had been used as the relaxation time (Delshad et al. 2008).Recently, specialized oscillatory V-E rheometer based on the oscillatory flow but with the capillary plug was used for characterizing the EOR polymers (Wilton and Thorabi 2013). Seright et al. (2011b) reported the inability of shear rheology to distinguish similar shear behavior polymers (HPAM and associative polymers) in the oscillatory field thereby resulting in the similar value of G' and G". However, the flow of polymer solution through porous media is both, shear and elongational (Delshad et al. 2008). The amount of deformation that the polymer molecules experience in the elongational field while undergoing the coil-stretch transition is much higher than the one in the relatively weak oscillatory field (Clasen et al. 2006). Relaxation attained using the extensional flow is higher than the one attained using oscillatory flow (Clasen et al. 2006). Extensional relaxation time can be the longest relaxation time. It can be used for polymer screening by distinguishing similar shear polymers differing in elasticity.

In this study, extensional relaxation time attained using the CaBER is used to calculate the Deborah number of HPAM and associative polymer. Deborah number is then used for correlating the bulk extensional performance of these two polymers in porous media along with other extensional

parameters. Investigating the role of extensional viscosity on the reduction of residual oil saturation in the porous media is not the scope of this study. However, the effect of elasticity on displacing fluid's propagation, oil recovery and pressure profile in porous media has been discussed using De_p and extensional viscosity.

3.2 Experimental methodology

3.2.1 Materials

3.2.1.1 Polymers used in this study

HPAM (FLOPAAM 3630) and its associative polymer (super pusher-C319) with similar MW and degree of hydrolysis (Perttamo 2013), but different hydrophobicity were used in this research. The polymers were provided by SNF Floerger. Table 3.1 lists their properties.

Table 3.1: Properties of the polymers used in this study

Name	Commercial Name	Molecular weight (MDa)	Hydrolysis degree (mol %)	Relative Hydrophobicity
HPAM 3630	FLOPAAM 3630S	16-20	25%	-
Associative polymer	Super pusher C- 319	16-20	25%	One hydrophobic content

Polymer solutions were prepared by dissolving the dry polymers in deionized water separately at a concentration of 2000 parts per million (ppm) using a magnetic stirrer.

3.2.1.2 Oil used in the study

Heavy oil with a viscosity of 0.540 Pa.s was used during both flooding experiments.

3.2.1.3 Porous nedia

Glass beads with a mesh size of ~40-80, which corresponds to the 354-177 microns were supplied by Potters industries and were used as sand for packing the core holder. Sands were packed uniformly with rubber vibrator in both experiments to ensure that pore volume; permeability and thus the residential time needed to calculate De_p were in the same range for comparison.

3.2.2 Characterization

3.2.2.1 Shear rheology

A BOHLIN CVOR rheometer was used to characterize the shear behavior of HPAM and its associative polymer. The cone and plate geometry is used. Samples were placed in a 150 microns gap between a rotating upper cone at a 4° angle with a diameter of 40 millimeters (mm) and a fixed

lower plate with a diameter of 60 mm. Shear rheology was carried out on the two polymers prepared at concentrations of 2000 ppm in deionized water at room temperature.

3.2.2.2 Extensional rheology

3.2.2.2.1 Extensional rheometer

HAAKE CaBER, a proprietary extensional rheometer from Thermo Scientific was used for characterizing the extensional properties with operating range of 0-80℃ and a Hencky strain of up to 10.

3.2.2.2.2 CaBER experimental procedure

A small quantity of each polymer sample was placed between two circular plates with diameters of 6 mm. The top plate was rapidly separated from the bottom plate, thereby forming a filament by imposing an instantaneous level of extensional strain on the fluid sample. A strike time of 50 milliseconds (ms) was given for the separation of plates. After stretching, the fluid was squeezed together by capillary force. A laser micrometer monitored the midpoint diameter of the thinning fluid filament as a function of time. The relevant extensional properties of the polymers were then quantified using appropriate equations. Table 3.2 report the operational parameters.

Table 3.2: *Test conditions during extensional rheology*

Parameters	**Values**
Temperature	Room temperature
Salinity	0 ppm
Concentration	2000 ppm
Initial gap distance	3 mm
Final gap distance	8.2 mm
Final aspect ratio	2.73

3.2.2.2.3 CaBER theory

The imposed step strain that stretches the droplet placed between the two plates results in the filament drainage that is governed by the balance between the driving capillary force and the resistive viscous and elastic force. Following the viscous dominated fluid drainage in the early phase, the intermediate time scale of viscoelastic fluids that have been reported to be governed by the balance between elasticity and surface tension is represented by the exponential decline in filament diameter (Entov and Hinch 1997). The upper convected Maxwell model accounting for elasticity is used to estimate the extensional relaxation time for two samples by regression. The solution to the upper convected Maxwell model is given in the Eq. (3.1). The linear data

representing the elastic region is extracted from the filament diameter versus time semi-logarithmic plot for the two polymer samples. The extracted data is then fitted with the solution to the upper convected Maxwell model in Eq. (3.1) using regression to match the exponential decline of fluid diameter. The extensional relaxation time is determined using the match. The value of 73 milli Newton/meter ($m\frac{N}{m}$) is used for the surface tension for both solutions.

$$D_{mid}(t) = D_o \left(\frac{GD_0}{4\sigma}\right)^{1/3} e^{\left(-t/3\lambda\right)} \quad (3.1)$$

where

$D_{mid}(t)$ – Midpoint diameter at time t, mm

D_o – Initial Diameter of the sample loaded, mm

G – Elastic Modulus, Pa

σ – Surface Tension of polymer samples, mN/m

λ – Relaxation time of polymer sample, s

The filament drainage in CaBER is driven by the capillary force and resisted by the viscous and elastic force. The axial force balance detailed in Anna and McKinley (2001), McKinley (2005) used recently by Kim et al. (2010) is given by Eq. (3.2):

$$\frac{2\sigma}{D_{mid}} = 3\tilde{\eta}_s\dot{\varepsilon} + (\tau_{zz} - \tau_{rr}) \quad (3.2)$$

where

$\tilde{\eta}_s$ is Solvent viscosity, Pa.s

τ_{zz} is First Normal stress, Pa

τ_{rr} is Second normal stress, Pa

$\dot{\varepsilon}$ is Strain rate, s^{-1}

The term $3\tilde{\eta}_s\dot{\varepsilon}$ represents the viscous, Newtonian stress. Multiplicative factor of 3 to the first term of right hand side in Eq. 3.2 implies the induction of extensional stress to the term as the Trouton's ratio for the Newtonian solvent is 3 (Renardy 1994). Non-Newtonian elastic stresses is represented by normal stress difference ($\tau_{zz} - \tau_{rr}$).

Both these terms suggest the existence of only elongational flow during filament drainage in CaBER experiment (Plog et al. 2004; Bhardwaj et al. (2007b); Anna and McKinley (2001), Clasen

et al. (2006). Capillary action is resisted only through the elongational stresses and viscosity calculated out of them represents the apparent extensional viscosity.

Hencky strain and strain rate were defined as per the standard analysis of Entov and Hinch (1997); Anna and McKinley (2001) of CaBER experiments by Eqs. (3.3 and 3.4):

$$\varepsilon(t) = 2\ln\left(\frac{D_o}{D_{mid}(t)}\right) \tag{3.3}$$

$$\dot{\varepsilon}(t) = -\frac{2}{D_{mid}(t)}\left(\frac{dD_{mid}(t)}{dt}\right) \tag{3.4}$$

where

ε – Hencky strain,

$\dot{\varepsilon}$ – Strain/Elongation rate, s^{-1}

Midpoint diameter data as such cannot provide any information relevant to EOR. It is essential to express the filament diameter data in terms of extensional viscosity. Extensional viscosity can be decoded from the filament diameter with time data by substituting Eq. (3.4) into Eq. (3.2) (Schummer and Tebel 1983; Anna and McKinley 2001). Upon substitution and rearrangement, apparent extensional viscosity ($\tilde{\eta}_{app}$) is represented by

$$\tilde{\eta}_{app}(e) = \left(-\frac{\sigma}{\frac{dD_{mid}}{dt}}\right) = 3\tilde{\eta}_s + \frac{(\tau_{zz}-\tau_{rr})}{\varepsilon} \tag{3.5}$$

where

$\tilde{\eta}_{app}(e)$ – Apparent extensional viscosity, Pa.s

The comprehensive analysis of extensional flow in the neck indicates that the apparent extensional viscosity incorporating non-zero tensile force is needed and the apparent extensional viscosity represented by Eq. (3.5) without correction factor is insufficient (Kim et al. 2010). Considering non-zero tensile stress in a force balance equation, the apparent extensional viscosity used by Kim et al. (2010) is represented by Eq. (3.6).

$$\tilde{\eta}_{app}(e) = -\frac{(2X-1)\sigma}{\frac{dD_{mid}}{dt}} \tag{3.6}$$

where

X- Axial correction factor.

The correction factor is required to account for the axial variation. The value of 0.7127 is assigned for the axial correction factor X in the CaBER experiment (McKinley and Tripathy 2000). The value of X depends on the local shape of the filament.

The extensional viscosity vs strain rate plot can be generated using the Eq. 3.4 and 3.6. During filament drainage, Entov and Hinch (1997) derived that fluid relaxes at the rate 2/3rd of the strain rate using finite extensible non linear elastic (FENE) theory. The details of the derivation can be found in Entov and Hinch (1997). Filament drainage is constant at the critical Deborah number of 0.66 and it represents the maximum elastic limit where the elongational viscosity tends to exhibit maxima (Clasen et al. 2010; Kim et al. 2010a). The maxima around the critical Deborah number will be used as the maximum extensional viscosity for comparing the polymers of different elasticity. During filament drainage, the fluids get strained that result in the increase of extensional viscosity with respect to strain, contrary to shear thinning that occur in the shear field. Strain can be calculated using the Eq. 3.3. Extensional viscosity vs strain around the critical Deborah number value is fitted with the power law to calculate the strain hardening index.

The dimensionless number that characterizes the inertial capillary breakup by relating material relaxation time (λ) and Rayleigh time scale (t_r) is called the intrinsic Deborah number. Since the strain rate during necking is self-selected and not externally controlled, it is called intrinsic (Rodd et al. 2005; Kim et al. 2010). The intrinsic Deborah number represented by Eq. (3.7) is calculated using the relaxation time and Rayleigh time scale defined in Eq. (3.8).

$$(De_{int}) = \frac{\lambda}{t_r} \tag{3.7}$$

$$t_r = \left(\frac{\rho * r_o^3}{\sigma}\right)^{\frac{1}{2}} \tag{3.8}$$

where

De_{int} – Intrinsic Deborah number, Dimensionless

t_r – Rayleigh time scale, Dimensionless

r_o – Initial midpoint radius of sathe mple, mm

ρ – Density of the solution, $\frac{kg}{m^3}$

3.2.3 Porous media studies

3.2.3.1 Core flood set up

A 6-inch long horizontal cylindrical core holder with a 1 ¼-inch diameter was used to carry out the flooding experiments. An ISCO syringe pump 500D was used to pump water to displace the oil and polymers upwards towards the core from the accumulators during oil saturation, polymer flooding, etc. The pressure was monitored using a pressure transducer. A graduated measuring cylinder was used for collecting the produced oil during flooding for every 0.25 pore volume (PV) injections. The schematic of the core flood set up is shown (Figure 3.1).

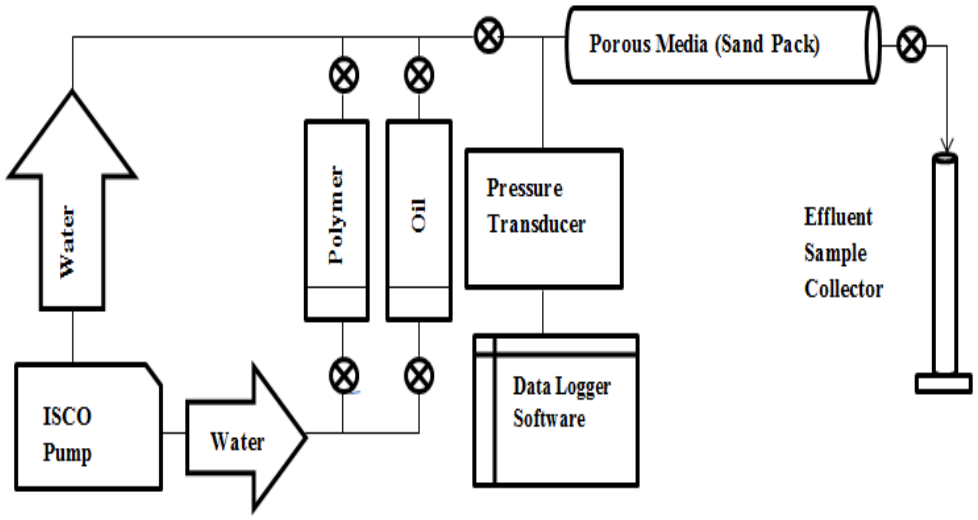

Figure 3.1: *Schematic of the core flood set up*

3.2.3.2 Core flood procedure

The performances of the associative polymers and HPAM in porous media were compared by two different flooding experiments under similar conditions. In both experiments, the cores were packed with glass beads of ~40-80 mesh size. The permeability and porosity of both cores were measured after water saturation. Initially, 2.5 PV of deionized water was injected into the oil-saturated cores during both experiments at a rate of 15 milliliter/hr. (ml/hr.). Then, 3 PV of polymer solutions (HPAM and associative polymer) at concentrations of 2000 ppm were injected into the water-flooded core at a rate of 15 ml/hr. Oil recovery for each 0.25 PV injections was recorded using the graduated cylinder along with the continuous pressure monitoring using pressure transducer. De_p was calculated from average grain diameter along with the extensional relaxation time attained from CaBER. The flow behavior of the two polymers in the porous media is

discussed based on De_p. 2.5 PV of chase water was injected in both the experiments and pressure profile was monitored. More than 10 PV of chase water was injected at different rates to determine the permeability reduction caused by the flooding of HPAM and associative polymer solutions.

3.3 Results and discussions

3.3.1 Shear rheology

Shear behavior of HPAM and its associative polymer solutions is shown (Figure 3.2).

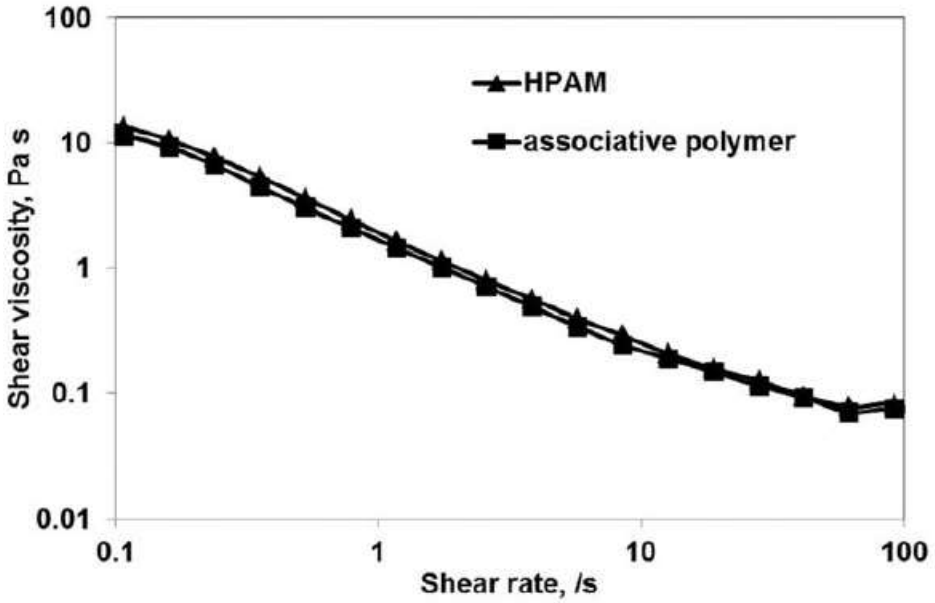

Figure 3.2: *Shear rheology of HPAM and associative polymer*

Both the polymer solutions exhibit shear thinning within the shear rate range studied here. The polymer molecules may roll while shearing, resulting in the cancellation of stresses. The inability of the rotational rheometer to distinguish these polymers in the shear field has been reported by Seright et al. (2011 b). However, those polymers behaved differently in the porous media (Seright et al. 2011b). Flow in the porous media is both shear and extensional (Delshad et al. 2008). Polymeric solutions that behave similarly in the bulk shear field were reported to behave differently in the bulk extensional field (Barnes 2010; Taha 2010). Since the polymer prepared using the deionized water showed similar shear behavior in this work, bulk extensional and porous media studies are also conducted using the same solutions. The saline water is not used because it will alter the similar shear behavior of these polymers. The prime focus of this study is to isolate the extensional influence from shear during the oil recovery process in porous media.

3.3.2 Extensional rheological results

3.3.2.1 Filament thinning images

The series of images captured by laser micrometer during the typical filament thinning of the viscoelastic polymer is presented (Figure 3.3).

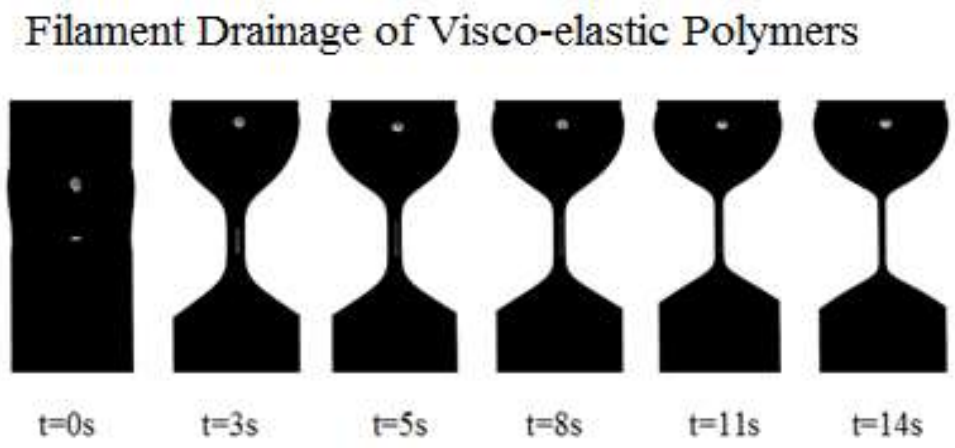

Figure 3.2: *Images representing filament thinning of the viscoelastic polymer during capillary drainage*

Viscoelastic samples that initially form the cylindrical column between the end plates undergo capillary thinning after stretching and tend to break due to driving capillary force. The capillary break up would be resisted by the viscous and elastic strength of the tested polymers.

3.3.2.2 Filament Diameter vs Time

The monitored mid-point filament diameter of the two polymer samples during filament thinning shown in the semi-logarithmic plot as a function of time is represented in Figure 3.4.

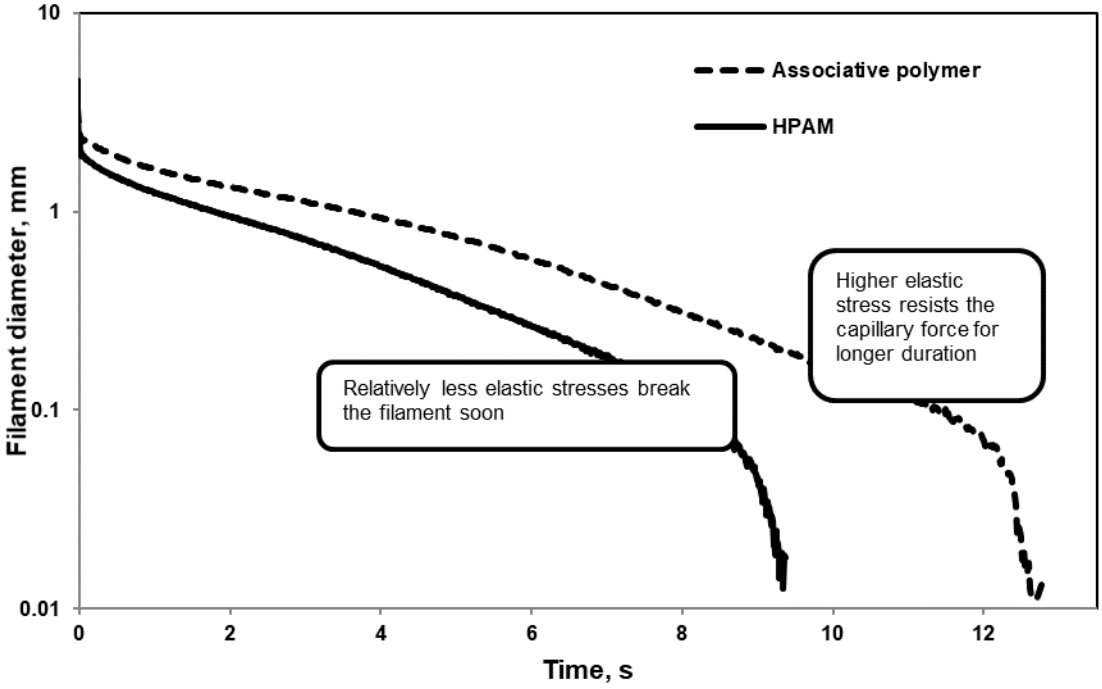

Figure 3.4: *Filament diameter as a function of time for HPAM and associative polymer*

The diameter of the associative polymer solution is higher than HPAM throughout drainage, indicating its higher resistance to counter the capillary breakup. The linear decline in the semi-logarithmic plot represents the intermediate time scale where the fluid drainage is balanced between the resistances offered by the polymer elasticity and driving surface tension (Entov and Hinch 1997). The higher diameter of the associative polymer solution characterized by hydrophobicity over HPAM throughout the linear decline is indicative of its higher elasticity. These linear decreases shown by two similar shear polymers have to be decoded to obtain more useful extensional properties that are discussed further.

3.3.2.3 Extensional relaxation time

The time required for the material to return to its original state after being perturbed is called relaxation time. The relaxation time attained while the samples undergo elongation is called extensional relaxation time. Between a diameter of 1 mm and the final breakup (Figure 3.4) during filament drainage, solutions of HPAM and its associative polymer show a linear decrease of the filament diameter in a semi-logarithmic plot. The filament that declines exponentially appears linear in a semi-logarithmic plot. These linear data were extracted for fitting with the upper convected Maxwell model to match the exponential decline of the fluid diameter as given in Eq.

(3.1). The extracted and fitted data for HPAM and associative polymer solutions are shown in Figure 3.5 and Figure 3.6. The slope and intercept of the fitted data are also shown in Figure 3.5 and Figure 3.6.

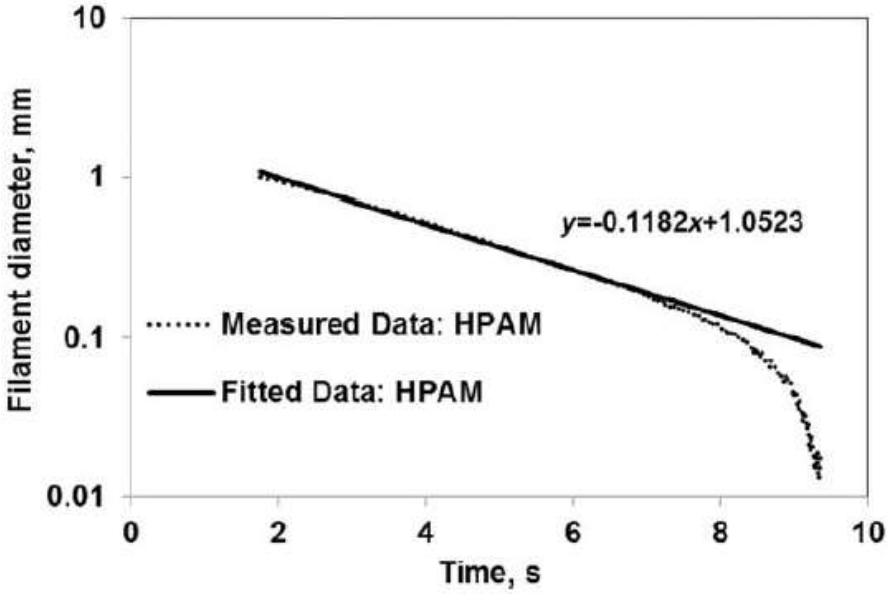

Figure 3.5: *Measured and fitted data from UCM model for HPAM*

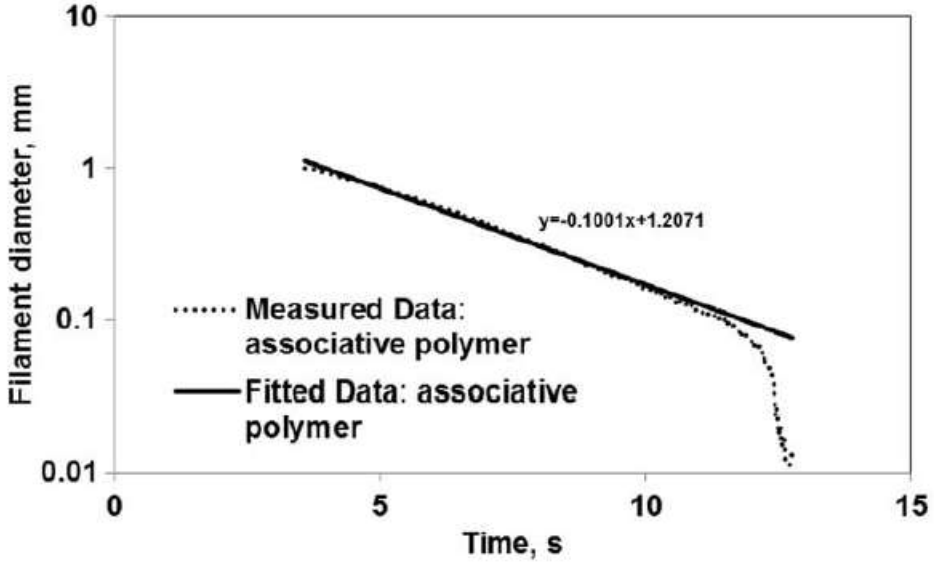

Figure 3.6: *Measured and fitted data from UCM model for associative polymer*

Elastic modulus can be calculated from the intercept using the initial diameter and surface tension. The slope represents the longest relaxation time (Plog et al. 2004; Rodd et al. 2005; Clasen et al. 2006; Bharadwaj et al. 2007b). The average value of the relaxation time is calculated using the Eq.

(3.1). The filament diameter vs time data is extracted from the semi-log plot. Natural logarithmic values are used for accounting the conversion from the semi-log to Cartesian. The calculated relaxation time and the experimental break up time for two polymer samples are summarized in Table 3.3.

Table 3.3: *Extensional relaxation time of HPAM and an associative polymer*

Sample	**Relaxation time (s)**	**Break up time (s)**
HPAM	1.02	9.36
Associative polymer	1.2	12.8

The associative polymer with the higher break up time could relax up to 1.2 seconds, indicating its dominant elastic nature over HPAM. HPAM could relax up to 1.02 seconds, indicating its relatively weaker resistance to break. Associative polymers were formed by adding a hydrophobic monomer to HPAM. The added hydrophobic monomer can promote intermolecular attraction (Bock et al. 1988). Thus, this substance possessing higher resistive strength would not let capillary action, driven by surface tension, to dominate and easily break the sample. This is an essential property for an EOR-displacing fluid that needs to provide stable displacement. Both polymers that exhibited similar shear behavior (Figure 3.2) exhibit different relaxation time, which is indicative of their different elasticity. Their elasticity could play a prominent role during oil recovery, which will be discussed later in the porous media section.

3.3.2.4 Extensional viscosity

Viscoelastic polymer solutions while flowing through tortuous porous media characterized by converging-diverging nature would exhibit both viscous and elastic nature. Polymer solutions flowing through such regions would be subjected to both elongation and shear. The relatively higher elastic polymers while getting elongated would generate higher extensional stresses (higher extensional viscosity) and higher resistance factor in porous media. In general, high resistance is expected from the displacing EOR fluid to enhance the sweep efficiency in conditions of adverse mobility ratio (Green and Willhite 1998). Usually a rotational rheometer is used to measure the shear viscosity of the EOR slugs. Shearing in the fixed volume results in the cancellation of stresses. Therefore, shear rheology cannot distinguish the behavior of polymers (Figure 3.2) with different elasticity represented by different relaxation times (Table 3.2). Also, it has been reported

that the shear viscosity of a polymer measured using a rotational rheometer is much lower than the apparent viscosity measured in porous media (Han et al. 2012). This implied the presence of usually ignored extensional flow in the reservoir and the need for extensional characterization.

3.3.2.4.1 Extensional viscosity vs Hencky strain

Hencky strain, also called true strain or logarithmic strain, corresponds to the final strain considering the strain path since beginning of deformation. During EOR, injected polymer molecules elongate and shear continuously as they travel from the injector to the producer. These molecules deform and may exhibit different ranges of viscosity while deforming with time. Thus, plotting the extensional viscosity of the polymer samples against Hencky strain can characterize the polymer's ability to retain its extensional properties while subjected to stresses and stretches in the reservoir. The extensional viscosity of HPAM and its associative polymer are measured with respect to strain using Eq. (3.3) and Eq. (3.5) by considering the filament diameter. The extensional viscosity against the generated strain for HPAM and its associative polymer solutions is shown (Figure 3.7).

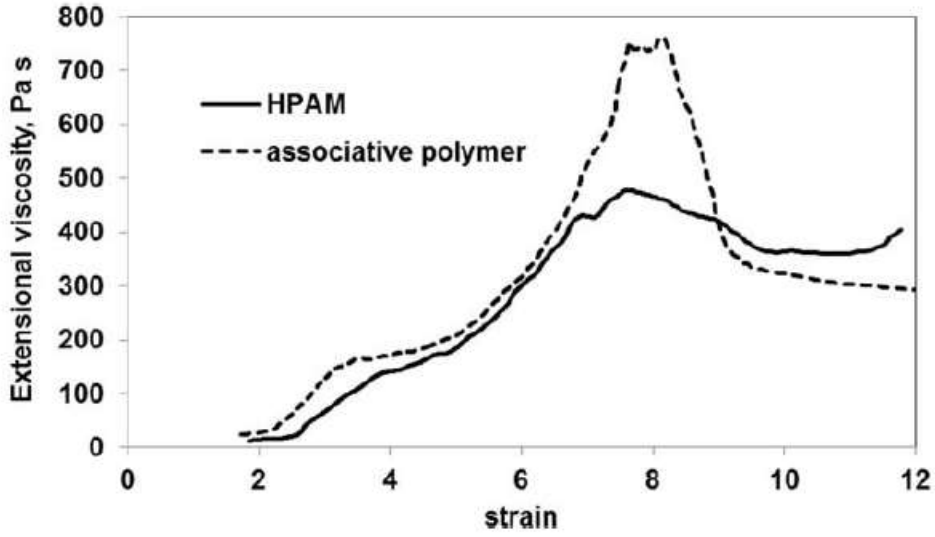

Figure 3.7: *Extensional viscosity as a function of generated Hencky strain for HPAM and associative polymer*

HPAM and its associative polymer solutions exhibit strain-hardening behavior in contrast to their pure thinning behavior seen in the shear field (Figure 3.2). This strain-hardening behavior for viscoelastic polymers have also been reported in previous studies (Yesilata et al. 2006; Bharadwaj et al. 2007b; Kim et al. 2010) and the thickening behavior can influence oil displacement efficiency

in the farthest part of the reservoir (Delshad et al. 2008). The associative polymer solution has shown higher strain-hardening behavior than HPAM. The maximum extensional viscosity for associative polymer was ~ 760 Pa.s before thinning sharply. This value was higher than the HPAM (Figure 3.7). The exhibition of maxima by associative polymer followed by thinning had been reported in the literature (Kennedy et al. 1995). It is an indicative of its higher elasticity and its susceptibility to degradation (Southwick and Manke 1988)

3.3.2.4.2 Extensional viscosity vs strain rate

General trend

The typical extensional viscosity vs strain rate plot determined from filament diameter data, using Eq. 3.4 and Eq.3.6 is shown in Figure 3.8. The behavior of extensional viscosity with respect to strain rate in the uniaxial extensional field is different than the conventional behavior seen in the shear field.

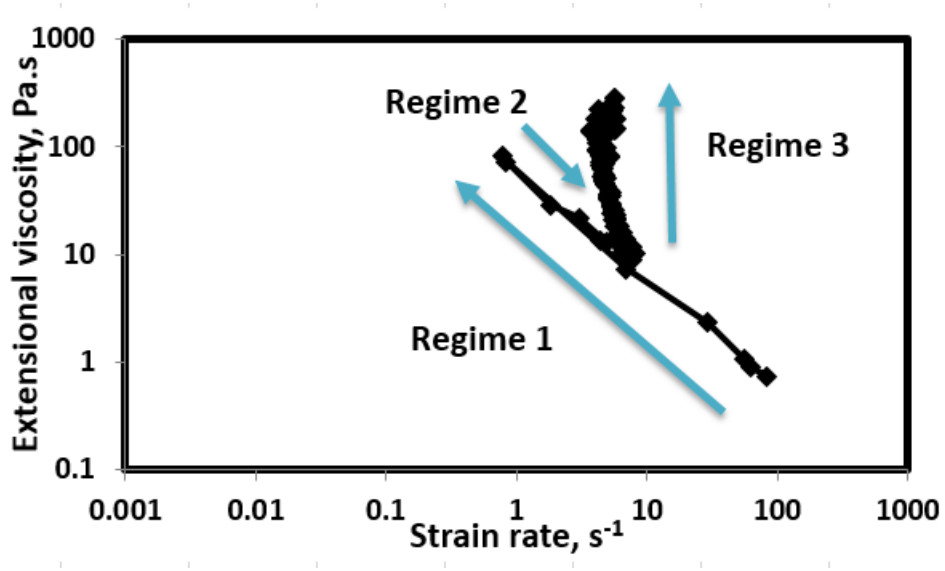

Figure 3.8: *The typical extensional viscosity vs the generated strain rate behavior during CaBER experiment*

Initially, the strain rate that is high; then it drops to the lower value and extensional viscosity increases (regime 1 in Figure 3.8). This increase in extensional viscosity accompanied by the drop in the strain rate is due to the gravitational sagging and doesn't represent any material function (Clasen 2010). In regime 2, the fluid begins to resist the capillary action by its viscosity. This regime is called visco-capillary balance where the viscosity drops and strain rate increases (regime 2 in Figure 3.8). Weak nature of viscous resistance is the reason that causes the strain rate to

increase due to high deformation (Anna and McKinley 2001). The strain rate increases until the elastic stresses of unraveling polymer chains develop to resist the deformation driven by the capillary action. Once polymer's elastic stress begins to resist the capillary action, the strain rate drops and approaches the constant critical Deborah number of 0.66 (Entov and Hinch 1997; Anna and McKinley 2001; Clasen et al. 2006; Bharadwaj et al. 2007a). The asymptotic drop in the strain rate to the critical Deborah number is accompanied by the sharp rise in the extensional viscosity (Kim et al. (2010a); Clasen 2010). Regime 3 in Figure 3.8 represents this phenomenon. The region around the critical Deborah number represents the elastic limit (Entov and Hinch 1997; Kim et al. 2010). The maximum elongational viscosity of polymer solutions around the critical Deborah number corresponded to its elastic limit (Clasen 2010). Using the extensional relaxation time, the critical strain rate corresponding to the critical Deborah number of 0.66 is determined by the simple division. The sharp increase in the elongational viscosities around the critical strain rate is seen in Figure 3.8. Maximum elongational viscosity that corresponds to the elastic limit around the critical Deborah number of 0.66 will be used as for representing the polymer's elasticity.

Extensional viscosity vs strain rate for HPAM 3630 and associative polymer

Strain rate defined as the rate of change of strain is represented by Eq. (3.4). Polymers are compared by plotting extensional viscosity with the attained strain rate using Eq. (3.4) and Eq. (3.5). The effects of strain rate generated by HPAM and its associative polymer solutions on extensional viscosity are shown in Figure 3.9.

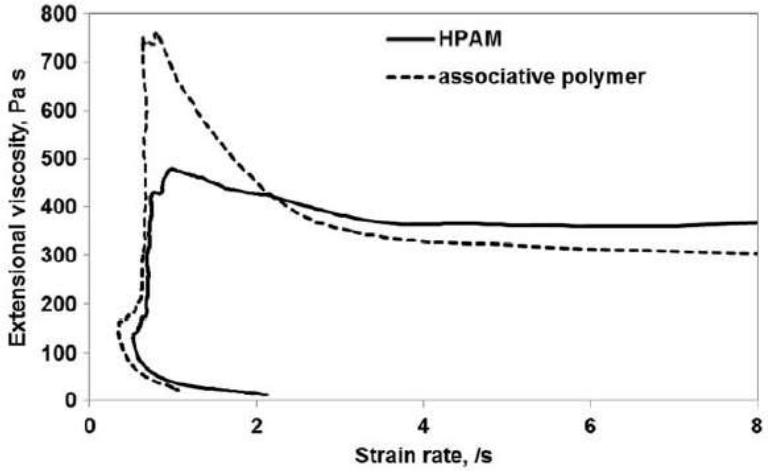

Figure 3.9: *Extensional viscosity as a function of generated strain rate for HPAM and an associative polymer*

Strain rate multiplied by relaxation time gives the non-dimensional strain rate in the form of a Deborah number (Kim et al. 2010). The drop in the strain rate and asymptotic rise shown by both polymers around the critical Deborah number of 0.66, which corresponds to the elastic limit (Entov and Hinch 1997), are indicative of their viscoelasticity (Anna and McKinley 2001; Kim et al. 2010). Extensional viscosity in this region represents the maximum elasticity. Around the critical Deborah number, the associative polymer and HPAM, with respective relaxation times of 1.2 seconds and 1.02 seconds, should deform at the rates of $0.55s^{-1}$ and $0.65s^{-1}$, respectively. The extensional viscosity of the associative polymer and HPAM solutions corresponding to these rates are ~760 Pa.s and ~470 Pa.s respectively (Figure 3.9). The higher extensional viscosity of the associative polymer characterized by bi-functionality is due to the relatively longer asymptotic rise of the dropping strain rate, which indicates its higher elasticity.

A comparatively strong strain loosening phenomenon is observed for associative polymer solution after its maximum elastic limit. This could be attributed to the predominance of mechanical disruption after the attainment of maximum elastic limit. The exhibition of maxima by associative polymer followed by thinning in the extensional field has also been reported earlier (Kennedy et al. 1995). HPAM on the other hand is less elastic and exhibited relatively weaker strain loosening behavior after maxima, indicating the possibility of HPAM undergoing mechanical deformation is lesser when compared with more elastic associative polymer solution at the studied concentration.

3.3.2.5 Intrinsic Deborah number

The variables needed to determine Rayleigh time scale is defined in Eq. (3.7). The densities of both samples were 1014.6 $\frac{kg}{m^3}$, and surface tensions of both samples were 73 m$\frac{N}{m}$. The initial midpoint radius during both experiments was 0.003 m. The intrinsic Deborah numbers of the two polymer samples were calculated using Eq. (3.6) and Eq. (3.7) by assigning the values of relaxation time from Table 3.3 and are reported in Table 3.4.

Table 3.4: *Intrinsic Deborah number of HPAM and associative polymer*

Sample	**Intrinsic Deborah number**
HPAM	53.68
Associative polymer	63.16

The intrinsic Deborah numbers corresponding associative polymer and HPAM are 63.16 and 58.68, respectively. The higher intrinsic Deborah number of the hydrophobic associative polymer

solution shows its higher elastic relaxation ability to the capillary action. It also indicates the potential to possess a higher Deborah number in porous media. The intrinsic Deborah number is another extensional parameter that distinguishes these two polymers.

3.3.3 Porous media studies

Two polymers that were identical in shear, but different in the extensional field were tested in porous media under the same conditions (i.e. by performing flooding experiments with the sand pack saturated with heavy oil to analyze its impact on oil recovery potential and pressure profile). Having uniformly packed the core with glass beads, the porosity and permeability of the core during both experiments were in the similar range. The porosity was 0.40 in both the experiments and permeability during the experiment carried out using the associative polymer and HPAM solutions were 1.55 Darcy and 1.56 Darcy respectively. The OOIP was 38 mL in both experiments. The recovery factors during 2.5 PV of water injection in both the experiments were ~ 32-34%.

3.3.3.1 HPAM vs Associative Polymer Flooding

Figure 3.10 depicts the incremental recovery factor during 3 PV injections of HPAM and its associative polymer after primary water flooding. The final incremental recovery during HPAM and associative polymer injection is 49.07% and 52.63%. Although, the recovery difference is only marginal, their pressure profile is quite different (Figure 3.11). This indicate that high elasticity doesn't result in the higher heavy oil recovery, which is consistent with the observation made by Seright (2018).

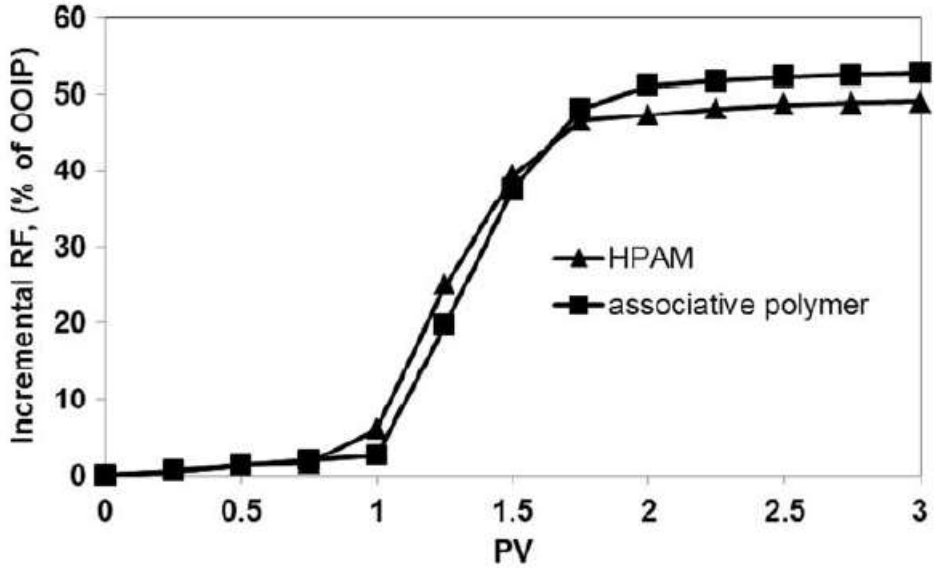

Figure 3.10: *Incremental recovery factor due to 3 pore volume injections of HPAM and associative polymer.*

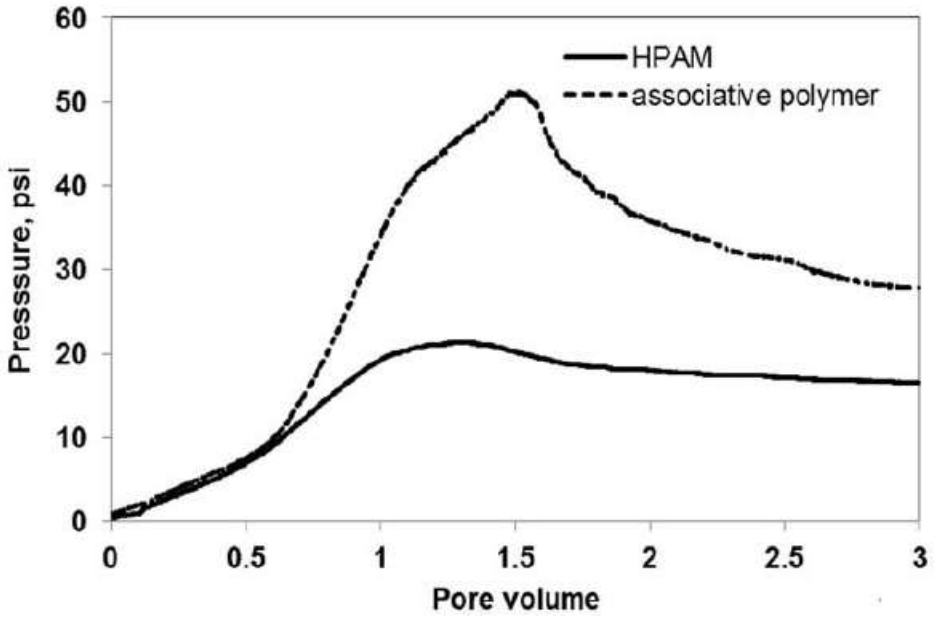

Figure 3.11: *Pressure behavior due to 3 pore volume injections of HPAM and associative polymer*.

Both HPAM and associative polymer exhibits similar pressure profile up to 0.7 PV after which significantly higher pressure drop was observed during injection of the associative polymer solution. This indicates the completely different in-situ rheology exhibited by these polymers while propagating through porous media. Similar shear rheology (Figure 3.2) exhibited by these polymers could not explain these in-situ differences because of their elongation flow in porous media. These differences are explained based on Deborah number in porous media (De_p) calculated using the extensional relaxation time in the following sections. Extensional viscosity at the critical Deborah number is also used for explaining the vast difference exhibited by these similar shear polymers in porous media.

3.3.3.2 Calculation of De_p

The Deborah number in porous media (De_p) is defined as the ratio between the fluid relaxation time and its residential time in the pore (Eq. 3.9).

$$De_p = \frac{\lambda}{t_p} \tag{3.9}$$

Extensional relaxation time (λ) is the fluid property that was estimated through extensional rheology as reported in Table 3.3. Residential time (t_p) during EOR in the reservoir depends on the pore structure, which dictates the time that injected slug would reside in the pores. The residential time is the inverse of the elongation rate (strain) rate (Hirasakhi and Pope 1974; Heemskerk et al. 1984; Haas and Durst 1982; Skartsis et al. 1992). Shear rates are also used for

calculation of residential time (Masuda et al. 1992; Koh 2015; Qi et al. 2017). Ehrenfried (2013) reported these discrepancies and suggested that Deborah number can be used for comparison purpose. Viscoelastic effects are more pronounced during elongation than shear. Therefore, in this work elongation rate is used for the calculation of residential time. A wide range of elongation rates could exist in the reservoir consisting of irregular grains (Heemskerk et al. 1984).The elongation rate is approximated by the first order approach (Maerker 1975) represented by Eq. (3.10).

$$\dot{\epsilon} = \frac{v}{D_p/_2} \tag{3.10}$$

where

$\dot{\epsilon}$ - Elongation rate, s^{-1}

v − Interstitial velocity, micron/s

D_p – Average grain diameter, micron

The average D_p of sand is 250 microns.

The elongation rate during both the polymer injection is calculated to be $0.13 s^{-1}$ and their inverse values (7.692 seconds) is the residential time. As the core properties and operational parameters, such as injection rate, are constant in both experiments, the residential time remains almost the same during both polymer flooding tests. Using the respective residential times and the relaxation time of two polymer samples as reported in Table 3.3, the Deborah numbers of those two polymer samples are calculated using Eq. (3.9). The calculated Deborah numbers in the pore (De_p) are tabulated in Table 3.5.

Table 3.5: *Deborah number of HPAM and associative polymer*

Sample	**Intrinsic Deborah number**
HPAM	0.132
Associative polymer	0.156

Typically, elastic effects become dominant in artificial porous media when the Deborah numbers are in the range of 0.1 and 10 (Heemskerk et al. 1984; Hestler et al. 1994). Vossoughi and Seyer (1974) found that increase in flow resistance, relative to Newtonian flow, during viscoelastic flows past cylinders in uniform arrays due to the onset of elastic effects occurred at critical Deborah number of 0.08, whereas Skartsis el al. (1992) reported the onset around De = 0.01. Heemskerk

et al. (1984) reported the onset of viscoelastic behavior to a Deborah Number of approximately 0.5. The experiments conducted by Stavland et al. (2010) suggested the onset around a Deborah Number of 0.2. In our experiments of polymer flooding, HPAM and its associative polymer correspond to Deborah numbers of 0.132 and 0.156, respectively.

3.3.3.3 Explanation of polymers behavior in porous media by De_p and other extensional parameters

It is seen from Figures 3.10 and 3.11 that both associative polymer and HPAM showed the similar recovery and pressure behavior up to 0.7 PV. However after that, the associative polymer exhibits a very high pressure drop before breakthrough. Early similar behavior could be due to the propagation of viscous front of hydrophobically modified associative polymer solution, which is comparable to water soluble polymers (HPAM) as reported by Dupuis et al. (2010) Consistent with the findings of Dupuis et al. (2010), Seright et al. (2011b) while studying the rheology of sulfonic associative polymer in porous media also concluded that associative polymer might contain the species that propagates at comparable rate to those for HPAM and another species that moves much slowly but creating a very higher resistance factor in porous media. Initial viscous front propagation was reported to generate lower differential pressure in the associative polymer (Klinke et al. 2016) and this explains the similarity in the early pressure profile and recovery of two polymers which is consistent with the similar shear rheology (Figure 3.2). Higher pressure drop exhibited by the associative polymer is due to the hydrophobic permeability impairment front (Klinke et al. 2016) that appeared to give the elastic (solid) component that in turn propagates very slowly. Recovery of associative polymer is marginally higher than HPAM especially in the later part of injection where the elastic component contributes to the front. Isolated role of elasticity on positive oil recovery had been reported (Urbissinova et al. 2010). Elasticity increases recovery due to both sweep (Veerabhadrappa et al. 2013) and displacement (Clarke et al. 2016). While 3 PV injections of HPAM results in the incremental recovery of 49%, associative polymer results in the incremental recovery of 52%. Wasmuth et al. (2012) observed similar behavior in the homogenous sand and reported that associative polymer resulted in the incremental recovery of 39% whereas HPAM with comparable shear viscosity resulted in the incremental recovery of 35%. Further, Wasmuth et al. (2012) reported that apparent viscosity of associative polymer was higher than HPAM despite their similar shear viscosity. The apparent viscosity of viscoelastic polymers in porous media is modelled by the combination of shear and extensional viscosity (Delshad et al.

2008). Higher apparent viscosity in porous media is due to the high elasticity that is modelled using the Deborah number and extensional viscosity (Delshad et al. 2008; Stavland et al. 2010). The associative polymer solution with a relaxation time of 1.2 seconds while residing in the pore corresponds to De_p of 0.156. HPAM with relaxation time of 1.02 seconds corresponds to the slightly lower value of Deborah number in porous media (De_p- 0.132). Break up time of associative polymer is also higher than HPAM (Table 3.3). Extensional viscosity of associative polymer is significantly higher than HPAM (by ~290 Pa.s) at their critical Deborah number as discussed. The presence of hydrophobic groups was reported to induce the higher extensional resistance in guar gum (Young et al. 1998).

Therefore, the pressure drop exhibited by HPAM injection through porous media was lower than its associative polymer. Maximum apparent viscosities exhibited by associative polymer and HPAM in porous media are 540 cP and 234 cP respectively. The difference in the maximum apparent viscosity between these two polymers is more than twice. However, both the polymer exhibits a similar shear viscosity of ~ 90 cP corresponding to the shear rate of ~40s^{-1}. HPAM relies on molecular weight to generate thickening viscosity whereas associative polymer characterized by the hydrophobicity generates additional resistance due to the combination of both molecular weight and intermolecular attraction (Klinke et al. 2013). Intermolecular attraction that becomes prominent in the extensional field where the polymer molecules become fully extended to induce increased interaction volume (Clasen et al. 2006) resulted in higher elastic resistance to the filament break up (Figure 3.4) during filament drainage as well as higher elastic extensional resistance to flow in porous media (Figure 3.11). Thus extensional rheology could clearly classify the similar shear polymers based on elasticity that exhibited a different viscoelastic pressure drop in porous media.

Although there is a difference in the recovery between these two viscoelastic polymers differing in elasticity, it is marginal but the pressure difference is very high. As per the definition of resistance factor (RF= $\frac{\mu_p k_w}{\mu_w k_p}$) , both permeability reduction (k_p) and viscosity augmentation (μ_p) of polymer can contribute to high pressure drop. k_w and μ_w represents the permeability and viscosity of water. A very high pressure drop exhibited by the associative polymer could be due to the high elastic resistance to flow as well as due to the permeability reduction. To analyze, 2.5 PV

of chase water is injected continuously in both the experiments and the monitored pressure profile is shown in the Figure 3.12.

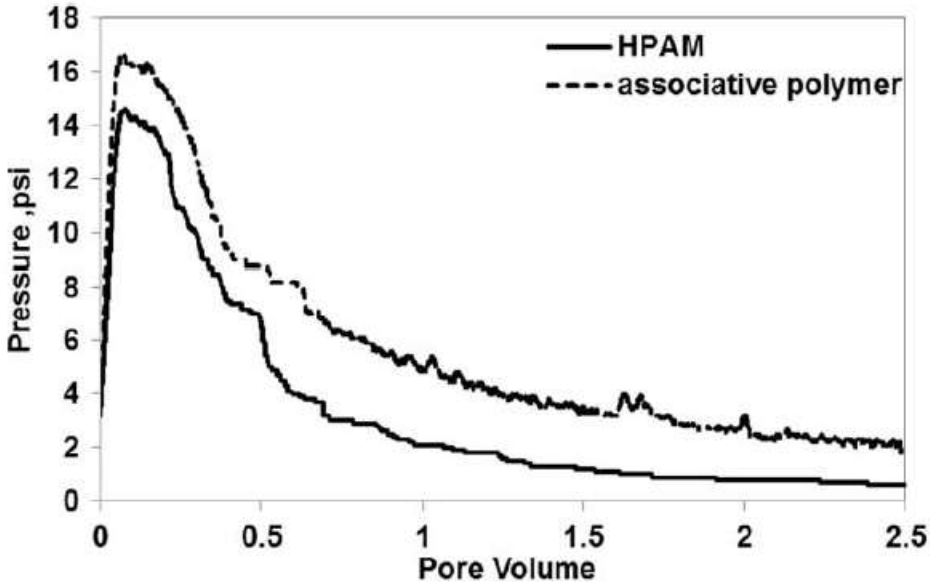

Figure 3.12: *Pressure behavior during chase water injections following HPAM and associative polymer flooding*

Based on it, it is clear that pressure drop due to the chase water injection following associative polymer flooding is higher than HPAM. But in both the cases, there is a continuous decrease with respect to the injection volume. Then at-least 10 PV of chase water is injected at different flow rates to measure the pressure drop. Figure 3.13 shows the measured pressure drop with respect to rate.

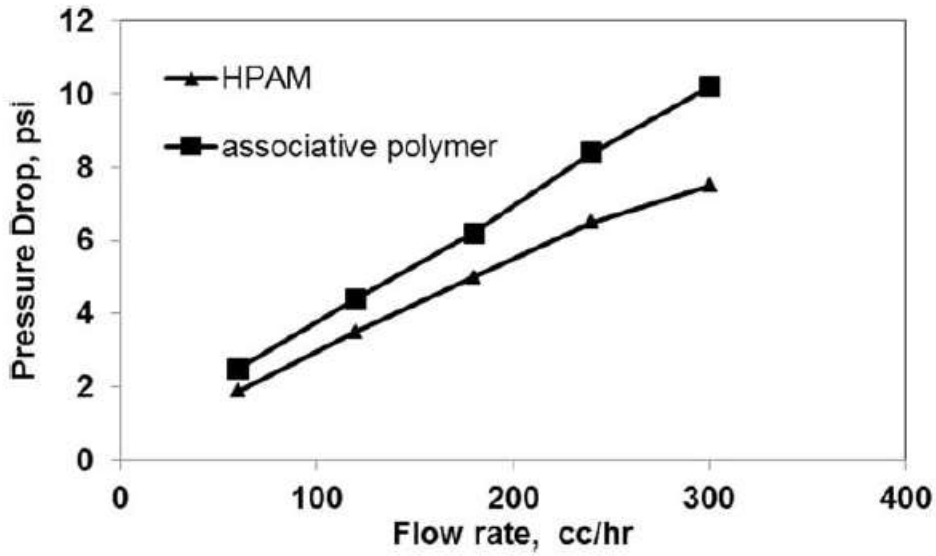

Figure 3.13: *Pressure drop exhibited by chase water at various flow rates*

Associative polymer exhibits a higher pressure drop than HPAM. This suggests that associative polymer might result in higher permeability reduction than HPAM. Multilayer adsorption could result in the higher permeability reduction for associative polymer than HPAM (Volpert et al. 1988; Taylor and Nasr-El-Din 1997). But Dupuis et al. (2010) reported that multilayer adsorption is not the sole reason and adsorption of minor polymeric species could be the reason for high permeability reduction with associative polymer. Klinke et al. (2016) attributed the permeability reduction in associative polymer to a combination of adsorption and reversible associative intermolecular network blocking the parts of pore structure. In accordance with Klinke et al. (2016), permeability reduction seemed to be due to the reversible associative intermolecular network in the associative polymer as seen from the drop in pressure in Figure 3.10. The permeability impairment component in associative polymer that causes the stronger intermolecular attraction results in the higher relaxation time (thus elasticity) in the extensional field and appeared to play the crucial role in higher permeability reduction in the porous media too. Besio et al. (1988) and Chauveteau et al. (2002) reported the role of extensional properties of polymer on permeability reduction. The polymers in extended form are likely to get adsorbed more than when being in the quiescent, coiled state due to a larger size (Besio et al. 1988). The polymer with higher extensional viscosity will be stretched more due to its high elastic limits. Associative polymer is characterized by much higher extensional viscosity and elastic limit (Figure 3.9). Therefore, the possibility of adsorption and permeability reduction with associative polymer is higher.

It can be concluded that higher apparent viscosity exhibited by associative polymer than HPAM in porous media is due to its elastic permeability impairment front that should have resulted in both the enhanced elastic resistance to flow and elasticity induced permeability reduction. The additional elasticity induced by the associative polymer with De_p of 0.156 and maximum elongational viscosity of 760 Pa.s resulted in the slightly higher recovery at the cost of higher permeability reduction and the possible injectivity issues. Considering the marginal oil recovery increment at the cost of injectivity issues, associative polymer may not be a preferred option for polymer flooding application in the homogeneous sand pack. HPAM with relatively lesser elastic limit and lesser permeability reduction but slightly reduced recovery could be a preferred option for mobility control applications where the injectivity is crucial.

3.4 Summary

- HPAM and associative polymers with similar MW, but different natures were investigated. A comprehensive study of the shear and extensional rheology of these solutions at room temperature were performed to understand their behavior in porous media.
- Core flooding experiments carried in this study revealed the significantly higher pressure drop of associative polymer over HPAM. Shear rheology measurements using cone and plate rheometer failed to explain this behavior as both polymers showed identical shear viscosity. The increase in pressure drop is likely due to the differences in extensional viscosity (Besio et al. 1988). This hypothesis was confirmed by transient extensional rheology measurements in uniaxial elongation flow using CABER. We have used CABER to measure the effect of hydrophobic association on extensional viscosity as a function of extension rate.
- Extensional rheological characterization performed with the CaBER system revealed the dominant elastic nature of associative polymer over HPAM. This includes larger midpoint diameters of associative polymer over HPAM while undergoing capillary drainage. The measurements of the mid-filament diameter as a function of time in the CaBER allowed direct determination of the dominant fluid relaxation time controlling chain stretching in the fluid, as well as the growth in the transient extensional stress in the filament due to the elongation of polymer chains.
- The extensional relaxation time calculated using the extracted midpoint diameter representing the elastic region and break time was higher for associative polymer. The

extensional relaxation time and breakup time of associative polymer solutions correspond to 1.2 and 12.8 seconds. For HPAM solutions, these values are 1.02 and 9.36 seconds. A higher relaxation time indicates the ability of the associative polymer to exhibit higher elasticity for the same residential time in porous media.

- The extensional viscosity of associative polymer (~760 Pa.s) was significantly higher than HPAM (~470 Pa.s) at the critical Deborah number of 0.66. The Deborah number in porous media calculated using the extensional relaxation time attained from CaBER and the residential time of the fluid in the pore for the associative polymer was 0.156 and that for HPAM was 0.132. It is to be noted that the difference in extensional viscosity at critical Deborah number between the two polymers is significantly higher than their differences in the Deborah number in porous media.
- Because of the significant differences in extensional viscosity, the pressure drop exhibited by the flow of lesser elastic HPAM solution through porous media was lower than the higher elastic associative polymer in the mid-stage of flooding when elastic impairment in the bifunctional associative polymer front begin to propagate. The maximum pressure exhibited by associative polymer and HPAM are ~51 and ~21 psi, respectively. However, the incremental oil recoveries caused by 3 PV injections of associative polymer and HPAM solutions are 52% and 49%. The difference in the incremental recovery between these two similar shear polymers in homogeneous sand pack is marginal which is consistent with the observation reported by Wasmuth et al (2012). This signifies that the extensional viscosity of associative polymer has a profound role on the pressure drop than on the oil recovery in the homogeneous sand pack.
- The results presented here signifies the limitation of preliminary polymer screening for different cEOR applications solely through conventional bulk shear rheology and need of extensional rheological characterization

Chapter 4: Understanding the flow behavior of Copolymer and Associative polymers in Porous Media Using Extensional Viscosity Characterization: Effect of Hydrophobic Association[3]

4.1 Introduction

The polymer solution injected during enhanced oil recovery (EOR) increases the sweep efficiency of the EOR process by reducing the mobility ratio (Green and Willhite 1998; Sheng 2015). Recently, heavy oil reservoirs are increasingly targeted with polymer flooding. Some examples include the Bohai field in China (Kang et al. 2001), Marmul field in Oman (Salim Al-Sadi et al. 2012), and Pelican Lake in Canada (Delamaide et al. 2014). High molecular weight (MW) polymer solutions are employed to control the adverse mobility effect in heavy oil reservoirs (Delamaide et al. 2014; Seright 2010; Wasmuth et al. 2012). High MW polymers solutions exhibit viscoelastic characteristics in porous media (Delshad et al. 2008). Viscoelasticity was reported to have a positive influence on oil recovery (Masuda et al. 1992; Delshad et al. 2008), and a negative influence on injectivity (Seright 2010). Injectivity is the measurement of the ease with which the fluid can be injected into the reservoir (Hynes 1991). The high pressure generated by the viscoelastic polymer solutions during EOR reduces the injectivity (Seright 1983; Zaitoun and Kohler 1987; Seright et al. 2009; Han et al. 2012; Glasbergeren et al. 2015; Sheng 2015) The generated pressure is much higher than predicted from the shear rheology (Hirasakhi and Pope 1984; Durst et al. 1987; Masuda et al. 1992; Delshad et al. 2008).

Partially hydrolyzed polyacrylamides (hereafter called HPAM) and hydrophobic associative polymers (hereafter called AP) are two commonly used high MW viscoelastic polymers for heavy oil recovery applications (Wassmuth et al. 2012). The difference between HPAM and AP is the presence of hydrophobic groups in AP making it bifunctional. HPAM and AP solutions were reported to behave similarly in the shear field but differently in the porous media (Seright et al. 2011b). However, the polymer solutions flowing in the porous media are subjected to both shear and elongational forces. Polymers that behaved similarly in the shear field may behave differently in the extensional field (Barnes 2010; Sochi 2010). Any two polymer solutions having similar viscosity but different elasticity will not be distinguished in the weak shear field that is applied in shear rheometers. It is important to understand the reported differences in the resistance factor

[3] A version of this chapter has been published in Canadian journal of chemical engineering

(RF) observed during flow through porous media of these two polymers, considering direct measurements in extensional fields.

Further, AP exhibits the typical behavior, with its RF higher than HPAM at low flux and lower than HPAM at high flux (McCormick and Johnson 1988; Bock et al. 1988; Taylor and Nasr-el-din 2007; Seright et al. 2011b). Previous studies have attributed the RF loss in AP to the transformation from intermolecular networks to intramolecular networks at high flux. Extensional rheology, if successfully applied to probe the structure and morphology of polymer systems (Silva et al. 2007; Ares et al. 2009; Silva et al. 2010; Andrade 2010) might provide better insights for understanding the typical porous media behavior of AP.

Retention and rheology are the two causes for higher injection pressure during polymer flooding (Green and Willhite 1998). Retention results in the permeability reduction. Besio et al. (1988) reported that the polymers in extended (stretched) form are likely to get adsorbed more than when being in the quiescent, coiled state due to a larger size. Further, for the same permeability, RF and residual resistance factor (RRF) increase for AP with the increase in the concentration (Xie et al. 2016). The authors attributed the increase in RF and RRF to the increased apparent viscosity caused by the intense association. Apparent viscosity is the combination of shear and extensional viscosity (Delshad et al. 2008). Han et al. (1995) attributed the viscoelastic extensional effects to the permeability reduction. It is vital to understand the link between the polymer's extensional limit and RF and RRF.

Conventionally, it is believed that at the concentration above critical association concentration (CAC), the viscosity of AP increases rapidly (McCormick and Johnson 1988). In the dilute regime, an intramolecular attraction in AP solutions exhibits similar or lesser shear viscosity than in HPAM polymer solutions (Schulz and Bock 1991; Taylor and Nasr-el-din 1997; Perttamo 2013; Viken et al. 2016). The intramolecular attraction that occurs within macromolecule, between the hydrophobic groups, contracts the polymer chains and reduces the viscosification power of AP below CAC (Wever et al. 2011). Above CAC, an intermolecular attraction in AP results in the higher shear viscosity than HPAM (Perttamo 2013). The polymer molecules that are in a coiled state in the shear flow will be in the stretched state in the elongational flow. Therefore, the frequency of intermolecular interaction and subsequent intermolecular hydrophobic attraction in AP solution might be different in extensional flow. The inter-chain interactions are stronger, more frequent, and intense in the stretched state during extensional flow than during the coiled state in

shear flow (Ferguson et al. 1990; Kennedy et al. 1995; Stolz et al. 2006; Clasen et al. 2006; Sharma et al. 2015). Because of the frequent inter-chain interactions, the onset of the semi-dilute regime may occur at lower concentrations in the dilute regime itself (Clasen et al. 2006). Above CAC, AP exhibits significantly high RF than HPAM. Polymer solutions are subjected to both shear and elongational flow in the porous media. Therefore, the RF of AP and HPAM in the porous media onset needs a comparative investigation, considering CAC in shear and extensional flow, and thereby, the effect of hydrophobic association onset. Similarly, the stronger the hydrophobic associations, the higher the RRF will be (Xie et al. 2015). Thus, considering the nature of hydrophobic association, the extensional role on permeability reduction by AP requires a comparative investigation with HPAM.

The Deborah number has been used to represent the viscoelastic effects in the porous media (Delshad et al. 2008). The Deborah number is defined a number as the ratio between the characteristic relaxation time of the material to its characteristic flow time (Macosko 1994; Barnes 2010). From an EOR perspective, the Deborah number can be defined as the ratio between the relaxation time of polymer slugs to its residential time in the porous media (Delshad et al. 2008). The inverse of frequency at which storage modulus and elastic modulus intersects is considered as the longest relaxation time. Recently, the cross over method is considered to be most efficient and quick method to determine the longest relaxation time (Volpert et al. 1988; Munoz et al. 2003; Castelleto et al. 2004; Delshad et al. 2008; Magbagbeolo 2008; Ehrenfried 2013; Koh 2015; Hincapie et al. 2015; Qi et al. 2017). Longest relaxation time determined by the cross-over method was reported to be with in the same range of rouse relaxation time (Qi et al. 2017). Wilton and Torabi (2013) recently used a specialized oscillatory V-E rheometer, based on the oscillatory flow, but with the capillary plug for characterizing the EOR polymers. Seright et al. (2011b) reported the inability of shear rheology to distinguish similar shear behavior polymers (HPAM and AP) in the oscillatory field, thereby resulting in the similar value of G' and G". However, the flow of polymer solution through porous media is both shear and elongational (Delshad et al. 2008). The amount of deformation that the polymer molecules experiences in the elongational field while undergoing the coil-stretch transition is much higher than the one in the relatively weak oscillatory field (Clasen et al. 2006). Relaxation attained using the extensional flow is higher than the one attained using oscillatory flow (Clasen et al. 2006). Extensional relaxation time can be the longest

relaxation time. Can the Deborah number calculated using the extensional relaxation time be used for the understanding the flow behavior of AP and HPAM in porous media?

In this work, we perform shear and extensional rheology of HPAM and AP (with similar MW) solutions at two different concentrations of 1000 ppm and 2000 ppm. Unlike shear rheology, extensional rheology is difficult to perform on the EOR displacing slugs characterized by a low viscosity in the range of 0.01 to 1 Pa.s. A capillary breakup extensional rheometer (CaBER), reported to handle lower viscosity fluid (Rodd et al. 2005), is used in this research. Porous media studies are also conducted at 1000 and 2000 ppm and RF and RRF are reported. The upper limit of 2000 ppm is chosen because AP solution in general is reported to exhibit higher shear viscosity than HPAM polymer solution above this concentration (Chang et al. 2007; Perttamo 2013; Viken 2016). The RF and RRF are used as the parameters for the comparison of two polymer solutions in porous media, and correlated with the shear and extensional rheology to ask a series of questions. Can we understand the type of hydrophobic association prevailing in the porous media using bulk rheology (shear and extensional)? Will the information about the critical association from the extensional rheological characterization be more useful for EOR applications? Can we explain the different flow behavior of AP and HPAM in the porous media using the direct measurements of the extensional rheology? Is there any link between the extensional viscosity and permeability reduction concerning the hydrophobic association? And, finally, can the Deborah number calculated using the extensional relaxation time be used for explaining the flow behavior of AP and HPAM in porous media?

4.2 Methodology

4.2.1 Materials

HPAM (FLOPAAM 3630) and AP (super pusher-C319) polymers are used in this study. They are characterized by similar MW and degree of hydrolysis but different natures (Perttamo 2013). Relative hydrophobic content is one in AP. Both polymers were provided by SNF Floerger. Their properties are shown in Table 4.1.

Table 4.1: *Properties of polymers used in this study*

Name	Commercial Name	Molecular weight (MDa)	Hydrolysis degree (mol%)	Relative hydrophobic content

HPAM	FLOPAAM 3630 s`	16-20	25	-
AP	Super pusher C-319	16-20	25	1

Polymer solutions were prepared by dissolving the dry polymers in deionized water separately at a concentration of 1000 ppm and 2000 ppm using a magnetic stirrer. The solutions were stirred until the polymers dissolved completely.

4.2.2 Rheological characterization

Shear rheology and extensional rheology are performed using the shear rheometer and CaBER. For more details about the shear rheometer, CaBER, CaBER operational procedure, CaBER theories please refer to section 3.2.2 in chapter 3. Also more details can be found in our publications (Azad and Trivedi 2017; Azad et al. 2018a; Azad et al. 2018b; Azad and Trivedi 2018a; Azad and Trivedi 2019).

4.2.3 Porous media studies

Glass beads with a mesh size of ~40-80, which corresponds to the 354-177 microns were supplied by Potters industries and were used as sand for packing the core holder. Sands were packed uniformly with rubber vibrator in both experiments to ensure that pore volume, permeability and thus the residential time needed to calculate De_p were in the same range for comparison. The permeability and porosity of the sand pack used in the four experiments are tabulated in Table 4.2.

Table 4.2: *Petrophysical properties of the sand pack used in the study*

Experiment (Polymer/Concentration)	Porosity	Permeability, Darcy
HPAM : 1000 ppm	0.398	1.554
AP: 1000 ppm	0.395	1.549
HPAM: 2000 ppm	0.398	1.554

AP: 2000 ppm	0.397	1.525

Flooding experiments are carried out using the 15.24 cm long horizontal cylindrical core holder with a 1 ¼-inch diameter. Polymer solutions were displaced upwards towards the core from the accumulators during polymer injection with the aid of ISCO syringe pump 500D. The pressure drop was monitored using a pressure transducer. A schematic of the core flood set up is shown (Figure 4.1). The packing was done with 140 g of sand using vibration. The uniformity of the packing was ensured, because the porosity and permeability values were very close in all the experiments. This also indicates that the wall channeling is not a critical factor in these experiments. The permeability for all four experiments were 1.534, 1,529, 1.534, and 1.506 μm^2 respectively (Table 4.2). The porosity values was 0.398, 0.395, 0.398, and 0.397, respectively (Table 4.2). The possibility of filter cake formation is less likely, because the polymer solutions are stirred enough to make sure that no residue remains in the solutions.

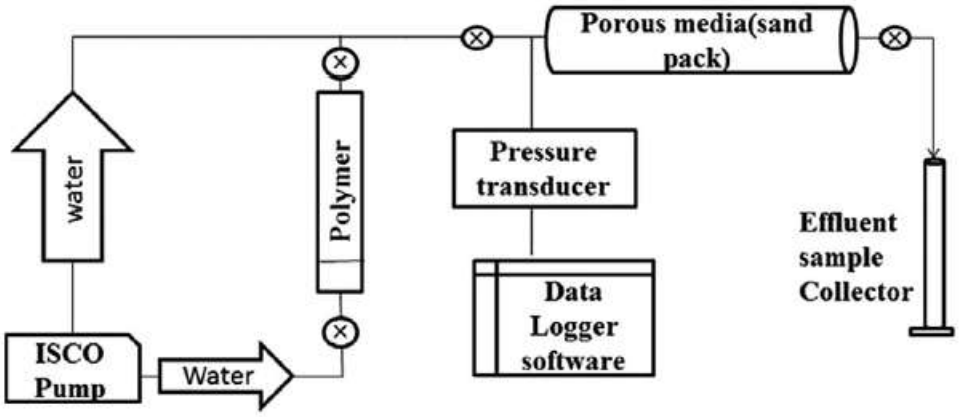

Figure 4.1: *Schematic of core flood set-up used for single phase studies*

Four different experiments were performed with AP and HPAM solutions of 1000 ppm and 2000 ppm concentrations. After water saturation and pore volume measurements, deionized water was injected into the sand pack at five different rates of 60cc/hr, 120 cc/hr, 180 cc/hr, 240 cc/hr and 300 cc/hr. The pressure drop ($dP_{primary\ water}$) which remained stable for 5 pore volumes was noted. Polymer solutions were injected into the sand pack at the same rates until the pressure remained stable($dP_{polymer}$) for another 5 pore volume. The stable pressure attained during

polymer injection was used for calculating RF. Following the polymer injection, the chase water injection was started at 60cc/hr and the pressure was noted to be higher and the chase water injection continued for another 5 pore volumes until the pressure decreases and attained the stabilized value. The rate was then increased and stable pressure drops for 5 pore volumes were noted. These stable pressure drops are used for RRF calculation.

4.2.3.1 Resistance factor (RF)

The RF at the fixed rate is a measure of the polymer resistance to flow when compared to the water's mobility (Pye 1964).

$$RF = {dP_{polymer}}\Big/{dP_{primary\ water}} \tag{4.1}$$

4.2.3.2 Residual resistance factor (RRF)

The RRF at the particular rate describes the ability of the polymer to reduce the permeability to water (Gogarty 1967).

$$RRF = {dP_{chase\ water}}\Big/{dP_{primary\ water}} \tag{4.2}$$

4.2.3.3 Flux rate (v) and shear rate (γ)

The Flux rate is given by

$$v = \left(\frac{q}{A*porosity}\right) \tag{4.3}$$

The average shear rate is calculated using the equation derived from the capillary bundle model of porous media (Zaitoun and Kohler 1987)

$$\gamma = \frac{4*\alpha*V}{r_p} \tag{4.4}$$

α is the shape parameter which is around 1.7 for packs of uniformly shaped spheres having the same diameter.

$$r_p = \left(\frac{8*Ke}{porosity}\right)^{0.5} \tag{4.5}$$

4.2.3.4 Deborah number (De_p) calculation in porous media

The Deborah number defined as the ratio of polymer's relaxation time (λ) to the residence time (t_p) classifies the viscoelastic polymer based on the elasticity. The polymers solutions having

higher relaxation time for the same observation time will be more elastic (Marshal and Metzener 1967). Residential time of the injected slugs during flooding is the time that the fluid would reside in the pore structure. Reciprocal of residential time is the elongation rate that can be calculated by first order approximation (Heemskerk et al. 1984). It is represented by Eq. 4.6.

$$\dot{\epsilon} = \frac{v}{D_p/_2} \tag{4.6}$$

The average D_p of sand is 250 microns.

Deborah number in porous media is calculated using the Eq.4.7.

$$De_p = \frac{\lambda}{t_p} \tag{4.7}$$

t_p is the residential time. Residential time is the reciprocal of elongation rate (ϵ).

4.3 Results and discussion

4.3.1 Shear rheology

The Shear behavior of HPAM and AP solutions of 1000 ppm and 2000 ppm concentrations are shown in Figure 4.2 and Figure 4.3, respectively.

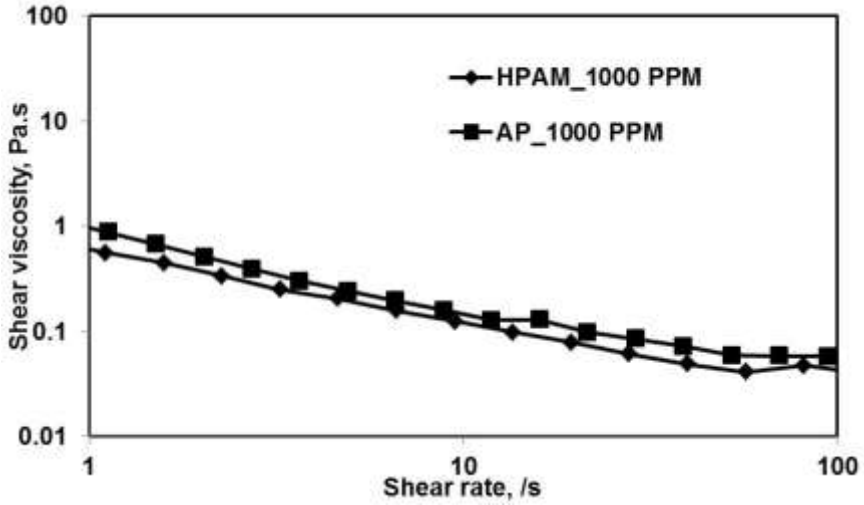

Figure 4.2: *Shear rheology of HPAM and AP solutions at 1000 PPM*

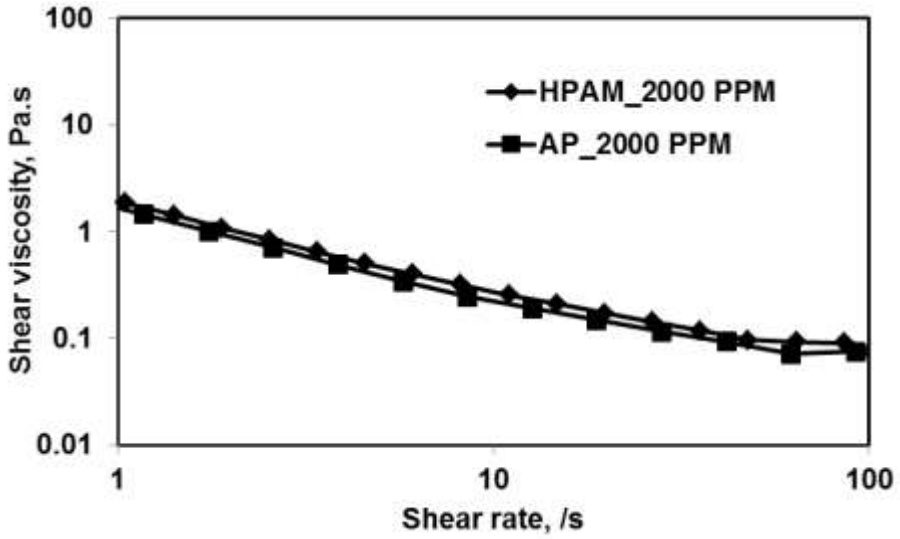

Figure 4.3: *Shear rheology of HPAM and AP at 2000 PPM*

Both the polymer solutions exhibit similar shear behavior within the shear rate range studied here at both the concentrations. The polymer molecules may roll while shearing; resulting in the cancellation of stresses (Zell et al. 2010). This makes the shear field, a weak and unable to distinguish these viscoelastic polymers differing in elasticity. The inability of the rotational rheometry to distinguish these polymers in the shear field has been reported by Seright et al (2011b). Since the viscosity of AP solution is not higher than HPAM solution, hydrophobic association in AP solution is dominated by weak intramolecular forces (Schulz and Bock 1991; Perttamo 2013; Viken et al. 2016). Even at a concentration of 2000 ppm, the shear viscosity of AP and HPAM solutions are similar. This indicates that the AP solution is not in the semi-dilute state at 2000 ppm and the CAC is above 2000 ppm.

4.3.2 Extensional rheology

4.3.2.1 Filament diameter vs time

The monitored mid-point filament diameter, as a function of time of the two polymer samples at two concentrations during filament thinning, is shown in semi-logarithmic plot (Figure 4.4).

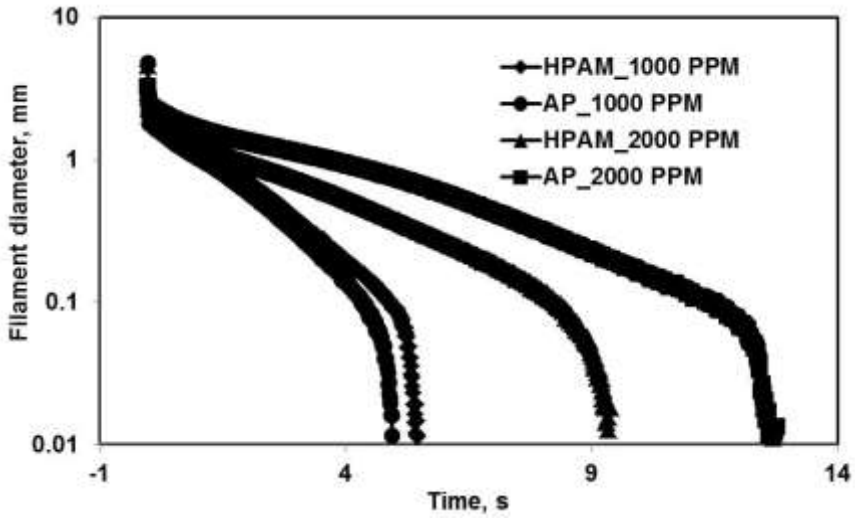

Figure 4.4: *Filament diameter with time for HPAM and AP solutions of 1000 and 2000 PPM*

Throughout drainage, the diameter of AP solution is higher than HPAM solution at 2000 ppm concentration and slightly lower when compared at 1000 ppm concentration. At 1000 ppm, both AP and HPAM solutions seem to exhibit a similar behavior in both shear and extensional fields (Figure 4.2 and Figure 4.4). However, at 2000 ppm, a notable difference is seen. AP solution resists the driving capillary action for a longer time due to its higher elasticity than HPAM solution in the extensional field contrary to similar behavior in the shear field (Figure 4.3 and Figure 4.4). A detailed explanation about these discrepancies will be made with respect to relaxation time and extensional viscosity in the forthcoming sections. These linear decreases shown by these polymers are analyzed with appropriate equations to obtain more usable extensional properties.

4.3.2.2 Extensional relaxation time

The HPAM and AP solutions of 2000 ppm show a linear decrease of the filament diameter in a semi-logarithmic plot between the diameter of 1mm and final break up during filament drainage. At 1000 ppm, these polymers show the linear decrease between around 0.85 mm and final break-up. The filament that declines exponentially appears linear in a semi-logarithmic plot. These linear data were extracted for fitting with the upper convected Maxwell model to match the exponential decline of the fluid diameter as given in Equation (3.1). The extracted and fitted data for HPAM and AP solutions at 1000 ppm and 2000 ppm are shown in Figures 4.5 to 4.8.

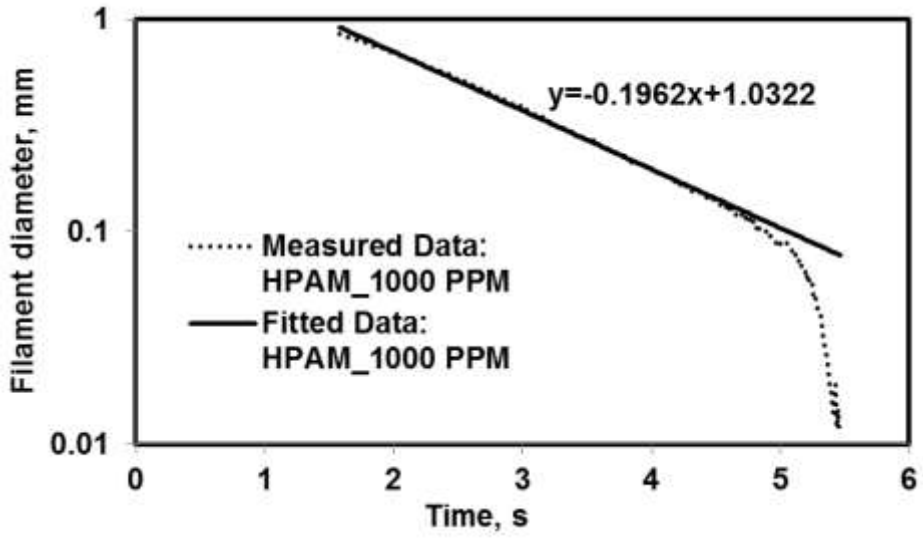

Figure 4.5: *Measured and fitted data from UCM Model for HPAM 1000 PPM*

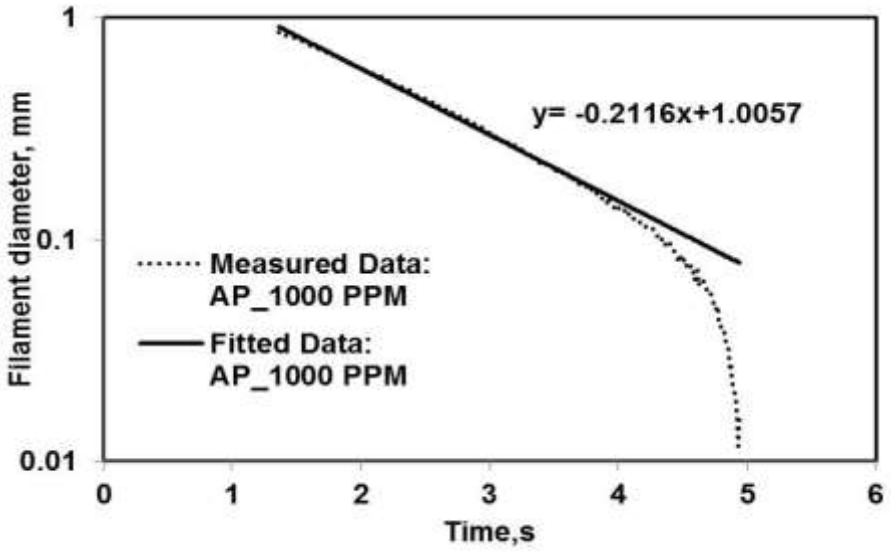

Figure 4.6: *Measured and fitted Data from UCM Model for AP 1000 PPM*

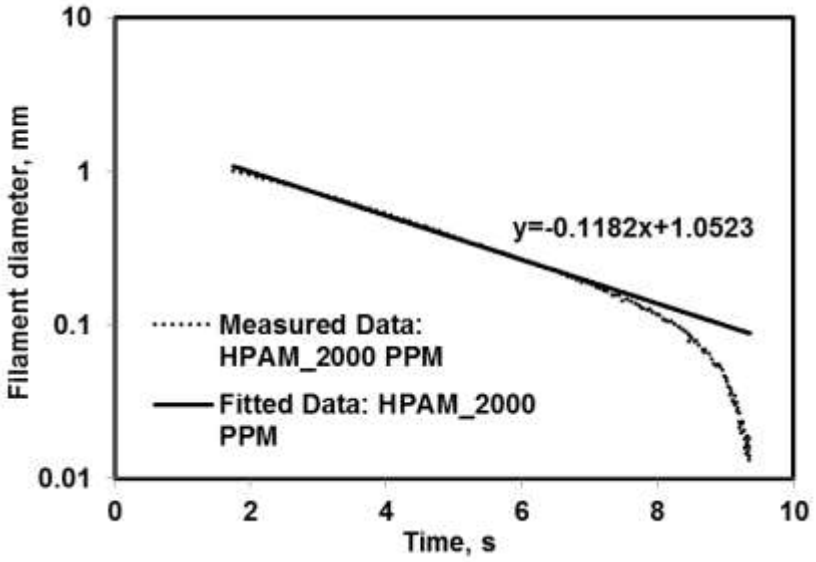

Figure 4.7: *Measured and fitted Data from UCM Model for HPAM 2000 PPM*

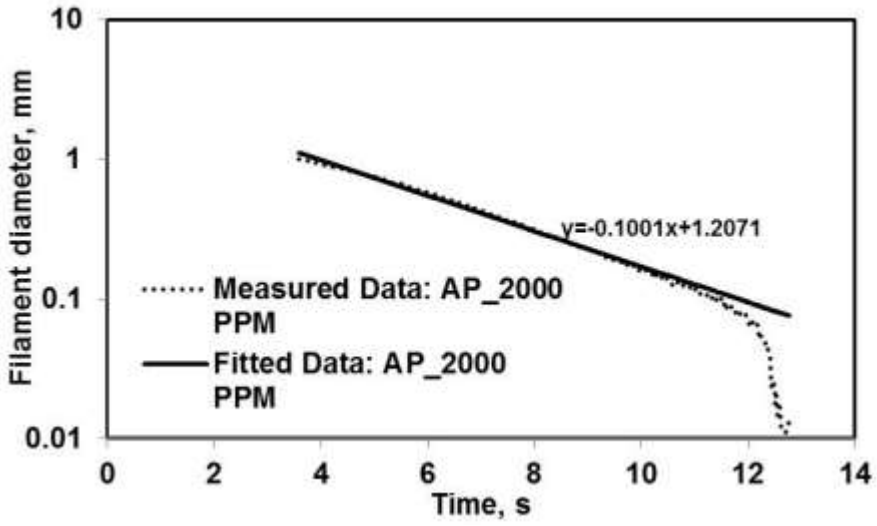

Figure 4.8: *Measured and fitted Data from UCM Model for AP 2000 PPM*

The slope and intercept of the fitted data are also shown in Figures 4.5 to 4.8. The slope represents the longest relaxation time (Plog et al. 2004; Rodd et al. 2005; Clasen et al. 2006). The average value of the relaxation time, calculated from the slope using the Eq. (3.1) and the experimental break up time for two polymer samples are summarized in Table 4.3.

Table 4.3: *Extensional rheological properties of the polymer solutions used in this study*		
Experiment (Polymer/Concentration)	**Break up time, s**	**Extensional relaxation time, s**
HPAM : 1000 ppm	5.4	0.53
AP: 1000 ppm	4.94	0.45
HPAM: 2000 ppm	9.36	1.02
AP: 2000 ppm	12.8	1.2

The break up time of AP and HPAM solutions at 2000 ppm is 12.8 seconds and 9.36 seconds. The break up time of these polymers is in the same range at 1000 ppm. At 1000 ppm, both shear and extensional rheology show similar results. However, at 2000 ppm, a stronger intermolecular attraction in AP leads to the high resistance to capillary break up mainly due to extensional properties. These are reflected in the relaxation time as well. The similar shear rheology shown by the HPAM and AP solutions at 2000 ppm suggests that intermolecular attraction is not dominant in AP at 2000 ppm. However, in the extensional flow, larger pervading polymer volume leads to frequent inter-chain interactions (Clasen et al. 2006) that eventually results in the intermolecular attraction in AP. Therefore, the resulting elastic response, in terms of relaxation time, calculated by the elastic model is higher for AP than HPAM. These observations suggest CAC for the studied AP may be lower than 2000 ppm in the bulk extensional field and it will be investigated further in the porous media studies.

4.3.2.3 Extensional viscosity vs strain rate

The strain rate defined as the rate of change of strain, is represented by Eq. (3.4). Plotting extensional viscosity with the attained strain rate using the Eq. (3.4) and Eq. (3.6) compares polymers. Figure 4.9 depicts the extensional viscosity as a function of a generated strain rate for the HPAM and AP solutions at 1000 ppm and 2000 ppm concentration.

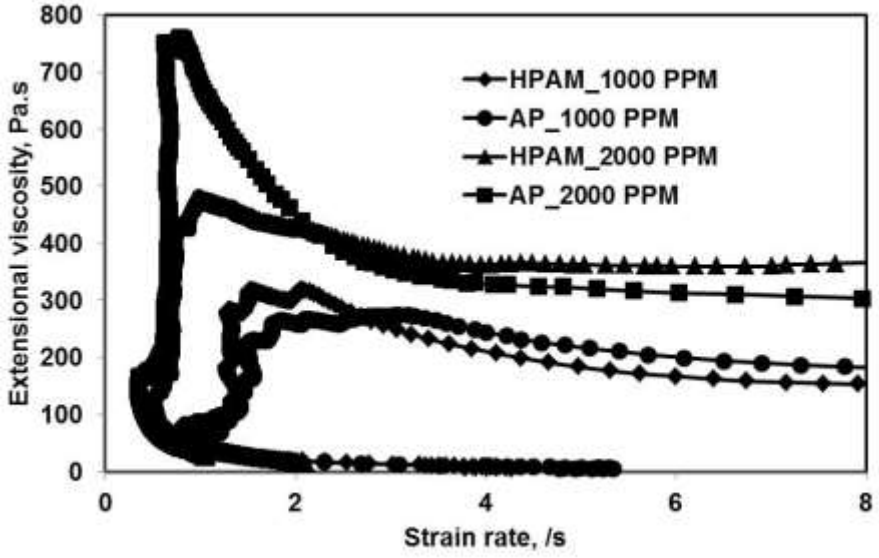

Figure 4.9: *Extensional viscosity as a function of strain rate for HPAM and AP at 1000 and 2000 PPM concentrations*

Using the finite extensible non-linear elastic (FENE) model, Entov and Hinch (1997) derived that the strain rate during filament drainage is 2/3 of the rate at which the fluid relaxes. This is widely recognized in the field of filament drainage (Clasen et al. 2006; Kim et al. 2010). The strain rate multiplied by relaxation time gives the non-dimensional strain rate in the form of a Deborah number, and an extensional viscosity around 0.66 represents the maximum elasticity (Kim et al. 2010). At a critical Deborah number, AP and HPAM at 2000 ppm corresponding to the relaxation time of 1.2 seconds and 1.02 seconds (Table 2.4) should deform around the rate of $0.55s^{-1}$ and $0.65s^{-1}$. At these rates, the extensional viscosity for HPAM and AP are ~470 Pa.s and ~760 Pa.s, respectively. This implies the higher elastic limit of AP at 2000 ppm due to the formation of intermolecular transitional network structure that generates higher viscosity, while responding to the capillary action. The maxima shown by the AP in the extensional field has been attributed to the intermolecular effects (Kennedy et al. 1995). Similarly, AP and HPAM solutions of 1000 ppm concentration, with a relaxation time of 0.45 and 0.53, respectively, should deform around the rate of $1.46s^{-1}$ and $1.24s^{-1}$ at the critical Deborah number of 0.66. Extensional viscosities of AP and HPAM corresponding to these rates are ~225 Pa.s and ~270 Pa.s, respectively. The difference in extensional properties at 1000 ppm is very small compared to 2000 ppm. Also, the extensional viscosity of the AP solution is slightly lower than the HPAM solution, indicating the dominance of the intra-molecular hydrophobic association at 1000 ppm concentration. The intermolecular

hydrophobic association that stretches the polymer chain increases the viscosity and intramolecular attraction that contracts the polymer chains decreases the viscosity even lower than HPAM (Schulz and Bock 1991; Viken et al. 2016).

Another interesting observation here is that once the maximum elastic limit is attained due to a stronger intermolecular attraction in the AP solution at 2000 ppm, a strong strain loosening phenomenon is observed. This can be due to the transformation of intermolecular attraction to intramolecular attraction (Klinke et al. 2016). The exhibition of maxima by AP followed by thinning in the extensional field has been reported (Tan et al. 2000; Sharma et al. 2015; Kennedy et al. 1995). AP solution exhibiting maximum elasticity at a lower strain rate itself is an indication that it is more elastic than HPAM solutions. Kennedy et al. (1995) reported that polymeric solutions with relatively high concentration show maxima at the relatively lower strain rate. HPAM on the other hand is relatively less elastic and exhibited the weak loosening and then continuous strain hardening behavior due to the delayed mechanical disruption. This behavior indicates that the possibility of HPAM solution undergoing mechanical deformation is lesser, at least in the relatively lower rates, than more elastic AP solution at 2000 ppm concentration. Similar observations of strain hardening followed by thinning in AP and continuous strain hardening in HPAM have also been reported (Sharma et al. 2015).

4.3.3 Porous media studies

The RF of AP and HPAM with respect to the shear rate at 1000 and 2000 ppm calculated using Eq. 4.1 is shown in Figure 4.10.

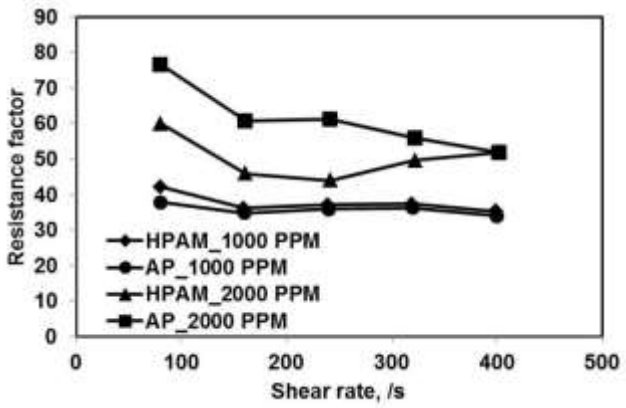

Figure 4.10: *Resistance factors for HPAM and AP solutions at 1000 and 2000 PPM concentrations in porous media*

At 2000 ppm, AP solution exhibits a higher RF than HPAM solution at all shear rate range studied here. Further, the RF of AP solution decreases at high rates in the porous media at 2000 ppm. The AP and HPAM solutions at a 1000 ppm concentration exhibit similar RFs. With increasing shear rates, no further drop in RF is observed for AP solutions at 1000 ppm. One of the characteristic of hydrophobic association is that an intermolecular network formed at a low rate will be changed to intramolecular network at high rates (Bock et al. 1988; Taylor and Nasr-el-din 2007; Klinke et al. 2016) and these will result in the loss of RF at high rates (Seright et al. 2011b). Therefore, the intermolecular hydrophobic association does not seem to play an important role at 1000 ppm concentration, and the AP solution appears to represent the dilute regime in porous media. However at 2000 ppm, higher RF of AP than HPAM at a lower rate and the subsequent loss of RF indicates the intermolecular hydrophobic association and existence of semi dilute regime in porous media.

The RRF of the AP and HPAM solutions at the 1000 and 2000 ppm concentrations is calculated using Eq. (4.2), and is shown in Figure 4.11.

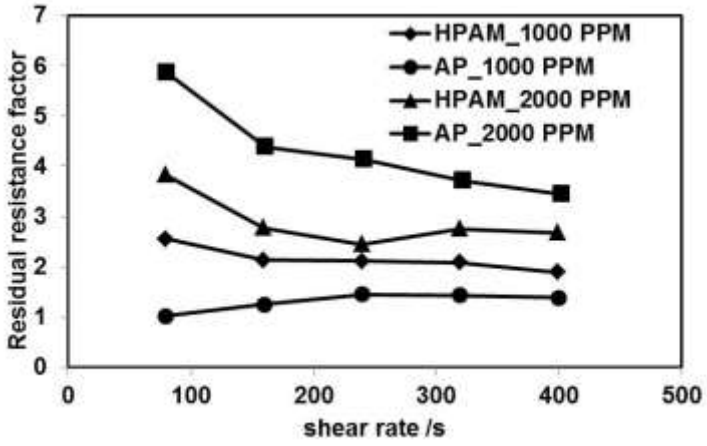

Figure 4.11: *Residual resistance factors for HPAM and AP solutions at 1000 and 2000 PPM concentrations in porous media*

AP exhibits a higher RRF for all ranges of shear rates at 2000 ppm. AP tends to exhibit multi-layer adsorption that was reported to result in a higher retention value than HPAM (Taylor and Nasr-el-din 2007). However, at 1000 ppm, the HPAM solution exhibits slightly higher residual RF than the AP solution despite the latter being characterized by the presence of hydrophobic groups. This implies that, as long as the hydrophobic association in AP is not triggered by intermolecular attraction, the RRF of AP are not higher than HPAM. Klinke et al. (2016) attributed the

permeability reduction effect of AP to the reversible intermolecular associative network. The RRF of AP at 2000 ppm decrease with the shear rate, indicating its reversibility. Therefore, it can be concluded that at 1000 ppm, hydrophobic association in porous media is dominated by intramolecular association at all the flux rates studied here. At 2000 ppm, the hydrophobic association is dominated by the intermolecular association at a low flux rate. Intermolecular attraction in AP at 2000 ppm results in stretching of polymer chains (Kennedy et al. 1995). Intra-molecular attraction in AP at 1000 ppm causes the compression of the polymer chain (Jiang et al. 2003). It is also clear that polymer solutions with a higher extensional viscosity (regardless of the nature of the groups) gets adsorbed more (Figure 4.9 and Figure 4.11). The polymer with higher extensional viscosity will be stretched more due to its high elastic limits. This indicates that the retention is related to the extensional effects, as reported by Besio et al. (1988), and the intermolecular networks are responsible for the higher permeability reduction (Klinke et al. 2016).

4.3.4 Correlating the porous media studies with bulk rheology

Having discussed the shear rheological, extensional rheological and porous media studies separately, we correlate their behavior in this section. A De_p, which represents polymer property (relaxation time) and porous media property (residential time) have been used to represent the viscoelastic effects (Delshad et al. 2008; Heemskerk et al. 1984). Using the respective residential times and the extensional relaxation time of two polymer samples at two different concentrations (reported in Table 4.3), the Deborah numbers of four polymer samples are calculated using Eq. (4.7). The calculated De_p are plotted in Figure 4.12 with respect to flux rate, in order to correlate with the injectivity results in porous media.

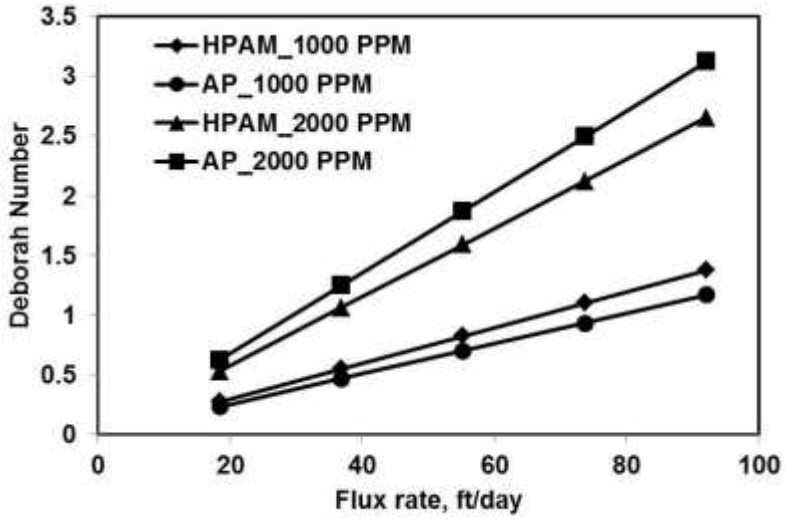

Figure 4.12: *Deborah number for HPAM and AP solutions at 1000 and 2000 PPM concentrations*

Typically, elastic effects become dominant in artificial porous media when the Deborah numbers are in the range of 0.1 and 10 (Klinke et al. 2016; Hestler et al. 1994; Stavland et al. 2010). Vossoughi and Seyer (1974) reported the elastic influence on the flow resistance occurs at the critical Deborah number of 0.08 in artificial porous media. Skartsis el al. (1992) reported the onset around De = 0.01. For the lowest flux rate investigated in this work, De_p of all the four polymeric samples are above 0.2. De_p increases monotonically with respect to the increasing flux rate for all the 4 samples (Figure 4.12). At 1000 ppm, similar behavior is shown by both the polymer solutions in shear rheology, extensional rheology, and porous media. As long as AP's behavior is similar to HPAM, association in it is aided by weak intramolecular attraction and its concentration is below CAC (Pertammo 2013). Thus 1000 ppm seems to be the diluted regime and below CAC.

However, at 2000 ppm, the influence of strong intermolecular attraction in AP is evident from the bulk extensional and porous media studies. In the extensional field, AP showed comparatively higher break-up and relaxation time, and therefore, higher De_p (Table 4) in porous media over HPAM at 2000 ppm. Also, the extensional viscosity of AP at critical Deborah number is almost ~300 Pa.s higher than HPAM at 2000 ppm indicating its higher elasticity. Comparing Figure 10 and Figure 11 with Figure 12, the De_p fairly explains higher RF and RRF of higher elastic AP solution at a 2000 ppm concentration over HPAM solution. The high elasticity is due to the intermolecular attraction, which was only possible to distinguish in the extensional field. From these observations CAC appears to be lower than 2000 ppm in porous media and in the extensional

field. However, similar shear rheology exhibited by these polymers failed to explain the difference in porous media behavior (Figure 4.3). However extensional rheology explains the difference. Further in contrary, similar shear rheology at 2000 ppm indicates CAC for AP solution is higher than 2000 ppm.

A closer look at Figure 4.10 reveals that at higher flux rates, RF of AP at 2000 ppm decreases. A higher loss of the RF by AP at high rates over HPAM was reported (McCormick and Johnson 1988; Bock et al. 1988; Taylor and Nasr-el-din 2007; Seright et al. 2011b). However, this is contrary to Figure 4.12 where the Deborah number of AP at 2000 ppm is higher than HPAM at 2000 ppm even at a high flux rate. The Deborah increases indefinitely with respect to flux rate. While Deborah number correlates the extensional behavior of elastic polymer with their behavior in porous media at low to intermediate fluxes well, at high fluxes, it could not correlate. This is because the highly elastic polymer tends to exhibit maximum elasticity, and is prone to degradation and losing its resistance. Flexible polymer molecules tend to get mechanically degraded at higher flow rate due to higher extensional stress it builds (Southwick and Manke 1988). The AP solution exhibits this phenomenon due to the transformation of intermolecular association to the intramolecular association in the range studied here. Indefinite increase in the extensional viscosity in earlier viscoelastic models (Masuda et al. 1992), with regard to the Deborah number has been reported as the limitation by Delshad et al. (2008) who used the maximum value of extensional viscosity in the unified apparent viscosity model. This implies that the Deborah number calculated using the extensional relaxation time or any fixed relaxation time alone is not sufficient to explain the viscoelastic behavior in porous media. However, the extensional viscosity vs strain rate plot (Figure 4.9) reveals that AP at 2000 ppm, after attaining the maximum at the critical Deborah number, undergoes a sharper thinning than HPAM. This results in the higher loss of extensional resistance for the AP solutions at 2000 ppm at a high strain rate, which is in accordance with its typical behavior in the porous media. A combination of Deborah number and extensional viscosity behavior explains the typical behavior of AP in porous media. The similar shear rheology exhibited by these polymers cannot explain the difference, and this emphasizes the need for bulk extensional characterization.

4.4 Summary

- Two viscoelastic polymers (HPAM and AP) with similar MW but different nature were tested in bulk shear and extensional field as well as in porous media to correlate their

behavior based on the hydrophobic associations. Single phase injectivity experiments were performed with the sand pack and shear rheological and extensional rheological experiments were performed using rotational and CaBER respectively. Two different concentrations (1000 ppm and 2000 ppm) were used throughout.

- At 2000 ppm, AP exhibits a higher RF and RRF than HPAM in porous media. The similar behavior exhibited by these flexible, viscoelastic polymers in the shear field could not explain the different level of RF they exhibited in porous media. However, extensional rheology of HPAM and AP performed using CaBER reveals the dominance of AP over HPAM, which is an indication that association is intermolecular and the CAC is around 2000 ppm.
    a. The extensional relaxation time and breakup time of AP solutions correspond to 1.2 and 12.8 seconds. For HPAM solutions, these values are 1.02 and 9.36 seconds.
    b. The extensional viscosity of AP (~760 Pa.s) was significantly higher than HPAM (~470 Pa.s) at the critical Deborah number of 0.66.
- At 2000 ppm, in the extensional viscosity vs strain rate plot, AP exhibits a high extensional viscosity at a low rate and a low extensional viscosity at a high rate due to the transformation of the intermolecular network to an intramolecular network. Similar behavior is observed in the porous media where AP exhibits a higher RF than HPAM at a low rate, and a comparable RF with HPAM at a high rate, due to the transformation of intermolecular to the intramolecular association. Thus, the typical intermolecular behavior of AP can be explained by the extensional viscosity characterization.
- At the flux rate of 92 ft/day, the RF of HPAM and AP solutions at 2000 ppm is ~53. At 92 ft/day, however, De_p for AP and HPAM solutions are 3.11 and 2.65. This signifies the limitation of using Deborah number alone for viscoelastic quantification, as reported by Delshad et al (2008). The trend shown by AP solutions in the porous media could be explained by the extensional viscosity behavior that shows the maximum and declines sharply at higher extension rates.
- Further evidence of intermolecular hydrophobic association of AP at 2000 ppm in porous media is the transformation of intermolecular to intramolecular effect at high rates, which is not observed with 1000 ppm.

- At 1000 ppm, AP exhibits a comparable RF with HPAM in porous media, even when there is no significant difference seen in the bulk shear and extensional field as well. Thus, 1000 ppm is well below CAC, thereby any additional resistance by virtue of association can't be expected for AP. While it has a negative impact on mobility control during recovery, it is good for injectivity.
- Extensional viscosity has a direct link with permeability reduction. A polymer with higher extensional viscosity stretches more and contributes to more retention and permeability reductions; AP will not contribute to drastic permeability reduction unless the hydrophobic association is aided by the intermolecular effects.
- Intermolecular attraction effects felt in the extensional field induces elasticity to AP and ignoring it while screening would be erroneous as it may lead to higher RF than HPAM at low/ intermediate rates and a quicker mechanical degradation than HPAM as observed by Seright et al. (2011b) in porous media.
- A prior accurate extensional characterization is essential, and CaBER is the viable option for classifying the similar MW and similar shear viscoelastic polymers differing in nature at various concentrations.

Chapter 5: Extensional Role to Viscoelastic Polymer Flooding: Unanswered Questions-Myth or Reality?[4]

5.1 Introduction

This paper addresses the research problems that exist in the upstream oil industry due to the misunderstanding of the flow of polymer solutions in porous media during enhanced oil recovery (EOR) operations. The additional oil recovery attained during polymer flooding is attributed to the enhanced sweep provided by viscous polymer solutions (Moffitt and Mitchell 1983; Greaves et al. 1984; James and Warren 1984; Hochanadel et al. 1990; De Melo et al. 2005; Clemens et al. 2016; Kumar et al. 2016). Viscoelastic polymers employed during EOR exhibit complex characteristics that cause an enhanced residual oil recovery and additional resistance factor (pressure drop), more than expected from the shear rheology. Several researchers attributed the viscoelastic characteristics of polymers in porous media to the extensional rheology empirically (Hirasaki and Pope 1974; Masuda et al. 1992; Delshad et al. 2008). However, there is no concrete proof to many of the empirical claims. Several misconceptions/deficiencies exist due to persistence in the usage of oscillatory rheology by EOR researchers to characterize the viscoelastic properties of EOR polymers (Garrouch and Gharbi 2006; Delshad et al. 2008; Ehrenfried 2013; Vermolen et al. 2014; Koh 2015; Qi et al. 2017; Erinick et al. 2018; Qi et al. 2018). Moreover, Deborah number (D_e) calculated using oscillatory relaxation time have failed to explain the different pressure drop (Garrouch and Gharbi 2006) and residual oil recovery (Ehrenfried 2013; Erinick et al. 2018) of EOR polymers with varying level of elasticity.

The conventional belief is that polymer flood cannot reduce S_{or} beyond the water flood (Taber 1969; Lake 1989; Sorbie 1991; Green and Willhite 1998). Recent studies have reported that viscoelastic polymers increase the overall oil recovery (Urbissinova et al. 2010; Azad et al. 2018). Several authors carefully isolated the polymer's viscoelastic influence on displacement from sweep and affirmed the polymer's viscoelastic effect on the S_{or} reduction specifically (Wang et al. 2001; Xia et al. 2004; Xia et al. 2007; Jiang et al. 2008; Vermolen et al. 2014; Clarke et al. 2015; Qi et al. 2017). However, capillary number (N_c), traditionally used for correlating the chemical slugs' potential to residual oil saturation (S_{or}) reduction, also fails to explain the additional residual oil recovery caused by viscoelastic polymers. Viscoelastic effects were deemed to cause the

[4] A version of this chapter will be submitted to SPE journal

reduced mobility of viscoelastic polymer solutions at high flow rates in porous media (Gogarty 1967; Marshall and Metzener 1967). However, high flow rates are not encountered in the major portion of the reservoir where most of the residual oil needs to be displaced from capillarity at the pore spaces. Thus, the mechanism causing the residual oil reduction at the typical low flooding rate remains elusive (Seright 2017).

These several issues are examined in detail with rheological and petrophysical insights. Quantification of extension rheology by ex-situ bulk measurements together with reported results were used to analyze the behavior of viscoelastic polymer flow through porous media. Attained results are discussed to explain the contradicting observations by various researchers.

5.2 Empirical claims

Biopolymer such as xanthan gum exhibit shear thinning phenomenon both in the shear field and in the porous media (Seright et al. 2009; Clarke et al. 2015). Synthetic polymers despite showing thinning phenomenon in the shear field, exhibit thickening behavior after a critical onset rate in the porous media. Figure 5.1 reproduced from Clarke et al. (2015) shows the behavior of xanthan gum and hydrolyzed polyacrylamide (HPAM) in the shear field and in the porous media. Figure 5.2a reproduced from Howe et al. (2015) reveals that the low molecular weight (Mw) polymer (at higher concentration) provided high shear viscosity than the high Mw polymers at low concentration.

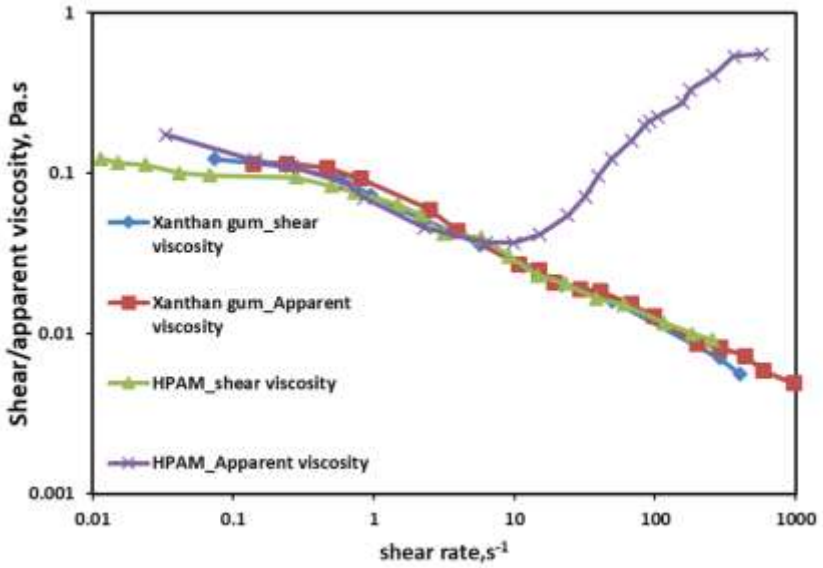

Figure 5.1: *Bulk rheological and Porous Media Behavior of xanthan gum and HPAM 3630 (Reproduced from Clarke et al. 2015)*

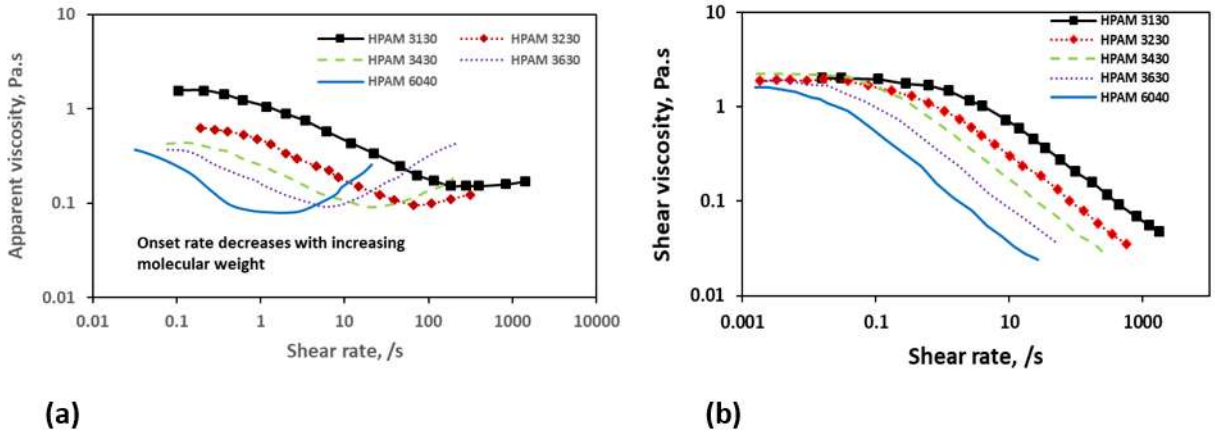

Figure 5.2: *a) Shear rheological behavior of series of HPAM polymers (reproduced from Howe et al. 2015) b) Porous media behavior of series of HPAM polymers (reproduced from Howe et al. 2015)*

Figures 5.2a and 5.2b, reproduced from Howe et al. (2015) shows that high Mw polymer with the lowest shear resistance corresponds to an early onset. Several researchers hypothesized that onset and shear thickening characteristics exhibited by synthetic viscoelastic polymers are due to its extensional characteristics (Hirasakhi and Pope 1974; Masuda et al. 1992; Delshad et al. 2008; Marshall and Metzener 1967; Stavland et al. 2010). However, there is no concrete evidence to it.

Performing extensional rheological measurements on xanthan gum and HPAM used by Clarke et al. (2015) may answer if the viscoelastic characteristics are specifically due to the extensional effect. The role of extensional viscosity on the viscoelastic onset, considering the Mw, concentration can be investigated by performing extensional rheology on the set of viscoelastic polymers used by Howe et al. (2015)

5.3 Deborah number and porous media behavior of viscous and viscoelastic polymers

Garrouch and Gharbi (2006) reported that D_e attained using the oscillatory rouse relaxation time for viscous xanthan and viscoelastic pusher-700 (HPAM) were almost similar at high salinity. However, in porous media, a different response is shown by these polymer solutions with HPAM exhibiting high pressure drop over xanthan gum. The authors explained this discrepancy with the viscoelastic number. The viscoelastic number N_v reported by Garrouch and Gharbi (2006) is represented by Eq. 5.1. N_v incorporates the oscillatory relaxation time, petrophysical parameters, Darcy velocity and power law constant to represent the polymer's viscoelasticity in porous media. Power law constant is determined from core flood experiments.

$$N_v = \frac{\sqrt{k * \phi}}{\theta_{f_1} * u^{\bar{n}-1}} \tag{5.1}$$

where

k is the permeability, Darcy

ϕ is the porosity

u is the velocity, $m.s^{-1}$

$\bar{n}$ is the power law exponent in the porous media, determined through core flood experiments

θ_{f_1} is the relaxation time, s

The viscoelastic number and D_e of these polymers reproduced from Garrouch and Gharbi (2006) are shown in the Figures 5.3a and 5.3b.

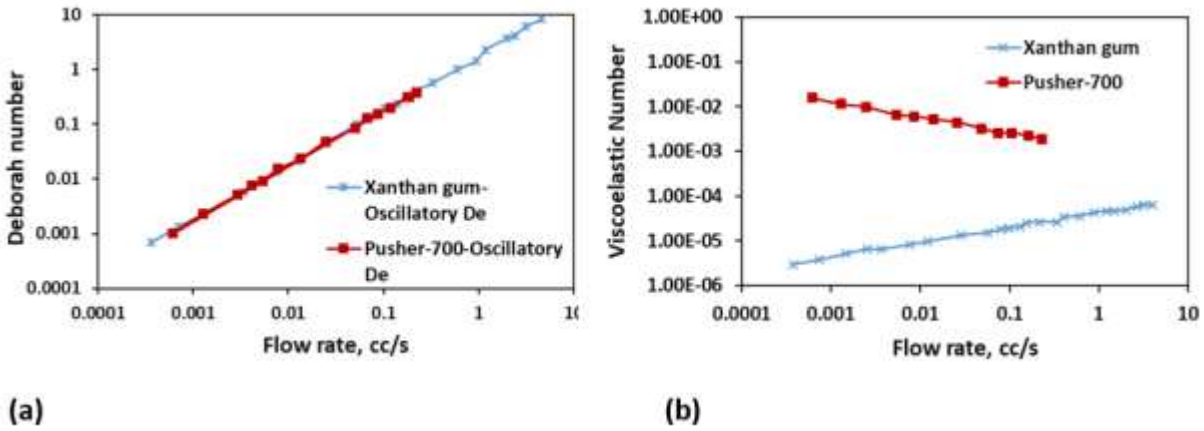

Figure 5.3: *a) Deborah number vs flow rate for Xanthan gum and Pusher-700 (reproduced from Garrouch and Gharbi 2006) b) viscoelastic number vs flow rate for Xanthan gum and Pusher-700 (reproduced from Garrouch and Gharbi 2006)*

Small amplitude oscillatory shear rheology, used to determine the relaxation time represents the weak, linear viscoelastic effects (Garrouch and Gharbi 2006). However, porous media has strong extensional flow component in the pore throat region of the reservoir as the normal stresses become higher around the pore constrictions (Nguyen 1999; Afsharpoor et al. 2012). Direct measurements of the extensional relaxation time on the viscous and viscoelastic polymer, reported in Garrouch and Gharbi (2006) could the compare the efficiency of oscillatory and extensional relaxation time for accounting the polymer's viscoelastic effects in porous media.

5.4 Capillary number and residual oil saturation reduction

Masuda et al. (1992) and Delshad et al. (2008) highlighted the inadequacy of shear rheology to explain the additional recovery caused by the viscoelastic polymers and used apparent viscosity for explaining the additional oil recovery caused by the viscoelastic effects. Clarke et al. (2015) recently attributed elastic turbulence as the reason for additional oil mobilization caused by the viscoelastic polymer solutions at the low flooding rate of 1ft/day. Clarke et al. (2015) reported the viscoelasticity can lead to the recovery more than expected from the shear and apparent viscosity (Figures 5.4 a, b and c).

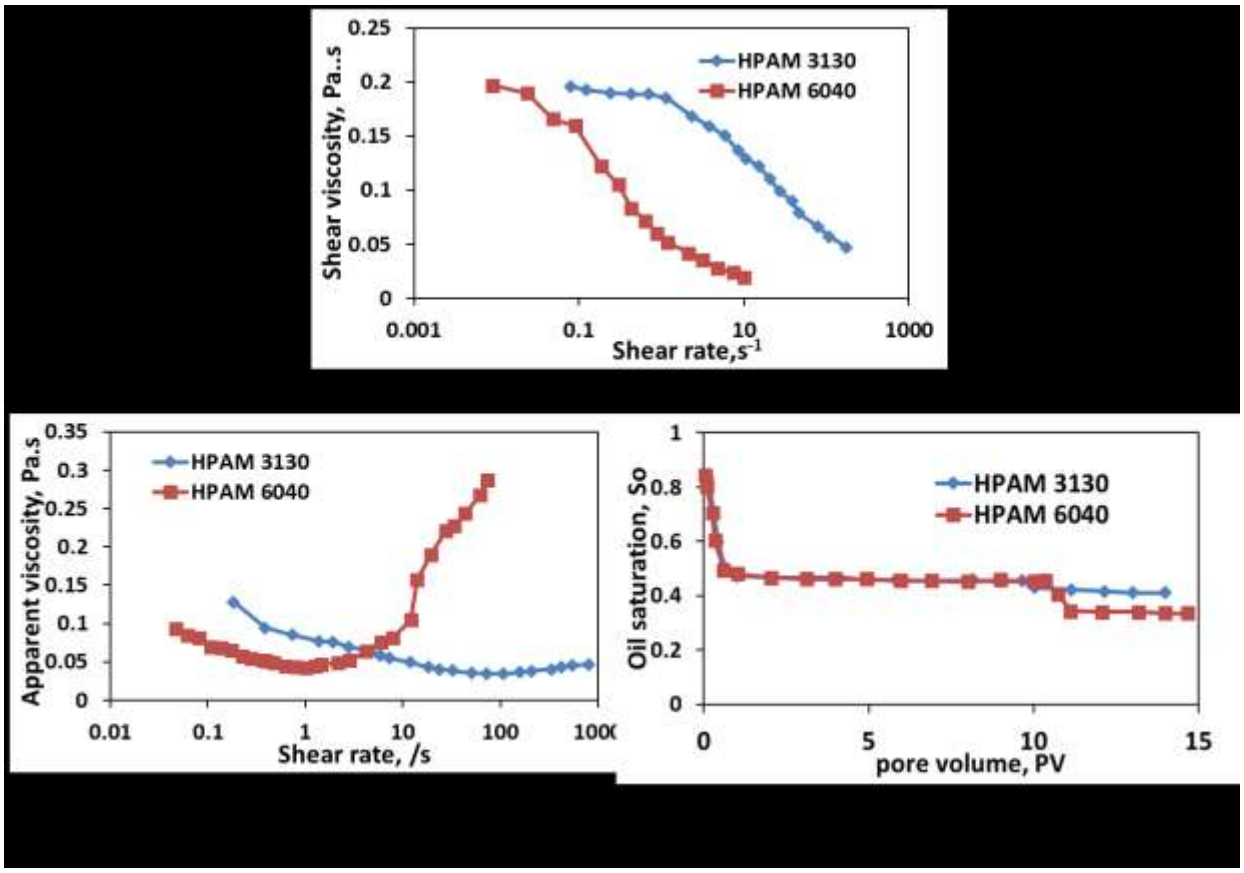

Figure 5.4: *a) Shear rheological plot reproduced from Clarke et al. (2015) for HPAM 3130 and HPAM 6040 b) Apparent viscosity plot reproduced from Clarke et al. (2015) for HPAM 3130 and HPAM 6040 c) Oil Recovery plot reproduced from Clarke et al. (2015) for HPAM 3130 and HPAM 6040*

Apparent viscosity is empirically treated as the sum of shear and extensional viscosity (Hirasaki and Pope 1974; Masuda et al. 1992; Delshad et al. 2008; Clarke et al. 2015; Stavland et al. 2010; Magbagbeola 2008). N_c normally used to study the residual oil saturation during chemical oil recovery (Green and Willhite 1998; Stegemeier 1977), fails to explain the polymer's viscoelastic effect on S_{or} reduction (Xia et al. 2007; Clarke et al. 2015; Qi et al. 2017). As per the capillary theory, residual oil cannot be mobilized unless the driving viscous force overcomes the trapping capillary force by at least two order (Taber 1969; Green and Willhite 1998; Peter 2002). Rapid oil mobilization begins to occur at the low N_c (Qi et al. 2017). N_c calculated using the apparent viscosity/shear viscosity remained the same for a set of polymers, with different normal stresses and recovery potential (Xia et al. 2004; Qi et al. 2017). Clarke et al. (2015) reported that the onset of rapid desaturation occurs at the lower N_c for HPAM than xanthan gum (Figure 5.5).

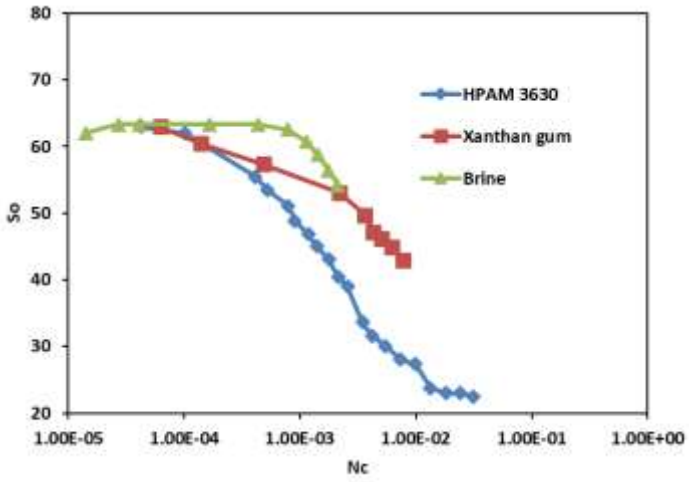

Figure 5.5: *CDC curve for HPAM 3630 and Xanthan gum (reproduced from Clarke et al. 2015)*

However, both the HPAM and xanthan gum were reported to exhibit similar shear viscosity, IFT, and linear viscoelastic effects. The authors reported that in addition to the viscous force, some other mechanism causes the rapid oil mobilization to occur at much lower N_c for HPAM. Figure 5.6 reproduced from Qi et al. (2017) reveals that viscoelastic HPAM causes the higher residual oil recovery than viscous glycerin, despite possessing the similar core scale pressure. The authors reported that both the glycerin and HPAM have similar IFT. The authors also reported HPAM 3630 were contributing to residual oil recovery even before the critical N_c.

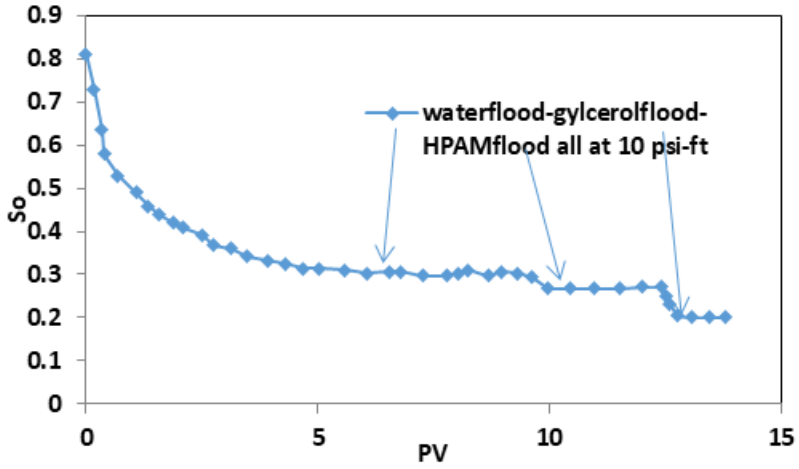

Figure 5.6: *Oil recovery plot showing the residual oil recovery potential of 2100 ppm HPAM 3630 over 75 cP Glycerin at the same core scale pressure and capillary number (reprinted from Qi et al. 2017).*

Extensional viscosity is related to normal stress. Extensional viscosity (normal stresses) tends to act in the protruding portion of the reservoir on the pore scale. On the pore scale, 75% of resistance

is offered by the polymer's elongational deformation (Haas and Durst 1982). On the core scale, apparent viscosity will be dominated by the shear forces, as the normal stress get nullified (Afsharpoor et al. 2012; Wang et al. 2007). However, Clarke et al. (2015) discounted extensional viscosity as the reason for residual oil recovery, based on the N_c calculated in psi/ft. Direct extensional measurements on the polymers used by Clarke et al. (2015) and Qi et al. (2017) may answer if is there any extensional rheological influence on the S_{or} reduction that is overlooked in the core scale terms such as apparent viscosity, pressure drop and N_c.

5.5 Deborah number and residual oil saturation reduction

Qi et al. (2017) developed the correlation between the D_e and S_{or}. Oscillatory relaxation time is used by the authors for D_e calculation. However, oscillatory D_e failed to explain the additional residual oil recovery caused by high saline polymer solutions (Erinick et al. 2018). Figure 5.7 reproduced from Erinick et al. (2018) reveals that the high saline polymer solutions, corresponding to the lower oscillatory D_e contributed to additional residual oil recovery.

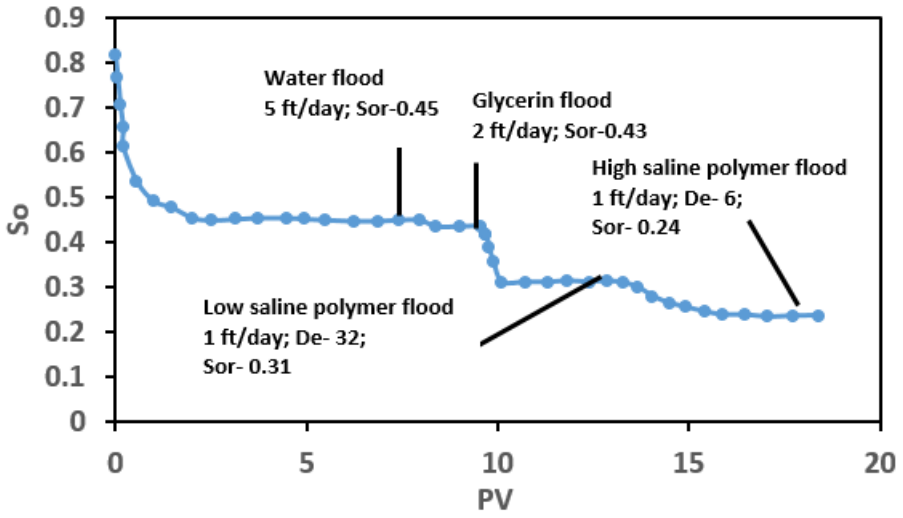

Figure 5.7: *Oil recovery plot, showing the residual oil recovery potential of high salinity polymer flood (3548 ppm HPAM 3630 in 24300 ppm salinity) over low salinity polymer solutions (2000 ppm HPAM 3630 in 1400 ppm salinity) in 1480 mD Bentheimer sandstone core (reproduced from Erinick et al. 2018)*

Erinick et al.'s (2018) findings create a difference of opinion on whether the polymer's viscoelasticity has an effect on S_{or} reduction. Magbagbeolo (2008) reported that strain hardening index, determined through UVM model fit, is higher for high saline polymer solutions than the low saline polymer solutions, despite the higher oscillatory relaxation time possessed by the later. At high salinity polymer solutions exist in the coiled state due to the electrostatic repulsion (Seright

et al. 2011a). However, at the low salinity, the polymer solutions exist in the elongated form because of unshielded electrostatic repulsion between the anionic groups along the polymer chains. More energy needs to be expended to uncoil the chains so that the polymer molecules can flow through the pore constriction. Contrarily, the energy needed to stretch the uncoiled polymer chains is relatively lesser. Direct measurements of the strain hardening index and other extensional parameters of the viscoelastic polymers used by Erinick et al. (2018) may answer if there is any extensional viscoelastic effect on high saline solutions that causes the additional S_{or} reduction.

5.6 Methodology

In order to answer the ambiguity surrounding the role of extension flow of viscoelastic polymers during oil displacement, discussed earlier, the literature reported results are reexamined with ex-situ measurement of bulk extensional rheology. The relevant polymers used by various researchers along with their concentration and salinity are provided in table 5.1. All the HPAM polymers were obtained from SNF Floerger (USA). Xanthan gum used by Garrouch and Gharbi (2006) was obtained from the Kelko (USA). Xanthan gum used by Clarke et al. (2015) as obtained from Qmax (Canada), the subsidiary of international drilling fluids.

The polymer solutions were prepared by low speed mixing at 200 rpm using a magnetic stirrer for 24 hours. Capillary breakup extensional rheometer (CaBER) is used to characterize the extensional properties of all the polymer solutions at similar operational conditions as reported in the literature. The polymer solutions taken in small quantity is placed between the top and bottom plate of the CaBER setup. A polymeric filament is created by lifting the top plate from the bottom plate. Filament diameter vs time data is obtained using the laser micrometer. From the filament diameter vs time plot, various extensional rheological parameters are obtained using appropriate theories. Extensional relaxation time is attained from filament diameter vs time plot using upper convected Maxwell (UCM) model. As per finite extensible non-linear elastic (FENE) theory, the maximum elongational viscosity is determined at the critical D_e of 0.66. Maximum elongational viscosity at the critical D_e corresponds to the elastic limit. Power law is used to determine the strain hardening index from the extensional viscosity vs strain values around the critical D_e. For more details about the experimental procedure of CaBER, CaBER theories and related equations, the readers are encouraged to refer to our previous publications (Azad and Trivedi 2017; Azad et al. 2018a; Azad et al. 2018b; Azad and Trivedi 2018a; Azad and Trivedi 2019).

5.7 Results and discussion

Extensional rheology is performed on the polymers, used by various researchers and all the relevant extensional properties are reported in Table 5.1.

Table 5.1: *Polymer solution used by various researchers, and their extensional rheological parameters*

Authors	**Polymer**	**Concentration (ppm)**	**Mw (MDa)**	**Salinity (ppm)**	τ_{ext} ,s	$\mu_{\max@De_{cr-0.66}}$ (cP)	n_2
Clarke et al. (2015)	HPAM 3130	6000	3.6	4900	0.026	40000	3.21
	HPAM 6040	640	30-36	4900	0.19	210000	3.6
	HPAM 3630	1300	18-20	4900	0.218	230000	3.64
	Xanthan gum	1400		4900	0.004	580	-2.02
Garrouch and Gharbi (2006)	Pusher-700	1000	8	10,000	0.0319	37000	3.37
	Xanthan gum	1000		10,000	0.0026	280	-2.2
Howe et al. (2015)	HPAM 3130	14600	3.6	4900	0.055	46000	2.94
	HPAM 3230	7280	6	4900	0.129	117000	3.15
	HPAM 3430	4220	11	4900	0.223	197000	3.17

	HPAM 3630	2250	18-20	4900	0.345	340000	3.81
	HPAM 6040	1200	30-36	4900	0.495	452000	4.09
Qi et al. (2017)	HPAM 3630	2100	18-20	11000	0.516	620000	3.74
	Glycerin	83000	0.000092	11,000	0.003	1000	-1.72
Erinick et al. (2018)	HPAM 3630 HPAM 3630	2000 3400	18-20 18-20	1400 26600	0.25 0.44	228000 813000	2.66 4.05

5.7.1 Shear thickening in porous media and extensional rheology

Clarke et al. (2015) reported that both xanthan gum and HPAM 3630 solutions show thinning behavior in the shear field (Figure 5.1). In porous media, xanthan gum solutions show thinning behavior (Figure 5.1).HPAM 3630 solutions show thickening behavior in porous media (Figure 5.1). Shear rheology fails to explain the different porous media behavior of viscous xanthan gum and viscoelastic HPAM 3630. Extensional rheology performed on xanthan gum and HPAM 3630 solutions reveals the strain loosening behavior (drop in the extensional viscosity with respect to strain) for xanthan gum (Figure 5.8 c)

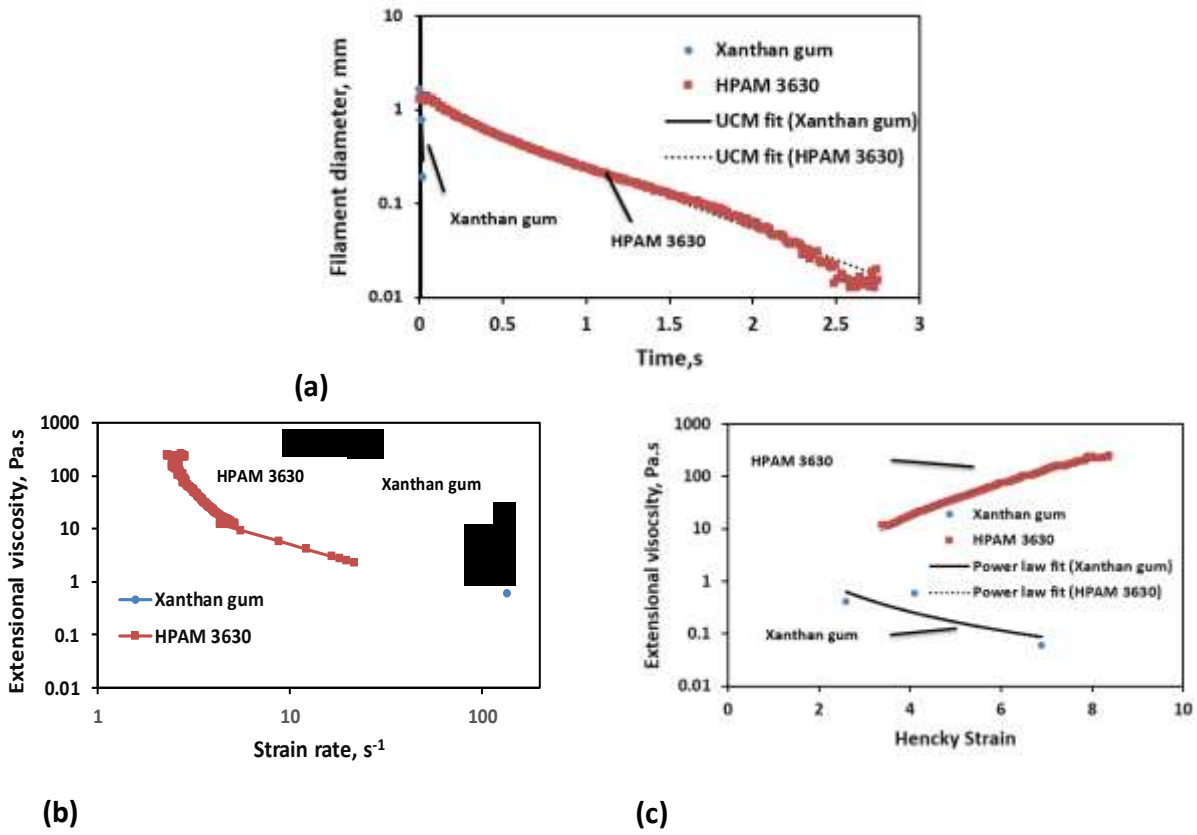

Figure 5.8: a*) Filament diameter as a function of time for xanthan gum and HPAM 3630 used by Clarke et al. (2015) b) Extensional viscosity as a function of generated strain rate, showing the Umax at the critical Deborah number c) Extensional viscosity vs strain values around the critical Deborah number*

The strain hardening index for xanthan gum is negative (Table 5.1). However, the strain hardening behavior of viscoelastic HPAM is clearly seen in Figure 5.8 c, despite its shear thinning behavior in the shear field (Figure 5.1). Therefore, increase in the viscosity with respect to the shear rate/flux (shear thickening,) shown by the viscoelastic polymer HPAM 3630 (Figure 5.1) in the porous media is due to the strain hardening. Failure of viscous polymer xanthan gum to exhibit strain hardening thickening indicates that strain hardening is the specific characteristics limited to viscoelastic polymers.

5.7.2 Onset and extensional rheology: Effect of Mw and concentration

Shear rheological experiments performed by Howe et al. (2015) on the series of HPAM polymers reveals that polymer with high Mw and lower concentration provides lesser shear resistance than the polymer with low Mw and higher concentration (Figure 5.2a). The high Mw polymer with the lowest shear resistance showed early onset than the low Mw polymers with higher shear resistance

(Figure 5.2b). Several researchers attributed the viscoelastic onset to the extensional viscosity empirically in their developed viscoelastic models (Hirasakhi and Pope 1974; Masuda et al. 1992; Delshad et al. 2008; Magbagbeolo 2008). Extensional rheological results attained with the series of HPAM polymers solutions, used by Howe et al. (2015) is shown (Figures 5.9 a, b, c).

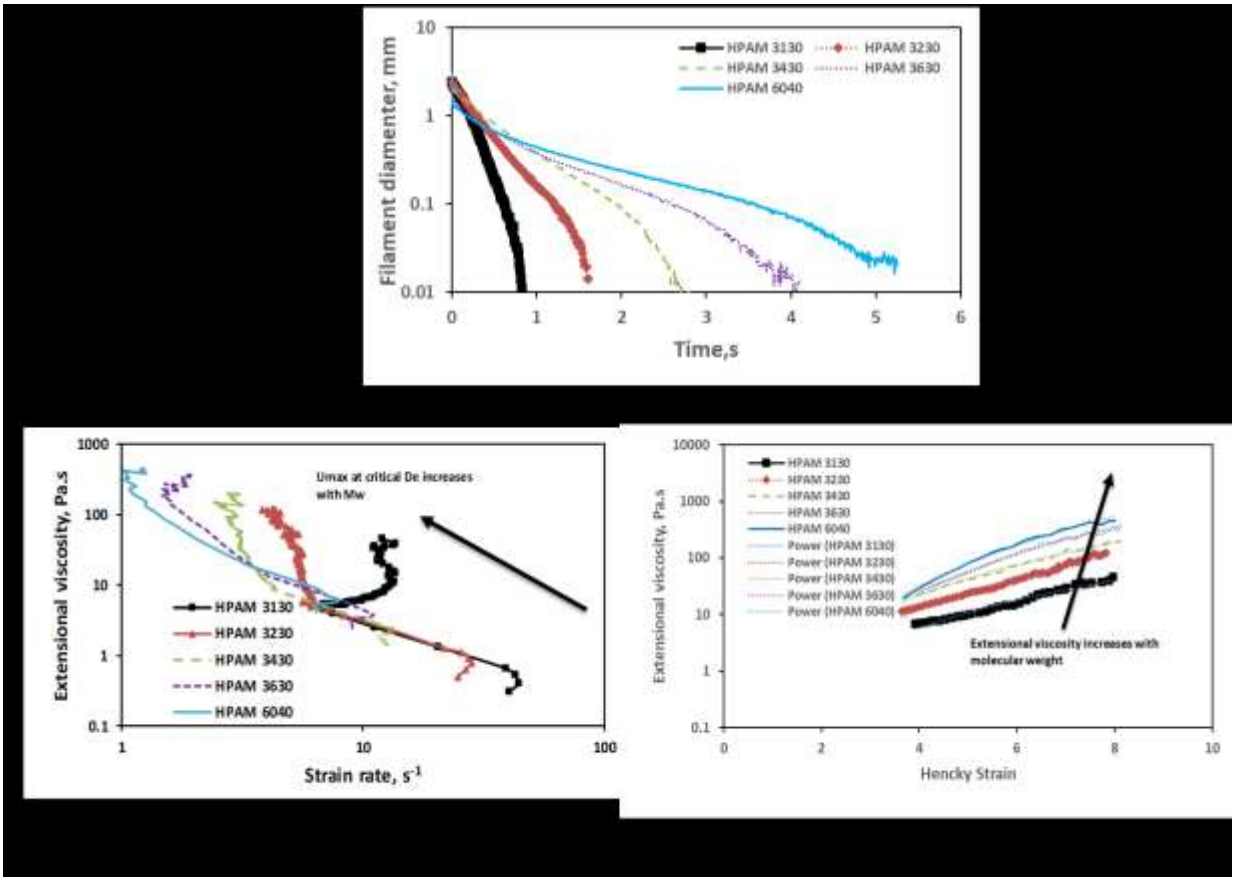

Figure 5.9: *a) Filament diameter as a function of time for five polymeric solutions used by Howe et al. (2015) b) Extensional viscosity as a function of generated strain rate, showing the Umax at the critical Deborah number c) Extensional viscosity vs strain values around the critical Deborah number*

Extensional relaxation time and the extensional viscosity of polymer with high Mw and lower concentration is higher than that of polymers with high concentration and low Mw (Table 5.1). HPAM 6040 and HPAM 3130 shows the highest and lowest extensional resistance, respectively. This behavior is completely different than their behavior in the shear field, where HPAM 6040 showed the lowest shear resistance and HPAM 3130 showed highest shear resistance (Figure 5.2a). Comparing the extensional rheological behavior of these polymers with the shear behavior (Figure 5.2a and Figures 5.9 a, b, c), it is clear that extensional resistance is directly related to the polymer's Mw whereas the shear resistance is directly related to polymer concentration. One key observation

in the rheological perspective is that the viscoelastic polymers possessing the highest viscosity will not necessarily possess the highest elasticity. Comparing the Figures 5.9 a, b, c with Figure 5.2b, it is clear, that the polymer solution with high extensional resistance causes early onset in the porous media. This reinforces the empirical belief existing in the industry since the 1970s that the onset shown by the viscoelastic EOR polymer solutions in reservoir cores is due to the extensional resistance. A small amount of deformation is enough for the polymer with higher extensional resistance (HPAM 6040) to cause the straining flow in the porous media. However, for the polymer with low extensional resistance (HPAM 3130), a higher rate is required to induce the straining flow in the porous media.

5.7.3 Porous media behavior of viscous and viscoelastic polymers: extensional vs oscillatory Deborah number

Garrouch and Gharbi (2006) reported that Deborah numbers calculated using the oscillatory relaxation time are equal for viscous xanthan gum and viscoelastic pusher-700 solutions (Figure 5.3a). However, these polymers have shown different pressure drop profile during their flow through porous media which is reflected in the viscoelastic number (Figure 5.3b). The viscoelastic number calculated using core flood experiments is higher for viscoelastic pusher-700 than viscous xanthan gum (Figure 5.3b). Deborah number fails to explain the higher pressure drop shown by pusher-700 over xanthan gum. Oscillatory relaxation time is similar (~0.01 seconds) for both of these polymers. However, the extensional relaxation time calculated using the UCM fit from the filament diameter vs time data are shown in the Figure 5.10a. The extensional relaxation time of xanthan gum and pusher-700 are 0.0026 seconds and 0.031 seconds, respectively (Figure 5.10a, and Table 5.1). The Deborah number ($D_{e\text{-}ext}$) values with respect to flow rate, calculated using extension relaxation time, are shown in Figure 5.11. It can be seen from Figure 5.11 that the $D_{e\text{-}ext}$ is higher for viscoelastic pusher-700 than viscous xanthan gum at any given flow rate (Figure 5.11), which explains the higher pressure drop and viscoelastic number shown by pusher-700 than xanthan gum during the flow through porous media over. This indicates that viscoelasticity effects observed in porous media are better represented through bulk extensional measurements than oscillatory shear.

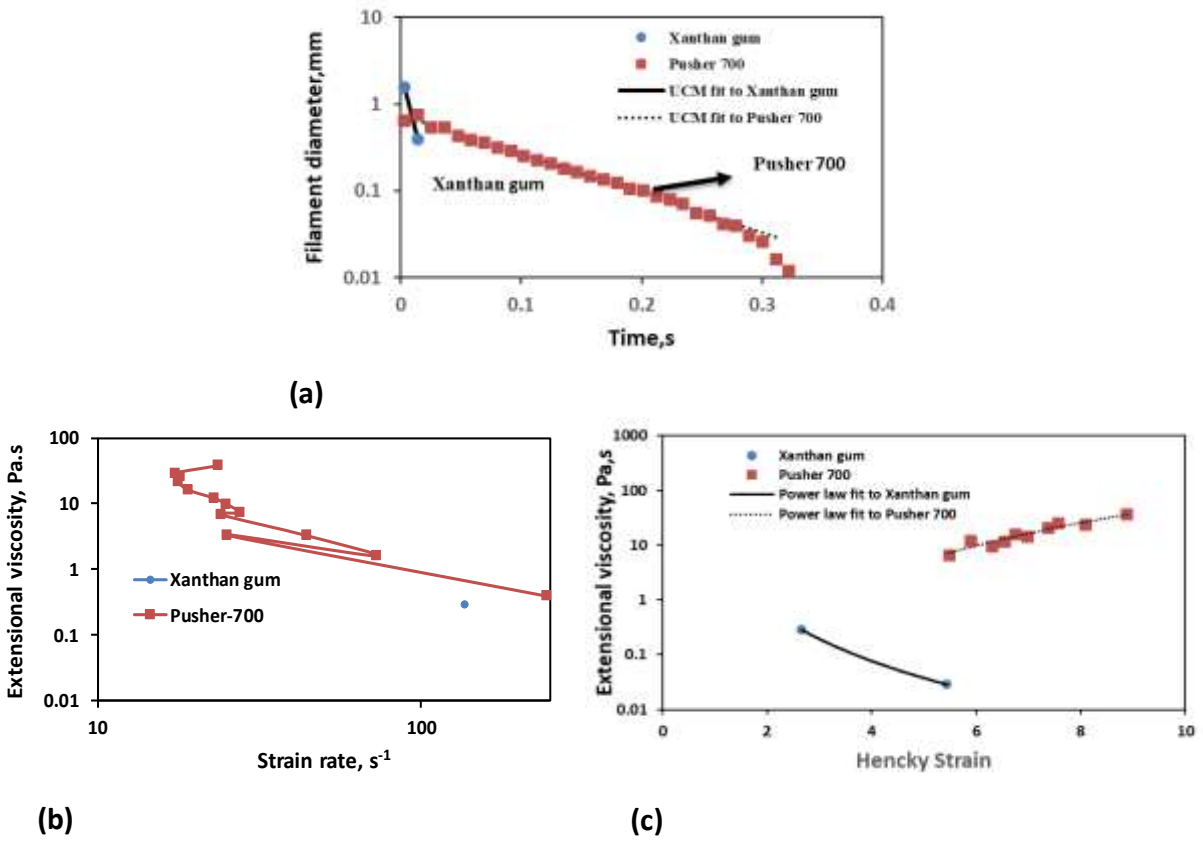

Figure 5.10: *a) Filament diameter as a function of time for xanthan gum and pusher-700 reported by Garrouch and Gharbi (2006) b) Extensional viscosity as a function of generated strain rate, showing the Umax at the critical Deborah number c) Extensional viscosity vs strain values around the critical Deborah number*

Hence, the D_e number calculated using the extensional relaxation time is higher for viscoelastic pusher-700 than viscous xanthan gum (Figure 5. 11) which is in accordance to the higher pressure drop and viscoelastic number shown by pusher-700 over xanthan gum (Figure 5.3b).

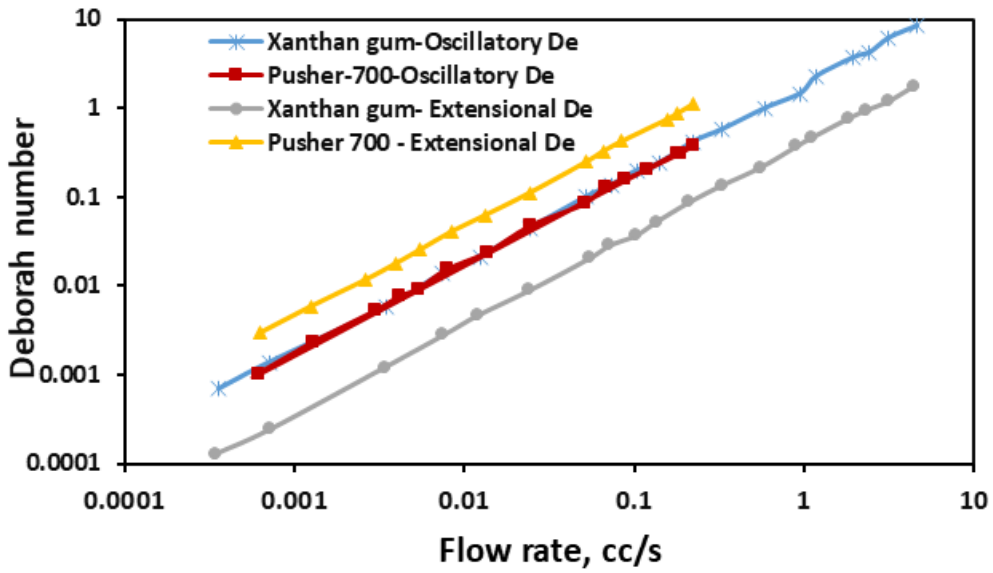

Figure 5.11: *Comparison between Deborah numbers calculated using oscillatory and extensional relaxation time for Xanthan gum and pusher 700, used by the Yuan (1981) and reported by Garrouch and Gharbi (2006)*

5.7.4 Influence of extensional rheology on the S_{or} reduction and injectivity

Clarke et al. (2015) reported that HPAM 6040 polymer solutions characterized by high Mw and lower concentration provided lower shear viscosity and apparent viscosity than HPAM 3130 polymer solutions characterized by low Mw and higher concentration (Figure 5.4a, Figure 5.4b and Table 5.1). However, HPAM 6040 solutions corresponded to higher S_{or} reduction than HPAM 3130 (Figure 5.4c). Several other researchers also reported residual oil saturation reduction during viscoelastic polymer flooding and termed additional micro-force or normal stresses as the main mechanism (Xia et al. 2004; Afsharpoor et al. 2012; Wang et al. 2007). Micro-force is a constituent of normal stress (Wang et al. 2007) and normal stress is directly related to extensional viscosity (Barnes 2010). Therefore, in order to understand the results reported by Clarke et al. (2015), it is utmost important to quantify extensional viscosity of HPAM 6040 and HPAM 3130 polymers.

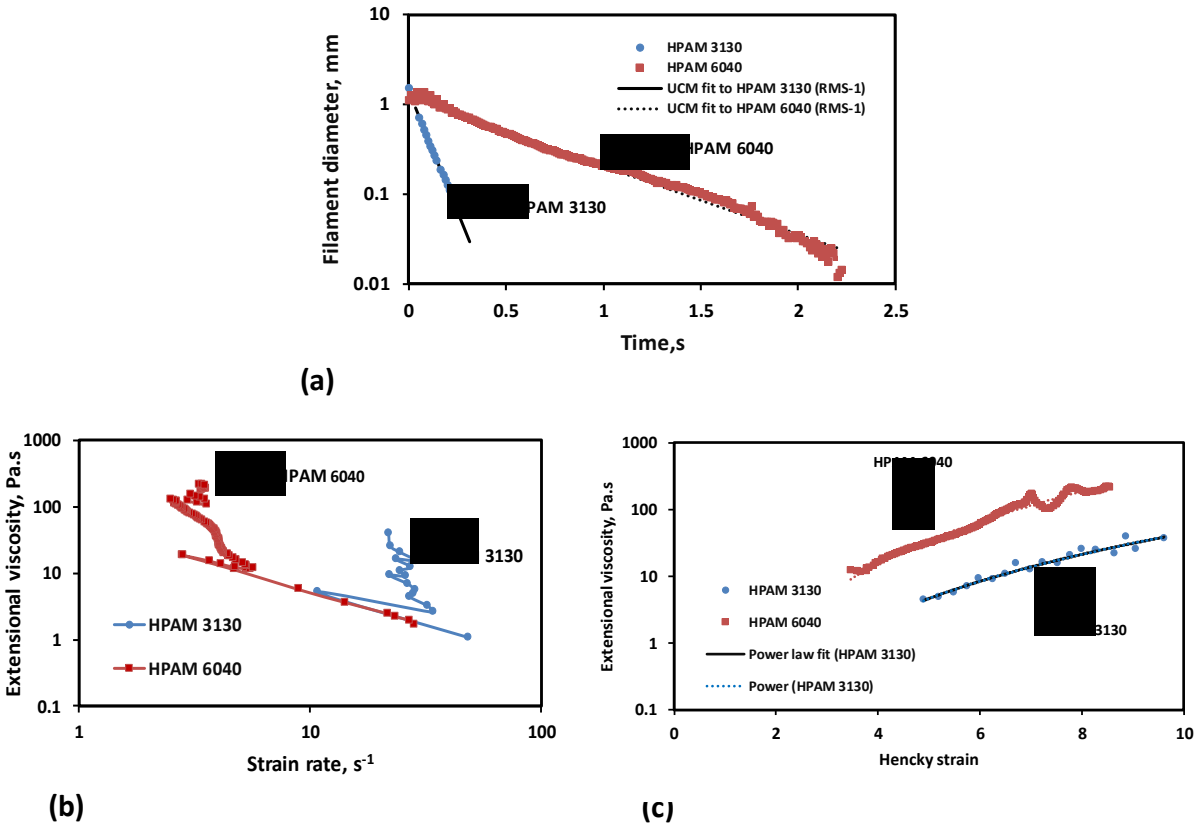

Figure 5.12: *a) Filament diameter vs time plot for HPAM 3130 and HPAM 6040, reported by Clarke et al. (2015) and the UCM fit to the linear elastic regimes for the determination of relaxation time b) Extensional viscosity as a function of generated strain rate plot showing the sharp rise in the extensional viscosity around the critical Deborah number c) Power law fit to the extensional viscosity vs Hencky strain values around the critical Deborah number for the determination of strain hardening index.*

Figure 5.12b shows that the measured values of maximum extensional viscosity around the critical D_e for HPAM 6040 and HPAM 3130 are 210 Pa.s and 40 Pa.s, respectively (Figure 5.12b and Table 5.1). The extensional viscosity of HPAM 6040 is higher than HPAM 3130 for all the ranges of critical strain values despite its lower shear viscosity and apparent viscosity (Figure 5.12c, Figure 5.4a and Figure 5.4b). This explains the S_{or} reduction reported by Clarke et al. (2015). Therefore, extensional viscosity of a polymer can be a dominating factor over shear viscosity for reducing residual oil saturation from the porous media. Further, the extensional viscosity is also a dominant factor than the apparent viscosity for reducing the residual oil saturation. There is a conventional notion that apparent viscosity should be treated as the summation of shear and extensional viscosity (Hirasakhi and Pope 1974; Masuda et al. 1992; Delshad et al. 2008;

Magbagbeolo 2008; Stavland et al. 2010). This conventional notion may not be applied to residual oil recovery applications.

It is important to note that the residual oil recovery is the pore-scale mechanism that can be attained through enhanced microscopic displacement efficiency (Green and Willhite 1998; Peter 2002). It has been reported that the magnitude and therefore the effect of forces exerted on pore-scale and core-scale are different. Afsharpoor et al. (2012) reported that normal (extensional) stresses become higher as the viscoelastic polymeric solution approaches the pore throat and therefore the pressure drop exerted around the pore throat is higher than the overall pressure drop. Similarly, apparent viscosity calculated on the core-scale will be lesser than the pore-scale apparent viscosity (Afsharpoor et al. 2012). Wang et al. (2007) reported that micro-force gets nullified on the core-scale and the pressure gradient is dominated by the macro-force or the shear force because, on the core-scale, shear flow predominates most of the regions. On the other hand, the extensional viscosity acting on pore-scale gets nullified on the core-scale and the measured apparent viscosity at core-scale is dominated mostly by the shear viscosity. Therefore, residual oil recovery potential of HPAM 6040 (with the maximum extensional viscosity of 210 Pa.s) was higher than HPAM 3130 (with the maximum extensional viscosity of 40 Pa.s) despite the lower apparent/shear viscosity exhibited by HPAM 6040. Thus, one cannot claim that apparent viscosity incorporates the extensional viscosity that plays a role in residual oil recovery at the pore-scale.

Injectivity defined as the measurement of the ease with which the fluid can be injected (Hyne 1991) is the ratio between the injection velocity and difference between wellbore pressure and reservoir pressure. Core-scale pressure drop is the pressure difference between the inlet and outlet of the core. For injectivity applications, the core-scale pressure drop is considered (Seright et al. 2009; Han et al. 2012; Azad and Trivedi 2017). Apparent viscosity is directly proportional to core-scale pressure drop (Delshad et al. 2008). The apparent viscosity generated by purely viscous polymers throughout the ranges of shear rates corresponds only to its shear resistance (Cannela et al. 1988; Seright et al. 2009). However the apparent viscosity generated by the viscoelastic polymers after the viscoelastic onset rate is more than expected from its shear viscosity (Magbagbeolo 2008). The difference between the apparent viscosity and the shear viscosity at higher rate is due to the extensional effect and several researchers have used the summation of extensional viscosity and shear viscosity in their viscoelastic models to match the apparent viscosity (Hirasakhi and Pope 1974; Masuda et al. 1992; Delshad et al. 2008; Stavland et al. 2010;

Magbagbeolo 2008; Azad and Trivedi 2019). It is important to point out here that extensional viscosity used in all the previous viscoelastic models were not the actual measured values but the reduced or the downscaled value. This can clearly be understood by referring to our previous publications (Azad and Trivedi 2018a; Azad and Trivedi 2019) where the measured extensional viscosity values of various EOR polymer systems are provided. The measured extensional viscosity values are ~3 orders higher than the downscaled extensional viscosity values (Azad and Trivedi 2017; Azad et al. 2018a; Azad et al. 2018b; Azad and Trivedi 2018a; Azad and Trivedi 2018b; Azad and Trivedi 2019). Directly measured bulk extensional viscosity values were not used in the core-scale viscoelastic models because bulk values are attained during the pure extensional flow but at core-scale, high speed shear flow dominates even at the high shear rate. The viscoelastic polymer tends to exhibit elongational characteristics during the high speed shear flow (Doshy and Dealy 1987). This is the reason for the difference that occurs between the apparent viscosity values and shear viscosity values only at high shear rates. Therefore only the reduced values of the extensional viscosity were used along with shear viscosity to match the apparent viscosity and core-scale pressure drop. Pure extensional flow and high speed shear flow are two different types of flow (Doshy and Dealy 1987) and it is important in chemical EOR perspective to treat them separately for different applications. For S_{or} reduction applications, which is a pore-scale phenomenon, one can use the actual measured extensional viscosity values because the flow field is extensional on the localized pore-scale scale. The general notion that the apparent viscosity is the summation of extensional viscosity and shear viscosity should hold only for core-scale injectivity applications but not for pore-scale residual oil recovery applications.

5.7.5 Extensional insights into the capillary theory

Clarke et al. (2015) reported that N_c that corresponding to the onset of rapid oil mobilization is significantly lower for viscoelastic HPAM 3630 than viscous xanthan gum (Figure 5.5). Since the N_c was calculated using the core-scale pressure gradients (in psi/ft), the authors made a claim that extensional viscosity is encompassed into the N_c. Authors also discounted extensional viscosity as the mechanism for additional S_{or} reduction shown by viscoelastic HPAM 3630. The extensional resistance of HPAM 3630 solutions and xanthan gum solutions, used by Clarke et al. (2015) are compared (Figure 5.8 a, b, c). HPAM shows more resistance to capillary breakup, due to its elastic characteristic when compared with purely viscous xanthan gum (Figure 5.8 a). Maximum extensional viscosity at the critical D_e is higher for HPAM 3630 than xanthan gum by more than

2 orders (Figure 5.8b and Table 5.1). The extensional viscosity of HPAM 3630 and xanthan gum is not similar and the claim that the extensional viscosity is incorporated into the N_c (calculated in the psi/ft) is not correct. Hence we are refuting the author's claim of discounting the extensional viscosity as the reason for additional S_{or} reduction shown by viscoelastic polymers. As discussed before for residual oil recovery applications, the apparent viscosity is not the summation of actual extensional viscosity and shear viscosity. Apparent viscosity is directly proportional to both core scale pressure drop and N_c. But residual oil recovery is a pore-scale phenomenon and the critical N_c that gives an estimate on the driving viscous force required to mobilize the residual oil is calculated based on the pore-scale parameters (Stegemeier 1977). Moreover, viscoelastic polymers show transient extensional/ normal stress resistance only at the pore scale (Nguyen 1999; Wang et al. 2007). Therefore using the N_c that is calculated based on the core-scale pressure measurements (in psi/ft) for representing the viscoelastic polymer's residual oil recovery potential is not ideal. This is the reason that CDC curve generated using viscoelastic polymers showed rapid oil mobilization at the N_c value lower value than critical N_c (Clarke et al. 2015). One of the ways to rectify and represent CDC curve for polymer enhanced oil recovery processes can be by incorporating extensional viscosity in N_c calculation. Since the value of extensional viscosity for viscoelastic HPAM 3630 is significantly higher than xanthan gum, the modified N_c of HPAM 3630 will be higher and represent oil mobilization beyond critical N_c.

To prove this rational, S_{or} reduction data reported by Qi et al. (2017) for HPAM 3630 and glycerin are analyzed together with experimental viscosity values measured in this study. The authors reported S_{or} reduction after the HPAM 3630 polymer flood, performed at the N_c lower than the critical N_c (0.0001). However, as per the capillary theory, residual oil cannot be mobilized unless the N_c overcomes the critical N_c (Peter 2002). Therefore, the capillary theory is considered to be invalid in the case of viscoelastic polymers with the conventional definition of N_c (Xia et al. 2007; Guo et al. 2014). On the other hand, CaBER experiments showed that viscoelastic HPAM 3630 solutions provided significantly higher resistance to the capillary breakup than viscous glycerin (Figure 5.13a). At critical strain rate, the extensional viscosity of HPAM 3630 and glycerin are 570 Pa.s and 1 Pa.s respectively (Figure 5.13 b and Table 5.1).

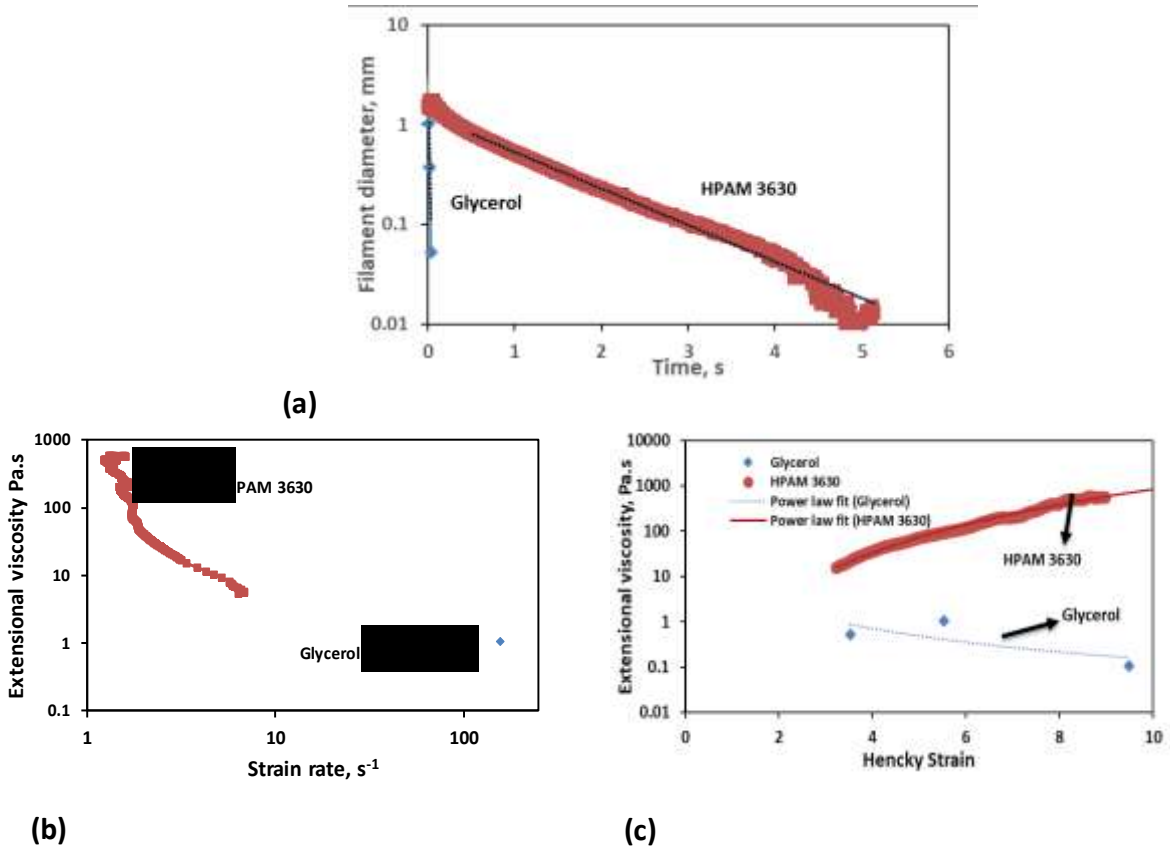

Figure 5.13: *a) Filament diameter vs time plot for HPAM 3630 and glycerin, reported by Qi et al. (2017) and the UCM fit to the linear elastic regimes for the determination of relaxation time b) Extensional viscosity as a function of generated strain rate plot showing the sharp rise in the extensional viscosity around the critical Deborah number c) Power law fit to the extensional viscosity vs Hencky strain values around the critical Deborah number for the determination of strain hardening index.*

As discussed before, extensional viscosity plays a role on the residual oil recovery at the pore-scale and the viscous force in the N_c should therefore incorporate extensional viscosity. Measured extensional viscosities were used for calculating modified N_c (N_{ce}). N_c and N_{ce} are represented by the Eq.5.2 and Eq.5.3.

$$N_c = \frac{\mu_a * \upsilon}{\sigma} \tag{5.2}$$

$$N_{ce} = \frac{\mu_e * \upsilon}{\sigma} \tag{5.3}$$

where

μ_a is the apparent viscosity, cP

μ_e is the extensional viscosity, cP

υ is the velocity, $m.s^{-1}$;

σ is the interfacial tension, $mN.m^{-1}$

The conventional N_c calculated using apparent viscosity and N_{ce}, calculated using the extensional viscosity at the critical D_e is plotted against the final residual oil saturation observed during polymer flooding for HPAM 3630 and glycerin (Figure 5.14).

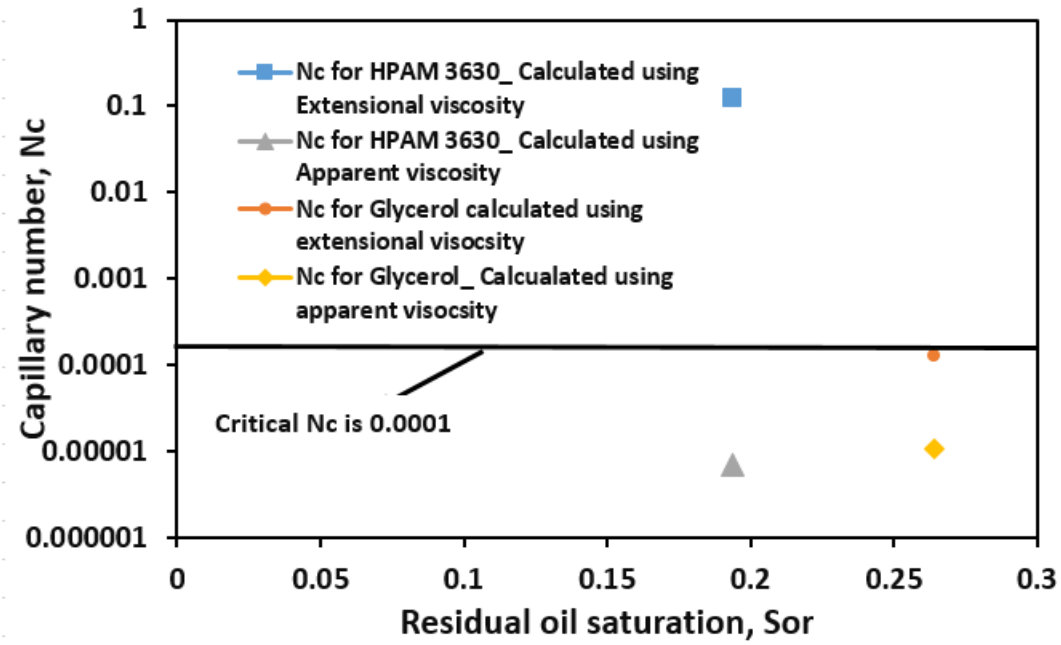

Figure 5.14: Sor vs capillary number calculated using extensional and apparent viscosity

Reported critical N_c of Bentheimer sandstone is also shown by the black line in Figure 5.14. Conventional N_c values for glycerin and HPAM 3630 are in the lower range ~ 0.000049 and 0.00001, whereas the N_{ce} values for glycerin and HPAM 3630 are 0.0001 and 0.087, respectively. Since the N_{ce} for HPAM 3630 was higher than the critical value (0.001), S_{or} reduction was observed; however this wasn't the case for glycerin. Thus, the capillary theory which is invalid for explaining the S_{or} reduction during viscoelastic polymer flooding with conventional N_c (Guo et al. 2014; Qi et al. 2017) can be validated with the N_{ce} calculated using the extensional viscosity (Figure 5.14).

5.7.6 Extensional insights into residual oil recovery potential of high saline viscoelastic polymer solutions

Erinick et al. (2018) reported that high saline viscoelastic polymer solutions with low Deborah number corresponded to the higher S_{or} reduction than the low saline viscoelastic polymer solutions with high Deborah number. Deborah number was calculated using the oscillatory rheology. However, the authors doubted the role of polymer viscoelastic effects on the S_{or} reduction. In this work, experimental results of Erinick et al. (2018) are reinvestigated using extensional rheological measurements

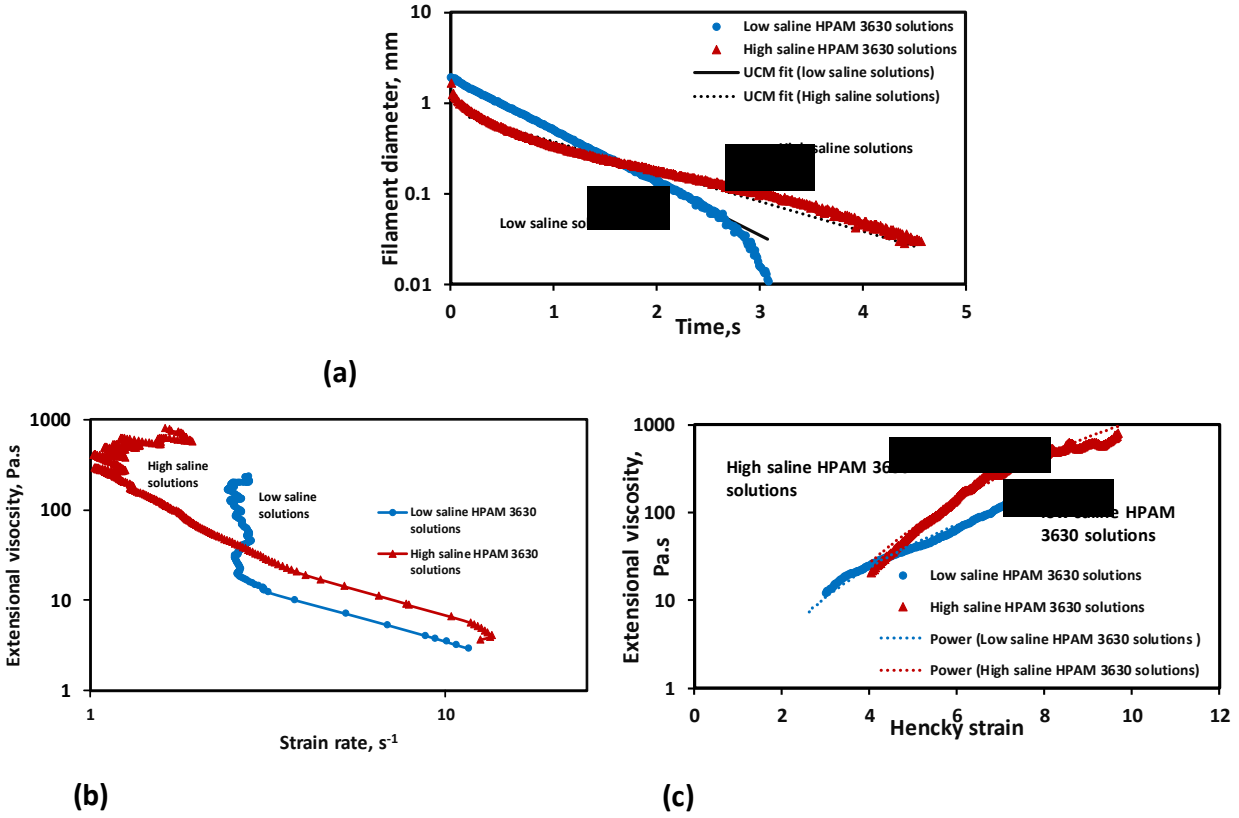

Figure 5.15: *a)Filament diameter vs time plot for 3548 ppm HPAM solutions at 24300 ppm salinity (High saline solutions) and 1200 ppm HPAM polymer solutions at 1400 ppm (low saline HPAM solutions), used by Erinick et al. 2018 b) extensional viscosity vs strain rate plot c) extensional viscosity vs strain value around the critical Deborah number.*

The breakup time of high saline HPAM 3630 solution and low saline HPAM 3630 solutions are 4.56 and 3.09 seconds respectively (Figure 5.15a). Extensional break up time of high saline solutions is higher than the lower saline solutions. The extensional relaxation time of high saline HPAM 3630 solutions and low saline HPAM 3630 solutions are 0.44 seconds and 0.22 seconds

(Table 5.1). The oscillatory relaxation time of high saline polymer and low saline polymer solutions are reported to be 0.12 seconds and 1.9 seconds respectively. Further, the maximum elongational viscosity at the critical D_e and the strain hardening index of the high saline solutions are 813 Pa.s and 4.05. These values are 228 Pa.s and 2.66 respectively (Figure 5.15 b, c and Table 5.1). In the extensional field, the high saline polymer solutions exhibit more elastic characteristics. Strain hardening index that quantifies the ability of the polymer to generate resistance during elongation and maximum extensional viscosity that corresponds to the stretchability and elastic-limit are significantly higher for a high saline solution than the low saline solutions. When the polymeric solutions pass from pore-body to the pore-throat, the chains elongate (Haas and Durst 1982). The higher extensional resistance offered during the course of elongation will provide the viscous force needed for overcoming the capillary force. Higher residual oil recovery by high saline solutions is indeed due to the viscoelastic effects, which is non-linear. Thus, ignoring the role of polymer's viscoelasticity (based on the linear oscillatory rheological results) on the residual oil recovery could be incorrect.

5.8 Summary

Direct extensional rheological measurements on the EOR polymers provided the following insights to the existing research questions/ hypothesis

a. Strain hardening behavior exhibited by viscoelastic HPAM that shows thinning in the bulk shear field indicates thickening shown by these polymers in porous media is due to its extensional characteristics. The complete shear thinning porous media behavior and strain loosening behavior shown by the viscous polymers confirms that porous media thickening will be shown only by the polymers that show the hardening behavior in the extensional field.
b. Higher extensional resistance shown by high Mw polymer solutions with the lowest shear resistance, when compared with low Mw with highest shear resistance indicates the Mw will influence the extensional flow behavior. Early viscoelastic onset shown by the polymers with higher extensional resistance proves the empirical claim that onset is due to the extensional resistance.
c. D_e calculated using the extensional relaxation time is the appropriate one for explaining the porous media behavior of viscoelastic polymers. Oscillatory rheology that represents

the linear viscoelastic effects is not the appropriate method to quantify the polymer viscoelastic effects for chemical EOR applications.

d. The claim by Clarke et al. (2015) that viscoelasticity can recover oil more than expected from the shear and apparent viscosity is true. However, the notion of ignoring extensional viscosity role on the S_{or} reduction based on the apparent viscosity, or conventional N_c is not correct. There is a strong correlation between extensional viscosity and S_{or}. N_c calculated in psi/ft condones the extensional effects occurring at the pore-scale. After all, the critical N_c is calculated on pore scale and residual oil recovery is a pore-scale recovery.
e. The extensional viscosity of the viscoelastic polymer is significantly higher than the purely viscous glycerin. N_c of viscoelastic HPAM, calculated using the extensional viscosity is higher than the critical N_c as well as the N_c calculated using apparent viscosity. The capillary theory is validated.
f. Maximum extensional viscosity and strain hardening index of high salinity polymer solution (with low D_e) is higher than the low salinity polymer solution (with high D_e). D_e calculated using oscillatory relaxation time mask the non-linear viscoelastic effects of high saline polymer solutions. Extensional viscosity and strain hardening index are the better parameter in describing the polymer viscoelastic effect on S_{or} reduction.

Chapter 6: Does polymer's viscoelasticity influence the heavy oil sweep efficiency and injectivity at 1ft/day?[5]

6.1 Introduction

Polymer flooding has been reported to be one of the successful EOR methods (Needham and Doe 1987; Sorbie 1991; Green and Willhite 1998; Sheng 2010). Several researchers have attributed the success of polymer flood to higher sweep (Moffitt and Mitchell 1983; Greaves et al. 1984; Mack and Warren 1984; Hochanadel et al. 1990; De Melo et al. 2005; Clemens et al. 2016; Kumar et al. 2016). If it is assumed, based on the conventional belief that polymer flood cannot reduce residual oil saturation (S_{or}) beyond water flood (Taber 1969; Lake 1989), theoretically both water flood and polymer flood should eventually result in the same ultimate recovery factor (Sorbie 1991). However, water flood will take an infinitely long time to recover the oil. Performing water flood for infinitely longer time will make the recovery process uneconomical. (Sorbie 1991). The higher sweep attributed to the polymer flood over water flood (Trantham and Moffitt 1982) will be reflected in the quicker production and economic gain, at least on a practical timescale. Hochanadel et al. (1990) demonstrated that the success of polymer flood over water flood can be attributed to the ability of polymer flood to recover more oil with less pore volume of injection. Fractional flow theory also indicates that the effect of polymer flood over water flood is that it enhances the oil flow, lowers the water-cut, delays the breakthrough, and aids in the quicker production of mobile oil (Sorbie 1991; Green and Willhite 1998; Peter 2002). Additional incremental oil is attributed to sweep efficiency, which is a function of flooding time or the injected pore volume (Trantham and Moffit 1982; Mack and Duvall 1984; Hochanadel et al. 1990; Green and Willhite 1998; Standnes and Skjevrak 2014).

Heavy oil reservoirs with thin payzone are not the ideal candidates for thermal EOR methods (Lyons and Plisga 2004; Delamaide et al. 2014; Azad et al. 2014). Recently, the usage of polymers for heavy oil recovery has gained increased attention (Wassmuth et al. 2009; Wassmuth et al. 2012; Delamaide 2014; Delamaide et al. 2014; Delamaide et al. 2016). Hydrolyzed polyacrylamide (HPAM), the most commonly used polymer for heavy oil recovery applications, exhibits viscoelastic characteristics (Delshad et al. 2008; Magbagbeolo 2008; Seright et al. 2011a,b; Sheng et al. 2015; Lotfollahi et al. 2016a,b; Qi et al. 2017; Azad and Trivedi 2017; Azad et al. 2018a;

[5] A version of this chapter was accepted for publication in SPE reservoir evaluation and engineering journal with revisions.

Azad et al. 2018b; Azad and Trivedi 2018; Azad and Trivedi 2019). The behaviour of viscous polymer and viscoelastic polymer are different in porous media, even though both the polymer exhibit thinning behavior in the shear field (Seright et al. 2009; Clarke et al. 2015). Viscoelastic polymer contributes to a higher residual oil recovery than viscous polymer (Clarke et al. 2015; Qi et al. 2017). Contradicting opinions exist on polymer's role on S_{or} reduction beyond waterflood residual oil (Wang et al. 2000; Wang et al. 2001; Xia et al. 2004; Xia et al. 2007; Jiang et al. 2008; Seright 2011; Vermolen et al. 2014; Clarke et al. 2015; Azad and Trivedi 2018c). Seright (2011) reported the positive influence of viscoelastic effects on the S_{or} reduction of 190 cP heavy oil. Vermolen et al. (2014) reported that viscoelastic effects do not have a significant role in S_{or} reduction of 300 cP heavy oil. Seright et al. (2018) didn't observe the influence of polymer's viscoelasticity on the S_{or} reduction of 990-1610 cP heavy oil. When it comes to polymer's viscoelastic effects, its effect on sweep efficiency has not been studied extensively.

Viscoelastic effects are expected to occur only at high rates (Gogarty 1967; Marshall and Metzener 1967; Seright et al. 2009; Seright 2017). However, Clarke et al. (2015) reported that the elasticity becomes dominant and contributes to higher S_{or} reduction even at a typical flux rate of 1ft/day. Since most parts of the reservoir away from the wellbore are likely to have lower flux, the contribution of elasticity to sweep efficiency at ~1ft/day requires a detailed study. In an attempt to history match the polymer's viscoelastic effects on oil recovery, Chen et al. (2011) accounted the sweep and displacement efficiency of polymer flooding through polymer's viscosity and elasticity respectively. Chen et al. (2011) accounted for the sweep through polymer's viscosity and displacement through polymer's elasticity. While it is proved by many researchers (Wang et al. 2000; Wang et al. 2001; Xia et al. 2004; Xia et al. 2007; Jiang et al. 2008; Clarke et al. 2015; Qi et al. 2017) that elasticity of the polymer solution has an effect on the microscopic displacement, there is no concrete proof that viscoelastic polymer with relatively higher viscosity provides higher sweep efficiency. Veerabhadrappa et al. (2013) reported that polymer with high elasticity provides a more stable displacement of 15 cP oil at 10 ft/day than the polymer with similar viscosity. However, the relative roles of viscosity and elasticity of viscoelastic polymers on sweeping the mobile heavy oil recovery at a typical reservoir flooding rate of 1ft/day is not explored. Askahri and Nagunti (2008) reported that the higher the polymer's concentration, the higher the recovery factor. Knight and Rudy (1977) performed polymer flooding using two different polymers at the same concentration but with different molecular weight (Mw). The authors reported that the

polymer with higher Mw corresponds to higher viscosity, higher screen factor, and higher recovery. Clarke et al. (2015) reported that the polymer with high concentration and low Mw provided higher shear resistance than the polymer with a low concentration and high Mw. However, high Mw polymer with low concentration but higher elastic turbulence corresponded to higher residual light oil recovery at 1ft/ day in the low permeable core. The relative role of concentration and Mw on the heavy oil recovery at low flux rate requires an investigation. Seright (2010) reported that reduced injectivity affects the economics of the heavy oil project more than the cost of the chemical itself. Polymer possessing an intense shear thickening regime corresponds to the higher apparent viscosity at a higher rate, which reduces the injectivity (Seright et al. 2009; Lotfollahi et al. 2016b). The relative role of concentration and Mw on the injectivity at higher rates also requires a comparison at the typical highly permeable heavy oil recovery conditions. Shear rheology is alone considered for polymer screening during heavy oil recovery applications (Wassmuth et al. 2009; Delamaide et al. 2014). The displacing polymer solutions are subjected to both shear and extensional resistance in porous media. Extensional rheology is overlooked in polymer selection criteria. The role of extensional rheology on heavy oil recovery and injectivity needs to be investigated. Clarke et al. (2015) reported that S_{or} to water flood was attained in low permeable light oil reservoirs. The ability of water flood to attain residual heavy oil recovery in high permeable conditions need to be ascertained and compared with light oil recovery conditions. Considering these research gaps, this study is designed to 1) study the extended waterflood potential to attain S_{or} during heavy oil recovery and 2) identify the polymer's dominant rheological behavior affecting a) the sweep efficiency during heavy oil recovery at 1 ft/day and b) injectivity at high fluxes. The importance of incorporating the extensional rheological parameters in polymer selection criteria for heavy oil recovery applications is emphasized.

6.2 Methodology

6.2.1 Polymer solutions used in this study

Two viscoelastic HPAM polymers, Flopaam 3130 and Flopaam 3630 (hereinafter referred to as HPAM 3130 and HPAM 3630), supplied by SNF Floerger, are used (Table 6.1). The composition of the brine used in the polymer preparation is shown in Table 6.2. The polymer solutions were prepared by low-speed mixing at 200 rpm using a magnetic stirrer for 24 hours.

Table 6.1: *Properties of viscoelastic polymers used in this study*		
Name	**Molecular weight (MDa)**	**Concentration (%)**
HPAM 3130	3.6	1.46
HPAM 3630	18-20	0.225

Table 6.2: *Composition of brine used in this study*	
Salts	**Concentration (mg/L)**
NaCl	3115
$NaHCO_3$	1310
Na_2SO_4	239
KCl	54
$CaCl_2.2H20$	96
$MgCl_2.6H20$	93
Total	4907

6.2.2 Oil used in this study

Heavy oil from the Western Canadian reservoir with a viscosity of 640 cP is used during the oil recovery experiments.

6.2.3 Capillary breakup extensional rheometer

A capillary breakup extensional rheometer (HAAKE CaBER, Thermo Scientific) was used for characterizing the extensional rheological properties of the viscoelastic polymers. The details about the CaBER operational procedure and the advantages it has over other methods for the extensional characterization of EOR polymers are detailed in section 3.2.2 of this thesis, as well as in our previous publications (Azad and Trivedi 2017; Azad et al. 2018a; Azad et al. 2018b; Azad and Trivedi 2018; Azad and Trivedi 2019). The conducted extensional rheology revealed that extensional resistance of HPAM 3630 characterized by higher Mw, lower concentration, and

lower shear resistance is higher than the extensional resistance of HPAM 3130 characterized by low Mw, high concentration, and higher shear resistance.

6.2.4 Porous media studies

6.2.4.1 Core flood set up

Two oil recovery experiments and two single-phase experiments were carried out using the 6-inch long horizontal cylindrical core holder with a 1.25 inch diameter. Polymer solutions were are displaced upwards towards the core from the accumulators during polymer injection with a syringe pump (ISCO Tyredene, 500D). Pressure drop was monitored using a pressure transducer. A schematic of the core flood set up used for the experiment is shown in Figure 6.1.

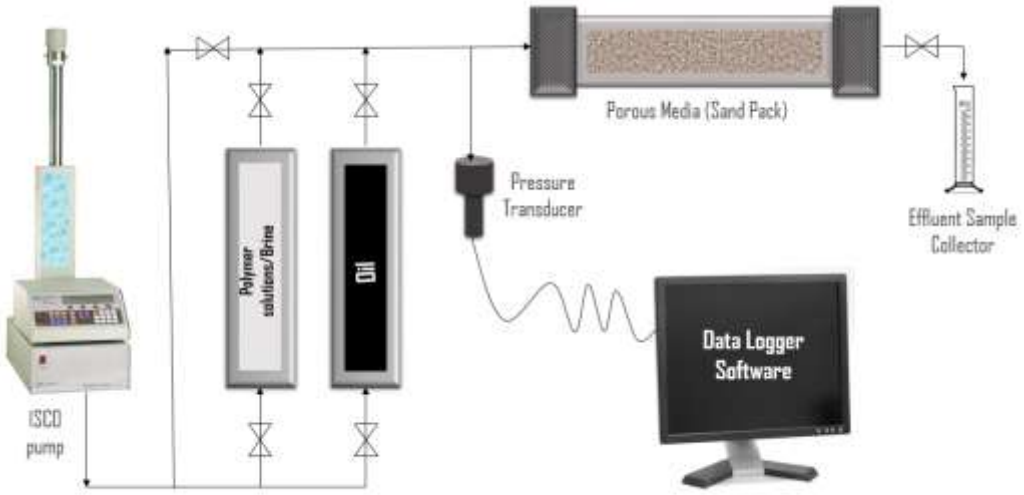

Figure 6.1: *The schematic of the core flood setup used for oil recovery experiments*

The core was packed with 40-mesh sand size uniformly in both the experiments. After water saturation, pore volume (PV) and permeability measurements were performed in all the experiments (Table 6.3). After oil saturation (in recovery experiments), water flooding was conducted at a rate of 2 ft/day to investigate the ability of water flood in attaining the residual heavy oil saturation. The water flooding was continued for 11 PV injection. Polymer solutions were injected into the sand pack at 1ft/day. Oil recovery corresponding to the injection of HPAM 3130 and HPAM 3630 was noted for 0.5 PV. Pressure drop was also recorded during both the experiments. During single-phase experiments, after pore volume measurements brine is injected into the sand pack at five different fluxes (shear rates) ranging from ~17 ft/day ($20s^{-1}$) to ~90

ft/day ($100s^{-1}$), respectively. The pressure drop, when it reached a stable value after ~ 2-3 PV injection, was noted and used for permeability measurements. Polymer solutions were injected into the core at the same flux rates until the pressure remained stable for 3-4 PV. The stable pressure drop attained during polymer injection is divided by the stable pressure drop attained during primary water injection at the respective rates to calculate the resistance factor.

Table 6.3: *Petro physical properties of the cores used in this study*

Experiment type/polymer	Porosity	Permeability (Darcy)
Multi-phase HPAM 3130	0.418	3.451
Multi-phase HPAM 3630	0.42	3.462
Single-phase HPAM 3130	0.41	3.423
Single-phase HPAM 3630	0.413	3.438

Shear rate is determined using the Eq. 6.1.

$$\dot{\gamma} = \alpha \frac{q}{A * \sqrt{k * \phi}} \tag{6.1}$$

Where

$\dot{\gamma}$ = Shear rate, s^{-1}

α = Constant factor taken to be 1.

q = injection rate, $cm^3.s^{-1}$

k = permeability, cm^2

ϕ = porosity

6.3 Results and discussions

6.3.1 Shear rheology

The bulk shear rheological data of HPAM 3130 and 3630, reproduced from Howe et al. (2015), is shown in Figure 6.2. Both the polymers show a shear thinning phenomenon up to $100s^{-1}$. The shear viscosity of HPAM 3130 around the shear rates (determined using Equation 5) of $1.25s^{-1}$ and $95s^{-1}$ (corresponding to the flux rate of 1 ft/day and 90 ft/day, respectively) are ~1500 cP and ~ 200

cP, respectively. For HPAM 3630, these values are significantly lower at ~300 cP and ~27 cP, respectively. Based on these results, it is clear that concentration plays a more major role than Mw during shear flow.

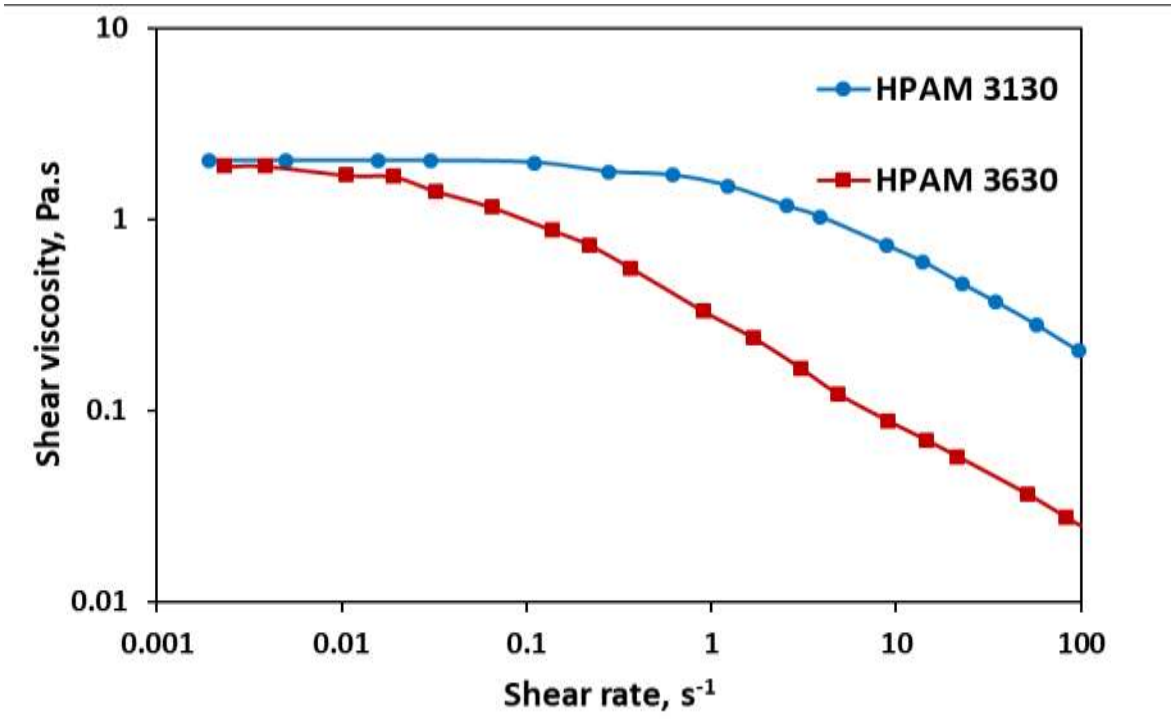

Figure 6.2: *Shear rheology of HPAM 3130 and HPAM 3630, reproduced from Howe et al. 2015*

6.3.2 Extensional rheology

6.3.2.1 Filament diameter vs time for HPAM 3130 and HPAM 3630

The mid-point filament diameter of the two polymer samples monitored during filament thinning and subsequent breakup time, reveals that HPAM 3630 characterized by high Mw shows higher extensional resistance to break up than HPAM 3130 characterized by higher concentration (Figure 6.3). Higher Mw indicates that the flexibility of individual polymer chains is higher. During polymer stretching, the individual flexible chains are stretched and the chains characterized by higher Mw (HPAM 3630) possess more resistance to the extensional flow. In shear flow, the polymer chains get rolled, resulting in the cancellation of stress and therefore the effect of elasticity was not observed in the shear field (Azad and Trivedi 2017; Azad et al. 2018a; Azad et al. 2018b).

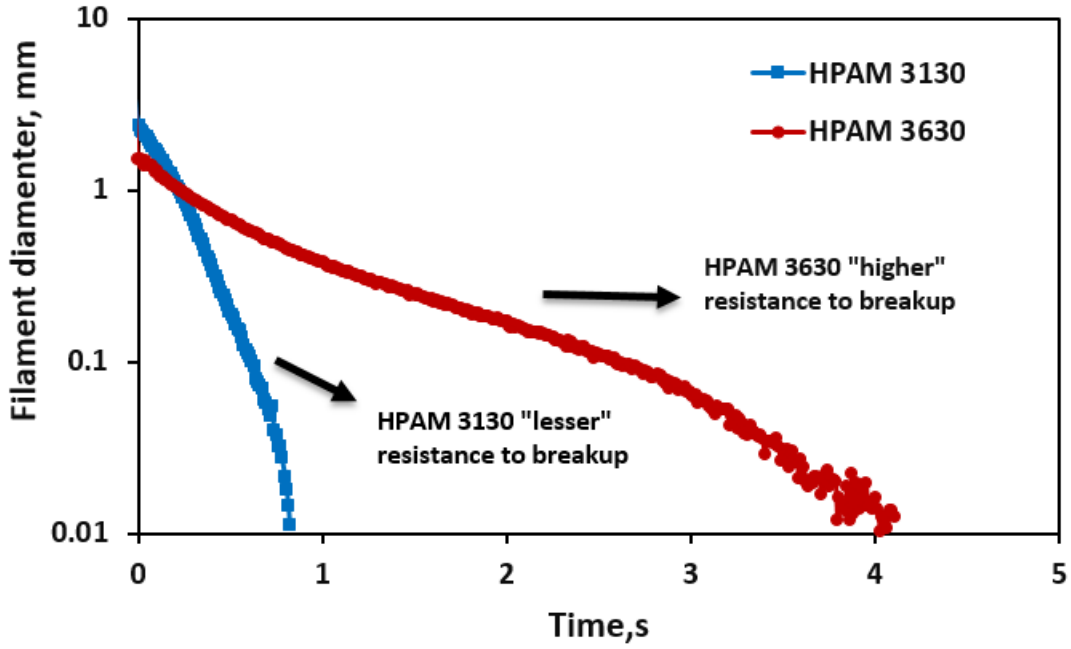

Figure 6.3: *Filament diameter vs time data for HPAM 3130 and HPAM 3630*

6.3.2.2 Extensional relaxation time for HPAM 3130 and HPAM 3630

The extension relaxation time for polymer solutions obtained using the UCM model (Eq. 3.1; Figure 6.4 and Figure 6.5), are reported in Table 6.4. The extensional relaxation of time HPAM 3630 is higher than HPAM 3130 by almost one order, which is an indication that HPAM 3630 is highly elastic over HPAM 3130.

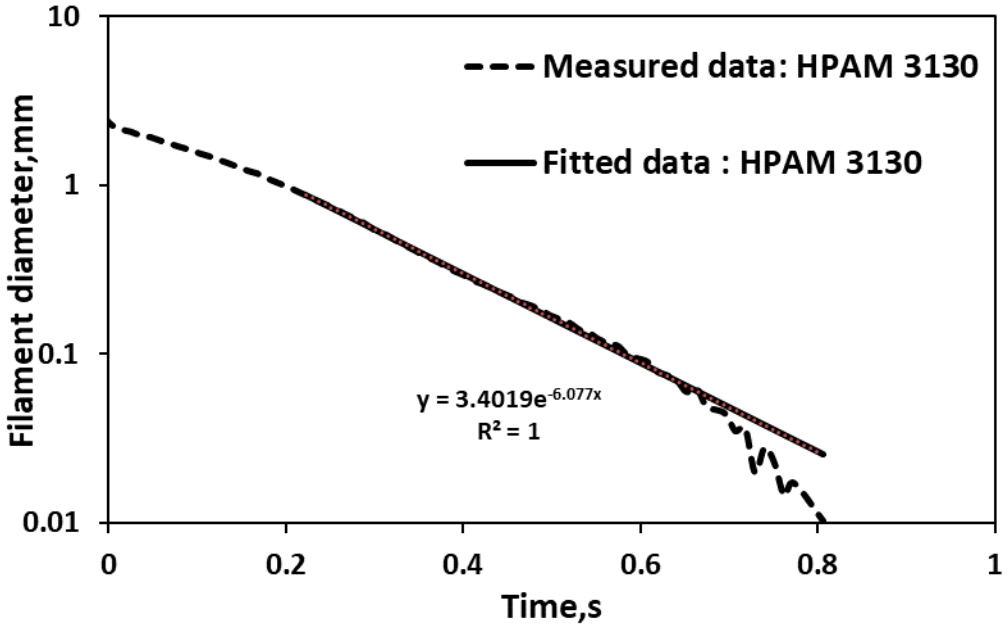

Figure 6.4: *UCM model fit to the elastic regime of the filament diameter vs time data for HPAM 3130*

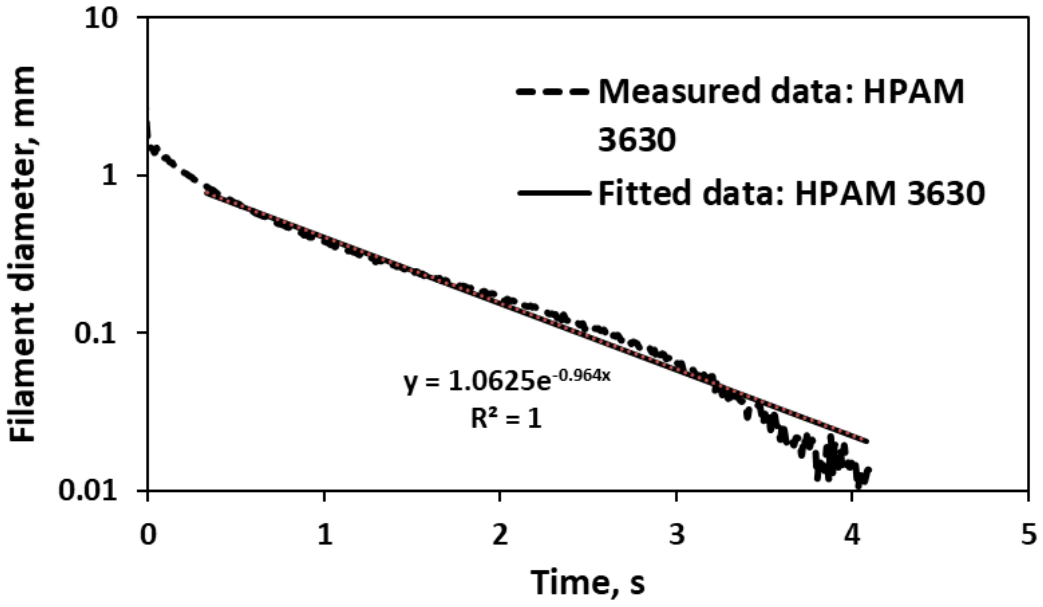

Figure 6.5: *UCM model fit to the elastic regime of the filament diameter vs time data for HPAM 3630*

Table 6.4: *Measured extensional rheological parameters of HPAM 3130 and HPAM 3630*			
Sample	τ_{ext} (s)	$\mu_{\max@cr.De}$,Pa.s	n_2

HPAM 3130	0.055	46	2.94
HPAM 3630	0.345	340	3.81

6.3.2.3 Extensional viscosity of HPAM 3130 and HPAM 3630

The extensional viscosity of HPAM 3130 and HPAM 3630, plotted with respect to Hencky strain and strain rate using Eq. 3.3, Eq. 3.4, and Eq. 3.6, is shown in Figure 6.6 and Figure 6.7. The details about the maximum extensional viscosity, corresponding to the elastic limit, can be found elsewhere (Entov and Hinch 1997; Kim et al. 2010; Clasen 2010; Azad and Trivedi 2017; Azad et al. 2018a; Azad et al. 2018b; Azad and Trivedi 2018; Azad and Trivedi 2019). Around the critical Deborah number, HPAM 3130 and HPAM 3630, with respective relaxation times of 0.055 seconds and 3.45 seconds, should deform at rates of $12s^{-1}$ and $1.9s^{-1}$, respectively. The maximum extensional viscosity of the HPAM 3130 and HPAM 3630 solutions corresponding to these rates are ~46 Pa.s and ~340 Pa.s, respectively (Figure 6.7 and Table 6.4). The higher extensional viscosity of the HPAM 3630 is due to the relatively longer asymptotic rise of the strain rate to its critical value, which indicates its higher elasticity.

Although both the polymers exhibit strain hardening behavior in the extensional field (Figure 6.6), the degree of hardening is less with HPAM 3130. The strain hardening index is obtained by power-law fit to the extensional viscosity vs. strain data around the critical Deborah number. The strain hardening index of HPAM 3130 and HPAM 3630 are 2.94 and 3.81, respectively (Table 6.4). The extensional viscosity of HPAM 3630 is significantly higher than that of HPAM 3130. Therefore, it can be said that the concentration influences the shear viscosity, whereas Mw influences the extensional viscosity.

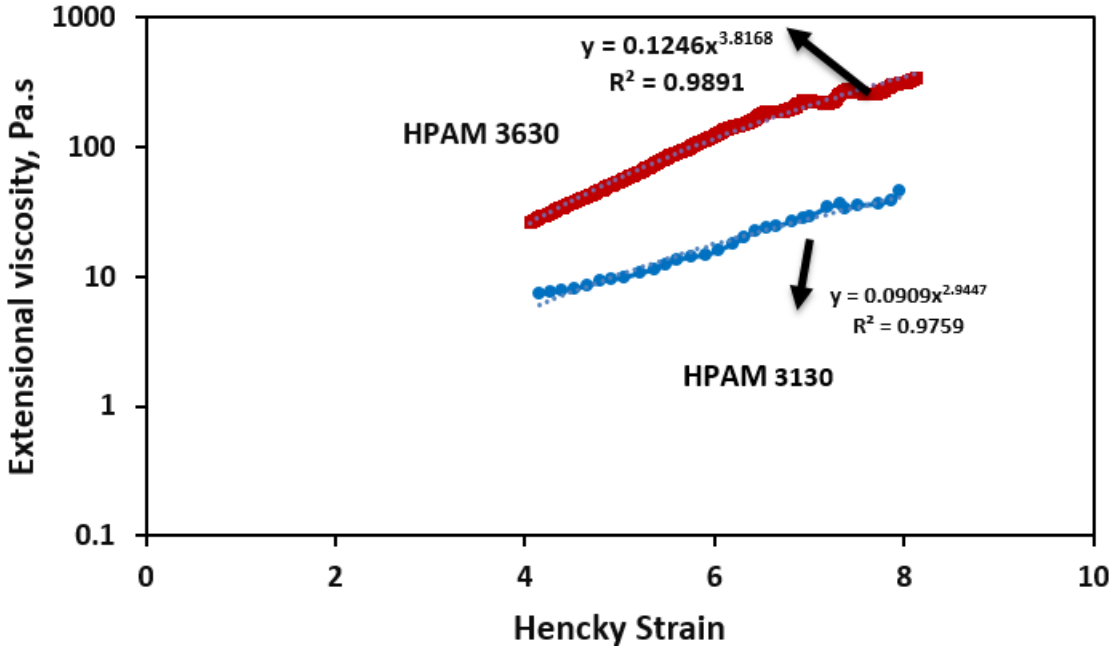

Figure 6.6: *Extensional viscosity as a function of generated strain for HPAM 3130 and HPAM 3630*

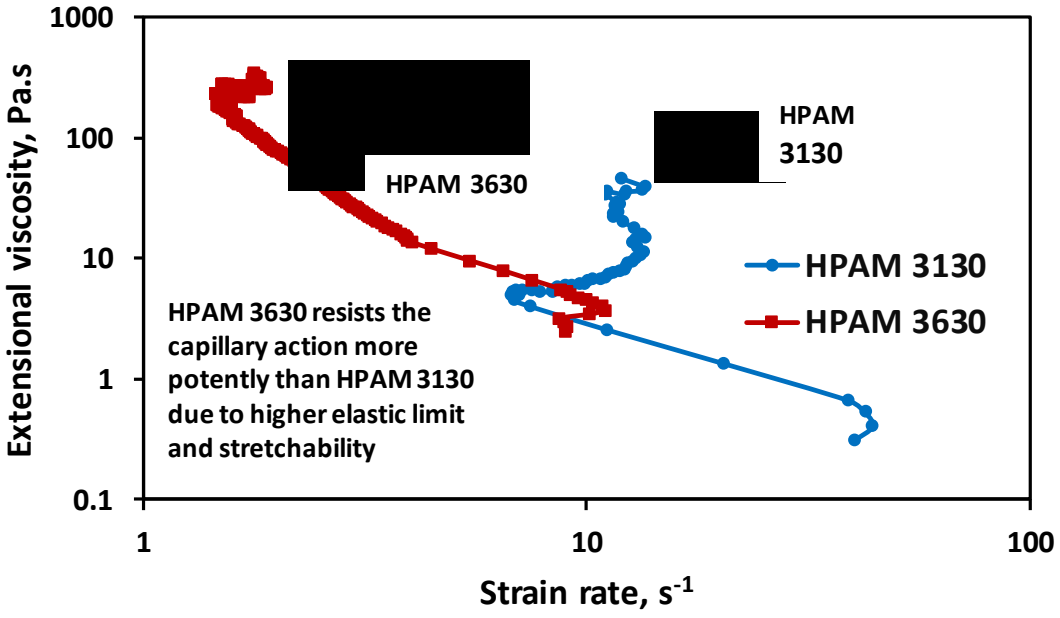

Figure 6.7: *Extensional viscosity as a function of generated strain rate for HPAM 3130 and HPAM 3630*

6.3 Porous media results

6.3.1 Does prolonged water flooding results in the residual heavy oil saturation?

After 11 PV of water injection, residual heavy oil saturation is not attained in Experiment 1 and Experiment 2 (Figure 6.8). However, Clarke et al. (2015) reported that residual oil saturation was attained in a light oil saturated core after ~1.5 PV of water flood. They used 40 cP oil and core

with ~450 mD permeability where the possibility of viscous fingering is less (Green and Willhite 1998) and the possibility of capillary trapping is high (Peter 2002). Comparing the experiments performed in this work with the results of Clarke et al. (2015), it is clear that water flood continued to recover heavy oil at the lower oil-cut. The decline in the oil saturation with respect to the pore volume indicates that the remaining oil can still be recovered if water flooding is continued. Therefore, there can be a significant amount of mobile heavy oil upswept. The limiting factor for the waterflood performance in the high permeable heavy oil reservoir is its poor sweep efficiency, whereas for the light oil reservoir, it is its poor displacement efficiency.

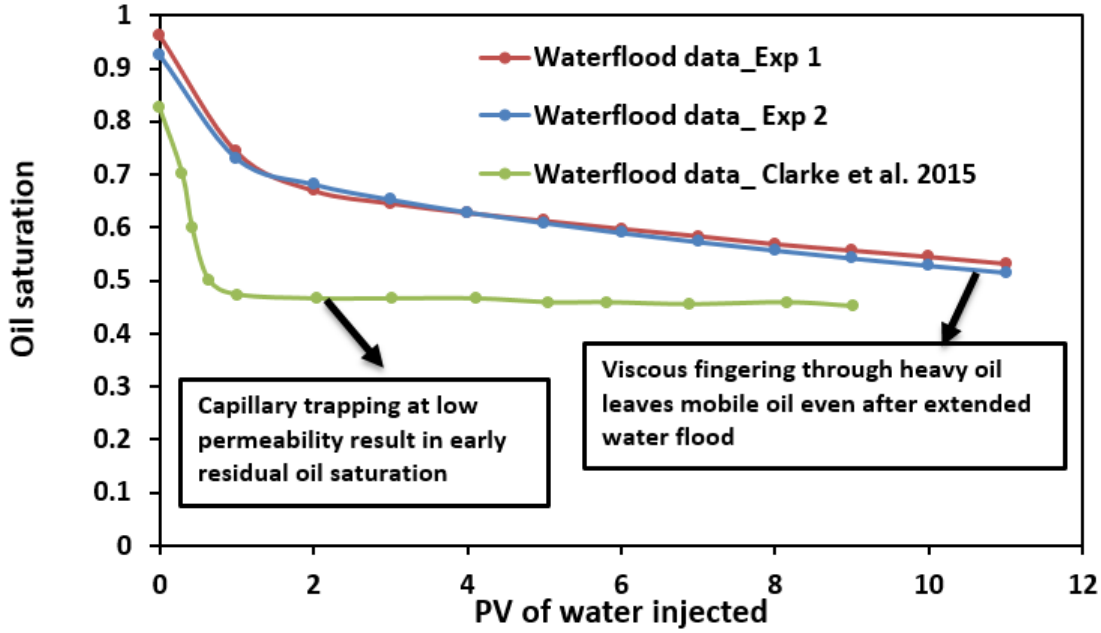

Figure 6.8: *Reduction in heavy oil saturation during the prolonged water flooding*

6.3.2 The dominant factor in the increasing the sweep recovery for heavy oil reservoirs: extensional or shear resistance?

Sweep efficiency determines the ability of the injection slug to sweep the oil to the total pore volume of oil present in the reservoir. Higher sweep efficiency means a higher production rate. After 11 PV water injections, the remaining oil saturation in Experiment 1 and Experiment 2 are 0.53 and 0.51. In terms of recovery factor, these values are 44.68% and 45.18%. The incremental recovery factor during subsequent 5.5 PV injections of HPAM 3130 and HPAM 3630 are shown in Figure 6.9.

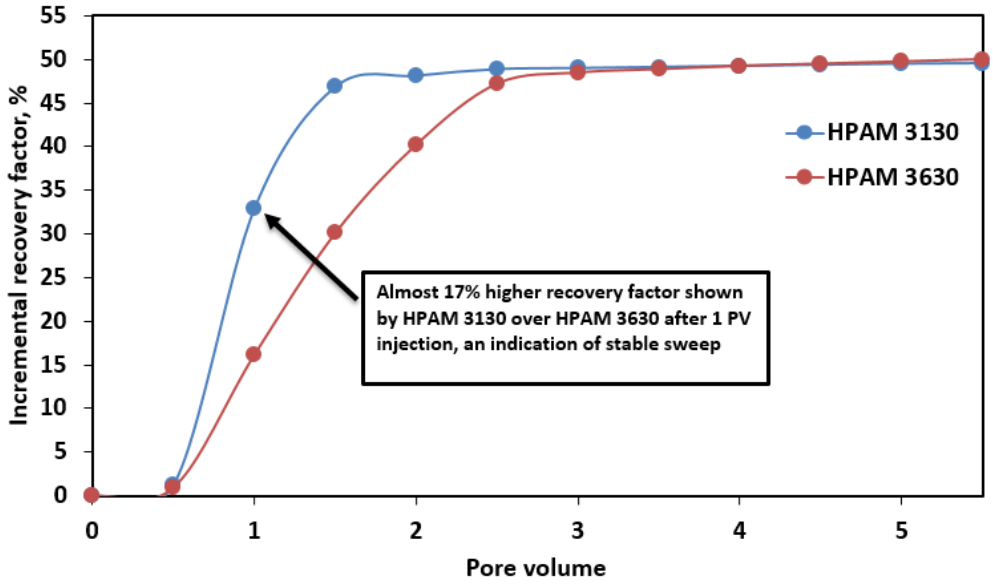

Figure 6.9: *Incremental recovery factor due to 5.5 PV of HPAM 3130 and HPAM 3630 injections*

The ultimate recovery for both polymer solutions is similar (~95%); however, HPAM 3130 showed faster recovery. The incremental recovery factor corresponding to the first PV injection of HPAM 3130 solution and HPAM 3630 solution are ~33% and ~16%, respectively. The difference in recovery is ~17%, which is similar to the observation made by Seright (2010). Here, it is important to note that the shear viscosity of HPAM 3130 is 1500 cP and the maximum elongational viscosity is 46 Pa.s, whereas the HPAM 3630 has a shear viscosity of 300 cP and a maximum extensional viscosity of 340 Pa.s. These results indicate that HPAM 3130, having higher shear viscosity, has the ability to recover the mobile oil (that is not trapped by the capillarity but bypassed by water) quicker and increases the sweep efficiency. Therefore, it can be said that the polymer solution with higher extensional resistance will not increase the sweep efficiency of the heavy oil studied here. Hence, the viscoelastic effects do not appear to play a significant role when it comes to increasing the sweep of mobile heavy oil at low flux conditions.

6.3.2.1 Why polymer with higher shear resistance contributes to better sweep at 1ft/day for heavy oil?

The pressure generated by injecting HPAM 3630 (with higher extensional resistance) at 1ft/day is lower than that of HPAM 3130 (Figure 6.10). Clarke et al. (2015) reported that the apparent viscosity generated during the injection of HPAM 6040 (with higher elastic turbulence) at 1 ft/day ($\sim \dot{\gamma}$ of $2s^{-1}$) is lower than that of HPAM 3130 in a 450 mD core (Figure 6.11b). The shear viscosity of HPAM 3130 is higher than that of HPAM 3630 and HPAM 6040 (Figure 6.2; Figure 6.11a).

This implies that the overall core scale pressure drop (or apparent viscosity) is dominated by the shear forces both in 3.4 Darcy sand (used in this work) and 450 mD core (used in Clarke et al.'s [2015] work). Contrary to higher sweep shown by HPAM 3130 (with higher shear resistance) in this work (Figure 6.9), HPAM 6040 (with lesser shear resistance) corresponded to the higher residual oil recovery in Clarke et al.'s work (Figure 6.11c). A careful look into Figure 6.11b reveals the HPAM 6040 used by Clarke et al. (2015) begins to show the viscoelastic onset before 1 ft/day ($\sim \dot{\gamma}$ of $2s^{-1}$). Elongational flow begins to occur in the core after the viscoelastic onset (Delshad et al. 2008; Magbagbeolo 2008; Sheng 2010). However, the higher apparent viscosity shown by HPAM 3130 (with higher shear resistance) at 1ft/day indicates that core scale pressure is not dominated by the elongational forces at low fluxes even in the 450 mD core (Clarke et al. 2015). The domination of elongational effects in the form of elastic turbulence causes the trapped residual oil mobilization from the pores in 450 mD sandstone core (Clarke et al. 2015).

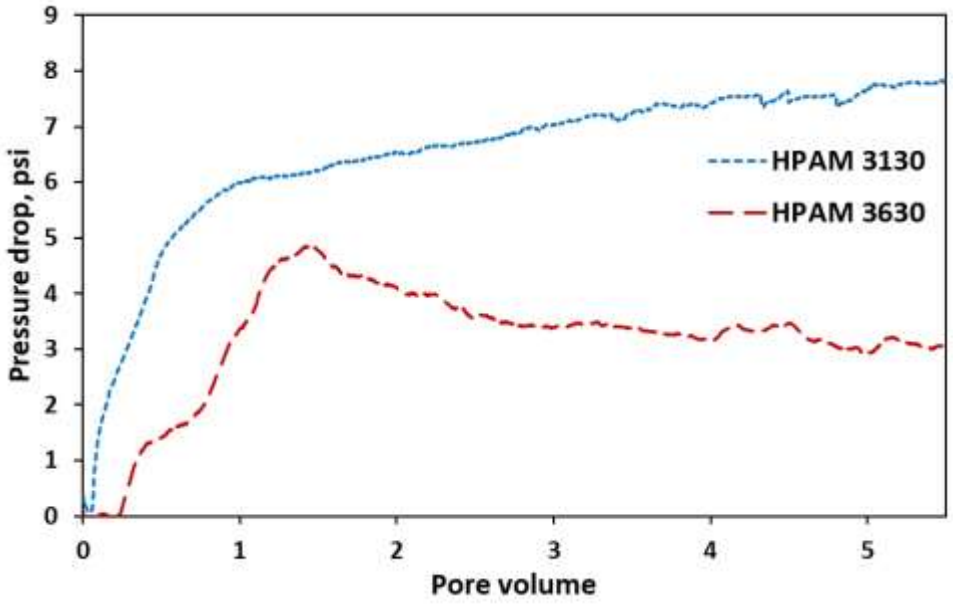

Figure 6.10: *Pressure drop exhibited by HPAM 3130 and HPAM 3630 at 1ft/day during oil recovery experiment*

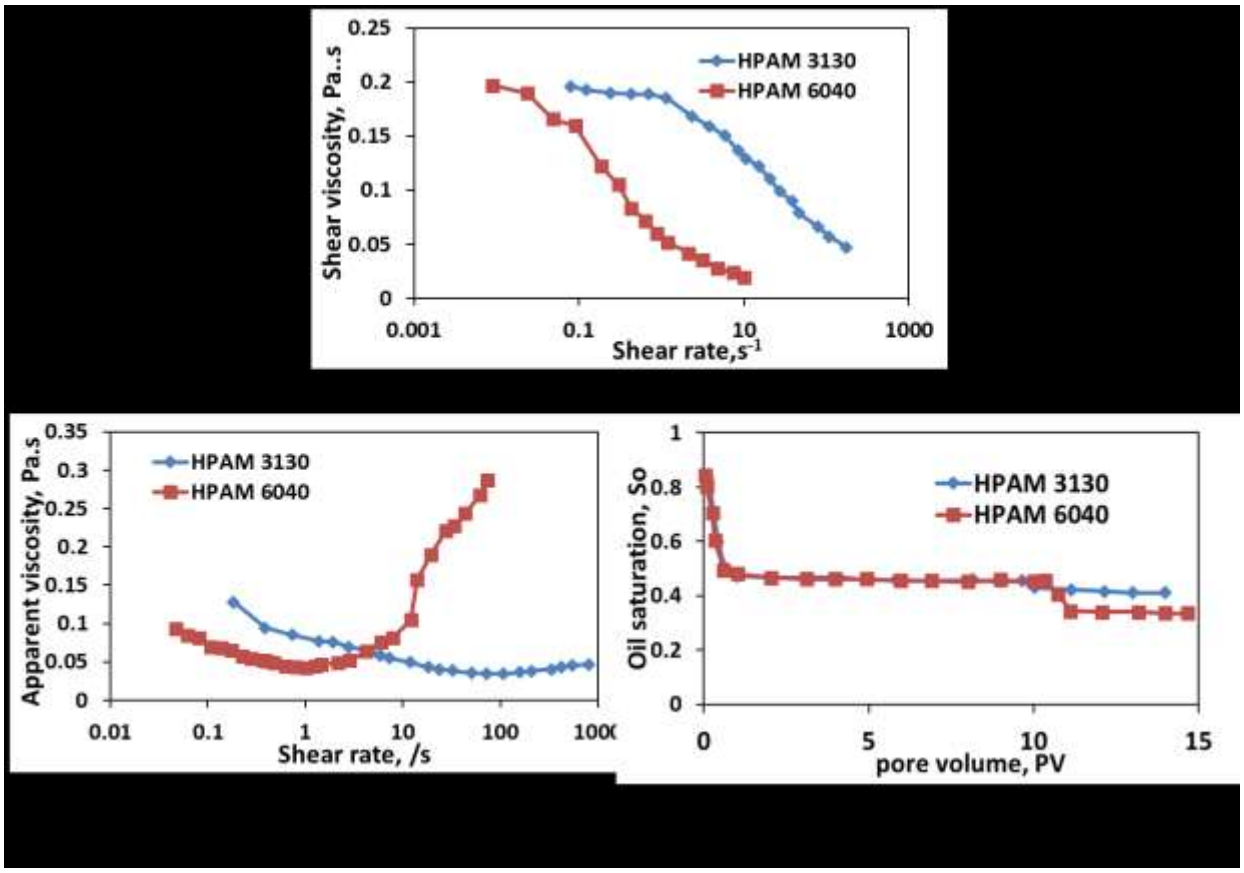

Figure 6.11: *a)Shear rheological plot reproduced from Clarke et al. (2015) for HPAM 3130 and HPAM 6040 b)Apparent viscosity plot reproduced from Clarke et al. (2015) for HPAM 3130 and HPAM 6040 c) Oil Recovery plot reproduced from Clarke et al. (2015) for HPAM 3130 and HPAM 6040*

Residual oil recovery is a pore-scale phenomenon and the critical capillary number that gives an estimate on the polymer viscous force needed to overcome the trapping capillary force is calculated based on the pore dimensions (Peter 2002). Normal stresses tend to act only in the pore throat region. Afsharpoor et al. (2012) reported that the pore-scale pressure drop of the viscoelastic polymer is higher than the overall core-scale pressure drop. Zamani et al. (2015) reported that extensional viscosity becomes dominant as the aspect ratio increases. However, the extensional viscosity becomes less dominant when the pore throat length is higher. Wang et al. (2007) reported that micro-force (normal/extensional stresses) gets nullified at the core scale and the pressure gradient is dominated by the macro-force or the shear force because shear flow predominates most of the regions at the core scale. Therefore, the HPAM 6040 possessing higher elastic characteristics corresponded to the higher residual oil recovery, despite possessing lower core-scale pressure at 1ft/day (Clarke et al. 2015). However, high core-scale pressure is essential for sweeping the mobile

heavy oil from the inlet to the outlet. Thus, the contribution of HPAM 3630 with higher extensional resistance in sweep efficiency of heavy oil at low flux conditions is significantly lesser than the contribution of HPAM 3130 with higher shear resistance.

High pressure at the core scale is an indication that the polymer solution possesses a higher apparent viscosity/resistance factor throughout the course of propagation. The role of extensional viscosity on permeability reduction has been documented in several studies (Han et al. 1995; Chauveteau et al. 2002; Besio et al. 1988; Azad et al. 2018a; Azad et al. 2018b). The higher core-scale pressure drop shown by HPAM 3130 with lesser extensional resistance is therefore solely due to its higher shear resistance. Higher apparent viscosity leads to effective mobility control, quicker recovery and better sweep of mobile heavy oil.

6.3.3 Should polymer screening criteria incorporate extensional viscosity for heavy oil recovery applications?

Comparing the results presented in Figure 9 with the ones from Clarke et al. (2015), the overall recovery factor during the experiments conducted in this study is higher despite the fact that oil is 12 times more viscous than the light oil used by Clarke et al (2015). However, the permeability of sand pack used in the conducted experiments is almost 10 higher than low permeable core used by Clarke et al. (2015). There is no notable difference seen in the ultimate recovery factor between the two experiments conducted using HPAM 3130 and HPAM 3630 polymers. It is an implication that HPAM 3630 with higher elasticity doesn't contribute significantly towards residual heavy oil recovery. Similar observations were reported by other researchers during heavy oil recovery. Vermolen et al. (2014) observed the S_{or} reduction with 9 cP light oil but not with the 300 cP heavy oil in Bentheimer core. Recently, Seright et al. (2018) performed the series of polymer flooding experiments at various polymer concentration using the Cactus Lake cores saturated with 1610 cP heavy oil. The authors did not report a significant residual heavy oil recovery with the high concentrated polymer flooding. Vik et al. (2018) didn't observe S_{or} reduction during the recovery of 500 cP heavy oil from Bentheimer core samples. However during light oil recovery, viscoelastic polymer were reported to contribute to S_{or} reduction. Cottins et al. (2014) and Clarke et al. (2015) observed the S_{or} reduction with 34 cP and 7 cP light oil in sandstone core. Qi et al. (2017) and Erinick et al. (2018) observed the S_{or} reduction with 120 cP and 114 cP oil in Bentheimer sandstone. Seright (2011) observed the S_{or} reduction during the recovery of 190 cP heavy oil in hydrophobic core. It appears that as the viscosity of oil goes lower, the elastic influence on the

residual oil recovery becomes significant. Residual oil recovery is an interplay between the driving viscous force and trapping capillary force. Residual oil recovery is well represented by the capillary number (Eq.6) (Green and Willhite 1998). Guo et al. (2014) reviewed the usage of capillary number and highlighted the importance of oil viscosity and mobility ratio. In the conventional capillary number term the effect of oil viscosity is usually ignored. Abrams (1975) modified the conventional capillary number (Eq. 6.2) by incorporating the effect of oil viscosity (Eq.6.3).

$$N_c = \frac{v * \mu_w}{\sigma_{o-w}} \qquad \text{(Eq.6.2)}$$

$$N_c = \frac{v * \mu_w}{\sigma_{o-w}} * (\frac{\mu_w}{\mu_o}) \qquad \text{(Eq.6.3)}$$

where

N_c = Capillary number

v = flux rate, $cm.s^{-1}$

σ_{o-w} = interfacial tension, $mN.m^{-1}$

μ_w = viscosity of displacing water-phase, cP

μ_o = viscosity of displaced oil-phase, c

Comparing the Eq.6.2 and Eq. 6.3, is clear that as the oil viscosity goes higher, N_c becomes lower for the same interfacial tension, flux and displacing fluid's viscosity. This implies that an additional force is preventing the mobilization of viscous oil at the pore-scale. The elasticity of the polymers doesn't seems to play a convincing role on the mobilization of the residual heavy oil at the pore-scale. While it is clear that extensional rheological property of polymer doesn't contribute to the sweep efficiency of mobile heavy oil significantly, its role on the residual heavy oil recovery is uncertain and questionable. Polymer's shear resistance controls the sweep efficiency, which is a major requirement in the heavy oil polymer flood projects. Therefore, shear rheology is sufficient to screen the viscoelastic polymers based on their potential to recover the mobile heavy oil.

6.3.3.1 Is there a role of extensional rheology on the injectivity?

Injectivity of the polymer solutions is indirectly proportional to the shear thickening regime at higher flux rates (Seright et al. 2009; Lotfollahi et al. 2016a). Shear thickening leads to the higher apparent viscosity at higher fluxes. The single-phase experiment conducted in this work shows that HPAM 3630 exhibits shear thickening, whereas HPAM 3130 exhibits shear thinning even up to ~90ft/day. At 90 ft/day (~95s^{-1}), the apparent viscosity of HPAM 3630 and HPAM 3130 are 92 cP and 72 cP, respectively (Figure 6.12).

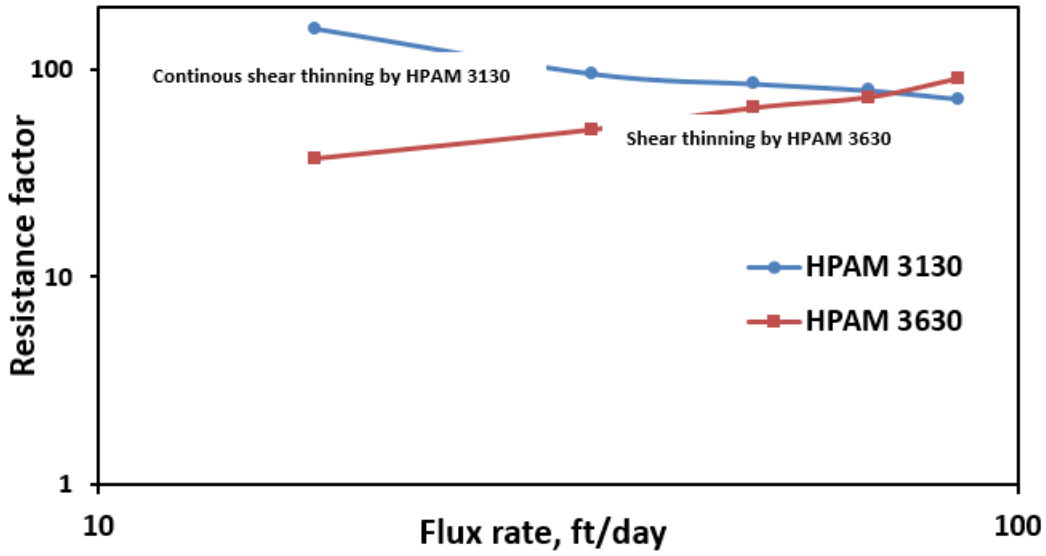

Figure 6.12: *Resistance factor exhibited by HPAM 3130 and HPAM 3630 at higher flux rates during single-phase experiments*

The shear viscosity of HPAM 3630 is lower than that of HPAM 3630 throughout the range of shear rates (Figure 6.2). Injectivity will be overestimated when only shear rheological measurements are used. Nonetheless, until now polymer selection for heavy oil recovery applications have been made based on the shear viscosity (Wassmuth et al. 2009; Delamaide et al. 2014). Much of the literature has empirically speculated the extensional viscosity of polymers as the reason for their shear thickening phenomenon (Hirasakhi and Pope 1974; Haas and Durst 1982; Masuda et al. 1992; Ranjbar et al. 1992; Delshad et al. 2008; Magbagbeolo 2008; Stavland et al. 2010; Sheng 2010; Taha 2010; Kim et al. 2010; Zamani et al. 2015; Van den Ende 2015). Extensional rheological measurements performed using CaBER revealed that extensional relaxation time, maximum elongational viscosity at the critical Deborah number, and strain hardening index are higher for HPAM 3630 than HPAM 3130 (Figure 6.6, Figure 6.7, and Table

6.4). Since HPAM 3130 has weaker extensional resistance, no thickening is observed in porous media and consequently, the injectivity is higher at higher flux.

A mobility ratio of one or less is deemed to be desirable for early polymer flood projects (Maitin 1992). In the case of 1000 cP heavy oil, Seright (2010) reported that the recovery and relative profit will be higher for the case employing 12000 ppm polymer corresponding to 1000 cP, if only the cost of the chemical and price of the oil are considered. However, he concluded that if the injectivity is taken into account, flooding with a highly concentrated viscous polymer solution can delay profitability. As per his observation, a higher concentration is better for heavy oil recovery but detrimental for injectivity. In this work, we are reporting that HPAM 3130 with higher concentration but lower molecular weight yield both higher injectivity and sweep efficiency than higher molecular weight HPAM 3630 at a lower concentration. If the injectivity is a more important factor than the cost of the chemical (Seright 2010), HPAM 3130 with higher shear resistance and lesser extensional resistance seems to be a better option than HPAM 3630. One may consider doing high concentration, low PV polymer flood (with low Mw polymer) in a certain region of poorly water flooded reservoir characterized by the presence of high mobile oil saturation for a quick return. Both enhanced sweep efficiency and injectivity will aid in a quick economic return. Regardless of the feasibility of applications, both shear and extensional characterization of EOR polymers is a must to screen them for heavy oil recovery applications, based on their recovery potential and injectivity.

6.4 Summary

- Two viscoelastic polymers (HPAM 3130 and HPAM 3630) with varying molecular weight (Mw) and concentration but similar zero shear viscosity are used in this study. A shear rheological study performed by Howe et al. (2015) revealed that low Mw polymer at a higher concentration exhibits higher resistance in the shear field than higher Mw polymer at a lower concentration. The ex-situ bulk extensional rheology performed using CaBER in this study revealed the dominant elastic behavior of HPAM 3630 over HPAM 3130. This includes
    a. the higher extensional relaxation time of HPAM 3630 (3.45 s) over HPAM 3130 (0.055 s),
    b. the higher breakup time of HPAM 3630 (4.1 s) over HPAM 3130 (0.83 s), and

c. the significantly higher extensional viscosity of HPAM 3630 (~340 Pa.s) over HPAM (~46 Pa.s) at the critical Deborah number of 0.66.

- Heavy oil core flooding experiments performed at a flux of 1 ft/day using HPAM 3130 and HPAM 3630 revealed that HPAM 3130 with higher shear viscosity contributes to the quicker recovery of mobile heavy oil unswept by the preceding 11 PV of water flood. For the initial 1 PV of polymer injection, the incremental mobile/remaining oil recovery attained by HPAM 3130 is almost 17% higher than that of HPAM 3630. The higher incremental recovery could be attributed to the very favourable mobility ratio between HPAM 3130 and heavy oil. The results signify the ability of polymer with higher concentration and higher shear viscosity to contribute to higher sweep efficiency.
- The core-scale pressure drop generated by HPAM 3130 was is more than twice the pressure drop generated by HPAM 3630 due to higher shear resistance that resulted in higher sweep efficiency at 1ft/day. Therefore, sweeping the mobile oil can be considered the core-scale phenomenon.
- Comparing the higher rate of heavy oil recovery shown by the polymer with higher shear viscosity but lower extensional resistance (HPAM 3130) in our experiments with higher residual oil recovery shown by the polymer with higher elasticity and extensional resistance (HPAM 6040) in Clarke et al.'s (2015) experiments, we conclude that extensional viscosity influences residual oil recovery and shear viscosity influences the sweep efficiency. Our observation also reinforces Chen et al.'s (2011) notion that viscosity influences the sweep.
- HPAM 3130 with higher shear viscosity corresponds to the lower apparent viscosity (72 cP) at a higher flux rate of 90 ft/day, whereas HPAM 3630 with higher extensional viscosity generated higher apparent viscosity (92 cP) at the same flux. At low fluxes, HPAM 3130 generated higher core-scale pressure than HPAM 3630, which is essential for better sweep efficiency. However, higher apparent viscosity at higher flux is detrimental to injectivity. Hence, both shear and extensional rheological characterization of polymers is a must to screen them for heavy oil recovery applications, based on their potential for recovery and injectivity.

Chapter 7: Novel Viscoelastic Model for Predicting the Synthetic Polymer's Viscoelastic Behavior in Porous Media using Direct Extensional Rheological Measurements[6]

7.1 Introduction

Polymer flooding is one of the most commonly used enhanced oil recovery (EOR) methods for improving the recovery factor in depleted oil reservoirs. Polymers are also used as mobility control agent in surfactant polymer (SP) flooding, alkali polymer flooding (AP) flooding and alkali surfactant polymer (ASP) flooding (Green and Willhite 1998). A large amount of oil remains as unswept oil in the water flooded reservoir. The amount of unswept oil after water flooding will be higher in the reservoirs characterized by high heterogeneity and high oil viscosity. Water is a Newtonian fluid with the unit viscosity that tends to channel/finger easily through high permeable streaks and high viscous oil. The added polymers viscosify the displacing slugs, control its mobility and thereby provide high sweep efficiency which is essential for higher overall recovery factor. The polymers solutions are non-Newtonian and the viscosity exhibited by them would be different at different shear rates. Shear rates are generally high near the wellbore. In the farthest part of the reservoirs, shear rates are generally low due to exposure of flood front to a larger area. Shear rates are also dependent on the injection rate, permeability, porosity etc. Reservoir characterized by the high oil viscosity requires high viscosity from polymer solutions for the optimal sweep. Injectivity is an issue with slugs providing high viscosity (Seright et al. 2009). Hydrolyzed polyacrylamide (HPAM) and Xanthan gum, the two commonly used EOR polymers (Green and Willhite 1998; Garrouch and Gharbi 2006; Seright et al. 2009; Sheng 2010), exhibit different in-situ behavior. Xanthan gum is rigid, viscous biopolymer without considerable elasticity. HPAM is the synthetic viscoelastic polymer. Viscoelasticity in HPAM provides higher in-situ viscosity than xanthan gum to the displacing slugs (Sheng 2010). Prior determination of the in-situ viscosity exhibited by the displacing slugs is essential for screening and simulation. Core flooding can be performed to determine the in-situ viscosity of polymer solutions. However, chemical EOR (cEOR) is an extensive process. Salinity variances in the reservoir necessitate core flooding to be done at different salinities. Different combinations of chemical EOR slugs include the different concentration of surfactant, polymer, and alkali. Performing core flooding with

[6] A version of this chapter has been published in Fuel and data in brief
A version of this chapter has also been filed for patent.

respect to these variables is a cumbersome process. Moreover, cores for representative reservoirs are not available in most of the cases, or obtaining the cores is an expensive process. Rheological experiments are performed to measure the viscosity at the desired shear rate and correlating them to the reservoir's shear rate by the appropriate mathematical models. Shear rheological experiments are used extensively in the oil industry for predicting the performance of polymer solutions (Cannella et al. 1988; Seright et al. 2011a, b; Han et al. 2012). Shear rheological experiments are also used for screening the chemical formulation for mobility control purpose (Azad and Sultan 2014). Carreau model, developed based on shear rheology, was successful in matching the porous media behavior for viscous biopolymers that shows thinning in both the bulk shear and porous media (Cannella et al. 1988; Seright et al. 2009).

Viscoelastic effects were deemed to cause the reduced mobility of synthetic HPAM solutions at high rates in porous media (Pye 1964; Gogarty 1967; Marshall and Metzener 1967). Marshall and Metzener (1967) correlated the viscoelastic effects with Deborah number. They reported that the viscoelastic effects become dominant in porous media when Deborah number is in between 0.1 to 10. At higher flow rates, the Deborah number increases. Smith (1970) observed that the mobility of polymer solutions decreases significantly at higher flow rates. Smith claimed that viscoelastic effects at high rates might reduce the channeling in the high permeable zone. Jennings et al. (1971) also reported the viscoelastic effects were prominent with high molecular weight polymers with flexible, linear chain structures. High rates are typically encountered around the wellbore where the injectivity is a major concern. Injectivity, defined as the measurement of ease with which the fluid can be injected into the reservoir (Hyne 1991) will be lower for viscoelastic polymers possessing higher apparent viscosity at the higher shear rate. Higher apparent viscosity results in the higher injection pressure. The excessive pressure generated during injection will result in the mechanical degradation and formation fracturing. Both degradation and unintended fracturing are undesirable and the amount of fluid that can be injected safely becomes lower in the case of viscoelastic polymers. Viscous polymer solutions exhibiting shear thinning will have higher injectivity. Viscoelastic polymers solutions exhibit thickening after a critical flow rate in the porous media (Yuan 1981; Masuda et al. 1992; Delshad et al. 2008; Magbagbeolo 2008; Seright et al. 2011a; Mansour et al. 2014; Laoroongroj et al. 2014). Thickening causes an increase in the viscosity with respect to shear rate. However, in the bulk shear field, its exhibits shear thinning. Polymer solutions that exhibit shear thinning in the shear field, exhibits thickening in the

extensional field (Barnes 2010). Carreau model that predicts the pure viscous biopolymer behavior fairly well, underestimated the apparent viscosity of the viscoelastic polymers in the porous media by a considerable margin (Delshad et al. 2008; Magbagbeolo 2008). Seright et al. (2009) studied the behavior of HPAM and biopolymer in porous media. Xanthan gum exhibits shear thinning behavior both in bulk shear field and in porous media. HPAM that exhibits shear thinning in bulk field, exhibited thickening in porous media. This was attributed to viscoelastic nature of HPAM. Predictions based on the Carreau model will result in the overestimation of injectivity that may lead to undesirable consequences such as fracturing and mechanical degradation.

The critical flow rate that results in the viscoelastic thickening may occur at the relatively lower rate experienced in the reservoir for high molecular weight polymers (Delshad et al. 2008; Clarke et al. 2016). Viscoelastic effects may result in poor injectivity. However, it influences the oil recovery positively (Masuda et al. 1992; Delshad et al. 2008; Clarke et al. 2016; Qi et al. 2017). Therefore, predicting the onset is crucial for screening or formulating the polymers solutions that could give better recovery due to viscoelasticity. Onset is not observed in the Carreau model for viscoelastic polymers solutions (Delshad et al. 2008). Thus, viscoelasticity has an influence on the injectivity and recovery. Predicting the shear thickening regime and onset is crucial for screening the polymers for optimal injectivity and recovery. Models were developed since 1970s, to quantify the viscoelastic effects (Garrouch 1999; Masuda et al. 1992; Delshad et al. 2008; Hirasakhi and Pope 1974; Heemskerk et al. 1984; Ranjbar et al. 1992; Yin et al. 2006; Kim et al. 2010 b; Stavland et al. 2010). Hirasaki and Pope (1974) developed the viscoelastic model based on the postulation that flow through varying cross-sectional pores is simply elongational. However, the physical meaning of the Hirasaki and Pope's model is lost when the Deborah number is greater than 1. Commonly used high molecular weight polymers exhibit Deborah number much higher than 1 (Qi et al. 2017). Heemskerk et al. (1984) performed detailed core flood studies to ascertain the viscoelastic onset. The authors quantified the viscoelastic effects through the critical flow rate causing the viscoelastic onsets. Also two power-law coefficients representing thinning and thickening effects were used. The conducted studies provided a detailed sensitivity analysis of polymer and porous media properties on the viscoelastic effects. However, it could not be used for quick screening as it relied completely on core flooding. Masuda et al. (1992) developed an improved version of the viscoelastic model representing the Darcy viscosity through the combination of elastic viscosity and viscous viscosity for accounting the viscoelastic effects. The

developed model was used to history match the additional oil recovery caused by the viscoelastic effects. Masuda's model depends on core flooding to determine the empirical parameters and relaxation time. Another limitation is the elastic force in the elongational part increases indefinitely when Deborah number increases. Ranjbar et al. (1992) developed a model based on the Maxwell-Fluid relation for accounting the additional apparent viscosity caused by the strain flow of viscoelastic polymer solutions. They reported that the model index to be an important parameter for viscoelastic quantification. The model index is determined through extensive core flooding experiments by observing the changes inducted to the polymer molecules before and after the reduction of injection rate and injection pressure. Garrouch and Gharbi (2006) highlighted the limitation of oscillatory relaxation time in explaining the different porous media behavior of viscous polymer and viscoelastic polymer. The author introduced a new viscoelastic number. The New number that explains the behavior of viscous polymer and the viscoelastic polymer is determined through core flood experiments. Yin-Hongjun et al. (2006) proposed the model that requires extensive core flooding experiment to calculate the apparent viscosity. Delshad et al. (2008) developed the unified apparent viscosity model (UVM) based on the postulation that the apparent viscosity of polymer solutions is the sum of shear and elongational viscosity. UVM models account for the viscoelastic thickening in the extensional part through oscillatory relaxation time, strain hardening index and maximum elongational viscosity. Deborah number is the product of the relaxation time and shear rate. UVM model addressed the limitation of previous viscoelastic models. However, UVM depends on the core flood data to predict the extensional parameters such as maximum elongational viscosity and strain hardening index. Recently, Kim et al. (2010 b) developed the empirical correlation using the generalized Maxwell model to determine relaxation time for various conditions of salinity; temperature etc. The relaxation time is used successfully in elongational dominated part of the UVM to predict the shear thickening. However, other extensional parameters such as maximum elongational viscosity and strain hardening index are obtained through core flood experiment. Stavland et al. (2010) developed an extended viscoelastic model that can predict four different viscosity regimes (Newtonian, shear thinning, shear thickening and shear degradation) exhibited by viscoelastic polymers in porous media. The empirical parameter required to model the shear thickening regimes are determined through extensive core flood experiments.

From these studies, it is clear that the polymer chain becomes stretched at large deformation that results in the eventual extensional flow. Large deformation occurs at a high rate that is typically encountered around the wellbore. Reservoirs characterized by the low permeability also induce large deformation to the viscoelastic polymer solutions. In the extensional field, the flow is in the direction of the stress. Contrarily in the shear field, the flow is in the direction perpendicular to applied stress. Extensional flow is the strong flow that causes the thickening of viscosity with respect to the flow rate (Barnes 2010; Taha 2010). A polymer that thins in shear field thickens in the porous media and in bulk extensional field. Previous viscoelastic models developed by various researchers (Garrouch 1999; Masuda et al. 1992; Delshad et al. 2008; Hirasakhi and Pope 1974; Heemskerk et al. 1984; Ranjbar et al. 1992; Yin et al. 2006; Kim et al. 2010 b; Stavland et al. 2010) relies on core flood data to predict the synthetic polymer's viscoelastic behaviour in porous media such as viscoelastic onset rate and shear thickening regime. Carreau model can predict the shear thinning behavior of viscous polymers such as xanthan gum through bulk shear rheological measurements. However, the Carreau model fails to predict the onset rate and shear thickening regime of viscoelastic polymers, and under predicts the apparent viscosity of viscoelastic polymers by a considerable margin (Delshad et al. 2008). Despite recognizing the extensional contribution to viscoelastic thickening, there was no effort being made to develop a universal model based on the direct extensional rheological measurements. Developing such a model for viscoelastic polymers will get rid of core flood experiments and is the objective of this study.

Unlike shear rheology measurements, extensional measurements of the low viscous polymer slugs remain the challenge. The difficulties involved in the extensional characterization of low viscous EOR polymers have been well documented in our previous publications (Azad and Trivedi 2017; Azad et al. 2018 a; Azad et al. 2018 b). Capillary breakup extensional rheometer (CaBER), reported to handle low viscous fluid (Rodd et al. 2005) is used in this research for extensional characterization.

In this work, we propose a novel viscoelastic model (similar to UVM) that can predict the onset, apparent viscosity in the shear thickening regime through measurable extensional parameters. Extensional parameters include the $\mu_{\max}$ (maximum elongational viscosity), n_2 (strain hardening index) and τ_{ext} (extensional relaxation time). These parameters are determined from filament drainage experiment performed using CaBER based on the upper convected Maxwell (UCM) model, finite extensible non-linear elastic (FENE) theory, and power law model. The proposed

model is validated by matching the 14 core flood experiments reported in the literature. Average downscaling power factor to maximum elongational viscosity and subtrahend to the strain hardening index are used for scaling down from the pure elongation in bulk extensional field to the combination of shear and extensional in the porous media. The accuracy of the prediction by the proposed model is compared with both the UVM (core flood-dependent) and Carreau model (core flood- independent) models.

7.2 Methodology

7.2.1 Polymer solutions

Shear thickening data exhibited by viscoelastic polymer solutions in porous media are extracted from published literature. The details about the polymer type, molecular weight, concentration and brine salinity are listed in Table 7.1.

Table 7.1: *Properties of viscoelastic polymers used in 14 experiments*

Data set	Authors	Polymer	Concentration (ppm)	Molecular weight (million Daltons)	Salinity
1	Magbagbeolo 2008	HPAM 3630	1500	18-20	20040 ppm (640 ppm Ca2+ ions)
2	Magbagbeolo 2008	HENGFLOC 63020	1500	20	20040 ppm (640 ppm Ca2+ ions)
3	Magbagbeolo 2008	HENGFLOC 63020	1500	20	20040 ppm (20 ppm Ca2+ ions)
4	Magbagbeolo 2008	HENGFLOC 63026	1500	26	20040 ppm (20 ppm Ca2+ ions)
5	Yuan 1981	Pusher 700	1000	8	10000 ppm
6	Yuan 1981	Pusher 700	1000	8	1000 ppm
7	Yuan 1981	Pusher 700	1000	8	10000 ppm

8	Mansour et al. 2014	HPAM 3630	850	18-20	20000 ppm
9	Mansour et al. 2014	HPAM 3630	850	18-20	10000 ppm
10	Mansour et al. 2014	HPAM 3630	600	18-20	10000 ppm
11	Seright et al. 2011a	HPAM 3230	2500	6-8	25200 ppm
12	Masuda et al. 1992	HPAM 3530	200	16-17	0 ppm
13	Laoroongroj et al. 2014	HPAM 3630	500	18-20	21963 ppm
14	Laoroongroj et al. 2014	HPAM 3630	500	18-20	21963 ppm

HPAM 3230, HPAM 3530, HPAM 3630 and pusher 700 polymers were obtained from SNF Floerger (USA). Hengfloc 63020 and Hengfloc 63026 were obtained from Henju Beijing (China). The details about the polymer type, molecular weight, concentration and brine salinity are listed in Table 7.1. The polymer solutions were prepared by low speed mixing at 200 rpm using a magnetic stirrer for 24 hours. All the samples were used in the experiments without any prefiltration. The results attained using the polymer preparation are consistent with the reported values. For example, the relaxation time of polymer used in experiments 1 to experiments 7 is in agreement with the reported relaxation time value (Magbagbeolo 2008). Extensional rheological measurements were performed on the prepared polymer solutions using CaBER to attain filament diameter vs time data. The relevant extensional parameters are determined from the filament diameter vs time plot using appropriate theories. Attained extensional parameters are coupled into the UVM and downscaling factors to be used in AT-VEM for predicting the experimental apparent viscosity data are determined. Assumptions made by Magbagbeola (2008) for validating the UVM model are considered in this work. This includes that the permeability during polymer flow is same as the brine permeability and experimental apparent viscosity is calculated using the brine permeability. Permeability is considered to be anisotropic. Shear rates corresponding to the experiment 11 to 14 are converted to the shear rates, used by Magbagbeola (2008) for validating

the UVM. The generalized steps involved in the model development are shown in the flow chart (Figure 7.1).

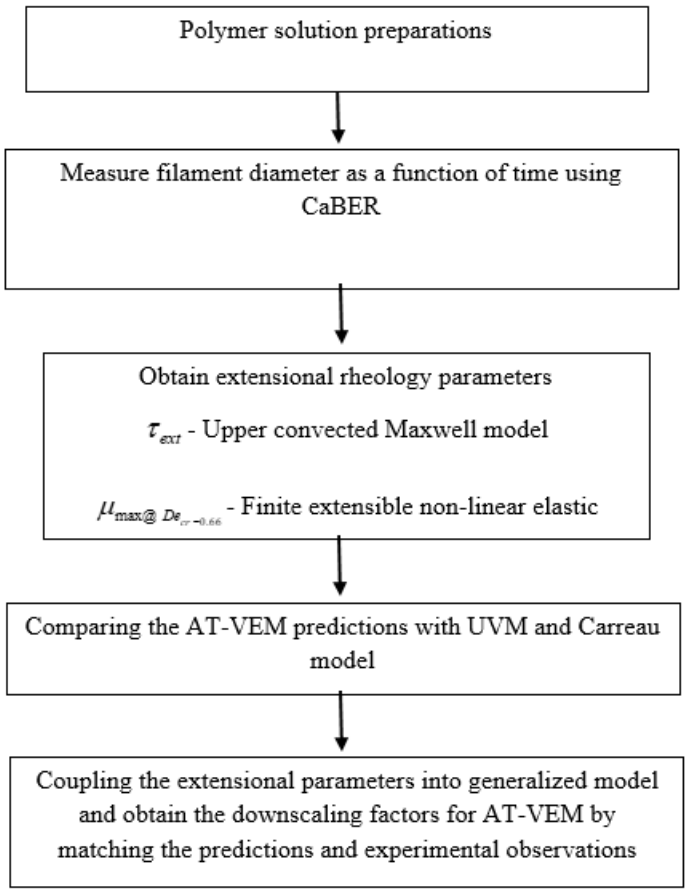

Figure 7.1: *Methodology in AT-VEM development*

7.2.2 UVM model

Unified apparent viscosity model represented by Eq. 7.1 is the sum of shear and extensional viscosity (Delshad et al. 2008; Magbagbeolo 2008).

$$\mu_{app} = \mu_{\infty} + \left(\mu_p^o - \mu_{\infty}\right)\left[1 + \left(\lambda * \gamma\right)^{\alpha}\right]^{\frac{(n-1)}{\alpha}} + \mu_{\max} * \left[1 - \exp\left(-\left(\beta * N_{Deb}\right)\right)\right]^{n_2 - 1} \quad (7.1)$$

Shear parameters such as μ_{∞}, μ_p^o, λ, α and n are determined through bulk shear rheology using Carreau model. Extensional parameters such as $\mu_{\max}$ and n_2 are determined from core flooding

experiments. Relaxation time used for Deborah number calculation is determined by oscillatory rheology.

7.2.3 Extensional rheological parameters to be used in AT-VEM

The readers are suggested to refer to section 3.2.1 for more details about the CaBER experimental procedure. Also, the readers can refer to section 3.2.1 for details about the CaBER theories, used in the calculation of the extensional relaxation time, maximum extensional viscosity at the critical Deborah number and strain hardening index. The readers can also find more information in our previous publications (Azad and Trivedi 2017; Azad et al. 2018a; Azad et al. 2018b; Azad and Trivedi 2018a; Azad and Trivedi 2018 b; Azad and Trivedi 2019). As discussed in section 3.2.1, upper convected Maxwell (UCM) model is used in the determination of extensional relaxation time from the filament diameter vs time plot (Eq. 3.1). During filament drainage, Entov and Hinch (1997) derived that fluid relaxes at the rate 2/3rd of strain rate using finite extensible non-linear elastic theory. The details of the derivation can be found in the Entov and Hinch (1997). Filament drainage is constant at the critical Deborah number of 0.66 and it represents the maximum elastic limit where the elongational viscosity tends to exhibit maxima (Clasen et al. 2010; Kim et al. 2010 a). The maxima around the critical Deborah number will be used as $\mu_{\max@De_{cr-0.66}}$ in the proposed model. Deborah number is the product of relaxation time and shear rate. The relaxation time is determined using the UCM model. Critical strain rate is determined by dividing the critical Deborah number by the relaxation time. During filament drainage, the fluids get strained that results in the increase of apparent viscosity with respect to strain, contrary to shear thinning that occur in the shear field. During filament drainage, the polymers tend to show an increase in the extensional viscosity with respect to strain. Extensional viscosity vs strain is fitted with the power law to calculate the average n_2

7.2.4 Coupling with UVM model

Core flood experiments that have shear thickening regime are selected from the literature to calibrate the model and compare the results. The properties and operational conditions of these literature reported experiments are shown in Table 7.1. Extensional rheology measurements are performed for the polymer at the operational conditions reported in Table 7.1. Extensional parameters are determined using the CaBER theories.

7.2.5 Determination of average downscaling factors

Modified UVM model incorporating the measured extensional parameters are used to match the experimental values using non-linear regression. Average factor needed to bring the pure elongation to a combination of shear and elongation is determined. The extensional viscosity of viscoelastic polymers in 100% extensional field is more than 3 orders higher than shear viscosity. Thus, average downscaling power factor is determined to downscale the maximum elongational viscosity attained at the critical Deborah number in the extensional field to the combination of shear and extensional field in the porous media. Index determined using the power law model indicates the degree of thickening or thinning exhibited by the polymer solutions. The degree of thickening in the porous media is less than the degree of thickening in the pure extensional field. Thus, subtrahend is determined to bring the strain hardening index measured using power-law fitting in the extensional field to the combination of shear and extension experienced in the porous media. Universal constant of 0.01 used along with Deborah number in UVM model is maintained in this model. Deborah number incorporating the shear rate controls the differences in the apparent viscosity caused due to the permeability.

7.3 Results and discussion

Laser micrometer monitors the mid-point diameter of the polymeric solutions during filament drainage. The monitored mid-point diameters of polymeric solutions during filament thinning are shown as a function of time in the semi-log plot in appendix (Figures A.1a to A.14a). The linear decline in the semi-logarithmic plot represents the intermediate time scale where the fluid drainage is balanced between the driving surface tension and polymer's elasticity (Entov and Hinch 1997). τ_{ext} is determined by fitting the UCM model (Equation 3.1) to the linear part of the filament diameter vs time data in the semi-log plot. The extracted and fitted data highlighted by the blue line are shown (Figures A.1a to A.14a). The slope represents the longest relaxation time (Plog et al. 2004; Rodd et al. 2005; Clasen et al. 2006; Bhardwaj et al. 2007). The average value of τ_{ext} is calculated from the slope using the Eq. 3.1. The calculated values of τ_{ext} are shown (Table 7.2).

Table 7.2: *Measured Extensional Parameters to be used in AT-VEM*

Data set	τ_{ext} (s)	$\mu_{\max,De_{Cr-0.66}}$	n_2	n

1	0.086	147000	3.520	0.755
2	0.048	26000	3.484	0.828
3	0.107	165000	3.586	0.72
4	0.146	285000	3.597	0.662
5	0.032	37000	3.372	0.75
6	0.0623	48000	3.029	0.6
7	0.032	37000	3.372	0.72
8	0.198	250000	3.975	0.49
9	0.216	340000	4.092	0.42
10	0.169	220000	3.948	0.5
11	0.0371	37000	3.602	0.7
12	0.073	30000	2.989	0.58
13	0.097	160000	3.531	0.483
14	0.097	160000	3.531	0.483

Comparing the Figures A.1a to A.14a with Table 7.2, it appears that τ_{ext} is generally higher for the polymeric solutions with the longer breakup time. τ_{ext} of experiment 1, 2, 3 and 4 are similar to the longest relaxation time determined using rouse method (Magbagbeolo 2008). The Deborah number used in most of the viscoelastic models (Masuda et al. 1992) is a product of the relaxation time and the shear rate. Higher Deborah number represents the higher elasticity of the viscoelastic polymeric solutions (Marshall and Metzener 1967; Delshad et al. 2008; Clarke et al. 2016). However, the Deborah number alone cannot be used for modeling the shear thickening regimes (Delshad et al. 2008). Extensional viscosity is used for modeling the shear thickening regimes by Delshad et al. (2008) and Stavland et al. (2010).

The extensional viscosity and strain rate determined from filament diameter data, using Eqs. 3.4 and 3.6 are shown (Figures A.1b to A.14b). The behavior of extensional viscosity with respect to strain rate in the uniaxial extensional field is different than the conventional behavior seen in the shear field. The typical extensional viscosity vs strain rate plot, generated from the CaBER experiment is shown earlier in Figure 3.2.

The maximum elongational viscosity of polymer solutions around the critical Deborah number corresponded to its elastic limit (Clasen 2010). Using the extensional relaxation time, the critical strain rate corresponding to the critical Deborah number of 0.66 is determined by the simple division. The sharp increase in the elongational viscosities around the critical strain rate for each experiment can be seen (Figure A.1(b) to A.14(b)). Maximum elongational viscosity that corresponds to the elastic limit around the critical Deborah number of 0.66 is noted and shown as in Table 7.2. In general, higher the relaxation time, lower the critical strain rate and higher the maximum elongational viscosity around the critical strain rate/critical Deborah number. For example, polymer solution used in experiment 4 and 5 possess the extensional relaxation time of 0.146 seconds and 0.032 seconds (Table 7.2). Critical strain rate corresponding to regime 3 for experiment 4 and 5 are around $5s^{-1}$ and $23s^{-1}$, respectively (Figures A.4 (b) and A.5 (b)). Around these critical strain rates, the maximum elongational viscosity for experiment 4 and 5 are 285 Pa.s and 37 Pa.s, respectively (Table 7.2).

The extensional viscosity of the polymer solutions can be measured with respect to strain using Eqs. (3.3) and (3.6). Strain hardening index is determined by the using power law to fit extensional viscosity vs strain values around the critical Deborah number. The power law fits for all the 14 experiments is shown (Figures. A.1c to A.14c). The strain hardening index (n_2) determined using the power law fit is also shown (Table 7.2). In general, the strain hardening index is higher for a polymer with higher relaxation time. However, for the high saline brine solutions, the strain hardening index is higher for the polymer solutions with lesser relaxation time. The polymer solution of 1500 ppm used in experiment 2 with brine salinity of 20,040 ppm possesses the extensional relaxation time of 0.048 seconds and the strain hardening index of 3.484. Contrarily, 200 ppm polymer solution used in experiment 12 with deionized water possess relatively the higher extensional relaxation time of 0.073 seconds. However, the strain hardening index of the polymer solution in experiment 12 is only 2.898. Similar behavior can also be observed by comparing the experiments 5 and 6. The polymer solution of 1000 ppm used in experiment 5 with the brine salinity of 10,000 ppm corresponds to the relaxation time of 0.032 seconds and strain hardening index of 3.372. The same polymer solution (at the same concentration) used in experiment 6 with a lower salinity of 1000 ppm corresponds to the higher relaxation time of 0.0623 seconds and the lower strain hardening index of 3.029. The attained results in our experiments are

in accordance with the Magbagbeolo (2008). Shear thinning index (n) is determined using Carreau model from the shear rheological experiment. The shear thinning index for all the experiments is reported in Table 7.2 along with the other extensional parameters.

The measured values of τ_{ext}, $\mu_{\max@De_{cr-0.66}}$ and n_2 are substituted in the extensional part of the UVM model. Shear parameters are used in the shear part of the UVM model. The average downscaling power factor to $\mu_{\max@De_{cr-0.66}}$ attained from the 14 data sets using non-linear regression is 0.35, and the average subtrahend to n_2 is 1.2. The proposed model incorporating the direct extensional measurements from CaBER experiment is shown in the Eq. 7.2.

$$\mu_{app} = \mu_{\infty} + \left(\mu_p^o - \mu_{\infty}\right)\left[1+\left(\lambda * \gamma\right)^{\alpha}\right]^{\frac{(n-1)}{\alpha}} + \mu_{\max@De_{cr-0.66}}^{0.35}\left[1-\exp\left(-\left(\beta * \tau_{ext} * \gamma\right)^{n_2-1.2-1}\right)\right] \quad (7.2)$$

Predictability of the proposed AT-VEM to match the experimental data is shown in the Figures 7.2 to 7.15.

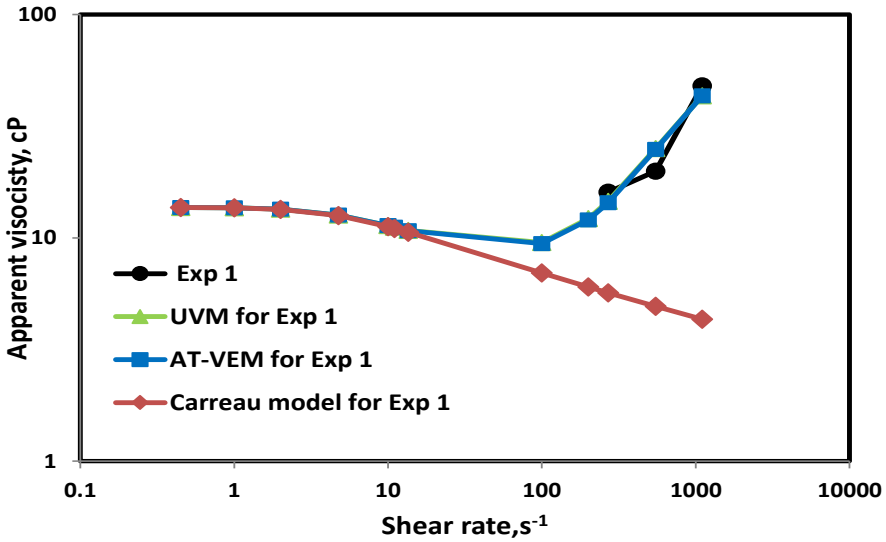

Figure 7.2: *AT-VEM fit for 1500 ppm HPAM 3630 at 20040 PPM TDS with 640 ppm calcium ions, 647 mD Berea sandstone core (Data from Magbagbeola 2008)*

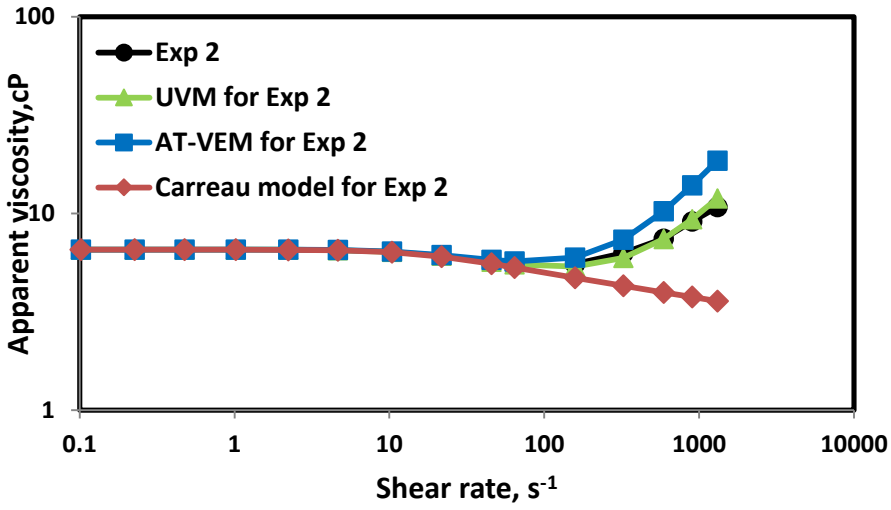

Figure 7.3: *AT-VEM fit for 1500 ppm HENGFLOC 63020 at 20040 TDS with 640 ppm calcium ions, 552 mD Berea sandstone core (Data from Magbagbeola 2008)*

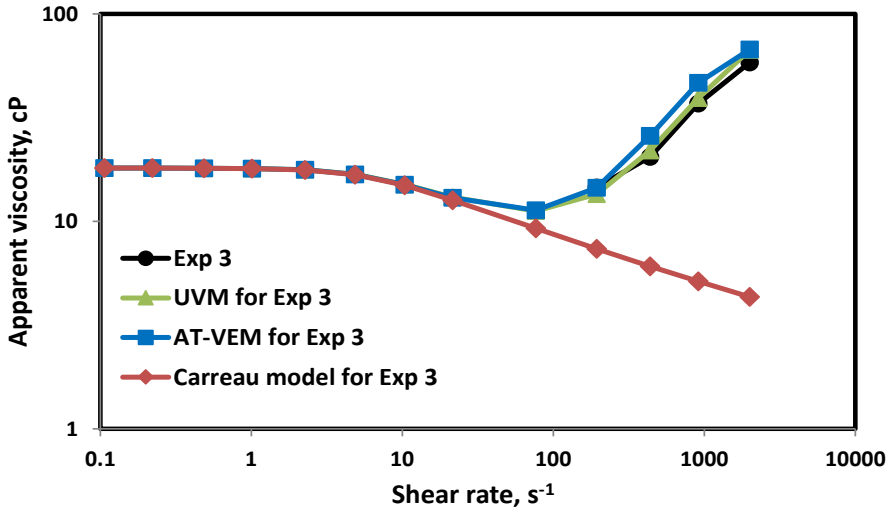

Figure 7.4: *AT-VEM fit for 1500 ppm HENGFLOC 63020 at 20040 TDS salinity with 20 ppm calcium ions, 372 mD Berea sandstone core (Data from Magbagbeola 2008)*

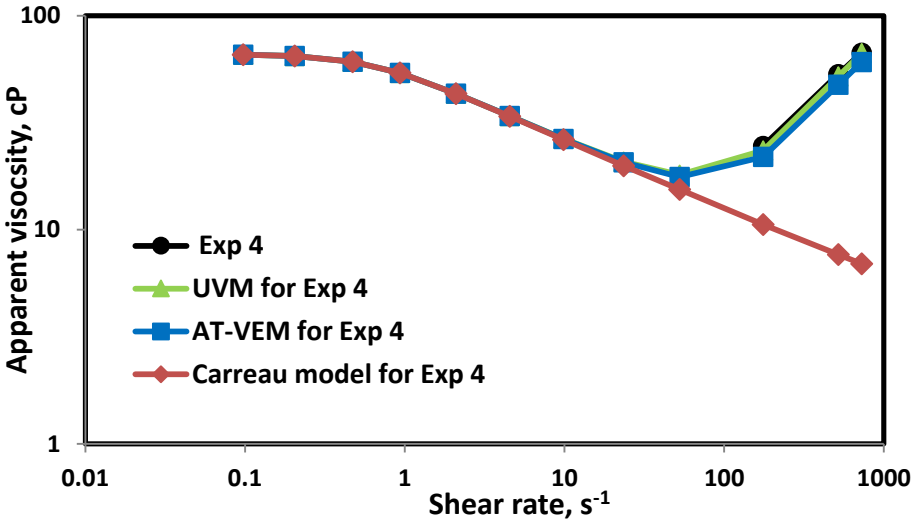

Figure 7.5: *AT-VEM fit for 1500 ppm HENGFLOC 63026 at 20040 PPM TDS with 20 ppm Calcium ions, 260 mD Berea sandstone core (Data from Magbagbeola 2008)*

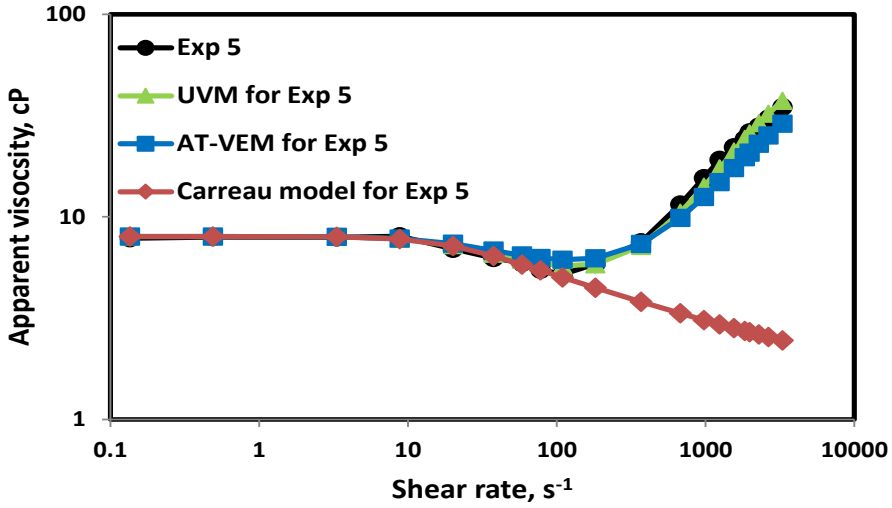

Figure 7. 6**:** *AT-VEM fit for 1000 ppm Pusher 700 at 10000 PPM NaCl, 4.2 D sand pack (Data from Yuan 1981)*

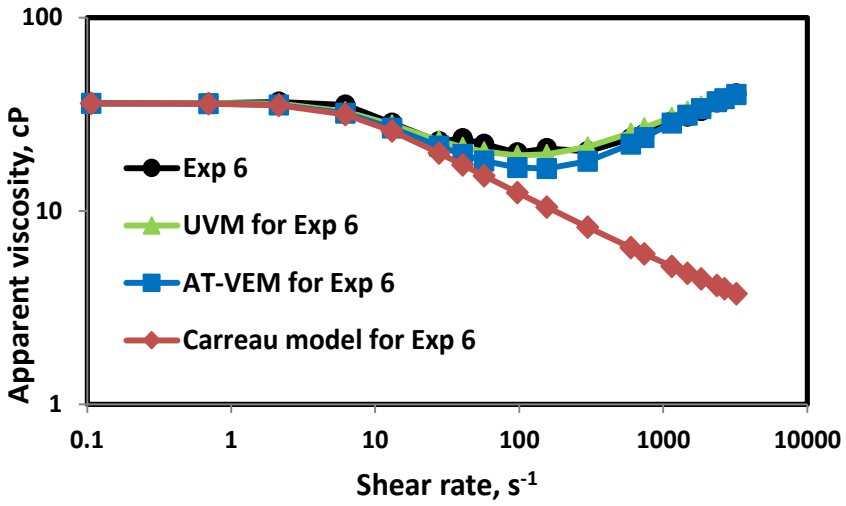

Figure 7.7: *AT-VEM fit for 1000 ppm Pusher 700 at 1000 PPM NaCl, 3.6 D sand pack (Data from Yuan 1981)*

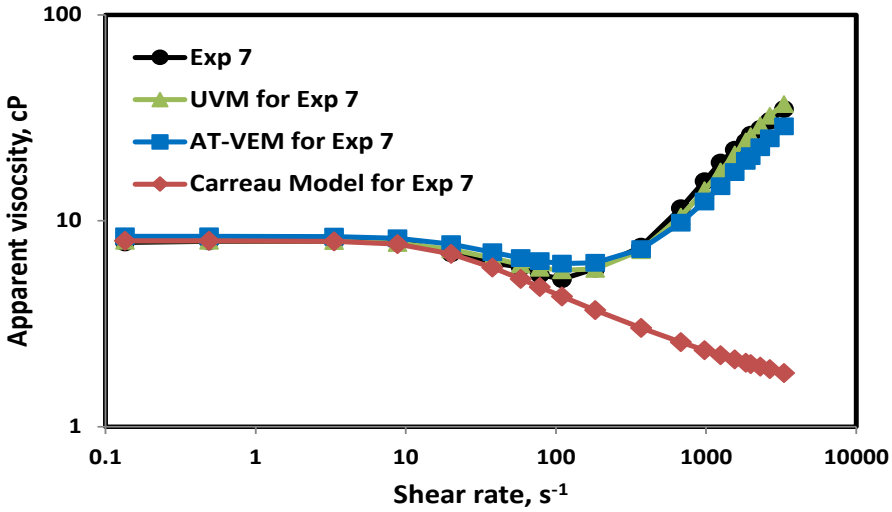

Figure 7.8: *AT-VEM fit for 1000 ppm Pusher 700 at 10000 PPM NaCl, 37 D sand pack core (Data from Yuan 1981)*

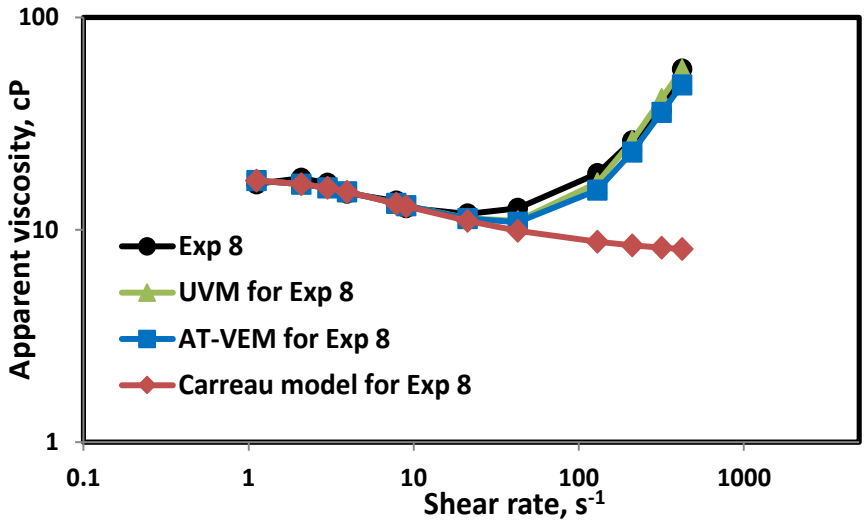

Figure 7.9: *AT-VEM fit for 850 ppm HPAM 3630 at 20000 PPM KCl, 301 mD reservoir sandstone core (Data from Mansour et al. 2014)*

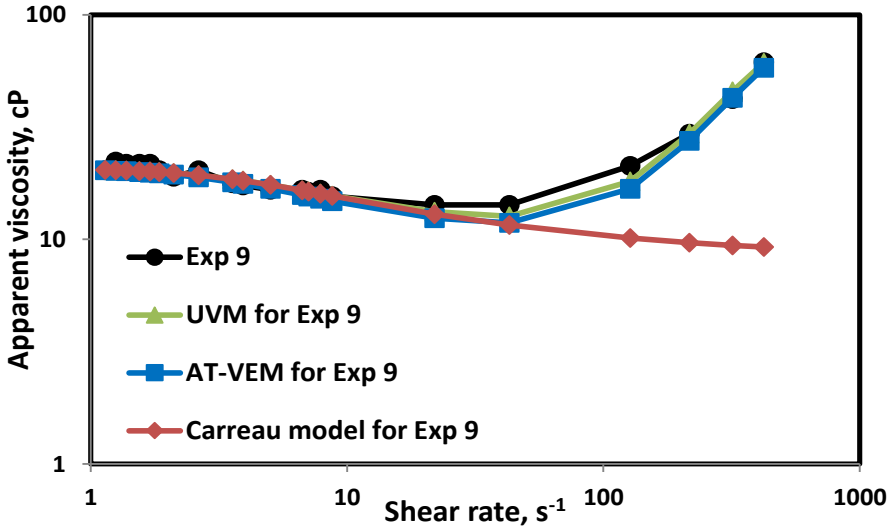

Figure 7.10: *AT-VEM fit for 850 ppm HPAM 3630 at 10000 PPM salinity, 301 mD reservoir sandstone core (Data from Mansor et al. 2014).*

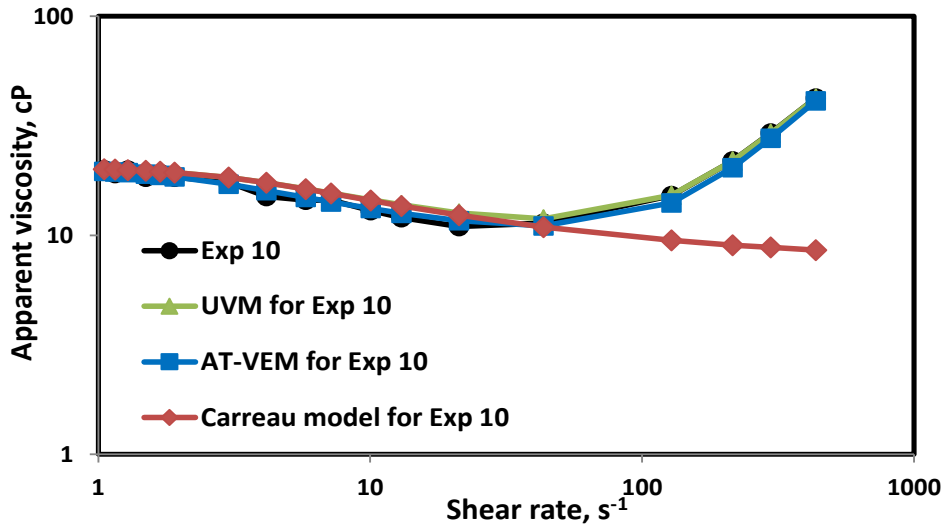

Figure 7.11: *AT-VEM fit for 600 ppm HPAM 3630 at 10000 PPM KCl, 301 mD reservoir sandstone core (Data from Mansor et al. 2014).*

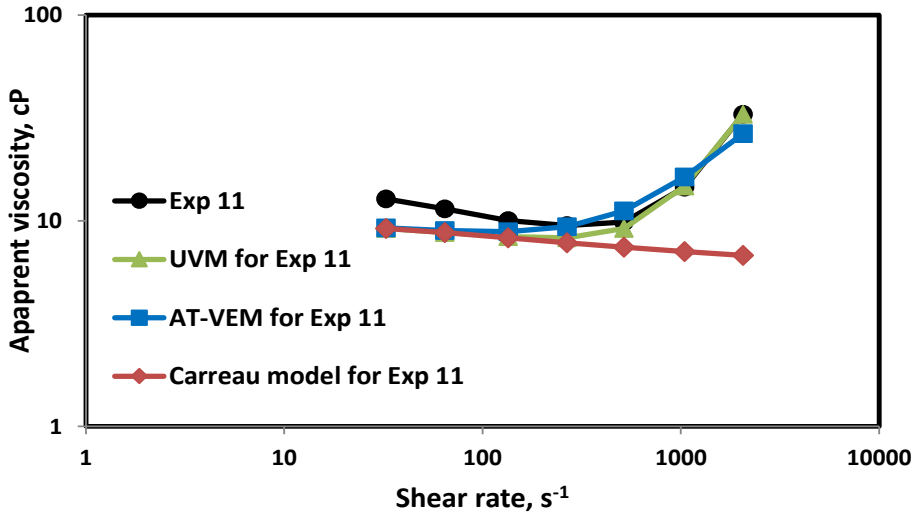

Figure 7.12: *AT-VEM fit for 2500 ppm HPAM 3230 at 25200 PPM TDS, 5.12 D polyethylene core (Data from Seright et al. 2011a).*

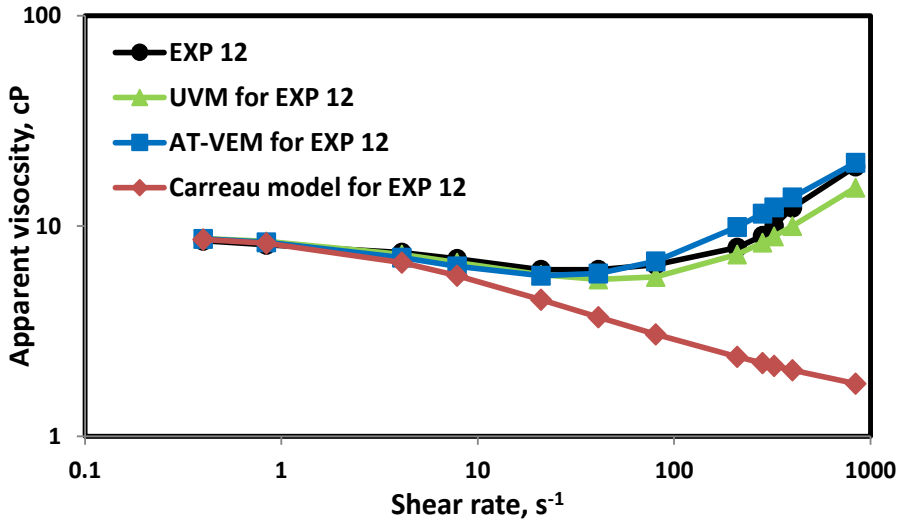

Figure 7.13: *AT-VEM fit for 200 ppm HPAM 3530 at 0 PPM salinity, 20 D sand pack core (Data from Masuda et al. 1992).*

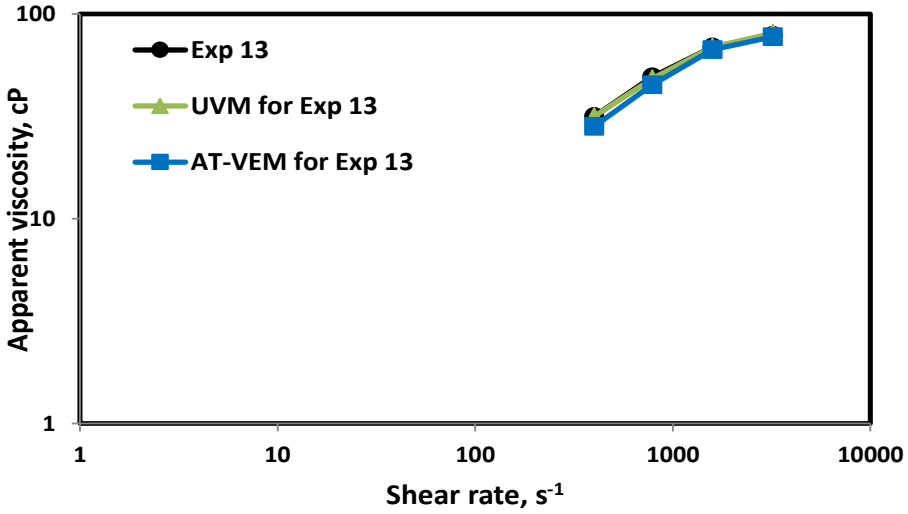

Figure 7.14: *AT-VEM fit for 500 ppm HPAM 3630 at 21969 PPM TDS, 200 mD sandstone core (Data from Laoroongroj et al. 2014).*

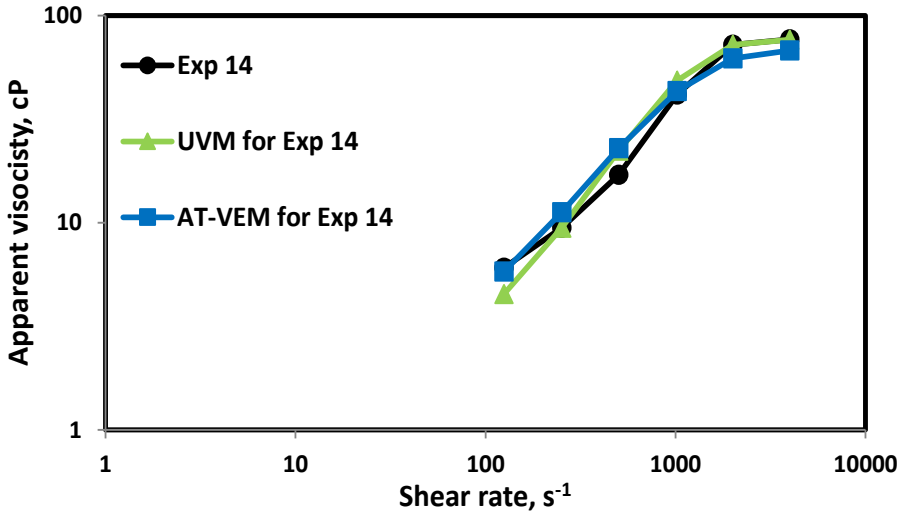

Figure 7.15: *AT-VEM fit for 500 ppm HPAM 3630 at 21969 PPM TDS, 2000 mD sandstone core (Data from Laoroongroj et al. 2014).*

Predictability of the AT-VEM is compared with UVM and Carreau model (Figure 7.2- 7.15). It is clear that AT-VEM model incorporating extensional parameters can predict the onset and shear thickening regime fairly well for all the experiments. The AT-VEM can also predict the differences in behavior because of the permeability variations between different experiments (Figures 7.6 and 7.8; Figures 7.14 and 7.15). The predictability of AT-VEM is comparable with core-flood dependent UVM. The proposed AT-VEM can predict the Newtonian, shear thinning and shear thickening behavior of viscoelastic polymers. The model cannot predict the drop in the viscosity with respect to the shear rate caused due to mechanical degradation. Please note that all the experiments used for validation of the AT-VEM are performed at room temperature.

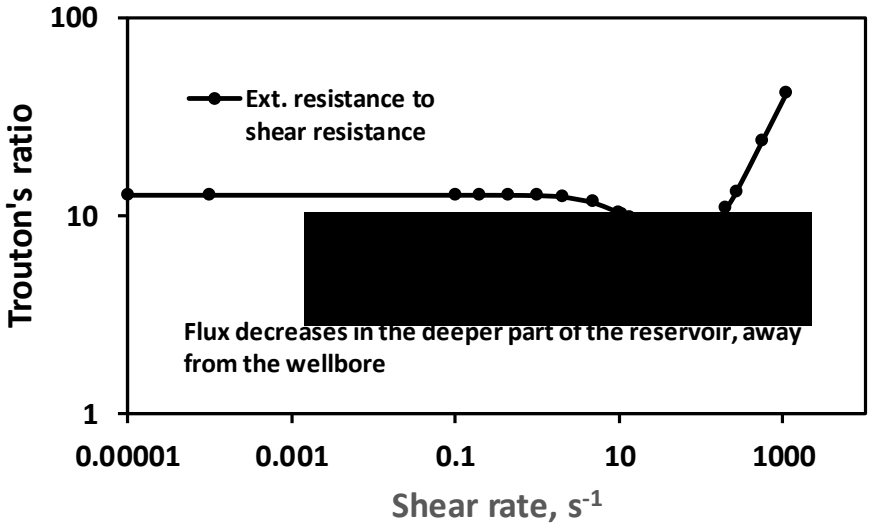

Figure 7.16: *Ratio of extensional contribution to shear contribution plotted for EXP 1 with respect to flux rates*

The ratio of the second term relative to the first term of the Eq. 7.2 is plotted for Exp 1 with respect to shear rate in Figure 7.16. This Figure shows the relative influence of extensional viscosity and shear viscosity at low shear rate. As the shear rate is approaching zero, the apparent viscosity is ~12 cP, which is closer to zero shear viscosity (Magbagbeolo 2008). This implies that at very low flux, the extensional contribution becomes insignificant and the core-scale apparent viscosity will be dominated by the polymer's shear resistance. Hence, core-scale viscoelastic effects will be of less importance as the polymer flood front propagates far away from the wellbore.

7.4 Summary

The novelty of the work can be summarised as a) measurement of extensional rheological parameters for EOR polymers, b) a new model for predicting viscoelastic onset and shear thickening in porous media, independent of core flooding parameters, and c) validation of proposed model using polymer solutions of different types, concentration, and brine salinity. Proposed AT-VEM is an extension to the Carreau model, which can predict the viscoelastic onset and shear thickening regimes of viscoelastic polymers using bulk shear and extensional rheological measurements. Thus, the limitation of existing viscoelastic model is addressed, and it is made possible by the direct measurements of the extensional parameters from CaBER. The measured extensional parameters include the strain hardening index, maximum elongational viscosity and extensional relaxation time. Power law, FENE and UCM theories are used for determining these

extensional parameters. The average downscaling factor of 0.35 to maximum elongational viscosity and subtrahend of 1.2 to strain hardening index is obtained based on 14 different experiments. These factors are attained for the polymer solutions possessing the extensional relaxation time of up to around 0.2 seconds. The downscaling factors are essential for downscaling the pure elongation in the uniaxial extensional field to the combination of shear and elongation experienced in the porous media by the polymeric solutions. The proposed model can predict the viscoelastic onset and the shear thickening regime for varying range of reservoir permeability (200 mD to 37 D), porosity (0.22 to 0.395), brine salinity (0 ppm to 25200 ppm), concentration (200 ppm to 2500 ppm) and polymer molecular weight (6 MDa to 26 MDa). AT-VEM can be used for a quick screening of viscoelastic cEOR polymers. It can also be incorporated in the reservoir simulators for the early prediction of injectivity and recovery caused by the viscoelastic effects.

Chapter 8: Quantification of S_{or} reduction during Viscoelastic Polymer Flooding Using Extensional Capillary Number

8.1 Introduction

Incremental oil recovered during enhanced oil recovery (EOR) processes could be due to both enhanced sweep and displacement efficiency. Sweep efficiency will be higher if the displacing slugs contact more oil with a minimal pore volume of injection. High oil viscosity and heterogeneity are the limiting factors affecting sweep efficiency. Sweep conventionally believed to be the field-scale mechanism has been reported to be a core-scale phenomenon, especially if the oil viscosity is high (Delshad et al. 2017; Azad and Trivedi 2018b). However, microscopic displacement efficiency is not a core-scale phenomenon; rather strictly, it is a pore-scale phenomenon. Residual oil by definition is the oil that is swept well by the displacing water but that failed to become mobilized due to high interfacial tension (IFT) between the water and oil. Capillarity will be higher when the IFT is high. Smaller pore radius also leads to higher capillary forces (Green and Willhite 1998). The interplay between the viscous and capillary force has been well described by the dimensionless number called capillary number (N_c). Generally, oil will be trapped at the capillary pressure of 1000 psi/ft while the viscous force is of the order of few psi/ft (Peter 2002). This residual oil can be recovered if the viscous force provided by the displacing slugs is sufficient enough to overcome the trapping capillary force (Peter 2002). The relation between S_{or} reduction and N_c is described by the capillary desaturation curve (CDC) (Green and Willhite 1998). As per the CDC curve, rapid oil mobilization begins to occur when N_c exceeds 10^{-5} to 10^{-4} for sandstone reservoirs (Melrose and Brander 1974; Stegemeier 1974; Abrams 1975; Chatzis and Morrow 1984; Chatzis et al. 1988; Johannesen et al. 2007; Humphry et al. 2014) and complete mobilization is expected to occur only when the N_c exceeds 10^{-2} (Foster 1973; Abrams 1975; Chatzis and Morrow 1984; Jr. et al. 1985). To increase the S_{or} reduction, N_c has to be increased. Mathematically, viscous force can be increased by either increasing the injection rate or by increasing the displacing fluid's viscosity. Both the options are not practically feasible, as increasing the viscosity by several orders may lead to injectivity issues and increasing the rate leads to the fracturing of reservoirs. Most of the residual oil is located in the farthest part of the wellbore, where low flux conditions prevail. The only way to recover residual oil that is practically feasible is to reduce the capillary trapping force for which the surfactant flooding capable of providing ultra-low IFT is employed (Green and Willhite 1998). IFT has been used a parameter to

screen or formulate the optimal surfactants for enhancing microscopic oil recovery (Azad 2014; Azad and Sultan 2014; Han et al. 2013; Kamal et al. 2017).

Polymer solutions are conventionally employed to increase the sweep efficiency by altering the mobility ratio between the displacing slug and displaced oil. Additional oil recovery attained during polymer flooding in the field has been attributed to enhanced sweep efficiency (Moffitt and Mitchell 1983; Greaves et al. 1984; Hochanadel et al. 1990; De Melo et al. 2014; Clemens et al. 2016; Kumar et al. 2016). Polymer solutions do not reduce the IFT significantly. They can increase the N_c by 1 or 2 order maximum with their viscosity, which will not be sufficient to mobilize the significant amount of residual oil. Therefore, conventionally it is believed that polymer flooding cannot reduce S_{or}. In recent times, however, viscoelastic polymers were reported to cause an additional residual oil recovery in the Daqing field (Wu et al. 2007). There were some studies which argued against the polymer's viscoelastic influence on the S_{or} reduction under certain conditions (Schneider and Owens 1982; Huh and Pope 2008; Vermolen et al. 2014; Erinick et al. 2018; Seright et al. 2018). Azad and Trivedi (2018c) listed those conditions that are relatively unfavourable for the viscoelastic polymer to recover the residual oil. Nevertheless, several recent results have asserted the polymer viscoelastic influence on S_{or} reduction beyond that of water flood (Wang et al. 2000; Wang et al. 2001; Wang et al. 2007; Xia et al. 2008; Jiang et al. 2008; Wang et al. 2010; Wang et al. 2011; Ehrenfried 2013; Vermolen et al. 2014; Clarke et al. 2015; Qi et al. 2017; Qi et al. 2018). It is to be noted that all the aforementioned literature has asserted the polymer's viscoelastic influence on S_{or} reduction specifically by ensuring the recovered oil is the true residual oil that is well swept. Some studies specifically emphasize the polymer's viscoelastic influence on the S_{or} reduction even at the flux of ~1ft/day and intermediate N_c of 10^{-5} to 10^{-6} (Ehrenfried 2013; Clarke et al. 2016; Cottin et al. 2014; Qi et al. 2017; Koh 2017). The polymer flood shows rapid oil mobilization even before the critical N_c (at low flux) which invalidates the capillary theory (Lotfollahi et al. 2016b; Qi et al. 2017). The proper mechanisms causing this S_{or} reduction at low flux are not understood and wettability alteration has been proposed as the mechanism (Seright 2017). Azad and Trivedi (2018c) speculated extensional viscosity might be the reason.

To account for the polymer's sweep efficiency, mobility ratio is widely used (Green and Willhite 1998). Mobility ratio by definition is the ratio between the mobility of displacing slugs and displaced oil. Mobility is the ratio between the permeability and viscosity. The higher the viscosity,

the lower the mobility ratio and the higher the sweep efficiency. Viscoelastic polymers possessing higher apparent viscosity contribute more to the higher sweep efficiency than polymers possessing higher elasticity (Azad and Trivedi 2018b). The role of the viscosity of viscoelastic polymers on sweep efficiency has been reported in more literature (Chen et al. 2011; Wang et al. 2013). These clearly indicate the apparent viscosity can be used in the mobility ratio calculation for accounting for the sweep efficiency. However, to account for the microscopic displacement efficiency of viscoelastic polymer flooding, apparent viscosity might not be appropriate, which is discussed below.

The surfactant solutions having lower IFT (higher N_c) were reported to contribute to higher S_{or} reduction (Foster 1973; Karnanda et al. 2013; Sheng 2015). However, higher S_{or} reduction is shown by the highly elastic polymers over viscous or less elastic polymers, despite possessing the similar N_c (Qi et al. 2017). It is important to point out here that conventional N_c is calculated using the apparent viscosity (Ehrenfried 2013 Qi et al. 2017; Koh 2017; Erinick et al. 2018). Micro-force or normal stress has been identified as the reason for higher S_{or} reduction by highly elastic polymers (Wang et al. 2001; Xia et al. 2004; Xia et al. 2008; Afsharpoor et al. 2012; Wang et al. 2013; Lotfallahi et al. 2016b). Normal stress is related to extensional viscosity (Barnes 2010). The conventional notion that core-scale apparent viscosity encompasses extensional viscosity (Hirasakhi and Pope 1974; Masuda et al. 1992; Delshad et al. 2008; Stavland et al. 2010; Clarke et al. 2015) is refuted by Azad and Trivedi (2018d) who show that actual extensional viscosity is three orders higher than the core-scale apparent viscosity. Azad and Trivedi (2018 d) reported that extensional viscosity should not be treated as the constituent of core-scale apparent viscosity for pore-scale applications such as S_{or} reductions. IFT that measures the tension between the water and oil interface is a microscopic property. Similarly, extensional viscosity which gives the measure of polymer's resistance to stretching around the pore is also a microscopic phenomenon (Haas and Durst 1982). The transient nature of elastic response means that normal stresses or extensional viscosity will be dominated only in the micro region of the pore (Wang et al. 2007). Coincidently, capillary pressure tends to be higher in that micro region characterized by the smaller radius, which in turn causes the higher trapping of residual oil. Microscopic residual oil displacement is a pore-scale phenomenon. So, if the microscopic property such as IFT has been used in the N_c for relating it with S_{or} (Green and Willhite 1998), the extensional viscosity should also be incorporated into N_c. Challenges involved in the extensional measurement of EOR

polymers were well documented in previous publications (Azad and Trivedi 2017; Azad et al. 2018a; Azad et al. 2018b; Azad and Trivedi 2018a; Azad and Trivedi 2018b; Azad and Trivedi 2019).

To quantify the polymer's viscoelastic effects on S_{or} reduction, few pore-scale models have been proposed. These include models proposed by Chen et al. (2012), Wang et al. (2013), and Lotfallahi et al. (2016b). All of these models fail to honour the capillary theory because they either rely on the normal stress and/or Deborah number. All the models that stress the importance of normal stress rely on empirical fitting parameters determined from core flooding. In the case of surfactant flooding, S_{or} reduction can be quantified through IFT, which is a bulk property. Any methodology that can quantify the S_{or} reduction through bulk properties alone is desirable, which can help in the quick screening of optimal slugs. It is worthwhile to mention here that the Azad Trivedi viscoelastic model (AT-VEM) that we have developed is the first viscoelastic model that can predict the apparent viscosity for various ranges of shear rates through bulk rheology alone (Azad and Trivedi 2018a; Azad and Trivedi 2019). Similarly, a methodology that can predict the S_{or} reduction potential of viscoelastic polymers is highly desirable. The model developed by Qi et al. (2018) is independent of core flood experiments. However, Qi et al.'s (2018) method is exclusively based on the conventional Deborah number (D_e).

D_e is widely used by chemical EOR researchers for quantifying the polymer viscoelastic effects during chemical EOR. If the transit time of the polymer solutions between pore body and pore throat is less compared to their relaxation time, then the fluid will exhibit elastic strain that causes a higher pressure drop, which would be more than expected from shear forces. It is to be noted that the relaxation time used by most EOR researchers are oscillatory based (Magbagbeola 2008; Delshad et al. 2008; Ehrenfried 2013; Vermolen et al. 2014; Koh 2015; Hincapie and Gazner 2015; Qi et al. 2017; Erinick et al. 2018; Qi et al. 2018), which represents the linear viscoelastic effects (Howe et al. 2015). Several misconceptions exist because of the usage of an oscillatory Deborah number, especially when there is variation in the salinity. High saline polymer solutions possessing lower D_e were reported to cause higher S_{or} reduction than the low saline polymer solutions possessing higher D_e (Ehrenfried 2013; Erinick et al 2018). Magbagbeolo (2008) reported that high saline polymer solutions (with the lower oscillatory Deborah number) resulted in the higher strain hardening index than the low saline polymer solutions (with the higher oscillatory Deborah number). Azad and Trivedi (2018d) also showed, using direct extensional measurements, that high

saline polymer solutions (with the lower oscillatory D_e) provided higher extensional resistance than the low saline polymer solutions (with the higher oscillatory D_e). When the polymer solutions flow from the pore body to pore throat, they stretch and generate extensional resistance to flow. Therefore, using the linear relaxation time determined from the oscillatory rheology for mimicking the flow from pore body to pore throat is not ideal for Deborah number calculation (Azad and Trivedi 2018c).

As discussed, N_c fails to explain the different residual oil recovery potential of viscoelastic polymers varying in the elasticity. Oscillatory D_e appears to be deficient in honouring the non-viscoelastic effects that the EOR polymer solutions are expected to exhibit. The objective of this work is to develop the N_c using the actual measured extensional viscosity (N_{ce}) and then using it for developing a correlation to be named the Azad Trivedi correlation (AT-C) for predicting the S_{or} reduction potential of viscoelastic polymers. Twenty-three different data sets, extracted from different experiments, are used for correlation. The AT-VEM used to predict the core-scale apparent viscosity of the viscoelastic polymers is modified for accounting for the extensional viscosity that occurs at the pore scale. The apparent pore-scale extensional viscosity predicted by the modified AT-VEM is used to account for the viscoelastic driving force in the N_{ce}, which is then correlated with the different S_{or} reduction of different polymers reported in the literature. The N_{ce} is compared with the conventional N_c and D_e. AT-C is compared for its predictability with the latest correlation developed at UT-Austin by Qi et al. (2018). It is ensured through comparative discussion that the deficiency persisting with the existing methods are addressed through the N_{ce}.

8.2 Methodology

S_{or} data corresponding to the viscoelastic polymer flooding is included from the different literature. Data sets are chosen only from the tertiary polymer flooding that was water flooded. S_{or} corresponding to the water flood and glycerin is also included. All the details pertaining to the polymer properties, flux, and oil viscosity can be found in Table 8.1.

Table 8.1: *Operational and petro physical conditions used in two phase core flood experiments*

Data Set	Authors	Slug	Conc. (ppm)	Salinity (ppm)	Temp℃	Flux (ft/day)	Formation	Porosity	Permeability (mD)	Oil viscosity (cP)
1	Qi	HPAM 3630	2100	11000	Room	0.96	Bentheimer sandstone	0.22	2200	120
2	Qi	HPAM 3630	1800	11000	Room	0.2	Bentheimer sandstone	0.22	2100	120
3	Erinick	HPAM 3630	3400	26000	Room	4	Bentheimer sandstone	0.24	1480	126
4	Erinick	HPAM 3630	2000	1400	Room	2	Bentheimer sandstone	0.24	1480	126
5	Erinick	HPAM 3630	2000	1400	Room	1	Bentheimer sandstone	0.25	1480	114
6	Erinick	HPAM 3630	3548	24300	Room	1	Bentheimer sandstone	0.25	1480	114
7	Ehrenfried	HPAM 3630	1500	4000	Room	5.28	Bentheimer sandstone	0.23	2398	149
8	Ehrenfried	HPAM 3630	1500	4000	Room	1.06-5.31	Bentheimer sandstone	0.23	2125	162
9	Ehrenfried	HPAM 3630	1000	1000	Room	1.07-5.34	Bentheimer sandstone	0.23	1597	162
10	Ehrenfried	HPAM 3630	1500	15000	Room	1.33	Berea sandstone	0.18	187	300
11	Ehrenfried	HPAM 3630	1500	15000	Room	0.14	Berea sandstone	0.18	169	300
12	Ehrenfried	HPAM	1500	15000	Room	0.91	Boise	0.27	475	300

		3630					Sandstone			
13	Clarke	HPAM 6040	640	4700	Room	1	Berea sandstone	0.23	435	34
14	Clarke	HPAM 3130	6000	4700	Room	1	Berea sandstone	0.23	465	34
15	Koh	HPAM 3630	1200	2000	68	1	Ottawa Sand	0.35	7900	80
16	Koh	HPAM 3630	1300	2000	68	1	Ottawa Sand	0.36	6650	120
17	Koh	HPAM 3630	2450	2000	68	1	Ottawa Sand	0.37	7311	250
18	Koh	HPAM 3330	3500	25878	55	1	Reservoir Sand	0.28	227	72
19	Cottins	HPAM 3630	500	5600	65	3	Sandstone Reservoir	0.359	2943	7
20	Clarke	Water	-	4700	Room	2	Berea Sandstone	0.23	435	34
21	Clarke	Water	-	4700	Room	2	Berea Sandstone	0.23	465	34
22	Erinick	Water	-	2000	Room	4.7	Bentheimer Sandstone	0.25	1480	114
23	Erinick	Glycerin	800000	2000	Room	2	Bentheimer Sandstone	0.25	1480	114

All of the series of HPAM polymers were supplied by SNF Floerger (USA). All the HPAM solutions were prepared by stirring at 200 rpm for 24 hours. Polymer samples were used in the experiments without any pre-filtration. Capillary breakup extensional rheometer (CaBER) is used to perform the extensional measurements on the polymer solutions to attain the filament diameter vs. time data. The extensional rheological parameters, such as extensional relaxation time (τ_{ext}), maximum extensional viscosity at the critical Deborah number ($\mu_{\max@De_{cr-0.66}}$), and strain hardening index (n_2), used in the AT-VEM (Azad and Trivedi 2018a; Azad and Trivedi 2019) will be attained using the appropriate theories. Please refer to our previous publications for details about the CaBER experimental procedure and related theories used in the calculation of extensional parameters (Azad et al. 2018a; Azad et al. 2018b; Azad and Trivedi 2018 a; Azad and Trivedi 2018 b; Azad and Trivedi 2018 d; Azad and Trivedi 2019).

The AT-VEM, developed using measured extensional rheological parameters to match the core-scale pressure drop, is modified in a way that accounts for the extensional resistance experienced by the polymer solutions at the pore scale. For example, a downscaling factor used to scale down the maximum extensional viscosity attained in the extensional field to the combination of shear and elongation in porous media is removed from the AT-VEM. Similarly, the subtrahend used to scale down the strain hardening index is also removed. Seventy-five percent of deformation experienced by the polymer solutions at the pore scale is due to elongational resistance (Haas and Durst 1982); therefore, seventy five of maximum extensional viscosity is used in the modified AT-VEM. Strain hardening index and extensional D_e are related exponentially in AT-VEM (Azad and Trivedi 2018a; Azad and Trivedi 2019). As per the AT-VEM, the higher the strain hardening index is, the more intense the shear thickening and the higher the apparent viscosity at high shear rates. Azad and Trivedi (2018c, 2018d) discussed that strain hardening and shear thickening are two different concepts. Here, we are considering the low flux rate with which the injected polymer solutions stretch and displace the residual oil in the farthest part of the reservoirs. Keeping the same functional relation between strain hardening index and Deborah number resulted in the lower pore-scale extensional viscosity for high saline solutions at low fluxes, which is not correct. Based on the experimental results (Azad and Trivedi 2018d), we observed that the higher the salinity was, the higher the strain hardening index and extensional viscosity, and the lower the S_{or}. So, the relation between the Deborah number and strain hardening index is modified to account for that

dependency accordingly. In the modified AT-VEM, strain hardening index is the direct multiplicative function of the Deborah number. Shear rate formulae used in the AT-VEM is used in the modified AT-VEM as well. A universal constant of 0.01, used in UVM and AT-VEM is retained. The modified AT-VEM is shown by Eq. 8.1.

$$\mu_{ext-pore} = \mu_{\infty} + \left(\mu_p^o - \mu_{\infty}\right)\left[1 + \left(\lambda * \gamma\right)^{\alpha}\right]^{\frac{(n-1)}{\alpha}} + 0.75 * \mu_{\max,De_{cr-0.66}}\left[1 - \exp\left(-\left(\beta * \tau_{ext} * \gamma * n_2\right)\right)\right] \quad (8.1)$$

where

$\mu_{ext-pore}$ is the extensional viscosity around the pore-scale

μ_{∞} is the infinite shear viscosity, Pascal second (Pa.s)

Pa.s; μ_p^o is the zero shear viscosity, Pa.s

λ is the shear characteristic time, s

γ is the shear rate, s^{-1}

α is the correction factor, 2

n is the shear thinning index

$\mu_{\max@\, De_{cr-0.66}}$ is the measured maximum elongational viscosity at the critical De, Pa.s

β is the universal constant, 0.01

τ_{ext} is the extensional relaxation time, s

n_2 is the measured strain hardening index

8.3 Results and discussion

8.3.1 Extensional capillary number

N_c can be defined by the ratio of viscous force to capillary force (Eq.8.2). N_{ce} is calculated from Eq. 8.2 by replacing the apparent viscosity with the $\mu_{ext-pore}$, calculated using the modified AT-VEM (Eq. 8.1).

$$N_c = \frac{v^* \mu_{app}}{\sigma} \tag{8.2}$$

$$N_{ce} = \frac{v^* \mu_{ext-pore}}{\sigma} \tag{8.3}$$

where

μ_{app} is the apparent viscosity, which can be calculated through core flood pressure data, cP

σ is the IFT, mN.m^{-1}

ϑ is the flux, ft/day

The relevant extensional rheological parameters for all 23 experiments to be used in Eq. 8.1 are measured using CaBER (Table 8.2).

Table 8.2: *Measured extensional rheological parameters, calculated N_{ce} and S_{or}*

Data set	Authors	τ (s)	n_1	τ_{ext} (s)	$\mu_{\max,De_{cr}=0.66}$ (cP)	n_2	$\mu_{ext-pore}$ (cP)	σ (mN/m)	N_{ce}	N_c	D_e	S_{or}
1	Qi	0.133	0.632	0.516	648000	3.60	340445	17.3	0.067	0.00005	14.8	0.198
2	Qi	0.1	0.6	0.352	560000	3.57	352401	17.3	0.014	0.00005	0.6	0.31
3	Erinick	0.11	0.32	0.456	760000	3.77	475739	17.3	0.388	0.000058	11	0.08
4	Erinick	0.11	0.32	0.25	250000	2.57	91818	17.3	0.037	0.000046	100	0.29
5	Erinick	0.11	0.32	0.25	250000	2.57	28523	17.3	0.0058	0.000056	32	0.32
6	Erinick	0.11	0.32	0.44	813000	4.05	223658	17.3	0.0456	0.000024	6	0.22
7	Ehrenfried	2	0.81	0.229	410000	3.12	230334	25	0.171	0.00006	4.34	0.151

8	Ehrenfried	2	0.81	0.229	410000	3.12	75148	25	0.011	0.000028	2.18	0.289
9	Ehrenfried	2.	0.81	0.117	117000	3.08	11484	25	0.00171	0.0000164	72.91	0.297
10	Ehrenfried	2	0.86	0.0879	250000	3.39	76059	25	0.014	0.000016	0.38	0.337
11	Ehrenfried	2	0.86	0.0879	250000	3.39	10007	25	0.000025	0.0000143	0.29	0.4
12	Ehrenfried	2	0.86	0.0879	250000	3.41	38254	25	0.00491	0.0000133	1.67	0.366
13	Clarke	33	0.88	0.19	210000	3.58	68640	25	0.009	0.0000705	2.2	0.32
14	Clarke	2.5	0.96	0.032	32000	2.65	865	25	0.0001	0.0000908	0.021	0.42
15	Koh	0.27	0.57	0.307	320000	3.16	72416	13.5	0.0189	0.0000006	2.94	0.26
16	Koh	0.45	0.82	0.36	370000	3.5	113090	13.5	0.029	0.0000017	4.2	0.24
17	Koh	1.62	0.62	0.72	600000	3.61	2554428	13.5	0.066	0.0000041	16	0.23
18	Koh	0.05	0.62	0.24	550000	3.69	344058	13.5	0.089	0.00000055	6.5	0.24
19	Cottins	1	0.72	0.082	197000	3.36	147401	17.5	0.089	0.00001	NA	0.24
20	Clarke	-	-	0.00048	173	-2.06	0.78	1	0.0000553	0.0000141	NA	0.45
21	Clarke	-	-	0.00048	173	-2.06	0.911	1	0.0000643	0.0000194	NA	0.45

22	Erinick	-	-	0.000 48	173	-2.06	0.84	15.6	0.000 0008 98	0.000 033	NA	0.45
23	Erinick	-	-	0.001	374	-2.18	45.37	21.3	0.000 015	0.000 052	NA	0.43

Filament diameter vs. time data for the 23 experiments is shown in the supplementary Figures (Figure S-8.1a to Figure S-8.23a). It is clear that water and glycerin solutions used in Experiment 20 through Experiment 23 possess negligible resistance to break up when compared to the viscoelastic polymer solutions used in Experiment 1 through Experiment 19. Extensional relaxation time is attained by fitting the upper convected Maxwell model to the filament diameter vs. time data (Figure S-8.1a to Figure S-8.23a) and the extracted relaxation time for all 23 solutions is shown in Table 8.2. The extensional relaxation time of water is in the range of $4*10^{-4}$ s. The extensional relaxation time of glycerin is in the range of $1*10^{-3}$ s. The extensional relaxation time of the viscoelastic polymer solutions is significantly higher than the extensional relaxation time of viscous glycerin (Table 8.2). Extensional viscosity vs. strain rate for all the experiments is shown (Figure S-8.1b to Figure S-8.23b). Readers are encouraged to read our earlier publication for the typical extensional viscosity vs. strain rate behaviour shown by the viscoelastic polymer solutions (Azad and Trivedi 2018 d; Azad and Trivedi 2019). As per finite extensible non-linear elastic theory, the maximum extensional viscosity at the critical Deborah number ($\mu_{\max@De_{cr-0.66}}$) corresponds to the polymer's elastic limit (Entov and Hinch 1997; Clasen 2010; Kim et al. 2010; Azad and Trivedi 2018 d; Azad and Trivedi 2019). $\mu_{\max@De_{cr-0.66}}$ is significantly higher for the viscoelastic polymer solutions than glycerin. For example, HPAM 3630 used in Experiment 1 corresponds to the $\mu_{\max@De_{cr-0.66}}$ of 648000 cP (Figure S-2b and Table 2). The glycerin used in Experiment 23 corresponds to $\mu_{\max@De_{cr-0.66}}$ of only 374 cP (Figure S-23b and Table 8.2). Also, strain hardening index (n_2), gives a measure of the polymer thickening ability in the extensional field. n_2 is determined by power law fit to the extensional viscosity vs. strain values around the critical De (Figure S-8.1c to Figure S-8.23c; Table 8.2). n_2 is negative for glycerin (Figure S-23c; Table 8.2). Strain hardening index for all the viscoelastic polymer solutions is positive (Figure S-8.1c to Figure S-8.19 c). These results clearly imply that elastic solutions possess more resistance

than viscous solutions in the extensional field. It is important to point out here that elastic pusher polymer possesses similar resistance to the viscous xanthan gum in the oscillatory field (Garrouch and Gharbi 2006). Shear rheological parameters and IFT, taken from the literature, are also reported in Table 8.2. $\mu_{ext-pore}$ calculated using Eq. 8.1 for all 23 slugs is shown in Table 8.2. N_{ce} calculated using Eq. 8.3 is also shown in Table 8.2.

8.3.2 Correlation between the extensional capillary number and residual oil saturation

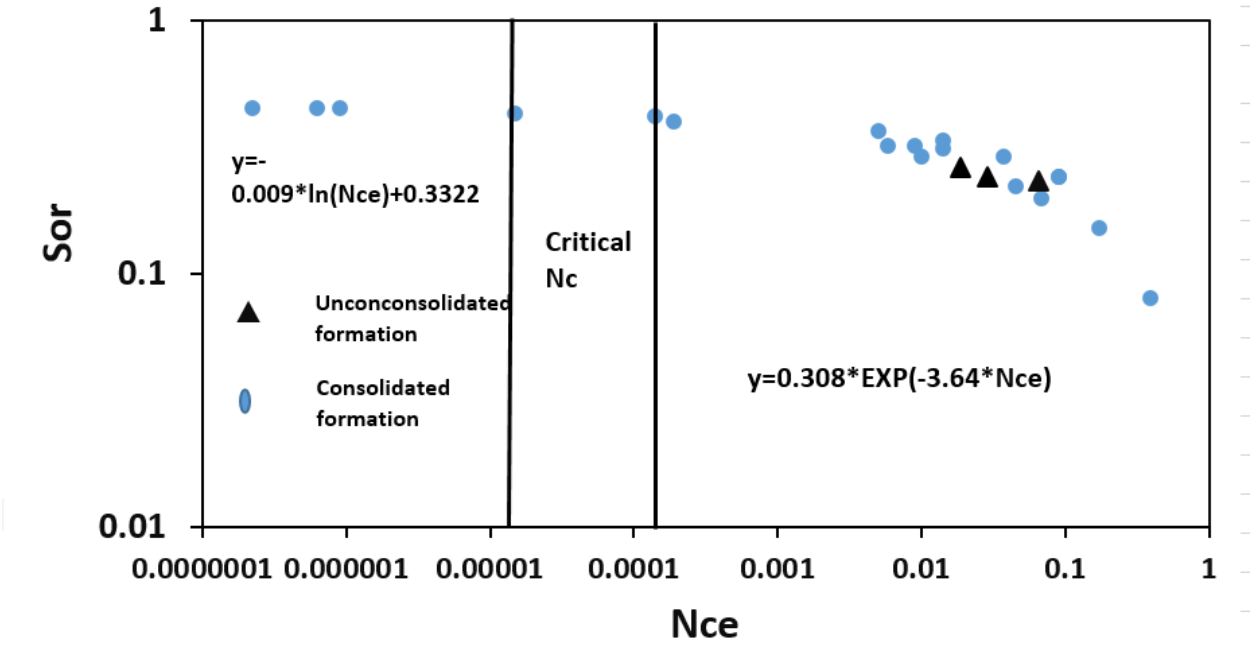

Figure 8.1: *N_{ce} vs S_{or} for 23 different data sets*

N_{ce} vs. S_{or} for all 23 solutions is shown in Figure 8.1. Both consolidated and unconsolidated formations were used (Table 8.1). Two sets of correlations (AT-C) are developed between the N_{ce} and S_{or} using 23 different experiments. As per the classical capillary theory, an increase in the N_c will not result in a drastic decrease in the S_{or} up to the critical N_c (Peter 2010). After the critical N_c, the increase in the N_{ce} will result in a significant increase in the S_{or} reduction. Critical N_c values were reported between $\sim 10^{-5}$ and 10^{-4} (Chatzis and Morrow 1984; Stegemeier 1974; Abrahams 1975) and are highlighted in Figure 8.1. N_{ce} values of the six slugs used in Experiment 18 to Experiment 23 lie on the left side to the critical N_c. The N_{ce} value of the slug used in Experiment 4 lies closer to critical N_c. Slugs used in these experiments are either Newtonian, water, viscous glycerin, or much less elastic HPAM polymer (Table 8.1 and Table 8.2). There is no significant

increase in the S_{or} reduction with the increase in the N_{ce} values up to critical N_c. The logarithmic fit made from these data is represented by Eq. 8.4. N_{ce} values of the remaining 17 data sets are higher than critical N_c values. A clear trend is seen that an increase in N_{ce} value results in a significant decrease in the S_{or} reduction. The relation between the N_{ce} and S_{or} after critical N_c is best fitted with the exponential function (Eq. 8.5).

For N_{ce} less than critical N_c,

$$S_{or} = -0.007 * \ln(N_{ce}) + 0.3523 \tag{8.4}$$

For N_{ce} greater than critical N_c,

$$S_{or} = 0.308 * Exp(-3.604 * N_{ce}) \tag{8.5}$$

Using these two fits, a predictive curve for 23 different sets is generated, which looks more like a typical CDC curve (Figure 8.2).

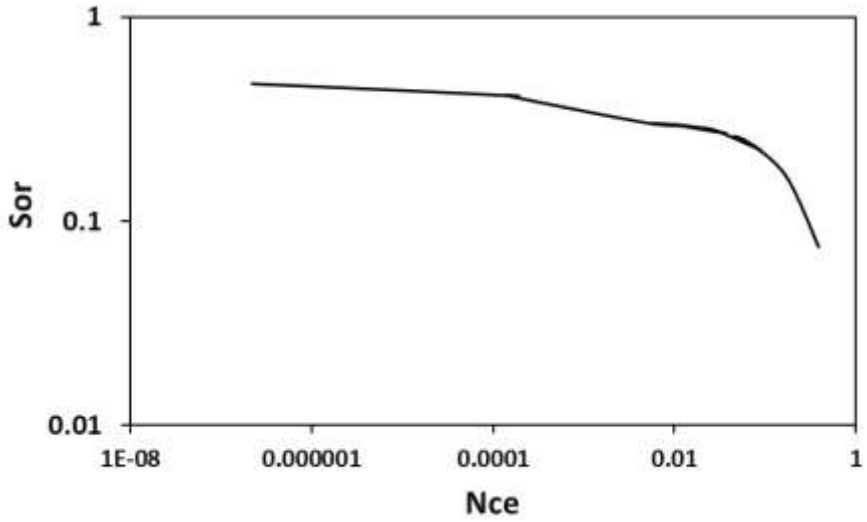

Figure 8.2: *Extensional CDC generated using the proposed correlations*

To predict the S_{or} reduction by viscoelastic polymers, only the bulk shear and extensional rheological properties of the polymer are needed. This can aid in the quick screening of optimal polymer for specific reservoir conditions. The curve is generated using 23 different data sets that have a wide variation in polymer properties, flux rates, formation nature, oil viscosities, and rheological behaviors. The polymer concentration ranges from 500 ppm to 6,000 ppm. The salinity

ranges from 2,000 ppm to 26,000 ppm. The temperature varies from room temperature to 68 ℃. The flux rate ranges from 0.14 ft/day to 5.28 ft/day. Different types of sandstone formation that were used are the Bentheimer sandstone, Berea sandstone, Boise sandstone, and Ottawa sand pack. Porosity ranges from 0.18 to 0.37. Permeability ranges from the 169 milli Darcy to 7,900 milli Darcy. Oil viscosity ranges from 7 cP to 300 cP. Viscoelastic polymers, viscous glycerin, and Newtonian water were also used in the development of correlation.

8.3.3. Extensional capillary number vs conventional capillary number

In this section, the predictability of N_{ce} is compared with N_c (Figure 8.3). The main limitation with the conventional N_c is that the N_c remains the same for the different sets of polymers that show drastic differences in the S_{or} reduction. For the similar value of N_c used in Experiment 1-12, 14, 17, 20-23, the S_{or} ranges from 0.08 to 0.45 (Table 8.2). Glycerin flooding used in Experiment 2 corresponding to the N_c of ~0.00005 at 2 ft/day resulted in the S_{or} of only 0.43, whereas HPAM 3630 used in Experiment 1 that corresponds to the N_c of ~ 0.00005 at 1ft/day resulted in the S_{or} of 0.198. This clearly implies that N_c cannot explain the relevant mechanisms causing S_{or} reduction by the viscoelastic polymers. Glycerin used in Experiment 23 corresponds to the N_{ce} of 0.000015. N_{ce} of HPAM 3630 used in Experiment 1 is 0.067, which is almost three orders higher than the N_{ce} of glycerin. HPAM 6040 and HPAM 3130 used in Experiment 13 and Experiment 14 correspond to the N_c of 0.000098 and 0.00007. S_{or} corresponding to HPAM 6040 and HPAM 3130 injections at 1ft/day are 0.32 and 0.42. Higher N_c of HPAM 3130, despite recovering lesser residual oil than HPAM 6040, again implies the inadequacy of conventional N_c. N_{ce} of HPAM 6040 and HPAM 3130 flooding are 0.009 and 0.0001 respectively. These results refute the conventional belief (Clarke et al. 2015) that apparent viscosity encompasses extensional viscosity or viscoelastic forces. Also, this discussion has reinforced Azad and Trivedi's (2018 d) claim that extensional rheology has a strong influence on the S_{or} reduction. Another interesting observation is the N_{ce} of all the viscoelastic polymers are higher than the N_c (Table 8.2). However, for the case of viscous glycerin, the N_c is slightly higher than the N_{ce} (Table 8.2). This is in accordance with Ashfargpour et al.'s (2012) observation that pressure drop exhibited by the viscoelastic polymers is higher around the pore scale when compared to pressure drop on the core-scale. Similarly, Ashfargpour et al. (2012) also reported that core-scale pressure drop is higher than pore-scale pressure drop for the viscous polymers. Azad and Trivedi (2018b) and Clarke et al. (2015) also reported that core-scale pressure drop is higher for the less elastic polymer (or more viscous polymer) at 1 ft/day

when compared to high elastic polymers (or less viscous polymer). These discussions clearly indicate that at low fluxes, shear viscosity representative of viscosity will be dominating the core-scale even if the extensional viscosity representative of elasticity of the viscoelastic polymers is dominating the pore scale.

Another discrepancy is that oil mobilization is occurring at the N_c values of less than 0.00001, which is less than the critical N_c value of 0.0001 (Abrams 1975; Qi et al. 2017). Complete oil mobilization up to S_{or} of less than 0.1 occurs only when the N_c value is 10^{-2} (Foster 1973; Abrams 1975; Chatzis and Morrow 1984; Jr. et al. 1985**)**. However, HPAM 3630 used in Experiment 3 that resulted in the S_{or} of 0.08 corresponds to the N_c and N_{ce} of 0.00058 and 0.438, respectively. This indicates that while N_c values are lower than the critical N_c, N_{ce} values are exceeding it. The proper relation between N_c and S_{or} is not seen. The best trend one can observe for these data sets has the R^2 value of only 2% to 5%. One cannot use the conventional N_c for predicting the viscoelastic polymer's residual oil recovery potential and it therefore cannot be used for screening optimal polymers. The first set of correlation developed using N_{ce} has an R^2 value of 82%. The second set of correlation using N_{ce} has a R^2 value of 91%. This clearly indicates the N_{ce} is a better method than N_c for quantifying the viscoelastic polymer's influence on S_{or} reduction.

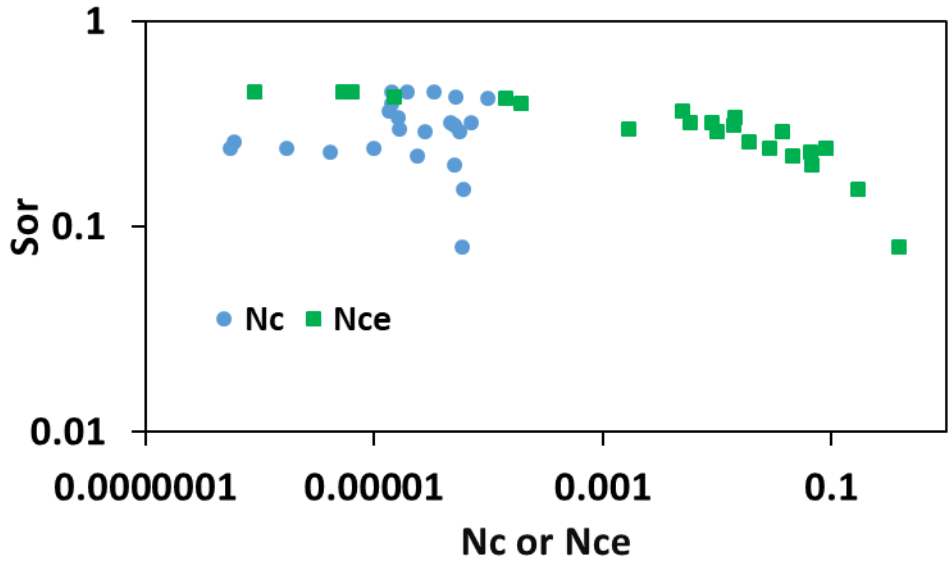

Figure 8.3: *A plot showing the relation between S_{or} verses N_c and N_{ce} of various polymers*

8.3.4 Extensional capillary number vs conventional Deborah number

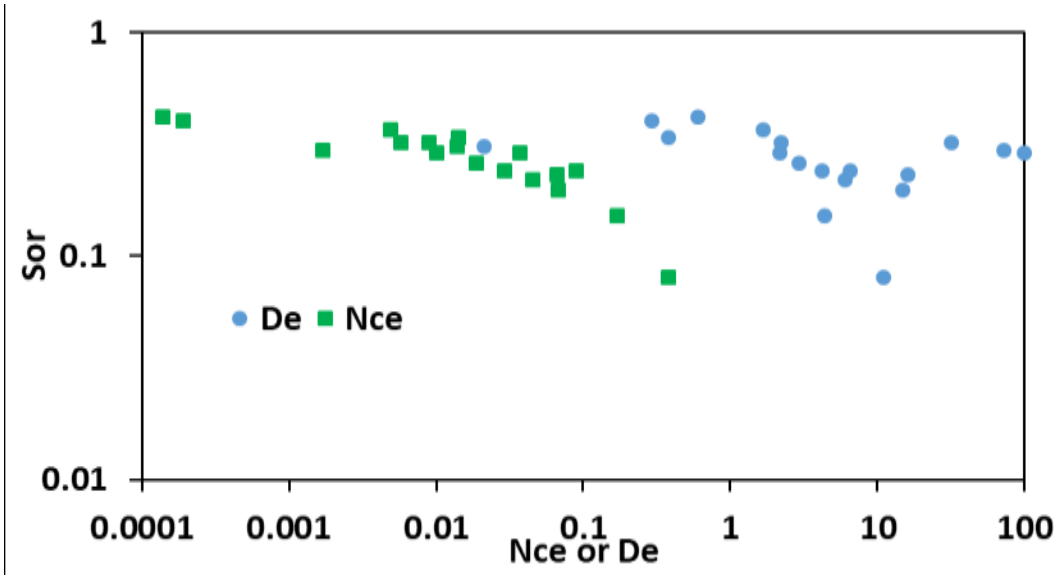

Figure 8.4: *The plot showing the relation between S_{or} verses N_c and N_{ce} of various polymers*

In this section, N_{ce} is compared with oscillatory D_e for 18 different data sets. D_e is widely used in the quantification of polymer's viscoelastic effects on the S_{or} reduction (Lotfollahi et al. 2016b; Qi et al. 2017; Erinick et al. 2018; Qi et al. 2018). As can be seen from Figure 8.4, there is no proper trend between D_e and S_{or}. An increase in D_e shows the rapid decrease in S_{or} up to a point, after which S_{or} increases rapidly with an increase in D_e. However, N_{ce} shows a clear trend: an increase in N_{ce} causes S_{or} reduction. These discrepancies are mainly caused by the salinity effect. Erinick et al. (2018) performed sequential flooding by injecting low saline polymer solutions and high saline polymer solutions. Erinick et al. (2018) reported that low saline HPAM solutions and high saline HPAM solutions used in Experiment 5 and Experiment 6 correspond to S_{or} reduction of 0.32 and 0.22 at the same flux rate of 1ft/day. However, the D_e of the high saline and low saline solutions are 32 and 6, respectively. Extensional rheological parameters are higher for the high saline solutions when compared to the low saline solutions (Table 8.2). Therefore, N_{ce} of the high saline solutions and low saline solutions are 0.045 and 0.0058, respectively. Similarly, in other sequential flooding performed by Erinick et al. (2018), high saline HPAM solutions used in Experiment 3 and operated at a flux rate of 4 ft/day resulted in the S_{or} of 0.08. However, low saline HPAM solutions used in Experiment 4 and flooded at a flux rate of 2 ft/day resulted in the S_{or} of 0.29. The D_e of high saline solutions used in Experiment 3 and low saline solutions used in Experiment 4 are 11 and 100. Higher values of extensional rheological parameters cause the N_{ce} of high saline solutions (0.438) to be one order higher than low saline solutions (0.042) (Table 8.2). Ehrenfried

(2013) performed two different flooding experiments using high saline and low saline viscoelastic polymer solutions (Experiment 7 and Experiment 9). The high saline polymer flooding experiments performed at a flux rate of 5.28 ft/day and with a D_e of 4.34 resulted in the S_{or} of 0.151. Low saline polymer flooding experiments performed with a flux rate of 1.07 and a much higher D_e of 72.9 resulted in the S_{or} of 0.297. It is also important to point out here that flux rates and D_e were increased up to 5.34 ft/day and 364.54 during the low saline polymer flooding (Ehrenfried 2013), but the S_{or} of low saline polymer flooding remains at 0.297. The oscillatory relaxation time of high saline solutions and low saline solutions, used in Experiment 7 and Experiment 9, are 0.11 seconds and 8.9 seconds, respectively (Ehrenfried 2013). The extensional relaxation time of these high saline and low saline polymer solutions are 0.229 seconds and 0.117 seconds, respectively (Table 8.2). It is an implication that oscillatory relaxation time of low saline polymer solutions is highly overestimated. The N_{ce} of low saline polymer solutions is 0.00171. The N_{ce} of high saline polymer solutions is 0.171, which is around two orders higher than the N_{ce} of low saline polymer solutions. These discussions clearly indicate the inefficiency of oscillatory rheology, which in turn is the reason for the skewed relation between oscillatory D_e and S_{or} (Figure 8.4). Polymer solutions flowing in porous media are subjected to a stretching phenomenon where the polymer solutions exhibit strong non-linear viscoelastic characteristics. Incorporating the oscillatory relaxation time calculated by using the linear oscillatory rheology is therefore not replicating the actual elastic resistance exhibited by the viscoelastic polymer solutions. It is clear that N_{ce} determined using the extensional rheological parameter is the most appropriate, best, and easiest method for predicting the S_{or} reduction caused by the viscoelastic polymer solutions.

8.3.5 Azad and Trivedi's correlation and Qi et al. (2018)'s correlation

Recently, Qi et al. (2018) proposed a relation between S_{or} and D_e. Two sets of correlations were developed based on the value of D_e (Eq. 8.6 and Eq. 8.7).

For D_e less than 1,

$$\frac{S_{orp}}{S_{orw}} = 1 \tag{8.6}$$

For D_e greater than 1,

$$\frac{S_{orp}}{S_{orw}} = 1 - 0.133 * \log(D_e) \tag{8.7}$$

where

S_{orp} is the residual oil saturation to polymer flood

S_{orw} is the residual oil saturation to water flood.

S_{or} to polymer flood can be predicted using Qi et al.'s (2018) correlation if the S_{orw} and D_e are known. AT-C represented by Eq. 8.4 and Eq. 8.5 also can predict the S_{or} to polymer flooding, if N_{ce} is known. Both of these methods do not require any core flood experiments. S_{orp} predictability by AT-C and Qi et al.'s (2018) correlation are compared with actual S_{or} values (Table 8.3). Figure 8.5 plots the actual S_{or} values and predicted S_{or} values for all the experiments (1-18)

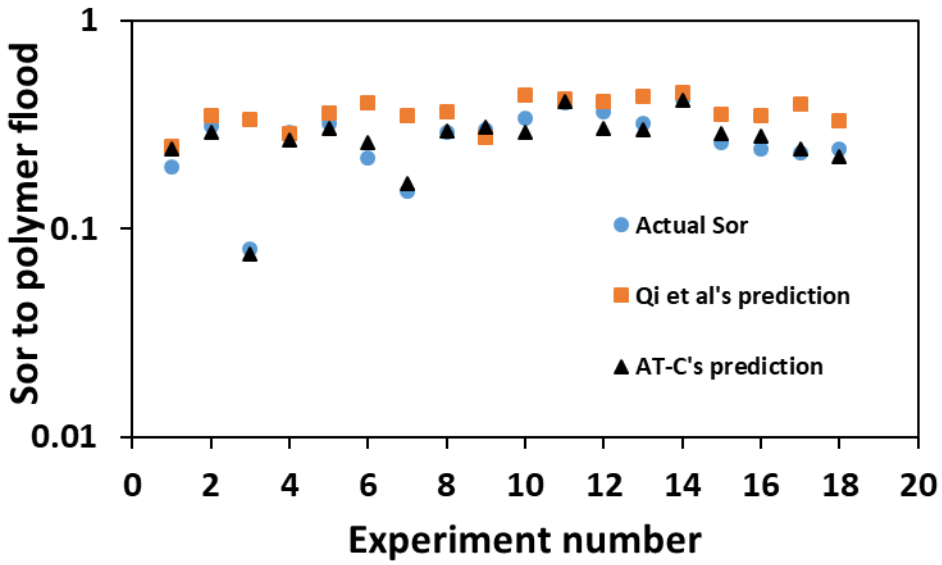

Figure 8.5: *The plot comparing the actual S_{or} values with the values predicted AT-C and Qi et al. (2018)'s correlation for various experiments*

Table 8.3: *Predicatability of correlation used by Qi et al. (2018) and AT-C*

Data set	Actual S_{or}	Qi et al. (2018)'s correlation predictions	AT-C's predictions

1	0.198	0.249	0.24
2	0.31	0.35	0.292
3	0.08	0.335	0.075
4	0.29	0.285	0.268
5	0.32	0.359	0.301
6	0.22	0.403	0.26
7	0.151	0.348	0.165
8	0.289	0.363	0.296
9	0.297	0.273	0.306
10	0.337	0.44	0.292
11	0.4	0.42	0.409
12	0.366	0.407	0.302
13	0.32	0.429	0.298
14	0.42	0.45	0.412
15	0.26	0.356	0.287
16	0.24	0.348	0.277
17	0.23	0.394	0.241
18	0.24	0.329	0.222

In general, it is clear that AT-C has a better predictability than the correlation proposed by Qi et al. (2018). For Experiment 3, S_{or} predicted by AT-C, Qi et al.'s correlation is 0.075 and 0.335, respectively (Table 8.3 and Figure 8.5). The actual S_{or} value for Experiment 3 is 0.08 (Table 8.3), which is very close to AT-C's predictions. Similarly for Experiment 6, S_{or} predicted by AT-C is 0.26, which is closer to its actual S_{or} value of 0.22 (Table 8.3). Again, the Qi et al.'s (2018) prediction for Experiment 6 is 0.403, which is very high when compared to the actual value. For Experiment 7, the predicted S_{or} values by AT-C and Qi et al.'s (2018) correlation are 0.163 and 0.348. Actual S_{or} value of 0.151 are again closer to AT-C's prediction. All of this analysis clearly indicates that S_{or} values are over predicted by Qi et al.'s (2018) correlation in these experiments.

Looking at Table 8.1, it is clear that all of these experiments (Experiment 3, Experiment 6, and Experiment 7) are carried out at high salinity and the values of the extensional rheological parameters are higher at high salinity (Table 8.2; Azad and Trivedi 2018c). An opposite behavior is seen in Experiment 9, where S_{or} predicted by the Qi et al.'s (2018) correlation is low, in the range of 0.273, whereas the actual values and AT-C's predicted values are relatively higher (0.297 and 0.306). The salinity of Experiment 9 is low, which overestimates the elastic effect and underestimates the S_{or} of polymer flood. Seright et al. (2011a) discussed that at high salinity, electrostatic repulsion causes the polymer solutions to exist in the coiled state. However, at the low salinity, electrostatic repulsion is not dominant, which causes the polymer to exist in the uncoiled form itself. The amount of energy needed to uncoil the coiled polymer chains for making it flow through the pore constriction is higher in the case of high salinity. For the uncoiled polymer chains, the energy needed to stretch the polymer chains around the pore-scale is relatively lesser. This could be the reason for the higher extensional values and lower extensional values shown by high saline and low saline polymer solutions, respectively (Table 8.1 and Table 8.2). Qi et al.'s (2018) correlation developed based on the oscillatory Deborah number overpredicts the elastic effect of low saline solutions and underpredicts the elastic effects of high saline solutions. Since AT-C developed based on the N_{ce} is calculated using the extensional parameters, it clearly distinguishes the polymer based on its actual residual oil recovery potential.

Another discrepancy is seen in Experiment 14, Experiment 15, and Experiment 17 where there is a slight difference in the prediction between Qi et al.'s (2018) correlation and actual value (Table 8.3). All these experiments were performed using sand packs of very high permeability Table 8.1). Generally, the capillarity will be less in the sand pack, which might have caused higher residual oil recovery for the similar viscous driving force. Capillarity and capillary pressure are indirectly proportional to permeability, pore radius, and IFT (Peter 2002). Since the Qi et al.'s (2018) correlation was developed using only Bentheimer and Berea sandstone, this effect might not have been captured in their proposed correlation. Particularly in Experiment 17, there is a notable difference between the S_{or} predicted by the Qi et al.'s (2018) correlation (0.394) and actual S_{or} value (0.23) (Table 8.3). Apart from the high permeability (7351 mD), oil viscosity (250 cP) is relatively very high in Experiment 17, which might have resulted in the poor sweep. Water flood resulted in the very high S_{or} because of both residual and unswept oil. As per the Qi et al.'s (2018) correlation, S_{or} to polymer flood will be higher when S_{or} to water flood is higher. But S_{or} to polymer

flood will become low in the sand pack characterized by high permeability and low capillarity once the viscous fingering is prevented by the polymer flooding. This highlights the deficiency of Qi et al.'s (2018) correlation, which was developed based on the experiments conducted using the Bentheimer and Berea formation. As discussed before, the main discrepancies with Qi et al.'s (2018) correlation is the persistent usage of oscillatory rheological parameters which affect its residual oil recovery predictability even in the Bentheimer and Berea formation.

8.4 Conclusions

The novelty of the work is that the extensional capillary number developed using the modified AT-VEM is the first and only version of the capillary number that can be used to quantify the S_{or} reduction caused by the viscoelastic polymer solutions. A comparative prediction is made between the N_{ce}, N_c, and D_e. The limitation associated with conventional N_c and D_e is clearly highlighted and a detailed discussion is provided on why the proposed N_{ce} is a better method. Capillary theory considered to be invalidated in the case of viscoelastic polymer flooding is validated using the N_{ce}. The correlation developed using the N_{ce} is the first and only method that can predict the S_{or} reduction caused by the viscoelastic polymer solutions through bulk extensional rheology. This will help in choosing the optimal polymer for specific reservoir conditions. Two sets of correlations are developed using 23 different data sets. The first correlation could predict the S_{or} reduction up to the critical N_c and the second correlation could predict the S_{or} reduction shown by the viscoelastic polymer solutions after the critical N_c. The proposed correlations can predict the S_{or} for a varying range of reservoir permeability (169 mD to 7.9 D), porosity (0.18 to 0.37), brine salinity (2000 ppm to 26000 ppm), concentration (500 ppm to 6000 ppm), polymer molecular weight (6 MDa to 35 MDa), flux (0.14 ft/day to 5.8 ft/day), sandstone (benthemier, boise, berea, and sand pack), and oil viscosity (7 cP to 300 cP). For high saline viscoelastic polymer flooding, AT-C has a better S_{or} predictability than Qi et al.'s (2018) correlation. N_{ce} and the proposed correlation can be incorporated into the reservoir simulator for predicting the S_{or} reduction potential of the viscoelastic polymers.

Supplementary figures

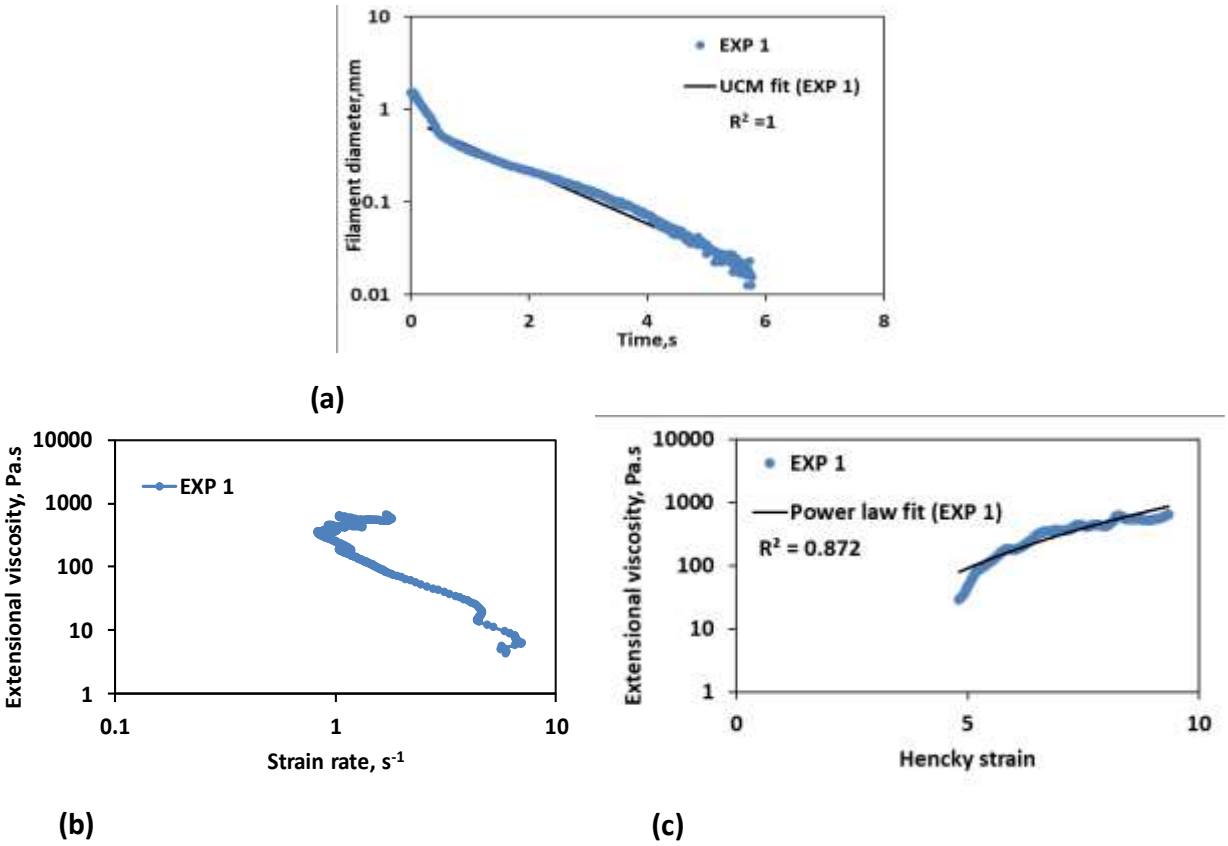

Figure S-8.1: *Filament diameter vs time plot for EXP 1 and the UCM fit to the linear elastic regimes for the determination of relaxation time b) Extensional viscosity as a function of generated strain rate plot showing the sharp rise in the extensional viscosity around the critical Deborah number c) Power law fit to the extensional viscosity vs Hencky strain values around the critical Deborah number for the determination of strain hardening index.*

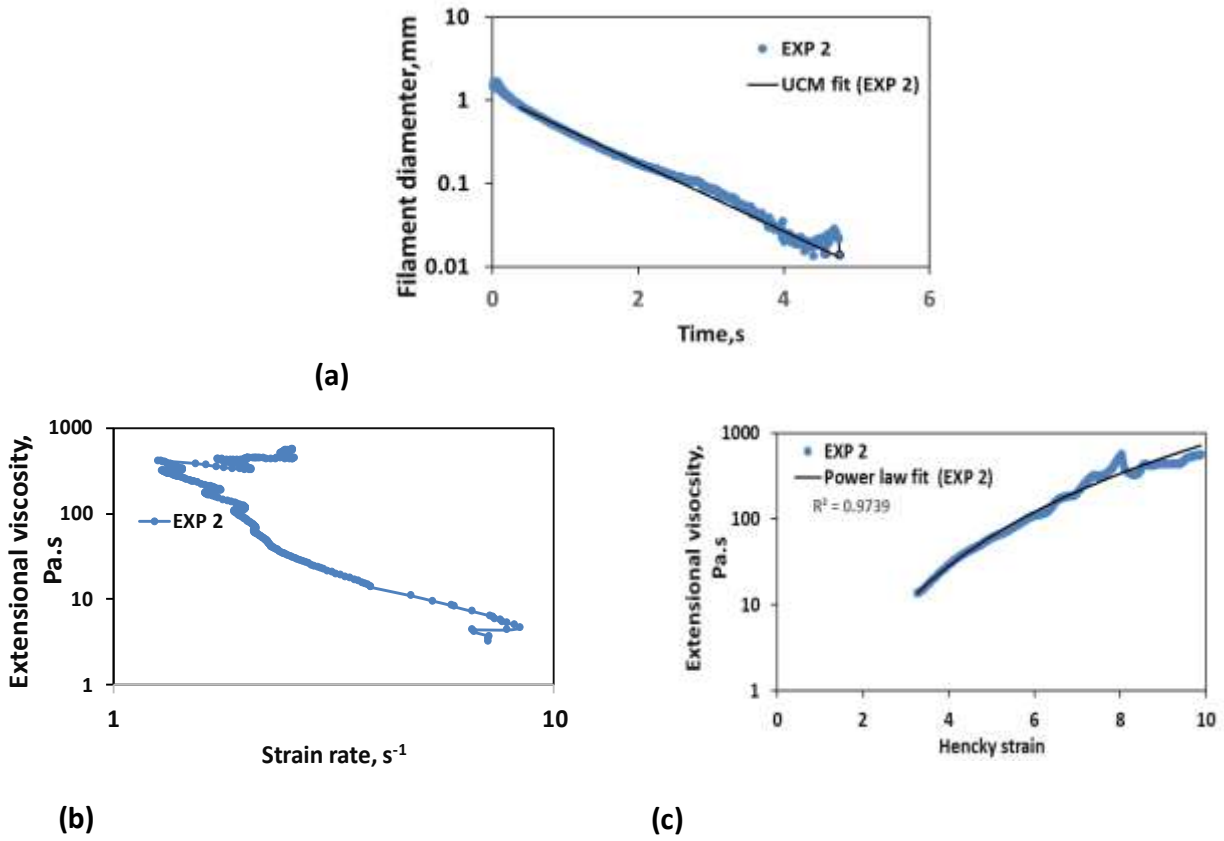

Figure S-8.2: *Filament diameter vs time plot for EXP 2 and the UCM fit to the linear elastic regimes for the determination of relaxation time b) Extensional viscosity as a function of generated strain rate plot showing the sharp rise in the extensional viscosity around the critical Deborah number c) Power law fit to the extensional viscosity vs Hencky strain values around the critical Deborah number for the determination of strain hardening index.*

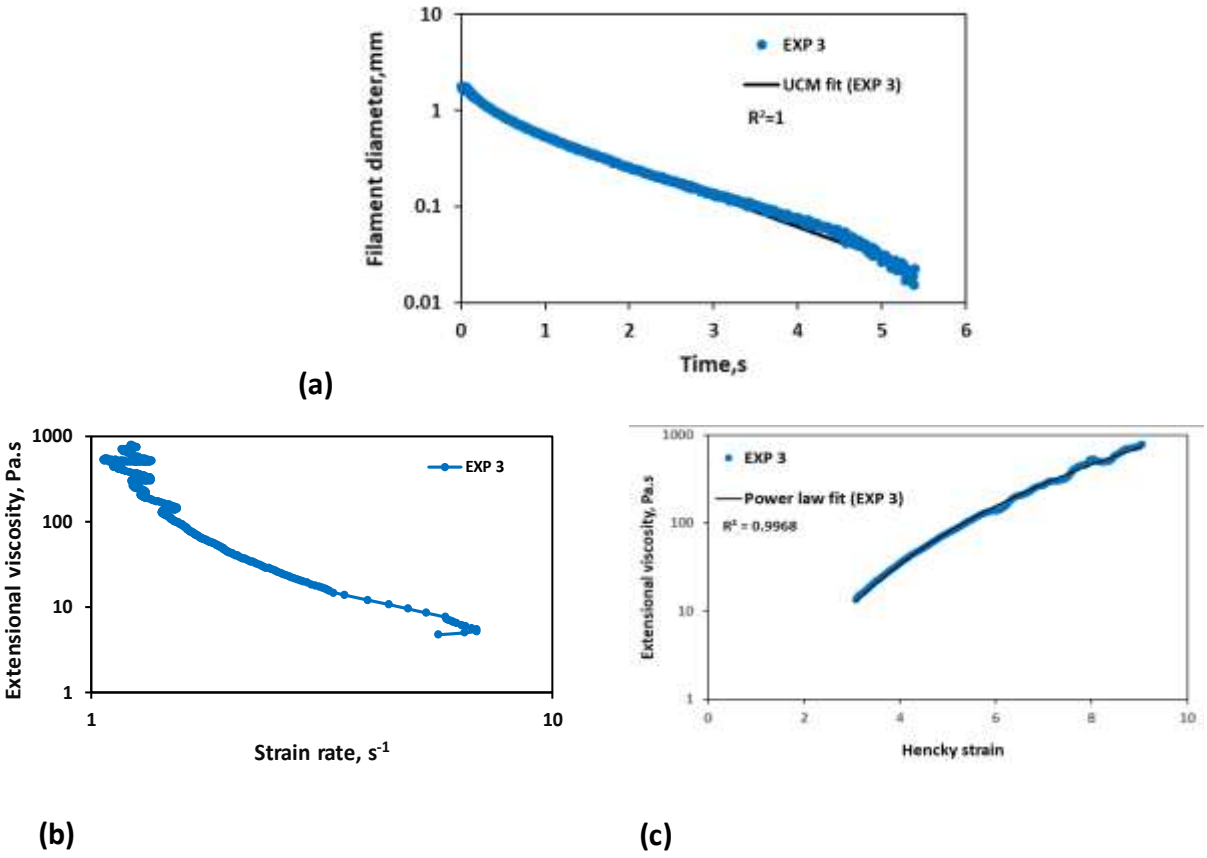

Figure S-8.3: *Filament diameter vs time plot for EXP 3 and the UCM fit to the linear elastic regimes for the determination of relaxation time b) Extensional viscosity as a function of generated strain rate plot showing the sharp rise in the extensional viscosity around the critical Deborah number c) Power law fit to the extensional viscosity vs Hencky strain values around the critical Deborah number for the determination of strain hardening index.*

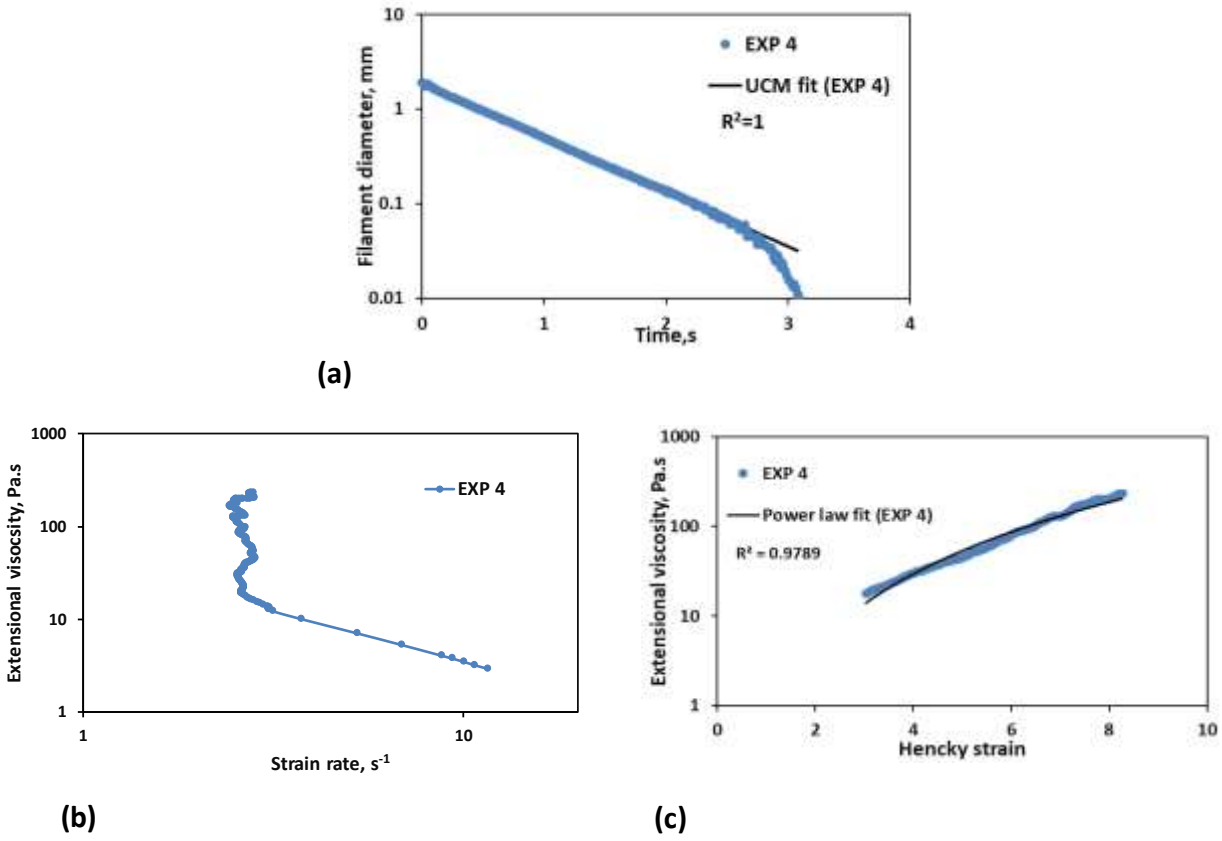

Figure S-8.4: *Filament diameter vs time plot for EXP 4 and the UCM fit to the linear elastic regimes for the determination of relaxation time b) Extensional viscosity as a function of generated strain rate plot showing the sharp rise in the extensional viscosity around the critical Deborah number c) Power law fit to the extensional viscosity vs Hencky strain values around the critical Deborah number for the determination of strain hardening index.*

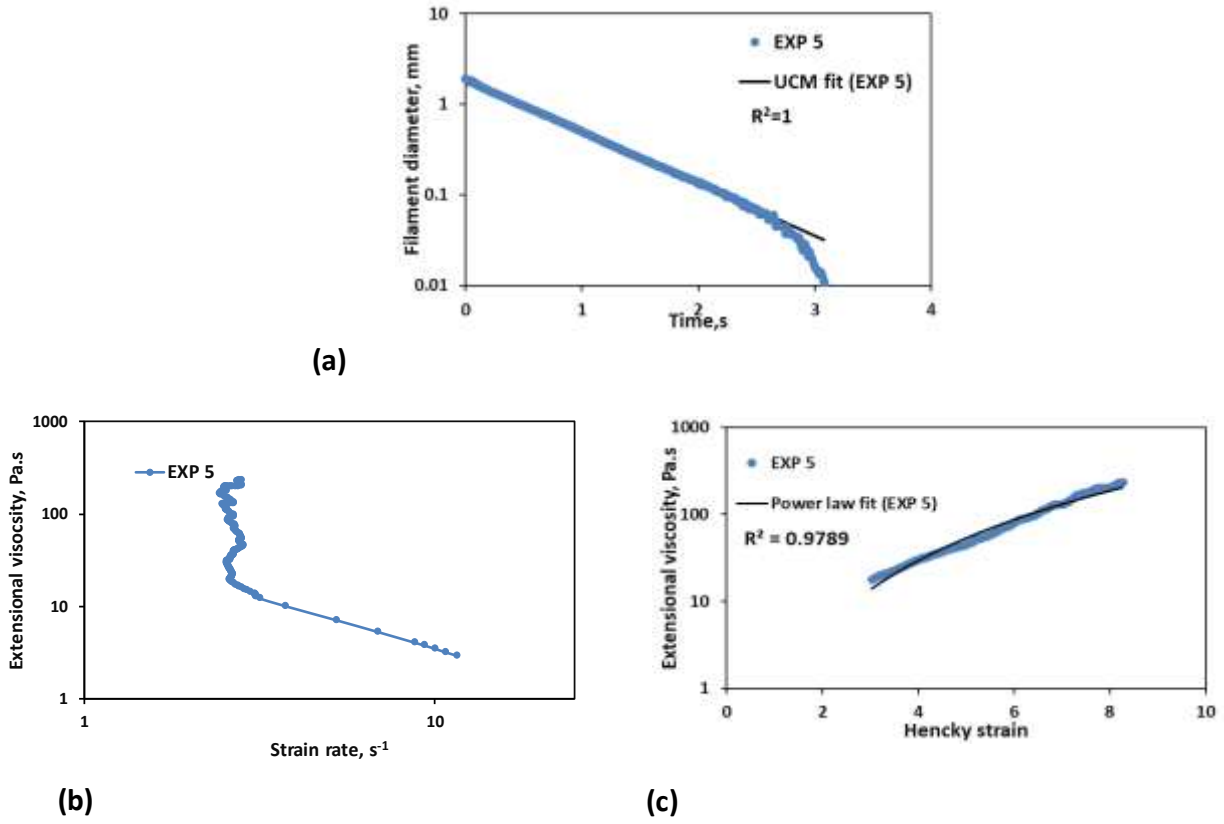

Figure S-8.5: *Filament diameter vs time plot for EXP 5 and the UCM fit to the linear elastic regimes for the determination of relaxation time b) Extensional viscosity as a function of generated strain rate plot showing the sharp rise in the extensional viscosity around the critical Deborah number c) Power law fit to the extensional viscosity vs Hencky strain values around the critical Deborah number for the determination of strain hardening index.*

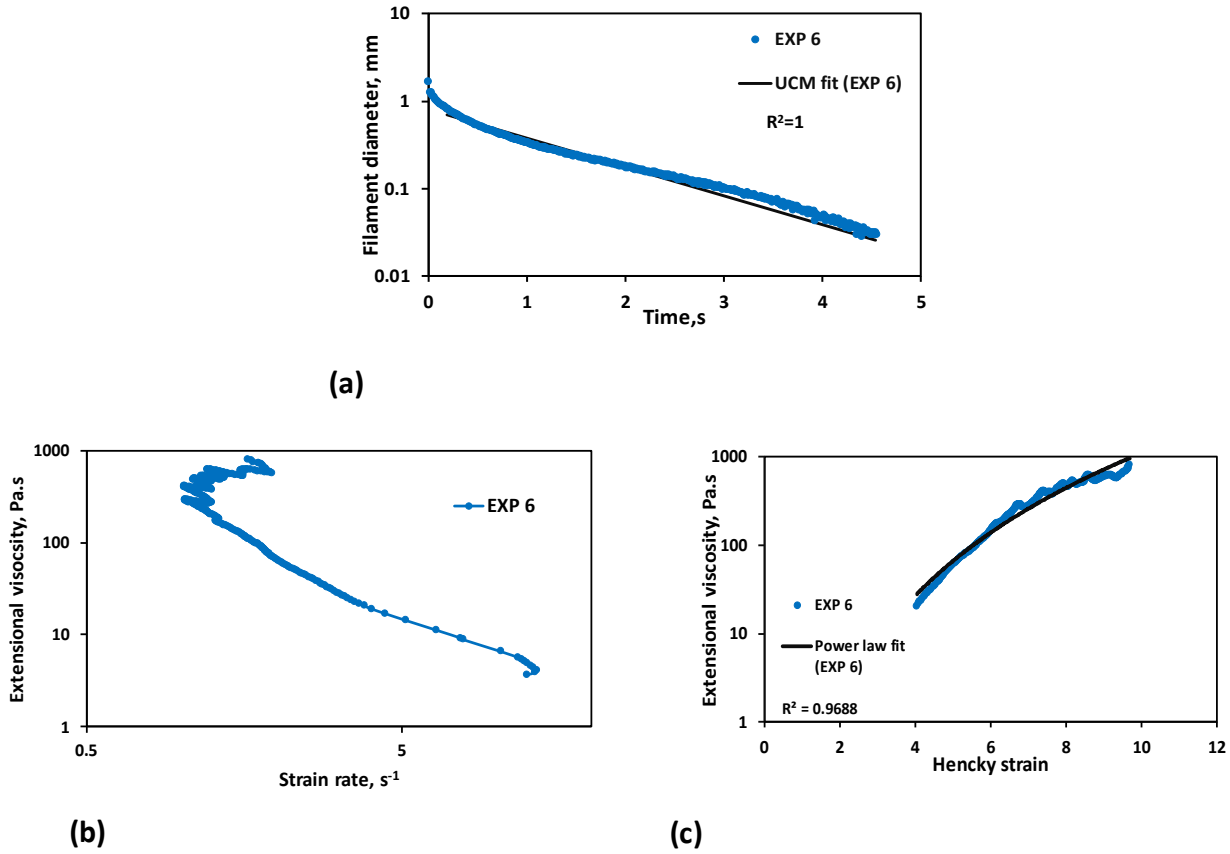

Figure S-8.6: *Filament diameter vs time plot for EXP 6 and the UCM fit to the linear elastic regimes for the determination of relaxation time b) Extensional viscosity as a function of generated strain rate plot showing the sharp rise in the extensional viscosity around the critical Deborah number c) Power law fit to the extensional viscosity vs Hencky strain values around the critical Deborah number for the determination of strain hardening index.*

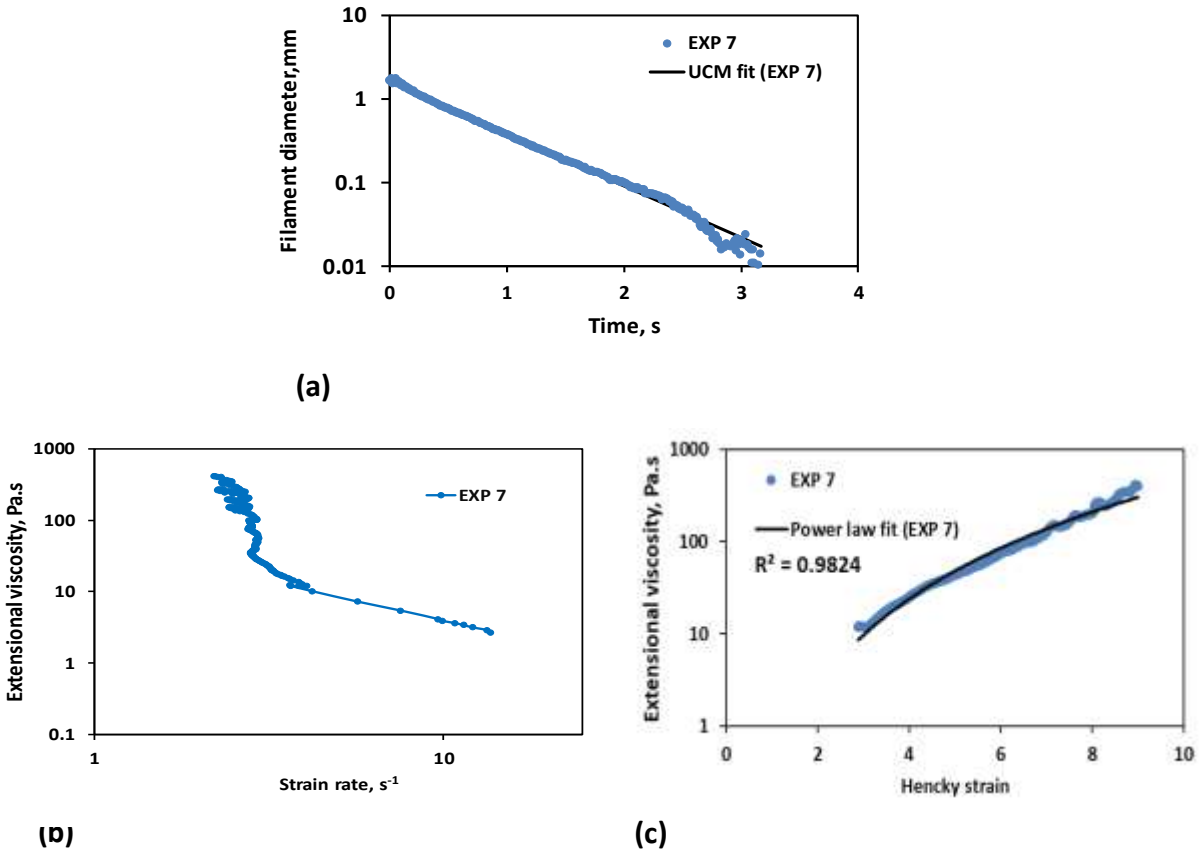

Figure S-8.7: *Filament diameter vs time plot for EXP 7 and the UCM fit to the linear elastic regimes for the determination of relaxation time b) Extensional viscosity as a function of generated strain rate plot showing the sharp rise in the extensional viscosity around the critical Deborah number c) Power law fit to the extensional viscosity vs Hencky strain values around the critical Deborah number for the determination of strain hardening index.*

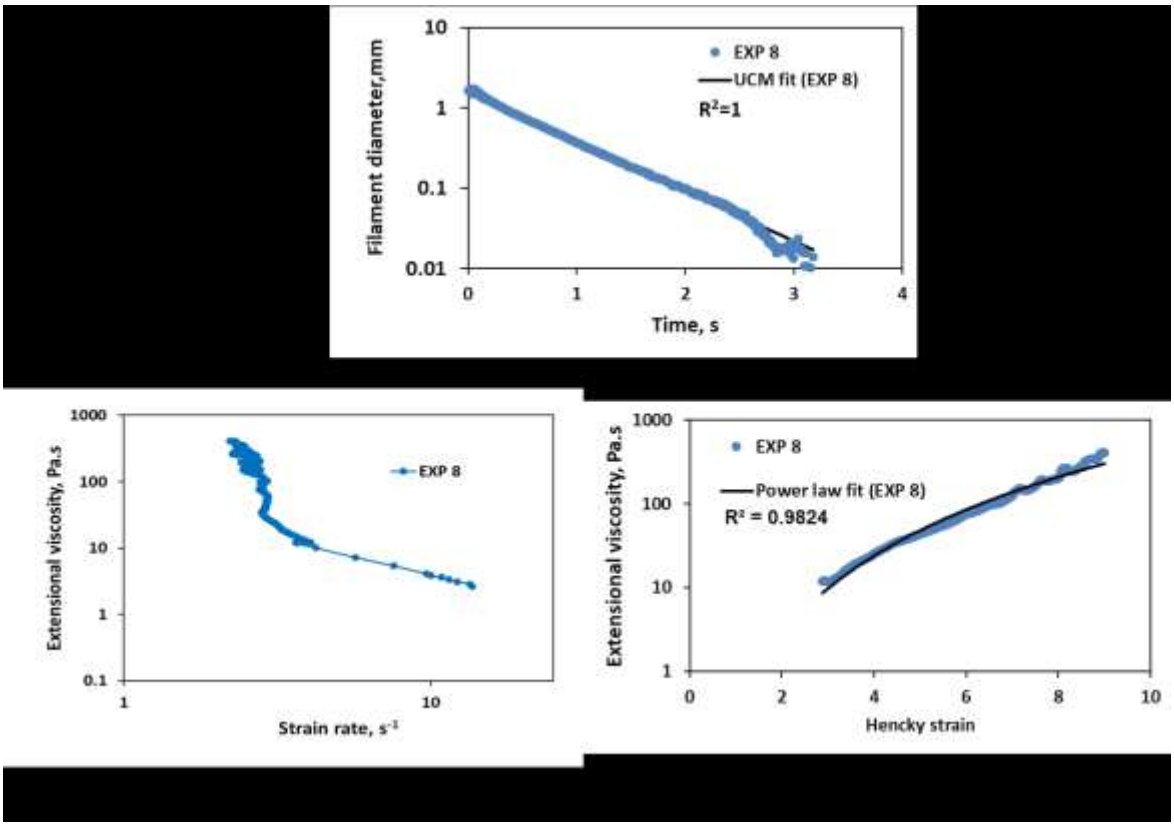

Figure S-8.8: *Filament diameter vs time plot for EXP 8 and the UCM fit to the linear elastic regimes for the determination of relaxation time b) Extensional viscosity as a function of generated strain rate plot showing the sharp rise in the extensional viscosity around the critical Deborah number c) Power law fit to the extensional viscosity vs Hencky strain values around the critical Deborah number for the determination of strain hardening index.*

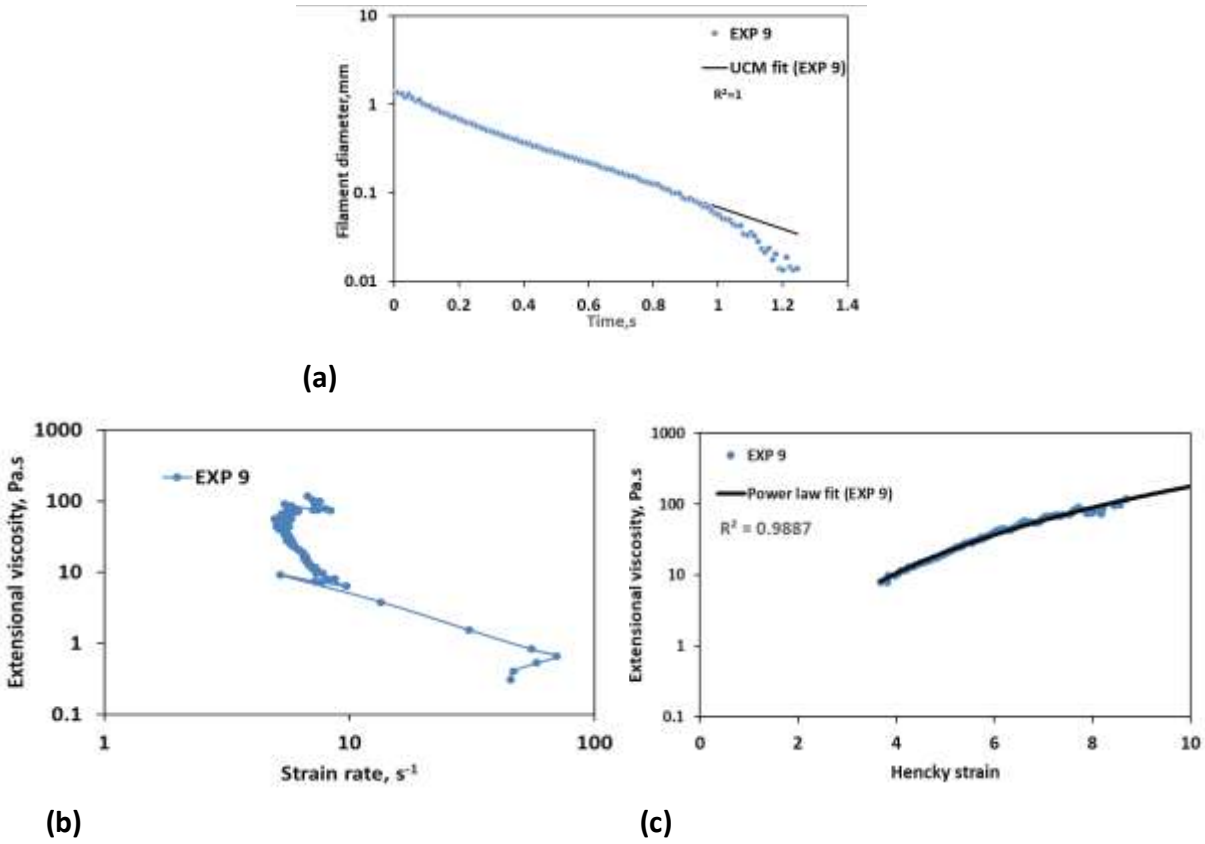

Figure S-8.9: *Filament diameter vs time plot for EXP 9 and the UCM fit to the linear elastic regimes for the determination of relaxation time b) Extensional viscosity as a function of generated strain rate plot showing the sharp rise in the extensional viscosity around the critical Deborah number c) Power law fit to the extensional viscosity vs Hencky strain values around the critical Deborah number for the determination of strain hardening index.*

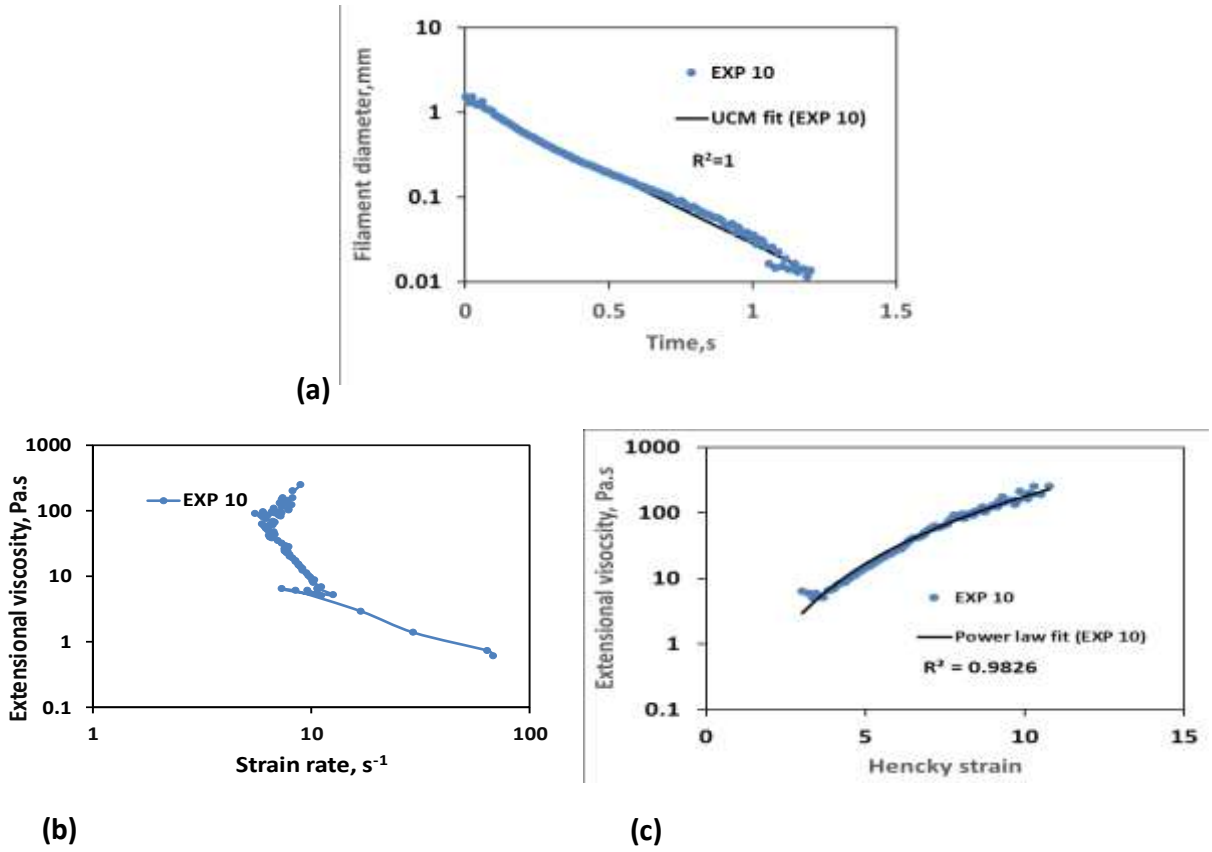

Figure S-8.10: *Filament diameter vs time plot for EXP 10 and the UCM fit to the linear elastic regimes for the determination of relaxation time b) Extensional viscosity as a function of generated strain rate plot showing the sharp rise in the extensional viscosity around the critical Deborah number c) Power law fit to the extensional viscosity vs Hencky strain values around the critical Deborah number for the determination of strain hardening index.*

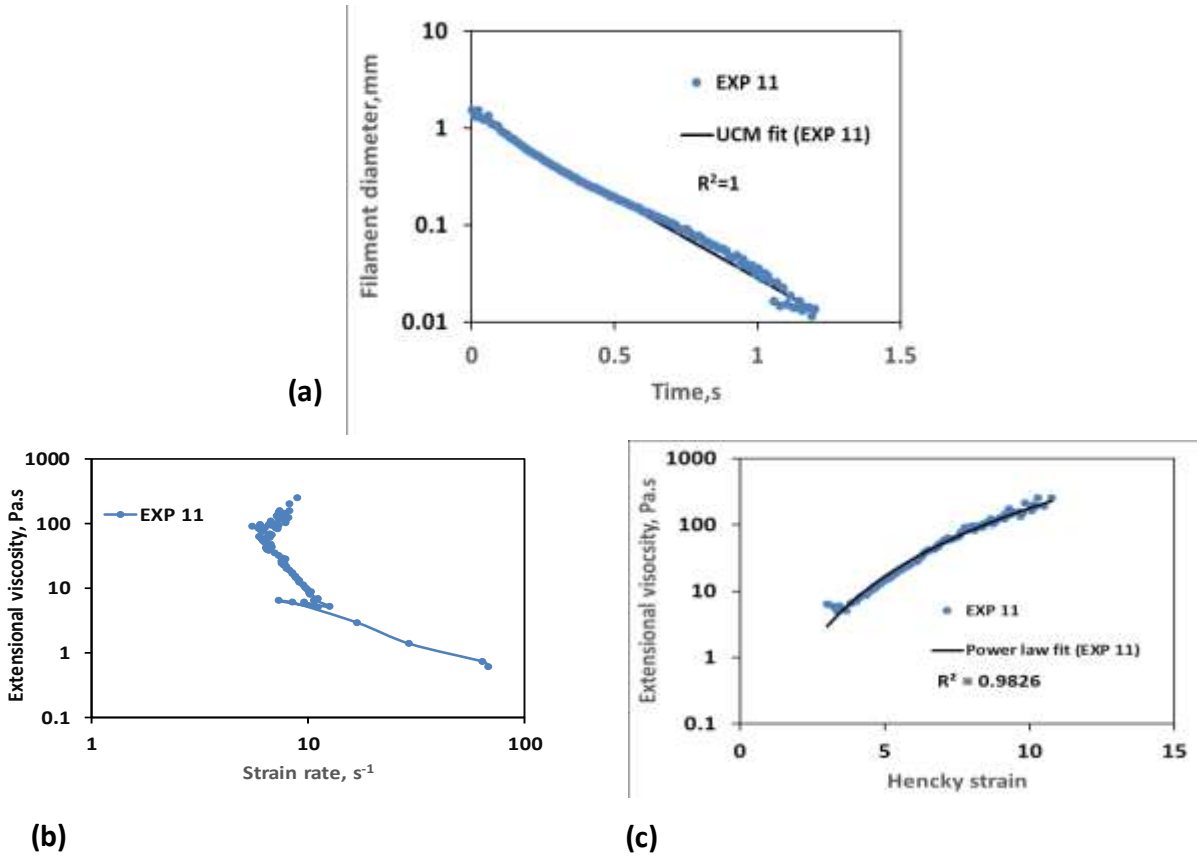

Figure S-8.11: *Filament diameter vs time plot for EXP 11 and the UCM fit to the linear elastic regimes for the determination of relaxation time b) Extensional viscosity as a function of generated strain rate plot showing the sharp rise in the extensional viscosity around the critical Deborah number c) Power law fit to the extensional viscosity vs Hencky strain values around the critical Deborah number for the determination of strain hardening index.*

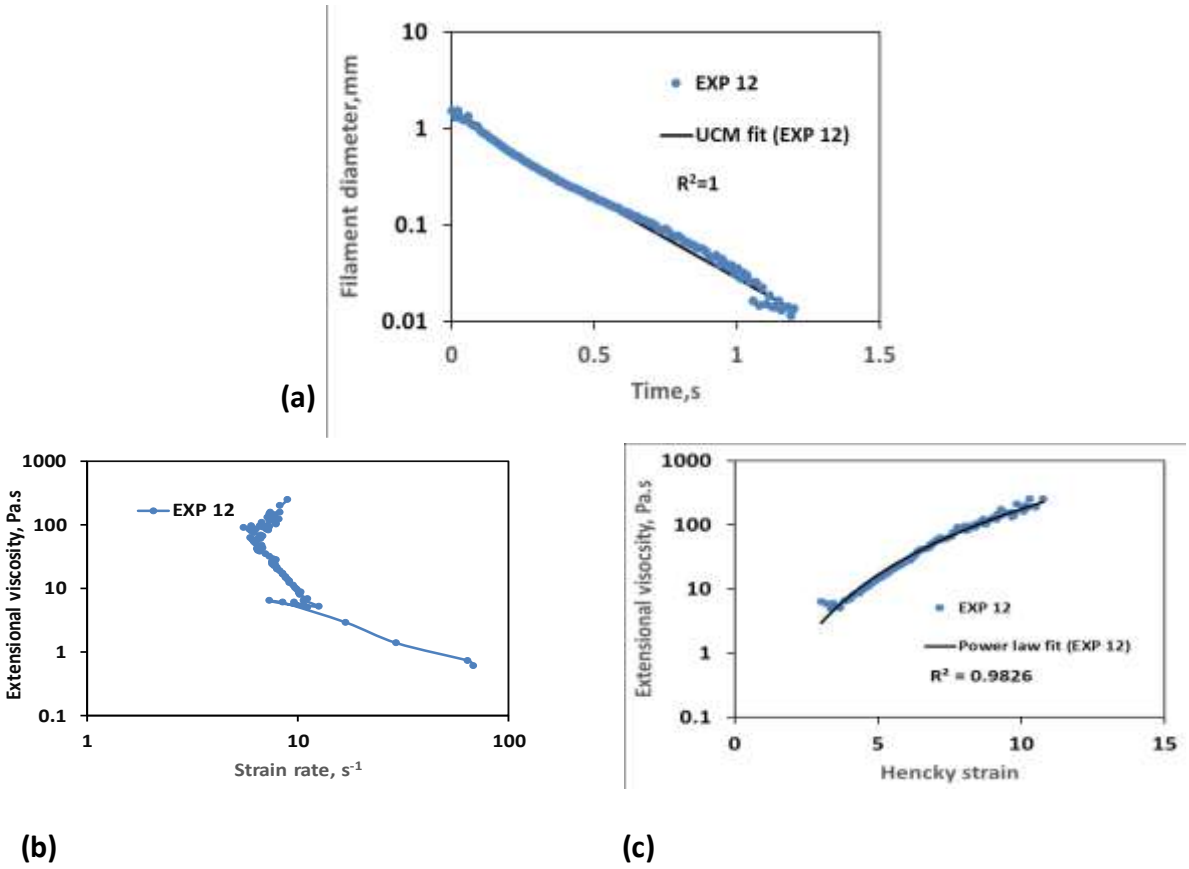

Figure S-8.12: *Filament diameter vs time plot for EXP 12 and the UCM fit to the linear elastic regimes for the determination of relaxation time b) Extensional viscosity as a function of generated strain rate plot showing the sharp rise in the extensional viscosity around the critical Deborah number c) Power law fit to the extensional viscosity vs Hencky strain values around the critical Deborah number for the determination of strain hardening index.*

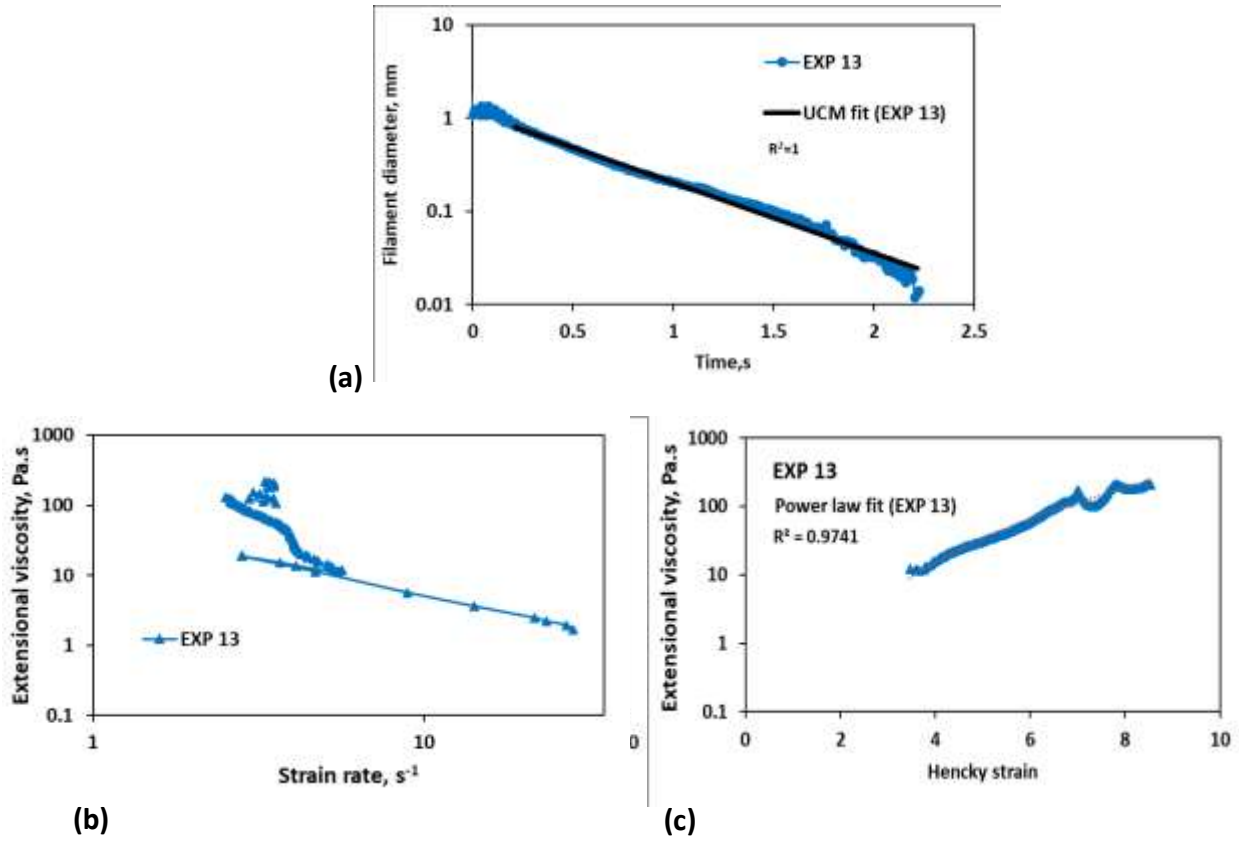

Figure S-8.13: *Filament diameter vs time plot for EXP 13 and the UCM fit to the linear elastic regimes for the determination of relaxation time b) Extensional viscosity as a function of generated strain rate plot showing the sharp rise in the extensional viscosity around the critical Deborah number c) Power law fit to the extensional viscosity vs Hencky strain values around the critical Deborah number for the determination of strain hardening index.*

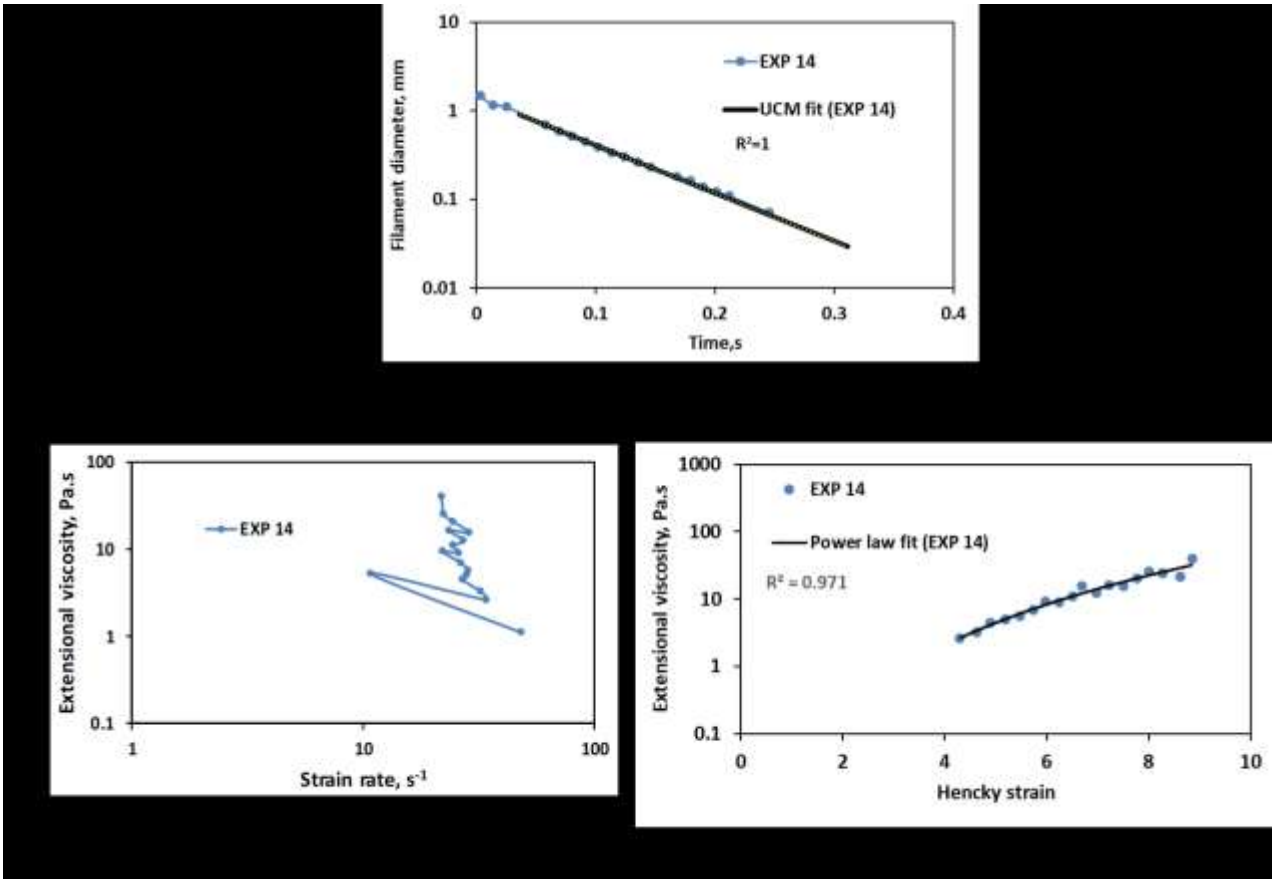

Figure S-8.14: *Filament diameter vs time plot for EXP 14 and the UCM fit to the linear elastic regimes for the determination of relaxation time b) Extensional viscosity as a function of generated strain rate plot showing the sharp rise in the extensional viscosity around the critical Deborah number c) Power law fit to the extensional viscosity vs Hencky strain values around the critical Deborah number for the determination of strain hardening index.*

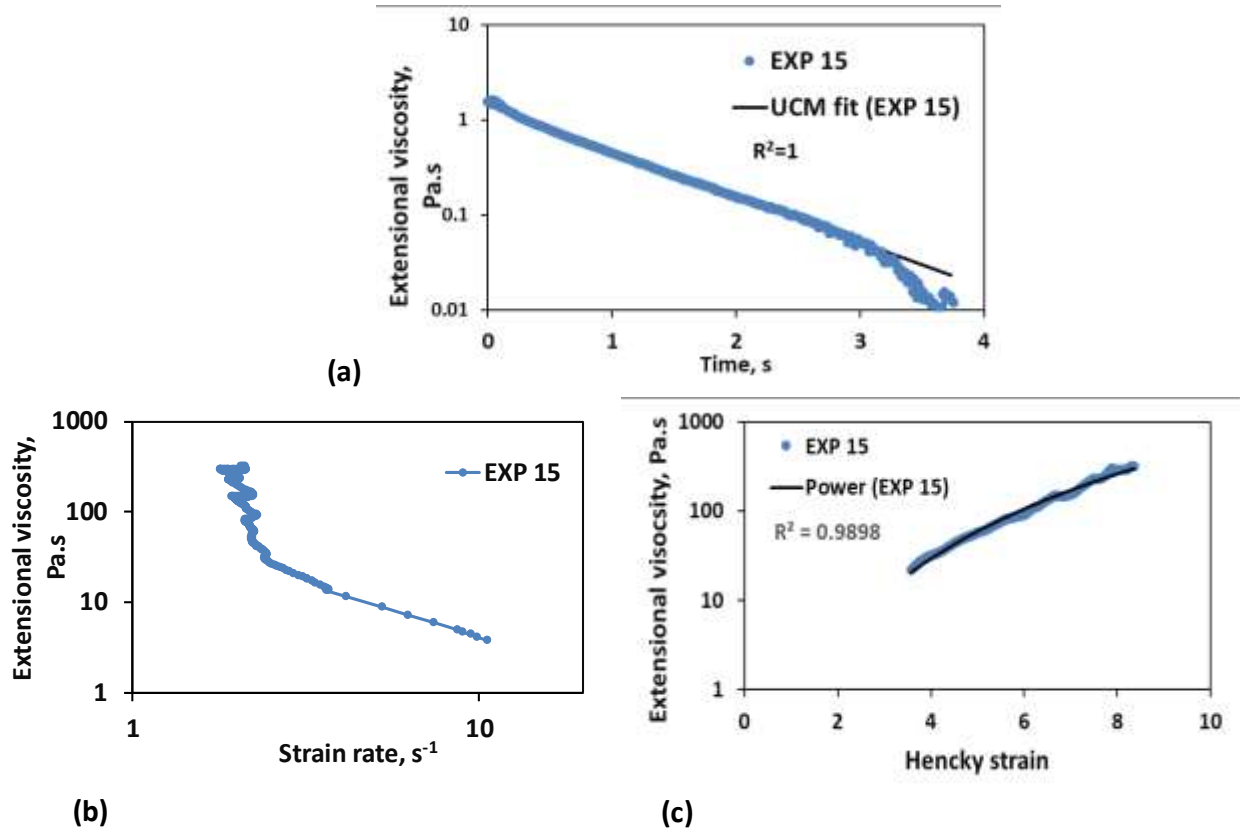

Figure S-8.15: *Filament diameter vs time plot for EXP 15 and the UCM fit to the linear elastic regimes for the determination of relaxation time b) Extensional viscosity as a function of generated strain rate plot showing the sharp rise in the extensional viscosity around the critical Deborah number c) Power law fit to the extensional viscosity vs Hencky strain values around the critical Deborah number for the determination of strain hardening index.*

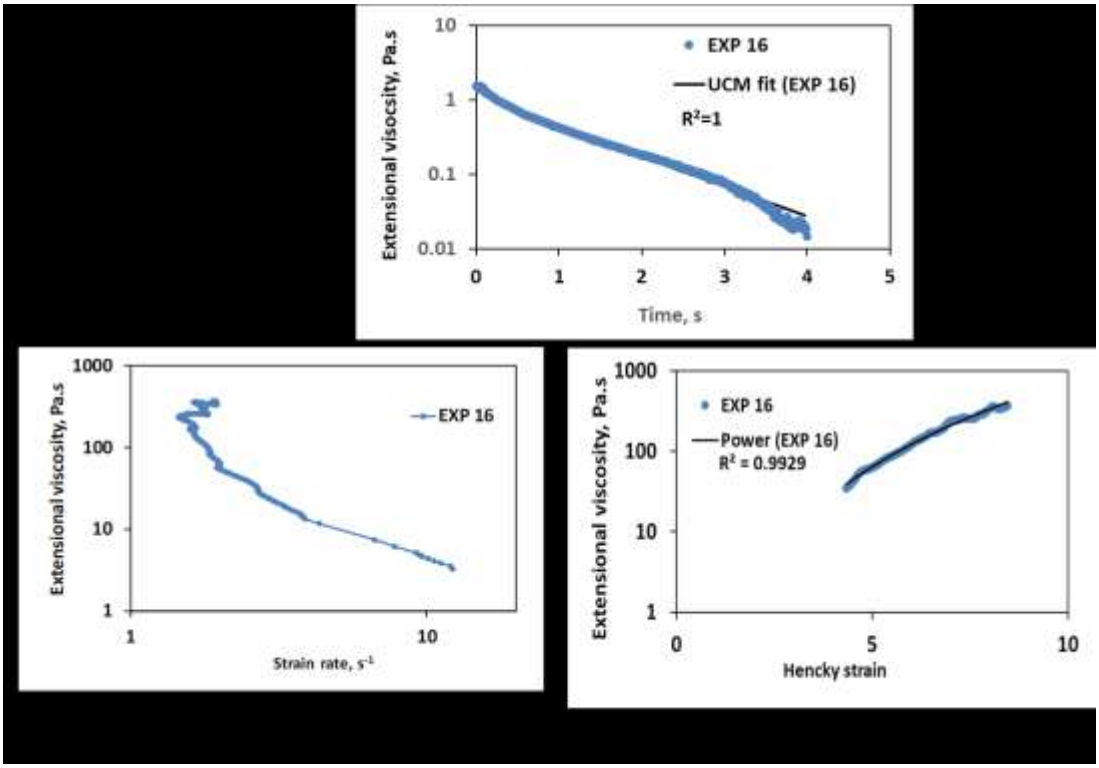

Figure S-8.16: *Filament diameter vs time plot for EXP 16 and the UCM fit to the linear elastic regimes for the determination of relaxation time b) Extensional viscosity as a function of generated strain rate plot showing the sharp rise in the extensional viscosity around the critical Deborah number c) Power law fit to the extensional viscosity vs Hencky strain values around the critical Deborah number for the determination of strain hardening index.*

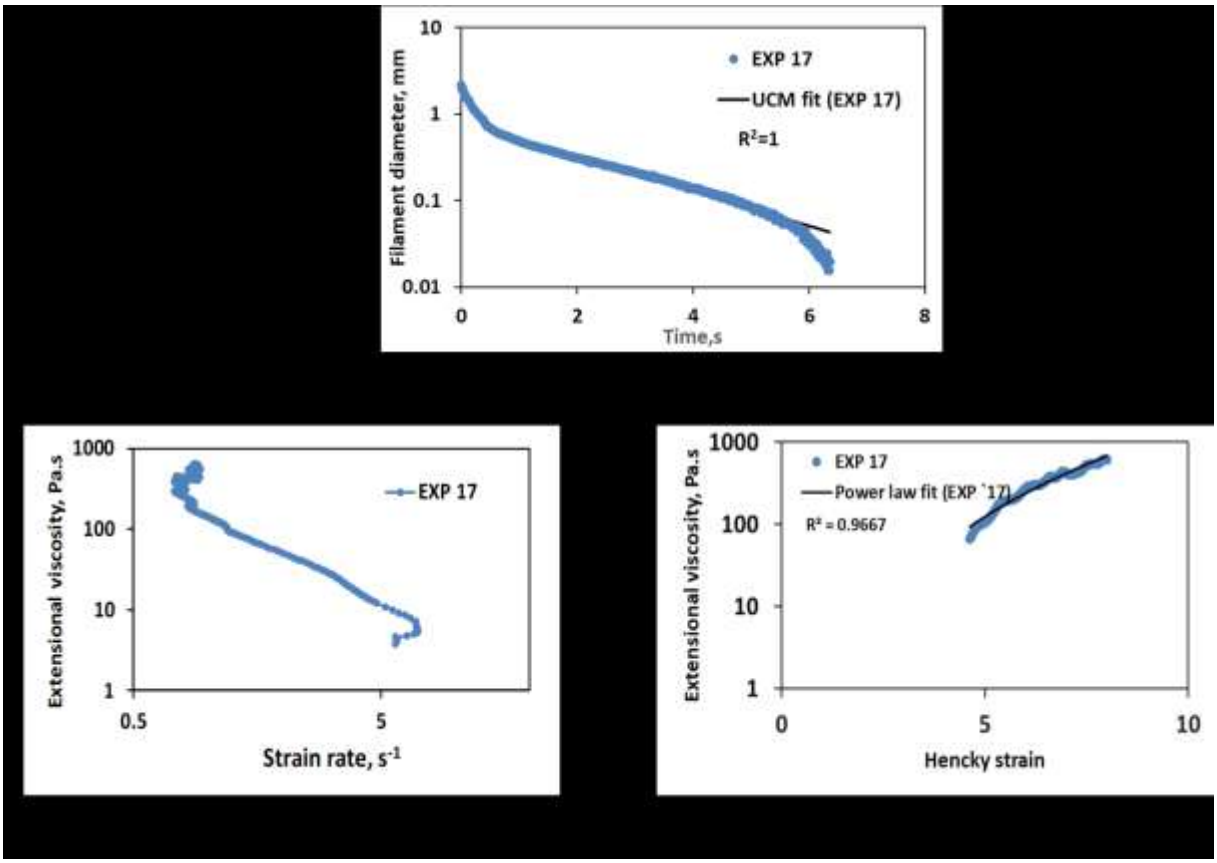

Figure S-8.17: *Filament diameter vs time plot for EXP 17 and the UCM fit to the linear elastic regimes for the determination of relaxation time b) Extensional viscosity as a function of generated strain rate plot showing the sharp rise in the extensional viscosity around the critical Deborah number c) Power law fit to the extensional viscosity vs Hencky strain values around the critical Deborah number for the determination of strain hardening index.*

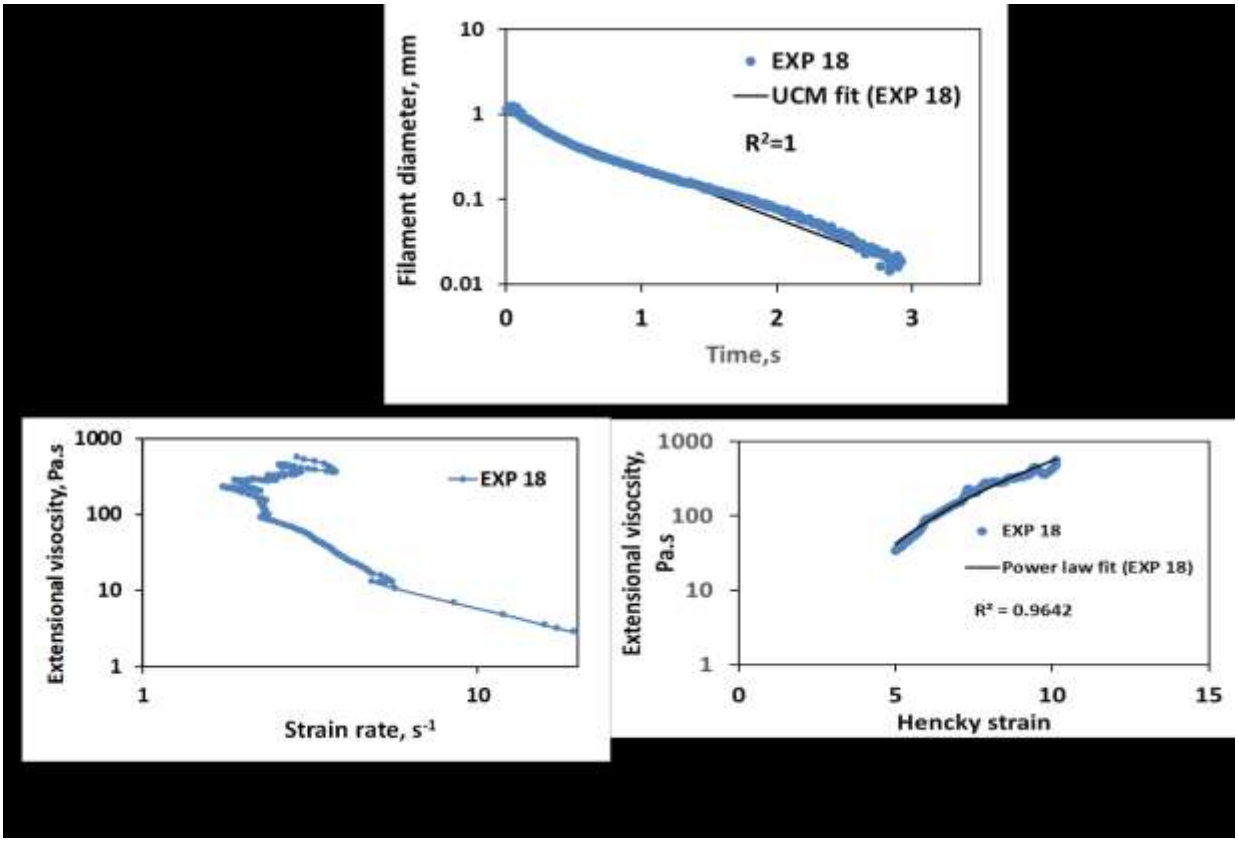

Figure S-8.18: *Filament diameter vs time plot for EXP 18 and the UCM fit to the linear elastic regimes for the determination of relaxation time b) Extensional viscosity as a function of generated strain rate plot showing the sharp rise in the extensional viscosity around the critical Deborah number c) Power law fit to the extensional viscosity vs Hencky strain values around the critical Deborah number for the determination of strain hardening index.*

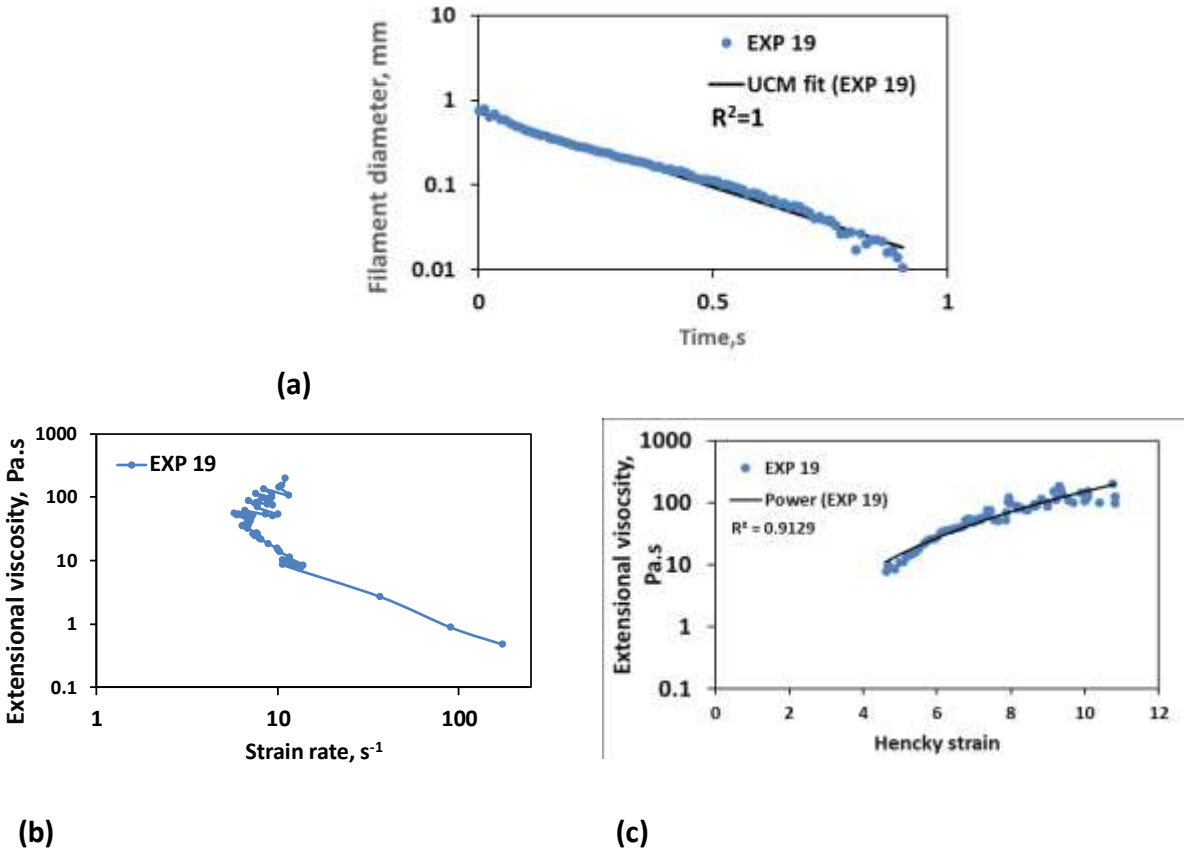

Figure S-8.19: *Filament diameter vs time plot for EXP 19 and the UCM fit to the linear elastic regimes for the determination of relaxation time b) Extensional viscosity as a function of generated strain rate plot showing the sharp rise in the extensional viscosity around the critical Deborah number c) Power law fit to the extensional viscosity vs Hencky strain values around the critical Deborah number for the determination of strain hardening index.*

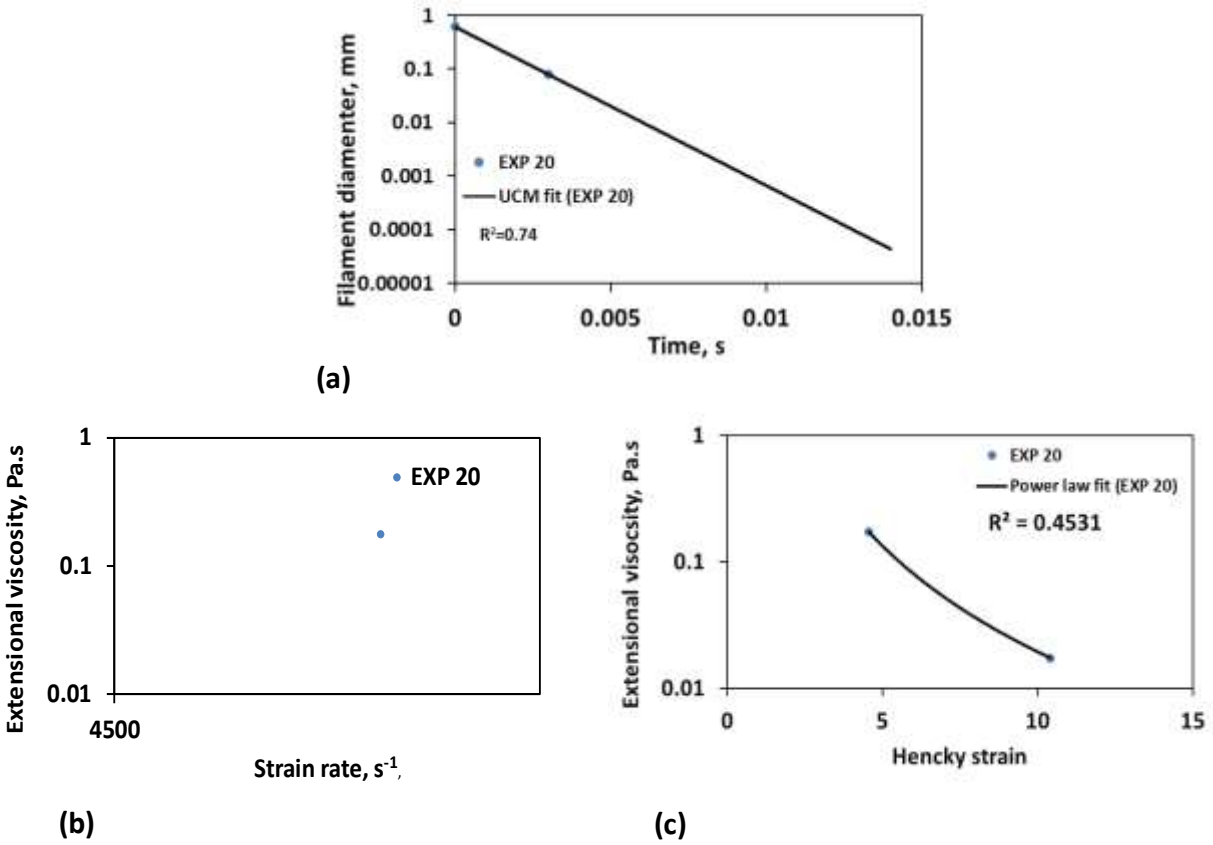

Figure S-8.20: *Filament diameter vs time plot for EXP 20 and the UCM fit to the linear elastic regimes for the determination of relaxation time b) Extensional viscosity as a function of generated strain rate plot showing the sharp rise in the extensional viscosity around the critical Deborah number c) Power law fit to the extensional viscosity vs Hencky strain values around the critical Deborah number for the determination of strain hardening index.*

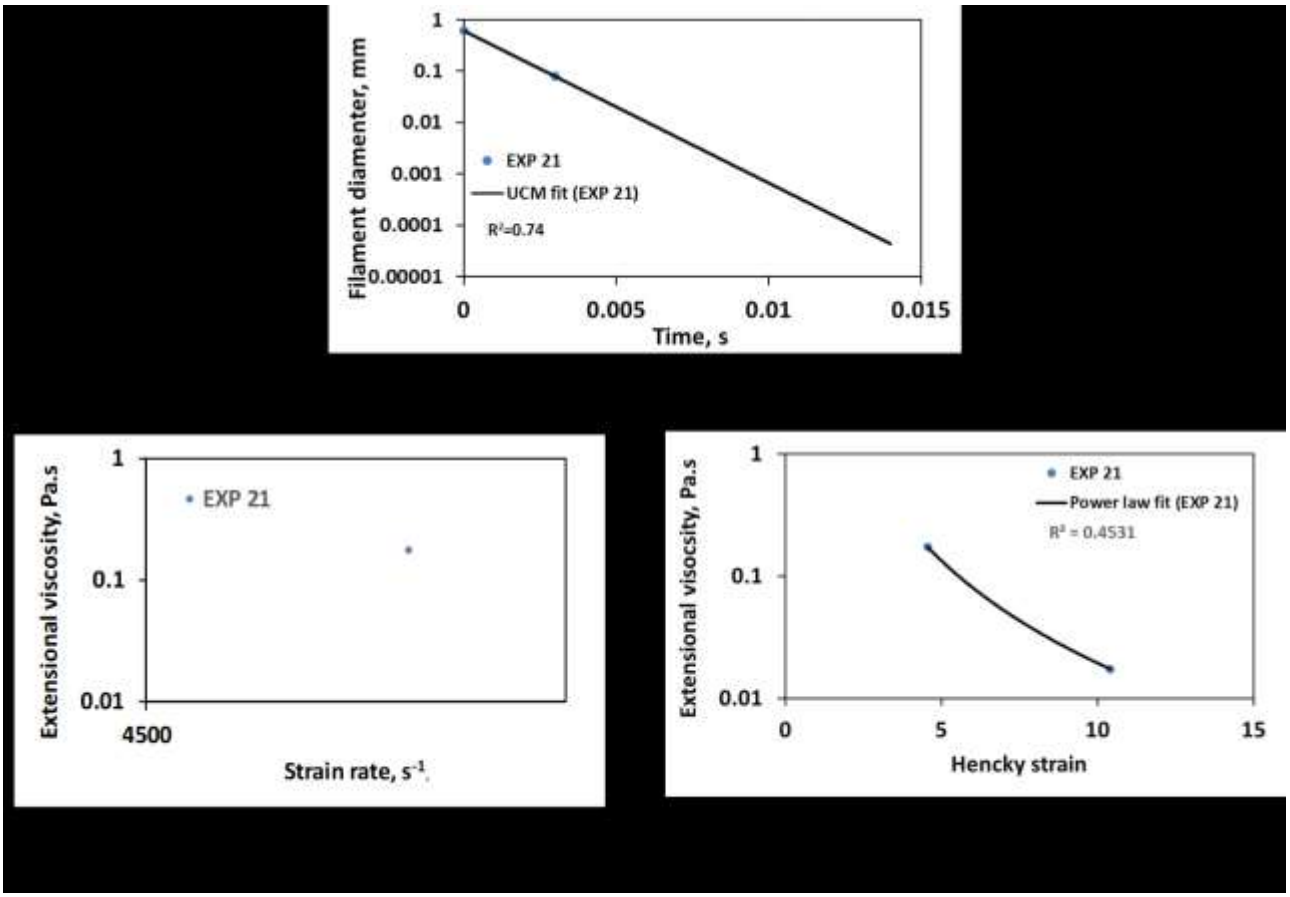

Figure S-8.21: *Filament diameter vs time plot for EXP 21 and the UCM fit to the linear elastic regimes for the determination of relaxation time b) Extensional viscosity as a function of generated strain rate plot showing the sharp rise in the extensional viscosity around the critical Deborah number c) Power law fit to the extensional viscosity vs Hencky strain values around the critical Deborah number for the determination of strain hardening index.*

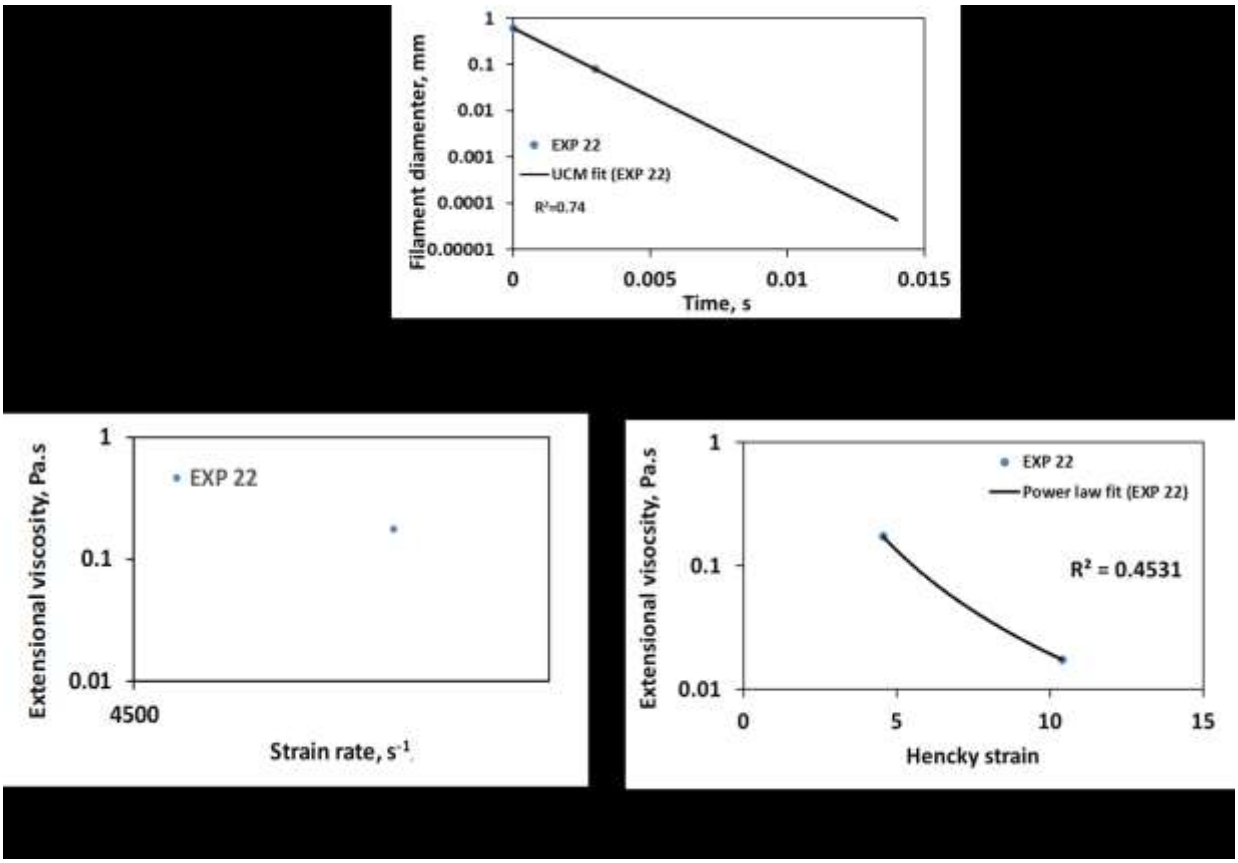

Figure S-8.22: *Filament diameter vs time plot for EXP 22 and the UCM fit to the linear elastic regimes for the determination of relaxation time b) Extensional viscosity as a function of generated strain rate plot showing the sharp rise in the extensional viscosity around the critical Deborah number c) Power law fit to the extensional viscosity vs Hencky strain values around the critical Deborah number for the determination of strain hardening index.*

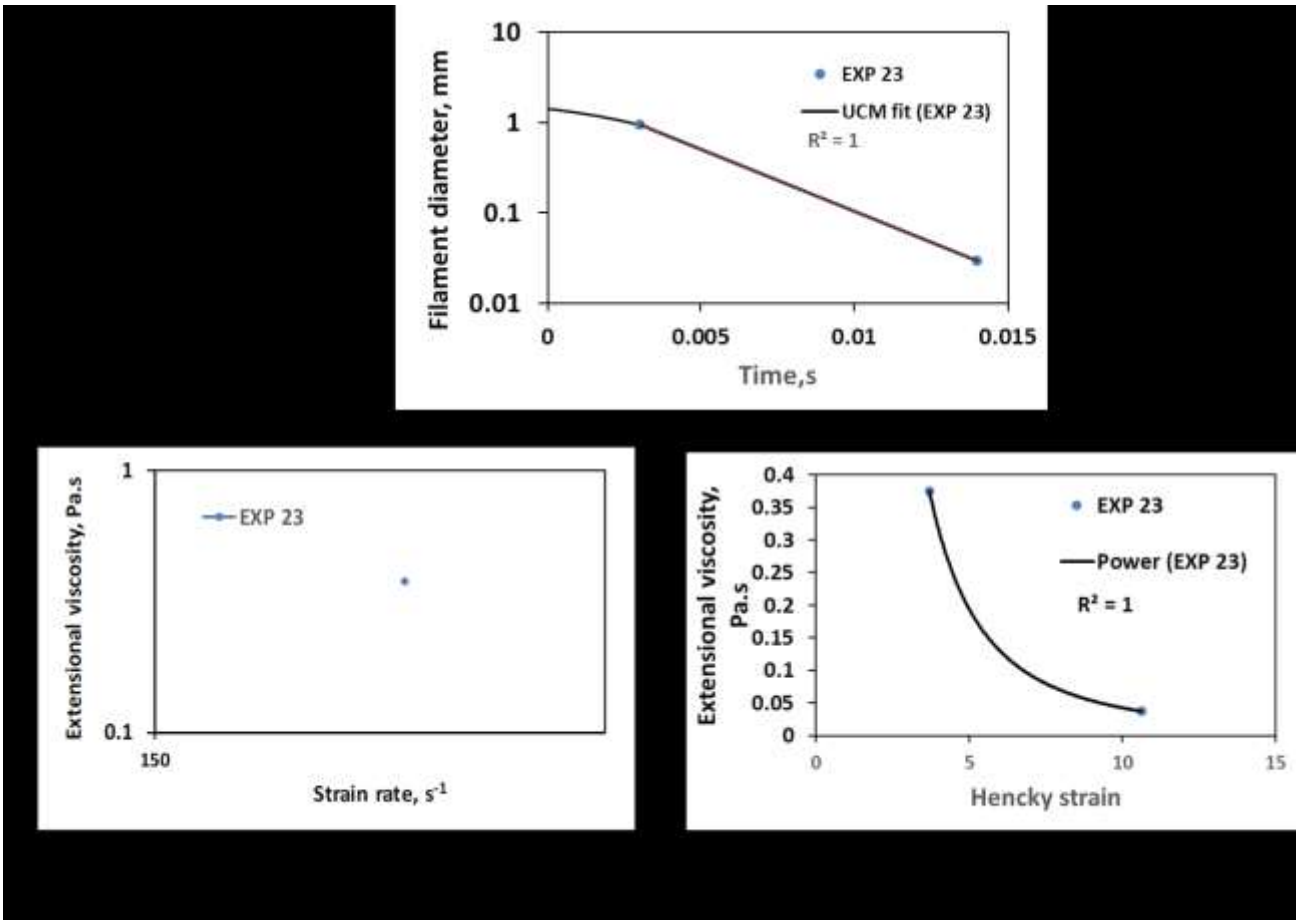

Figure S-8.23: *Filament diameter vs time plot for EXP 23 and the UCM fit to the linear elastic regimes for the determination of relaxation time b) Extensional viscosity as a function of generated strain rate plot showing the sharp rise in the extensional viscosity around the critical Deborah number c) Power law fit to the extensional viscosity vs Hencky strain values around the critical Deborah number for the determination of strain hardening index.*

Chapter 9: Conclusions

9.1 Conclusions

HPAM and an associative polymer having similar shear viscosity were during the oil recovery experiments. However, the maximum pressure generated during associative polymer injection in the homogeneous core is more than twice the pressure generated during the injection of HPAM. Despite the significant differences in pressure profile, the incremental oil recoveries caused by the associative polymer is only slightly higher than HPAM solutions. The maximum extensional viscosity of the associative polymer is significantly higher than HPAM. This implies that extensional viscosity of associative polymers influences the pressure profile more than the oil recovery in the relatively homogenous formation. The pressure generated during the injection of chase water as follow up slug to associative polymer is also higher when compared to HPAM. This indicates that extensional rheology influences the permeability reduction. These observations also provide insights into the hypothesis put forth by Besio et al. (1988) that the extensional rheology has a role on the polymer's adsorption.

The single phase study conducted using an associative polymer and HPAM of 1000 ppm concentration, indicates that both the polymers exhibit a similar resistance factor. Both shear and extensional rheology of associative polymer and HPAM were also similar at 1000 ppm. This indicates the hydrophobic association of associative polymer in porous media, shear and extensional field is dominated by intramolecular effects at 1000 ppm concentration. However, at 2000 ppm concentration, associative polymer exhibit higher resistance factor than HPAM at low flux and a comparable resistance factor at higher flux. At 2000 ppm, the associative polymer exhibits a high extensional viscosity at a low strain rate and a low extensional viscosity at a high strain rate due to the transformation of the intermolecular network to an intramolecular network. Therefore at 2000 ppm, the hydrophobic association appears to be dominated by the intermolecular effects at low fluxes and the typical intermolecular behavior of associative polymer can only be explained by the extensional viscosity characterization. At 2000 ppm, intermolecular effects dominate the hydrophobic association in porous media as well as in the extensional rheology. Residual resistance factor of the associative polymer is higher than HPAM only at 2000 ppm which indicates that the permeability reduction is related to intermolecular effects and the extensional viscosity. Deborah number (*De*) and shear rheology cannot explain the typical porous media behavior of associative polymers and HPAM.

The 640 ppm viscoelastic polymer with the molecular weight (Mw) of 30-36 Million daltons (MDa) possesses lower apparent viscosity and shear viscosity than 6000 ppm viscoelastic polymer with the Mw of 3.6 MDa. However, high Mw low concentrated polymer contributed to higher S_{or} reduction than the high concentrated low Mw polymer. The conventional belief is that extensional viscosity is a constituent of apparent viscosity. Rheological measurements performed using CaBER revealed that low concentrated high Mw polymer provided significantly higher extensional viscosity than the high concentrated low Mw polymer. It is therefore concluded that extensional viscosity has a strong role in S_{or} reduction. The extensional viscosity should not be treated as the constituent of the apparent viscosity during pore-scale residual oil recovery applications.

The viscoelastic polymer causes residual oil recovery at the value of N_c lower than the critical N_c. N_c is calculated using the apparent viscosity. As per the capillary theory, rapid residual oil mobilization occurs only at the N_c values higher than the critical N_c. N_c of viscoelastic polymers calculated using the extensional viscosity becomes higher than the critical N_c. While the N_c calculated using core-scale apparent viscosity is similar for both viscous glycerin and viscoelastic HPAM, viscoelastic HPAM showed higher S_{or} reduction at the flux of 1 ft/day. However, extensional N_c is higher for viscoelastic HPAM than viscous glycerin at this flux which indicates the N_c correlation break down even at 1ft/day. This also implies that apparent viscosity is not appropriate to be used in N_c calculation during viscoelastic polymer flooding.

Viscoelastic pusher-700 resulted in the higher pressure drop than viscous xanthan gum during their flow through porous media. *De* calculated using the oscillatory relaxation time were reported to be the same for both viscous and viscoelastic polymers. *De* calculated using the extensional relaxation time is higher for viscoelastic polymers than viscous polymers, which explains their porous media behavior. Further, high saline polymer solutions characterized by lower oscillatory *De* resulted in the higher S_{or} reduction than the low saline polymer solutions characterized by higher oscillatory *De*. However, the extensional rheological parameters such as strain hardening index and extensional viscosity are higher for the high saline polymer solutions than the low saline polymer solutions. Therefore, it can be concluded that extensional rheology, which represents the non-linear viscoelastic effects is an ideal method for characterizing the viscoelastic properties of EOR polymer solutions.

Viscoelastic polymers with the Mw of 30-36 MDa, 18-20 MDa, 11 MDa, 6 MDa, and 3.6 MDa were prepared at the concentrations of 1200 ppm, 2250 ppm, 4220 ppm, 7280 ppm, and 14600 ppm respectively. Higher extensional resistance shown by high Mw polymers at lowest concentration indicates polymer's molecular weight influence the elasticity. Whereas, higher shear resistance shown by low molecular weight polymer at higher concentration indicates that polymer's concentration influence the viscosity. It is to be concluded that the viscoelastic polymer with higher viscosity will not necessarily possess higher elasticity.

Viscoelastic polymer solutions with low Mw of 3.6 MDa and higher concentration of 14600 ppm possess higher shear viscosity and lower extensional viscosity when compared to the high Mw (18-20 MDa) and low concentrated (2250 ppm) viscoelastic polymers solutions. Low Mw, high concentrated viscoelastic polymer solutions with high shear flow resistance corresponds to the higher pressure drop and mobile heavy oil recovery at low flux when compared to the high Mw, low concentrated viscoelastic polymer solutions with lower shear viscosity. However, at high fluxes, the high Mw viscoelastic polymer with higher extensional viscosity contributes to higher pressure drop and lower injectivity due to the shear thickening phenomenon. This clearly indicates that polymer's viscosity contributes to higher sweep efficiency and injectivity. Chen et al. (2011)'s claim that viscosity influences the sweep efficiency is also reinforced. As per the shear rheology, at higher fluxes, high Mw polymer possessed low resistance. However, due to higher strain hardening, high Mw polymer possessed higher pressure drop. It is, therefore, important to incorporate extensional rheology in polymer selection criteria during heavy oil selection criteria.

Unified apparent viscosity (UVM) model developed at UT-Austin could predict the viscoelastic onset and shear thickening regimes through the combination of bulk steady shear, oscillatory shear and core flooding experiments. Oscillatory relaxation time is used in the UVM model. UVM model requires core flood experiments to measure the maximum extensional viscosity and strain hardening index of viscoelastic polymers. Proposed Azad Trivedi viscoelastic model (AT-VEM) is developed to predict the viscoelastic onset and shear thickening regimes of viscoelastic polymers using bulk shear and extensional rheological measurements. Extensional relaxation time, maximum extensional viscosity and strain hardening index used in AT-VEM are measured directly with an extensional rheometer. The average downscaling factor of 0.35 to maximum elongational viscosity and subtrahend of 1.2 to strain hardening index is obtained based on 14 different

experiments. These factors are attained for the polymer solutions possessing the extensional relaxation time of up to around 0.2 seconds. The proposed model can predict the viscoelastic onset and the shear thickening regime for varying range of reservoir permeability (200 mD to 37 D), porosity (0.22 to 0.395), brine salinity (0 ppm to 25200 ppm), concentration (200 ppm to 2500 ppm) and polymer molecular weight (6 MDa to 26 MDa). Predictability of AT-VEM is comparable to core flood-dependent UVM model and better than the core flood independent Carreau model.

Extensional capillary number (N_{ce}) is developed using the modified AT-VEM which is the first and only version of the N_c that can be used to quantify the S_{or} reduction caused by the viscoelastic polymer solutions. Capillary theory considered to be invalidated in the case of viscoelastic polymer flooding even at 1ft/day is validated using the N_{ce}. Based on 23 experimental data sets, it was concluded that for predicting the S_{or} reduction of viscoelastic polymers, N_{ce} is much better than conventional N_c. Based on 18 experimental data sets, it was concluded that N_{ce} can predict the S_{or} reduction of viscoelastic polymers much better than D_e.

Azad and Trivedi correlation (AT-C) developed using the N_{ce} can predict the S_{or} reduction caused by the viscoelastic polymer solutions through bulk rheology alone. Predictability of AT-C is better than the Qi et al. (2018)'s correlation, especially at high salinity. The proposed correlations can predict the S_{or} for varying range of reservoir permeability (169 mD to 7.9 D), porosity (0.18 to 0.37), brine salinity (2000 ppm to 26000 ppm), concentration (500 ppm to 6000 ppm), polymer molecular weight (6 MDa to 35 MDa), flux (0.14 ft/day to 5.8 ft/day), rock type, and oil viscosity (7 cP to 300 cP).

9.2 Contributions

Prior prediction of the apparent viscosity and injectivity of viscoelastic polymers during EOR is crucial for oil field development. Shear based Carreau model that fairly predicts the porous media behavior of viscous polymers, under predicts the apparent viscosity of viscoelastic polymers by a huge margin (Delshad et al. 2008). Viscoelastic models that were in existence since 1974 depends on the core flooding experiments to predict the in-situ rheological behavior. Performing core flooding with respect to many variables is a cumbersome process. Moreover, cores are difficult to attain during the early stage of field development. In this thesis, AT-VEM is proposed that can predict the onset and shear thickening regime without any core flood experiments. AT-VEM is recommended for incorporating into the commercial simulator for quick prediction of injectivity

which may help in the perforation design, well location, polymer selection, and injection rate selection.

Prediction of the S_{or} reduction especially at low flux will give an estimate about the expected recovery potential of different viscoelastic polymers. The existing numerical simulators lack the ability to predict residual oil recovery during polymer enhanced oil recovery. Existing analytical models such as the one proposed by Lotfollahi et al. (2016) relied on the core flooding experiments. The model proposed by Qi et al. (2018) relied on the oscillatory *De*, which has its own drawbacks. In this thesis, AT-C developed using N_{ce} is proposed that can predict S_{or} reduction potential of viscoelastic polymers. AT-C can be used in numerical simulators for a quick prediction of the oil recovery potential viscoelastic polymer flooding.

9.3 Limitations

The proposed AT-VEM has been validated using the experiments performed at room temperature. The predictability of AT-VEM at high temperature has not been tested. CaBER with its current feature cannot be used to perform the experiments at high temperature. Further, AT-VEM has been validated for HPAM polymers of varying molecular weights and operational conditions. Other polymers such as co- and terpolymers of polyacrylamide, star or comb polymers are to be tested in the future. AT-C for predicting the S_{or} reduction has been developed using the experimental data reported in the literature. Most of these experiments are performed with the flux rate of 1ft/day to 5.25 ft/day. Hence, the possibility of viscoelastic polymer solutions reducing S_{or} and therefore predictivity of AT-C model at the flux rate of lower than 1ft/day and relatively longer cores require more experimental investigation.

References

AbdelAlim, A.H. and Hamielec, A.E. 1973. Shear Degradation of Water-Soluble Polymers. I. Degradation of Polyacrylamide in a High-Shear Couette Viscometer. *Journal of Applied Polymer Science.* 17(12): 3769-3778. https://doi.org/10.1002/app.1973.070171218

Abrams, A. 1975. The Influence of Fluid Viscosity, Interfacial Tension, and Flow Velocity on Residual Oil Saturation Left by Waterflood. *SPE Journal.* 15(05): 437-447. SPE 5050-PA. https://doi.org/10.2118/5050-PA

Adams, D.M. 1982. Experiences with Water Flooding Lloydminster Heavy oil reservoirs. Journal of Canadian Petroleum Technology. 34 (08): 1643-1650. https://doi.org/10.2118/10196-PA

Afsharpoor, A., Balhoff, M.T., Bonnecaze, R., and Huh, C. 2012. CFD Modelling of the Effect of Polymer Elasticity on the Residual oil saturation at the pore-scale. *Journal of Petroleum Science and Engineering.* 94:79-88. https://doi.org/10.1016/j.petrol.2012.06.027

Alboudwarej, H. and Helix, J. 2006. Highlighting Heavy Oil. *Oil field review.* 18 (2):34-53

Andrade, R. J. E. Extensional Rheology and Structure Development in Polymer System, PhD thesis, Case Western Reserve University, Cleveland, Oklamaho, 2014.

Doda, A. 2014. Effect of Viscoelasticity and alkali on heavy oil EOR performance using HPAM, AA-NVP co- and cross-linked Polymers. MS Thesis, University of Alberta, Edmonton, Canada.

Anna, S.L. and McKinley, G.H. 2001. Elasto-Capillary Thinning and Breakup of model Elastic Liquids. Journal of Rheology. 45 (01):115-138. https://doi.org/10.1122/1.1332389

Ares, A.J., Silva, J.M. Maia, L., Barral, L., and Abad, M.J. 2009. Rheomechanical and Morphoological Study of the Compatibilized PP/EVOH Blends. *Rheological Acta.* 48: 993-1004

Asghari, K. and Nakutnyy, P. 2008. Experimental Results of Polymer Flooding of Heavy oil Reservoirs. Presented at the Canadian international petroleum conference, Calgary, 17-19 June, Paper 2008-189

Azad, M.S. 2014. Evaluation of Novel Viscoelastic System as a Potential Chemical EOR method in Carbonate Reservoirs. MS Thesis, KFUPM Library, Saudi Arabia

Azad, M.S., Sultan, A.S., Nuaim, S.A., Mahmoud, M.A., and Hussein, I.A. 2014. Could VES be a Part of Hybrid Option to Recover Heavy oil in Complex Heavy oil reservoirs. Presented at SPE Heavy oil Conference, Calgary, 10-12 June, SPE 170191-MS. https://doi.org/10.2118/170191-MS

Azad, M.S., and Sultan, A.S. 2014. Extending the Applicability of Chemical EOR to High Temperature, High Salinity and Fractured Carbonate Formation through Viscoelastic Surfactants. Presented at SPE Annual Saudi Technical symposium, Khobar, 21-24 April. SPE 172188-MS. https://doi.org/10.2118/172188-MS

Azad, M.S. and Trivedi, J.J. 2017. Injectivity Behavior of Copolymer and Associative polymers Decoded Using Extensional Viscosity Characterization: Effect of Hydrophobic Association. Presented at the SPE Western Regional Meeting, Bakersfield, 23-27 April. SPE 185668-MS. https://doi.org/10.2118/185668-MS

Azad, M.S., Dalsania, Y., and Trivedi, J.J. 2018a. Capillary breakup Extensional Rheometry of associative and hydrolyzed polyacrylamide for oil recovery applications. *Journal of Applied Polymer Science.* 135. 46253-46264. https://doi.org/10.1002/app.46253

Azad, M.S., Dalsania, Y., and Trivedi, J.J. 2018b. Understanding the Flow Behavior of Copolymer and Associative polymer using Extensional Viscosity Characterization: Effect of Hydrophobic Association, *Canadian Journal of Chemical Engineering.* 96 (11): 2498- 2508. https://doi.org/10.1002/cjce.23169

Azad, M.S. and Trivedi, J.J. 2018a. Extensional rheological data from ex-situ measurements for predicting porous media behavior of the viscoelastic EOR polymers. *Data in Brief*. 20: 293-305.

Azad, M.S. and Trivedi, J.J. 2018b. Does polymer's Viscoelasticity Influence the Heavy oil Sweep Efficiency and injectivity at 1ft/day? To be presented at the SPE International Heavy oil Conference and Exhibition, Kuwait city, 10-12 December. SPE 193771-MS.

Azad, M.S. and Trivedi, J.J. 2018c. Quantification of Viscoelastic Effects during Polymer Flooding: A Critical Review. Accepted in *SPE Journal* with revision

Azad, M.S. and Trivedi, J.J. 2019. A Novel Viscoelastic Model for Predicting the Synthetic Polymer's Viscoelastic Behavior in Porous Media Using Direct Extensional Rheological Measurements. *Fuel*. 235: 218-226. https://doi.org/10.1016/j.fuel.2018.06.030

Bargas, C.L. and Yanosik, J.L. 1988. The Effect of Vertical Fractures on Areal Sweep Efficiency in Adverse Mobility Ratio Floods. Presented at the SPE International Meeting on the Petroleum Engineering, Tianjin, 1-4 November, SPE-17609-MS. https://doi.org/10.2118/17609-MS

Barnes, H.A., Hutton, J.F., and Walter, K. 1989.An Introduction to Rheology. Elsevier, Amsterdam.

Barnes, H.A. 2000. A Handbook of Elementary Rheology. Introduction to Rheology. 1st edition. Elsevier Science Publishers B.V. Amsterdam.

Beeder, J., Skartsad, A., and Prasad, D. 2018. Biopolymer Injection in Offshore Single-Well Test. Presented at the 80th EAGE Conference and Exhibition, Copenhagen, 11-14 June. SPE 190758-MS. https://doi.org/10.2118/190758-MS

Besio, G.J., Prud'homme, R.K., and Benziger, J.B. 1988. Effect of Elongational Flow on Polymer Adsorption. *Macromolecules.* 21 (4): 1070-1074. 10.1021/ma00182a038

Bhardwaj, A., Richter, D., Chellamuthu, M., and Rothstein. 2007a. Rheological Acta. 46, 861-875

Bhardwaj, A., Miller, E., and Rosthein, J.P. 2007b. Filament Stretching and Capillary Breakup

Extensional Rheometry Measurements of Viscoelastic Wormlike Micelle Solutions. *Journal of Rheology.* 51(4): 693-719. http://dx.doi: 10.1122/1.2718974.

Bock, J. Valint, P. L, Pace, P. L., Siano, D. B., Schulz, D. N., and Turner. S. R. 1988. Hydrophobically Associating Polymers, *Water-Soluble Polymers for Petroleum Recovery*, G. A. Stahl, D. N. Schulz, Eds., Plenum Press, New York,147.

Boni, L., Fischer, P., Boker, L., Kuster, S., and Ruhs, P.A. 2016. Hagfish Slime and Mucin Flow Properties and their Implications for Defense. *Scientific Report.* 6: 30371. https://doi.org/10.1038/srep30371

Burnett, D.B. 1975. Laboratory Studies of Biopolymer Injectivity Behavior Effectiveness of Enzyme Clarifications. Presented at SPE California Regional Meeting, Ventura, California, 2-4 April. Paper SPE 5372-MS. https://doi.org/10.2118/5372-MS

Cakl, J., and Machac, I. 1995. Pressure Drop in the Flow of Viscoelastic Fluids through Fixed Beds of Particles. *Collection of Czechoslovak Chemical Communications* 60: 1124– 1139. https://doi.org/10.1135/cccc19951124

Cannela, W.J., Huh, C., and Seright, R.S. 1988. Prediction of Xanthan Rheology in Porous Media. Presented at the SPE Annual Technical Conference and Exhibition, Houston, 2-5 October. SPE-18089-MS. https://doi.org/10.2118/18089-MS

Carreau, P.J., De Kee, D.C.R., and Chhabra, R.P. 1997. Rheology of Polymeric Systems, Principles and Application. Hanser/Gardner publications, Cincinnati, Ohio, USA.

Castelleto, W.J., Hamley, I.W., Xue, W., Sommer, C., Pederson, J.S., and Oimsted, P.D. 2004. Rheological and Structural Characterization of Hydrophobically Modified Polyacrylamide solutions in the semi-dilute regime, *Macromolecules* 37 (4): 1492-1501.

Castor, T.P., Edwards, J.B., and Passman, F.J., 1981. Response of Mobility Control agents to Shear, Electrochemical, and Biological Stress. In: Shah, D.O. (Ed.), Surface Phenomena in Enhanced Oil Recovery. Plenum, 773–820.

Chang, H.L. 1978. Polymer Flooding Technology Yesterday, Today and Tomorrow. *J Petroleum Technology.* 30 (08):1113-1128. SPE 7043-PA. https://doi.org/10.2118/7043-PA.

Chang, P.E.K., Gouveia, L., Fernandez, I.J., Muller, A.J., Barrios, A.D., and Saez, E. 2007. Rheology of aqueous solutions of hydrophobically modified polyacrylamides and surfactants. *Colloids and Surfaces: A Physiochemical and Engineering Aspects.* 295 (1-3): 99–106. 10.1016/j.colsurfa.2006.08.038

Chatzis, I. and Morrow, N.R. 1984. Correlation of Capillary Number Relationship for Sandstone. *SPE Journal.* 24 (05): 555-562. SPE 10114-PA. https://doi.org/10.2118/10114-PA

Chatzis, I., Kuntamukkula, M.S., and Morrow, N.R. 1988. Effect of Capillary Number on the Microstructure of Residual oil in the Strongly Water-Wet Sandstones. *SPE Reservoir Engineering.* 3 (3): 902-912, SPE 13213-PA. https://doi.org/10.2118/13213-PA

Chauveteau, G. 1981. Molecular Interpretation of Several Different Properties of Flow of Coiled Polymer Solutions through Porous Media in Oil Recovery Conditions. Presented at SPE Annual Technical Conference and Exhibition, San Antonia, Texas, 4-7 October, SPE 10060-MS. https://doi.org/10.2118/10060-MS

Chauveteau, G. 1986. Fundamental Criteria in Polymer Flow through Porous Media and their Relative Importance in the Performance Differences of Mobility Control Buffers. *Water Soluble Polymers, Advances in Chemistry* 213. Chapter 14: 227-267 10.1021/ba-1986-0213.ch014

Chauveteau, G., Denys, K., and Zaitoun, A. 2002. New Insight on Polymer Adsorption Under High Flow Rates. Presented at SPE Improved Oil Recovery Symposium, Tulsa, 13-17 April, SPE 75183-MS. https://doi.org/10.2118/75183-MS

Chen G. 2006. Mathematical Model of Enhanced Oil Recovery for Viscous-Elastic Polymer Flooding. *Journal of Tsinghua University* 46 (6): 882-885.

Chen, G., Han, P., Shao, Z., Zhang, X., Ma, M., Lu, K., and Wei, C. 2011. History Matching Method for High Concentration Viscoelasticity Polymer flood in the Daqing Oilfield. Presented at the SPE EOR conference, Kuala Lampur, 19-21 July. SPE 144538-MS. https://doi.org/10.2118/144538-MS

Chiou, C.S. and Kellerhals, G.E. 1981. Polymer/Surfactant Transport in Micellar Flooding. *SPE Journal.* 21 (05): 603-612. SPE 9354-PA. https://doi.org/10.2118/9354-PA

Choplin. L. and Sabatie, J. 1986. Threshold-type Shear thickening in Polymeric Solutions. *Rheological Acta* 25 (6): 570-579. https://doi.org/10.1007/BF01358165

Christoper, R.H. and Middleman, S. 1965. Power Law Flow through a Packed Tube. *Industrial & Engineering Chemistry Fundamental.* 4(4): 422-426. 10.1021/i160016a011

Clarke. A., Howe. A.M., Mitchell, J., Staniland, J., and Hawkes, L.A. 2015. How Viscoelastic Polymer flooding Enhanced Displacement Efficiency. Presented at the SPE Asia Pacific Enhanced Oil Recovery Conference, Kuala Lampur, 11-13 August. SPE 174654-MS. https://doi.org/10.2118/174654-MS

Clarke. A., Howe. A.M., Mitchell, J., Staniland, J., and Hawkes, L.A. 2016. How Viscoelastic Polymer flooding Enhanced Displacement Efficiency. *SPE Journal*. 21 (3): 675-687. SPE 174654-PA. https://doi.org/10.2118/174654-PA

Clasen, C., Plog, J.P., Kulicke, W.M., Owens, M., Macosko, C., Scriven, L.E., Verani, M., and McKinley, G. 2006. How dilute are dilute solutions in extensional flows? *Journal of Rheology.* 50(6): 849-881. http://dx.doi.org/10.1122/1.2357595

Clasen, C. 2010. Capillary Breakup Extensional Rheometry of Semi-Dilute Polymer Solutions. *Korea Australian Rheology Journal*. 22 (04): 331-338.

Clemens, T., Kornberger, M., and Lueftenegger, M. 2016. Polymer Injection to Rejuvenate a Super mature oil field, Polymer pilot results, 8 TH Reservoir, Austria. Presented at the Abu Dhabi International Petroleum Exhibition and Conference, Abu Dhabi, 7-10 November. SPE 183010-MS. https://doi.org/10.2118/183010-MS

Cottin, C., Bourgeois, M., Bursaux, R., Jimenez, J., and Lassalle, S. 2014. Secondary and Tertiary Polymer Flooding on the Highly Permeable Reservoir Cores: Experimental Results. Presented at the SPE EOR Conference at Oil and Gas West Asia, Muscat, 31 March- 2 April. SPE 169692-MS. https://doi.org/10.2118/169692-MS

Crawford, F.B. and Collins, R.E. 1954. Estimated Effect of Vertical Fractures on Secondary Recovery. *Journal of Petroleum Technology.* 6 (8):41-45. SPE 325-G. https://doi.org/10.2118/325-G.

Culter, J.D., Mayhan, K.G., Patterson, G.K., Sarmasti, A.A., and Zakin, J.L. 1972. Entrance Effects on Capillary Degradation of Dilute Polystyrene Solutions. *Journal of Applied Polymer Science.* 16 (12): 3381-3385. https://doi.org/10.1002/app.1972.070161227

Culter, J.D., Zakin, J.L., and Patterson, G K. 1975. Mechanical Degradation of Dilute Solutions of High Polymers in Capillary Tube Flow. *Journal of Applied Polymer Science.* 19(12): 3235-3240. https://doi.org/10.1002/app.1975.070191210

Dauben, D.L. and Menzie, D.E. 1967. Flow of Polymer Solutions through Porous media. *Journal of Petroleum Technology.* 19 (08): 1065-1073. SPE 1688-PA. https://doi.org/10.2118/1688-PA

Dealy, J. M. 2010. Weissenberg and Deborah Numbers and Their Definition and Use. *Rheological Bulletin.* 79 (2): 14−18.

Dehghangpour, H. and Kuru, H. 2009. A New Look at the Viscoelastic Fluid Flow in the Porous Media- A possible Mechanism of Internal Cake Formation and Formation Damage Control. Presented at the SPE International symposium on Oil Field Chemistry, Woodlands, Texas, 20-22 April. SPE 121640-MS. https://doi.org/10.2118/121640-MS

eiber, J. A. and Schowalter, W. R. 1981. Modeling the Flow of Viscoelastic Fluids Through Porous Media. *American Institute of Chemical Engineering Journal* 27 (06), 912-920.
https://doi.org/10.1002/aic.690270606

Delamaide, E. 2014. Polymer flooding of Heavy oil- From Screening to Full Field Extension. Presented at the SPE Heavy and Extra Heavy oil Conference, Medellin, 24-26 September, SPE 171105-MS. https://doi.org/10.2118/171105-MS

Delamaide, E., Zaitoun, A., Renard, G., and Tabary, R. 2014. Pelican Lake Field: First Successful Application of Polymer Flooding in Heavy oil reservoir. *SPE Reservoir Evaluation & Engineering*. 17(03): 340-354. SPE 165234-PA. https://doi.org/10.2118/165234-PA

Delamaide, E. 2016. Comparison of Primary, Secondary and Tertiary Polymer Flood in the Heavy oil- Field Results. Presented at SPE Trinidad and Tobago Section Energy Resources Conference, Port of Spain, 13-15 June, SPE 180852-MS.
https://doi.org/10.2118/180852-MS

Delshad, M., Kim, D.H., Magbagbeola, Huh, C., Pope, G.A., and Tarahhom, F. 2008. Mechanistic Interpretation and Utilization of Viscoelastic Behaviour of Polymer Solutions for Improved Polymer-Flood Efficiency. Presented at SPE Improved Oil Recovery Symposium, Tulsa, 24-28 April, SPE 113620-MS. http://dx.doi.org/10.2118/113620-MS.

De Melo, M.A., De Holleben, C.R.C., Da Silva, I.G. Correia, A.D.B., Silva, G.A., Rosa, A.J., Jr, A.J.L., and Lima, J.C.D. 2005. Evaluation of Polymer Injection Projects in Brazil. Presented at the SPE Latin American and Caribbean Petroleum Engineering Conference, Rio de Janeiro, 20-23 June, SPE 94898-MS. https://doi.org/10.2118/94898-MS

Dinic, J., Zhang, Y., Jimenez, L.N., and Sharma, V. 2016. Extensional Relaxation time of Dilute, Aqueous Polymer Solutions. *Macro letters.* 4 (7): 804-808. 10.1021/acsmacrolett.5b00393.

Doshi, S. R. and Dealy. J. M. 1987. Exponential Shear: A Strong Flow. *Journal of Rheology.* 31 (7): 563. https://doi.org/10.1122/1.549936

Doughty, J. O. and Bogue, D. C. 1967. Experimental Evaluation of Viscoelastic Theories. *Industrial Engineering and Chemistry Fundamental* 6 (3): 388–393. https://doi.org/10.1021/i160023a011.

Dunlap, P.N. and Leal, L. 1987. Dilute Polystyrene Solutions in Extensional Flows—Birefringence and Flow Modification, *Journal of Non Newtonian Fluid Mechanics.* 23 : 5-48

Dupas, A., Henaut, I., Rousseau, D., Poulain, P., Tabary, R., Argillier, J.F., and Aubry, T. 2013. Impact of Mechanical degradation on the shear and extensional viscosities: Towards Better Injectivity forecasts in Polymer flooding applications, Presented at the SPE International Symposium on Oil Field Chemistry, Texas, 8-10 April. SPE 164083-MS. https://doi.org/10.2118/164083-MS

Dupuis, G., Rousseau, D., Tabary, R., and Bruno, G. 2011. Flow of Hydrophobically Modified Water-Soluble-Polymer Solutions in Porous Media: New Experimental Insights in the Diluted Regime. SPE *Journal.* 16 (01):43-54. SPE 129884-PA. https://doi.org/10.2118/129884-PA.

Durst, F., Haas, R., and Interthal, W. 1987. The Nature of Flows through Porous Media. *Journal of Non-Newtonian Fluid Mechanics.* 22 (2):169–189. http://dx.doi.org/10.1016/0377-0257(87)80034

Dyes, A.B., Kemp, C.E., and Caudle, B.H. 1958. Effect of Fractures on the Sweep-out Pattern. In *Petroleum Transactions* AIME, 213: 245-249. SPE 1071-G. Richardson, Texas: SPE.

Ehrenfried, D. 2013. Impact of Viscoelastic Polymer Flooding on Residual oil Saturation in Sandstones. MS thesis, University of Texas at Austin, Austin, Texas.

Entov V.M. and Hinch E.J. 1997. Effect of a Spectrum of Relaxation Times on the Capillary Thinning of a Filament of Elastic liquid. *Journal of Non-Newtonian Fluid Mechanics*. 72: 31-41.

Erincik, M.Z., Qi, P., Balhoff, M.T., and Pope, G. 2018. New Method to Reduce the Residual Oil Saturation by Polymer flooding. *SPE Journal.* 23 (05): 1944-1956. SPE 187230-PA. https://doi.org/10.2118/187230-PA

Farinato, R.S. and Yen, W.S. 1987. Polymer Degradation in Porous Media Flow. *Journal of Applied Polymer Science* 33 (7): 2353-2368. https://doi.org/10.1002/app.1987.070330708

Ferguson, J., Walters, K., and Wolff, C. 1990. Shear and Extensional Flow of Polyacrylamide Solutions. *Rheological Acta.* 29 (6):571-579.10.1007/BF01329303

Flew, S. and Sellin, R.H.J. 1993. Non-Newtonian Flow in Porous Media- A Laboratory Study of Polyacrylamide Solutions. *Journal of Non-Newtonian Fluid Mechanics*, 47, 169-210. https://doi.org/10.1016/0377-0257(93)80050-L

Foster, W.R. 1973. A Low Tension Water flooding Process. *SPE Journal.* 25 (02):205-210. SPE 3803-PA. https://doi.org/10.2118/3803-PA

Fred, H.L.W. 1979. Influences of Polymer Solution Properties on the Flow in the Porous Media. Presented at the SPE Annual Conference and Exhibition, Las Vegas, Nevada. 23-26 September. SPE 8418-MS. https://doi.org/10.2118/8418-MS

Fuller, G.G., Cathey, C.A., Hubbard, B., and Zebrowski, B.E. 1987. Extensional Viscosity Measurements of Low-Viscosity Fluids. *Journal of Rheology* 31 (03): 235-249. https://doi.org/10.1122/1.549923

Garrouch, A.A. and Gharbi, R.B. 2006. A Novel Model for Viscoelastic Fluid flow in the Porous Media. Presented at the SPE Annual Technical Conference and Exhibition, 24-27 September, Texas, San Antonio, SPE 102015-MS. https://doi.org/10.2118/102015-MS

Gennes, D.P. G. 1974. Coil-Stretch Transition of Dilute Flexible Polymers Under Ultra-High Velocity Gradients. *Journal of Chemical Physics* 60 (12): 5030. https://doi.org/10.1063/1.1681018

Glasbergen, G., Wever, D., Keijzer, E., and Farajzadeh, R. 2015. Injectivity loss in Polymer floods: Causes, Prevention and Mitigations. Presented at the SPE Kuwait oil and gas show conference, Kuwait city, 11-14 October. SPE 175383- MS. https://doi.org/10.2118/175383-MS

Gogarty, W.B. 1967. Mobility Control with Polymer Solutions. *SPE Journal.* 7(02): 161-173

Greaves, B.L. Marshall, R.N., and Thompson, J.H. 1984 Hitts lake Unit Polymer Project. Presented at 59th Annual Technical Conference and Exhibition. Dallas, Texas, 16-19 September. SPE 13123-MS. https://doi.org/10.2118/13123-MS

Green, D. and Willhite, P. 1998. Enhanced Oil Recovery, Vol. 6. Richardson, Texas: SPE. Textbook Series

1566-B. http://dx.doi.org/10.2118/1566-B

Gumpenberger, T., Deckers, M., and Kornberger, M. 2012. Experiments and Simulation of the Near Wellbore Dynamics and Displacement Efficiencies of the Polymer Injection, Matzen field, Austria. Presented at the Abu Dhabi International Petroleum Conference and Exhibition, Abu Dhabi, 11-14 November. SPE 161029-MS. https://doi.org/10.2118/161029-MS

Guo, H., Dou, M., Hanqing, W., Wang, F., Yuanyuan, G., Yu, Z., Yansheng, W., and Li, Y. 2014. Review of capillary number in chemical enhanced oil recovery. Presented at SPE Kuwait oil and gas show conference, Mishref, 11-14 October. SPE 175172-MS. https://doi.org/10.2118/175172-MS

Haas, R. and Durst, F. 1982. Viscoelastic Flow of Dilute Polymer Solutions in Regularly Packed Beds. *Rheological Acta.* 21: 566−571.

Han, X.Q., Wang, W.Y., and Xu, Y. 1995. The Viscoelastic Behavior of HPAM solutions in Porous media and its effect on the displacement efficiency. Presented at International meeting on Petroleum Engineering, Beijing, 14-17 November. SPE 30013-MS. https://doi.org/10.2118/30013-MS

Han, M., Zhou, X., Fuseni, A.B., Al-Zahrani, B.D., and Al Soofi, A.K. 2012. Laboratory Investigation of the Injectivity of Sulfonated Polyacrylamide Solutions into Carbonate Reservoir Rocks. Presented at the SPE EOR Conference at Oil and Gas West Asia, Muscat, 16-18 April. SPE 155390-MS. https://doi.org/10.2118/155390-MS

Han, M., Alsofi, AK., Fuseni, A., Zhou, X., and Hassan, S. 2013. Development of Chemical EOR Formulations for the High Temperature and High Salinity Carbonate Reservoir. Presented at the International Petroleum Technology Conference, Beijing, 26-28 March. IPTC 17084-MS. https://doi.org/10.2523/IPTC-17084-MS

Harrison, G.M., Remmelgas, J., and Leal, L.G. 1999. Comparison of Dumbbell- Based Theory and Experiment for a Dilute Polymer Solution in a Co rotating Two-roll Mill. *Journal of Rheology.* 43 (1): 197. http://dx.doi.org/10.1122/1.550982.

Heemskerk, J., Rosmalen, R., Janssen-Van, R., Holtslag, R.J., and Teeuw, D. 1984. Quantification of Viscoelastic effects of Polyacrylamide Solutions. Presented at SPE Enhanced Oil Recovery Symposium, Tulsa, 15-18 April 1984. SPE 12652-MS. http://dx.doi.org/10.2118/12652-MS.

Hester, R.D., Flesher, L.M., and McCormick, C.L. 1994. Polymer Solution Extensional Viscoelastic Effects during Reservoir Flooding. Presented at SPE Improved Oil Recovery Symposium, Tulsa, Oklahoma, 17-20 April. SPE 27823-MS. https://doi.org/10.2118/27823-MS

Hill, H.J., Brew, J.R., Claridge, E.L., Hite, J.R., and Pope, G.A. 1974. The Behavior of Polymer Solutions in the Porous Media. Presented at SPE Improved Oil Recovery Symposium, Tulsa, Oklahoma, 22-24 April. SPE 4748-MS. https://doi.org/10.2118/4748-MS

Hincapie, R.E. and Ganzer, L. 2015. Assessment of Polymer Injectivity with Regards to Viscoelasticity; Lab Evaluations towards Better Field Operations. Presented at the EUROPEC, Madrid, 1-4 June. SPE-174346-MS. https://doi.org/10.2118/174346-MS

Hirasakhi, G. and Pope, G. 1974. Analysis of Factors Influencing Mobility and Adsorption in the Flow of Polymer Solutions through Porous Media. *SPE Journal.* 14 (4): 337-346. SPE-4026-PA. http://dx.doi.org/10.2118/4026-PA.

Hochanadel, S.M., Lunceford, M.L., and Farmer, C.W. 1990. A Comparison of 31 Minnelusa polymer floods with 24 Minnelusa water floods. Presented at the SPE Improved Oil Recovery symposium, Tulsa, Oklahoma. 20-22 April, SPE 20234-MS. https://doi.org/10.2118/20234-MS

Howe, A.M., Clarke, A., and Giernalczyk, D. 2015. Flow of Concentrated Viscoelastic Polymer Solutions in Porous Media; Effect of MW and concentration on the Elastic Turbulence Onset in Various Geometries. *Soft Matter.* 11 (32): 6419-6431.

Humphry, K.J., Suijkerbuijk, B.M.J.M., Van der Linde, H.A., Pieterse, S.G.J., and Masalmeh, S.K. 2014. Impact of Wettability alteration on Residual Oil Saturation and Capillary Desaturation Curves. *Petrophysics.* 55 (04): 313-318.

Huh, C. and Pope, G.A. 2008. Residual Oil Saturation from Polymer Floods: Laboratory Measurements and Theoretical Interpretation. Presented at SPE/DOE symposium on Improved Oil Recovery Symposium, Tulsa, Oklahoma, 20–23 April. SPE 113417-MS. https://doi.org/10.2118/113417-MS

Hyne, N. 1991. Dictionary of Petroleum exploration, production and drilling" Penn Publication, Tulsa, USA

James, C.M. and Warren, J. 1984. Performance and operations of a cross linked polymer flood at sage spring creek unit a, Natrona county, Wyoming. *Journal of Petroleum Technology*. 36 (07): 1145-1156.

James, D.F. and Saringer, J.H. 1980. Flow of Dilute Polymer Solutions through Converging Channels. *Journal of Fluid Mechanics* 97 (3-4): 317-339. https://doi.org/10.1016/0377 0257(82)80038-4

Jennings, R.R., Rogers, J.H., and West, J.T. 1971. Factors influencing mobility control by polymer solutions. *Journal of Petroleum Technology.* 23(03): 391-401. SPE 2867-PA. https://doi.org/10.2118/2867-PA

Jiang, H.F., Wu, W.X., Wang, D.M., Zeng, Y., Zhao, S., and Nie, J. 2008. The Effect of Elasticity on Displacement Efficiency in the Lab and Results of High Concentration Polymer Flooding in the Field. Presented at SPE Annual Technical Conference and Exhibition, Denver, Colorado, 21-24 September, SPE 115315-MS. https://doi.org/10.2118/115315-MS

Johannesen, E.B. and Graue, A. 2007. Mobilization of Remaining oil- Emphasis on the Capillary number and Wettability. Presented at the International Oil Conference and Exhibition in Mexico, Veracrux, 27-30 June. SPE 108724-MS. https://doi.org/10.2118/108724-MS

Jones, W.M. 1976. The Flow of Dilute Aqueous Solutions of Macromolecules in Various Geometries: VI. Properties of the Solutions. *Journal of Physics D Applied Physics* 12 (3) http://iopscience.iop.org/article/10.1088/0022-3727/12/3/006

Jones, D.M. and Walter, K. 1989. The behavior of polymer solutions in the extension- dominated flows with applications to enhanced oil recovery. *Rheological Acta.* 28 (6):482-498. https://doi.org/10.1007/BF01332919

Jouenne, S. and Heurteux, G. 2017. Flow of Polymer Solutions through Porous Media- Prediction of mobility reduction from ex-situ measurements of elasticity. European Symposium on the Improved Oil Recovery, Stavanger, 24-27 April.

Jr. R.A.F., Ertekin, T., and Stahl, C.D. 1985. Effect of Capillary Number and Its Constituent on the Two-Phase Relative Permeability Curves. *Journal of Petroleum Technology* 37(02): 249-260. SPE 12170-PA. https://doi.org/10.2118/12170-PA

Kamal, M.S., Sultan, A.S., Al- Mubaiyedh, U., and Hussein, I.A. 2015. Review on Polymer flooding; Rheology, Adsorption, Stability and Field Applications of Various Polymer Systems. *Polymer Reviews.* 55(3): 491-530. 10.1080/15583724.2014.982821

Kamal, M.S., Hussein, I.A., and Sultan, A.S. 2017. Review on Surfactant flooding: Phase Behavior, Retention, IFT, and Field Applications. *Energy and Fuels.* 31 (08): (7701-7720). 10.1021/acs.energyfuels.7b00353

Kang, X., Zhang, J., Sun, F., Zhang, F., Feng, G., Yang, J., Zhang, X., and Xiang, W. 2011. A review of Polymer EOR on Offshore Heavy Oil Field in Bohai bay, China. Presented at SPE EOR Conference, Kuala Lampur, SPE 144932-MS. https://doi.org/10.2118/144932-MS

Karnanda, W., Benzagouta, M.S., Al Quraishi, AR., and Amro, M.M. 2012. Effect of temperature, pressure, salinity, and surfactant concentration on IFT for surfactant flooding optimization. *Arabian Geo Science.* 6: 3535-3544. 10.1007/s12517-012-0605-7

Keller, A., Muller, A.J., and Odell, J.A. 1987. Entanglements in Semi-Dilute Solutions as Revealed by the Elongational Flow Studies. *Progress in Colloid and Polymer Science* 75:179-200. https://doi.org/10.1007/BFb0109421

Kemblowski, Z. and Michniewicz, M. 1979. A New Look at the Laminar Flow of Power Law Fluids through Granular Beds. *Rheological Acta* 18 (06):730-739. https://doi.org/10.1007/BF01533348

Kemblowski, Z. and Dziubinski, M. 1978. Resistance to Flow of Molten Polymers through Granular Beds. *Rheological Acta* 17 (02):176-187. https://doi.org/10.1007/BF01517709

Kennedy, J.C., Meadows, J., and William, P.A. 1995. Shear and Extensional Viscosity Characteristics of a Series of Hydrophobically Associating Polyelectrolytes. *Journal of Chemical Society Faraday Transactions.* 91 (5): 911-916. 10.1039/FT9959100911.

Keshavarz B, Sharma V, Houze E.C., Koerner, M.R., Moore, J.R., Cotts, P.M., Holmes, P.T., and McKinley, G.H. Studying the Effects of Elongational Properties on Atomization of Weakly Viscoelastic Solutions Using Rayleigh Ohnesorge Jetting Extensional Rheometry (ROGER). *Journal of Non- Newtonian Fluid Mechanics* 222: 171-189. https://doi.org/10.1016/j.jnnfm.2014.11.004

Kim, N.J., Pipe, C.J., Ahn, K.H., Lee, S.J., and McKinley, G.H. 2010a. Capillary Breakup Extensional Rheometry of a Wormlike Micellar Solution. *Korea Australia Rheology Journal*. 22 (1): 31-41

Kim, D.H., Lee, S., Ahn, C.H., Huh, C., and Pope, G. 2010b. Development of a Viscoelastic Property Database for EOR polymers. Presented at the SPE Improved Oil Recovery Symposium, 24-28 April, Tulsa, Oklahoma, SPE 129971-MS. https://doi.org/10.2118/129971-MS

Knight, B.L. and Rhudy, J.S. 1977. Recovery of High Viscosity Crudes by Polymer flooding. *Journal of Canadian Petroleum Technology*. 16 (04). PETSOC-77-04-07.

Koh, H. Ph.D. dissertation, University of Texas at Austin, 2015.

Koh, H., Lee, V. B., and Pope, G. A. 2017. Experimental Investigation of the Effect of Polymers on Residual Oil Saturation. *SPE Journal*. 23 (1): 1–17. SPE-179683-PA. https://doi.org/10.2118/179683-PA.

Kozicki, W. 2002. Flow of FENE Fluid in Packed Beds or Porous Media. *Canadian Journal of Chemical Engineering.* 80: 818−829. https://doi.org/10.1002/cjce.5450800505

Kulicke, W.M. and Haas, R. 1984. Flow Behavior of Dilute Polyacrylamide Solutions through Porous Media. Influence of Chain length, concentration, and thermodynamic quality of the solvent. Industrial & Engineering Chemistry Fundamentals. 23 (03): 308-315. 10.1021/i100015a008

Kumar, P., Raj, R., Koduru, N., Kumar, S., and Pandey, A. 2016. Field Implementation of Mangala Polymer Flood: Initial Challenges, Mitigation and Management. Presented at the SPE EOR

conference at Oil and Gas, West Asia, 21-23 March, Muscat, SPE 179820-MS. https://doi.org/10.2118/179820-MS

Lake, L. 1989. Enhanced Oil Recovery. Englewood Cliffs, New Jersey, Prentice Hall.

Laoroongroj, A., Gumpenberger, T., and Clemens, T. 2014. Polymer flood Incremental Oil recovery and Efficiency in Layered Reservoir including Non-Newtonian and Viscoelastic effects. Presented at SPE Annual Technical conference and Exhibition, Amsterdam, 27-29 October. SPE 170657-MS. https://doi.org/10.2118/170657-MS

Levitt, D. and Pope, G. 2008. Selection and Screening of Polymers for Enhanced Oil Recovery. Presented at the SPE Improved Oil Recovery Symposium, Tulsa, 19-23 April. SPE 113845-MS. https://doi.org/10.2118/113845-MS

Li, Z and Delshad, M. 2014. Development of an Analytical Injectivity Model for Non-Newtonian Polymer Solutions. *SPE Journal.* 19 (3): 381-389. https://doi.org/10.2118/163672-PA

Lim, T., Uhl, J.T., and Prud'homme, R.K. 1986. The Interpretation of Screen-Factor Measurements. *SPE Reservoir Engineering.* 1 (3): 272–276. https://doi.org/10.2118/12285-PA

Liu, G., Sun, H., Rangou, S., Ntetsikas, K., Avgeropoulos, A., and Wang, S.Q. 2013. Studying the Origin of Strain Hardening: Basic Difference between Extension and Shear. *Journal of Rheology.* 57 (1): 89. https://doi.org/10.1016/0377-0257(93)85023-4

Lotfollahi, M., Farajzadeh, R., Delshad, M., Al-Abri, A.K., Wassing, B.M., Al-Mjeni, R., Awan, K., and Bedrikovestky, P. 2016. Mechanistic Simulation of Polymer Injectivity in Field Tests. *SPE Journal.* 21(04):1178-1191. SPE 174665-PA. http://dx.doi.org/10.2118/174665-PA.

Lotfallahi, M., Koh, H., Li, Z., Delshad, M., and Pope, G.A. 2016. Mechanistic Simulation of Residual Oil in the Viscoelastic Polymers Floods. Presented at SPE Enhanced Oil Recovery Conference at Muscat, Oman, 21-23 March. SPE 178844-MS. https://doi.org/10.2118/179844-MS

Lyons, W. and Plisga, G. 2004. Handbook of Petroleum and Natural Gas Engineering, Gulf Professional Publishing, USA.

Ma, Y. and McClure, M.W. 2017. The Effect of Polymer Rheology and Induced Fracturing on Injectivity and Pressure Transient- Behavior. *SPE Reservoir Evaluation & Engineering* 20 (02):394-402. SPE 184389-PA. https://doi.org/10.2118/184389-PA

Machac, I. and Dolejs, V. 1982. Flow of Viscoelastic Liquids through Fixed Beds of Particles. *Chemical Engineering Communications* 18 (1-4): 29-37. https://doi.org/10.1080/00986448208939954

Mack, J.C. and Warren, J. 1984. Performance and Operation of a Cross linked Polymer Flood at Sage Spring Creek Unit A, Natrona County, Wyoming, *Journal of Petroleum Technology*. 36 (07): 1145-1156. SPE 10876-PA. https://doi.org/10.2118/10876-PA.

Mack, J.C. and Duvall, M.L. 1984. Performance and Economics of Minnelusa Polymer Floods. Presented at the SPE Rocky Mountain Regional Meeting, Casper, Wyoming, 21-23 May. SPE 12929-MS. https://doi.org/10.2118/12929-MS

Macosko, C.W. 1994. Rheology: Principles, Measurements and Applications. Whiley VCH, New York.

Maerker, J.M. 1975. Shear Degradation of Partially Hydrolyzed Polyacrylamide Solutions. *Society of Petroleum Engineering* 15(04): 311-322. SPE 5101-PA. http://dx.doi.org/10.2118/5101-PA

Magbagbeola, O.A. 2008. Quantification of Viscoelastic Behavior of High Molecular weight polymers used chemical enhanced oil recovery, MS thesis, UT Austin, Texas, USA.

Maitin, B.K. 1992. Performance Analysis of Several Polyacrylamide Floods in North German Oil Fields. Presented at the SPE/DOE Enhanced Recovery Oil Symposium, Tulsa, 22–24 April. SPE 24118-MS. https://doi.org/10.2118/24118-MS

Manichand, R.N., Let, K.P.M.S., Gil, L., Quillien, B., and Seright, R.S. 2013. Effective Propagation of HPAM Solutions through the Tambaredjo Reservoir during a Polymer Flood. *SPE Production & Operation.* 28 (04): 358-368. https://doi.org/10.2118/164121-PA

Mansour, A.M., Al-Maamari, R.S., Al-Hashim, A.A., Zaitoun, A., and Al-Sharji, H. 2014. In-situ rheology and mechanical degradation of EOR polyacrylamide solutions under moderate shear rates. *Journal of Petroleum science and engineering.* 115: 57-65.
https://doi.org/10.1016/j.petrol.2014.02.009

Martin, F.D. 1974. Laboratory Investigations in the Use of Polymers in Low- permeability Reservoirs. Presented at SPE-AlME 49th Fall Meeting of SPE of AIME, Houston, Texas, October 6-9, 1974. SPE 5100-MS. https://doi.org/10.2118/5100-MS

Martin, F.D. 1986. Mechanical Degradation of Polyacrylamide solutions in the Core Plugs from the Several Carbonates. *SPE Formation Evaluation* 1 (2): 139-150. SPE 12651-PA. https://doi.org/10.2118/12651-PA

Marshall, R.J and Metzener, A.B. 1966. Flow of Viscoelastic fluids Through Porous Media. Presented at Symposium on Mechanics of Rheologically Complex Fluids, Houston, Texas, 15-16 December 1966. SPE 1687-MS. http://dx.doi.org/10.2118/1687-MS.

Marshall, R.J. and Metzener, A.B. 1967. Flow of Viscoelastic Fluids through Porous media. *Industrial and Engineering Chemistry Fundamentals*. 6 (03): 393-400.

Martischius, F.D., 1982. The Rheological Behavior of Polymer Solutions: Flow Consolidation in Shear and Expansion flows. *Rheological Acta.* 21 (03); 288-310. 10.1007/BF01515717

Masuda, Y., Tang, K.C., Miyazawa, M., and Tanaka, S. 1992. 1D Simulation of Polymer flooding including the viscoelastic effect of Polymer solutions. *SPE Reservoir Evaluation and Engineering.* 7 (02): 247-252.SPE19499-PA. http://dx.doi.org/10.2118/19499-PA.

McCormick, C.L. and Johnson, C.B. 1988. Structurally Tailored Macromolecules for Mobility control in Enhanced Oil Recovery. Water-Soluble Polymers for Petroleum Recovery, 161 – 180

McKinley, G.H. and Sridhar, T. 2002. Filament Stretching Rheometry of Complex Fluids. *Annual Review of Fluid Mechanics.* 34:375-415. https://doi.org/10.1146/annurev.fluid.34.083001.125207

McKinley, G. H. 2005. Visco-elasto-capillary thinning and breakup of complex fluids, In: *Annual Rheology Reviews*, edited by D. M. Binding and K. Walters. British Society of Rheology, Aberystwyth, 1–48

Melrose, J. C. and Brandner, C. F. 1974. Role of Capillary Forces in Determining Microscopic Displacement Efficiency for Oil Recovery by Water flooding. *Journal of Canadian Petroleum Technology.* 13(4): 54–62.10.2118/74-04-05.

Moffitt, P.D. and Mitchell, J.F. 1983. North Burbank Unit Commercial Scale Polymer flood Project. Presented at the Production Operation Symposium, Osage County, Oklahoma, February 27 – March 1. SPE 11560-MS. https://doi.org/10.2118/11560-MS

Moreno, R.A., Muller A.J. and Saez, A.E. 1996. Flow Induced Degradation of Hydrolyzed polyacrylamide in Porous Media. *Polymer Bulletin* 37 (5): 663-670. https://doi.org/10.1007/BF00296613

Moorhouse, R., Walkinshaw, M.D., and Arnott, S. 1977. Xanthan Gum- Molecular Conformation and Interactions. Extracellular Microbial Polysaccharides. *American Chemical Society Symposium Series* 45 (7): 90-102. 10.1021/bk-1977-0045.ch007

Muller, A.J, Odell, J.A., and Keller, A. 1988. Elongational Flow and Rheology of Monodisperse Polymers in the Solutions. *Journal of Non-Newtonian Fluid Mechanics* 30 (2-3): 99-118. https://doi.org/10.1016/0377-0257(88)85018-3

Munoz, M.E. and Santamaria, A. 2003. Enhancement of the first Normal Stress Coefficient and Dynamic Moduli during Shear Thickening of a Polymer Solutions. *Journal of Rheology.* 47 (4): 1041-1050. https://doi.org/10.1122/1.1579690

Needham, R.B. and Doe, P.H. 1987. Polymer Flooding Review. *Journal of Petroleum Technology.* 39(12): 1503-1507. SPE 17140-PA. https://doi.org/10.2118/17140-PA

Nguyen, T. 1999. Flexible Polymer Chain Dynamics in Elongational Flow: Theory and Experiment. Springer. Berlin

Odell, J. A and Keller, A. 1986. *Journal of Polymer Science Part B: Polymer Physics.* 24 (9): 1889-1916. https://doi.org/10.1002/polb.1986.090240901

Odell, J.A. and Carrington, S.P. 1999. Polymer Solutions in Strong Stagnation Point Extensional Flows. In: Nguyen, T.Q., Kausch, H.H. (eds). Flexible Polymer Chains in Elongational Flow. Springer, Berlin. https://doi.org/10.1007/978-3-642-58252-3_7

Perttamo, E. V. 2013. MS Thesis, University of Bergen, Bergen.

Peter, E.J. 2002. Advanced Petro physics, Live Oak Book Company, Texas.

Plog, J.P., Kulicke, W.M., and Clasen, C. 2004. Influence of the Molar mass distribution on the Elongational Behavior of Polymer Solutions in Capillary Break up. *Applied Rheology*. 15 (1): 28-37.

Pope, G.A., Wu, W., Narayanaswamy, G., Delshad, M., Sharma, M.M., and Wang, P. 2000. Modelling Relative Permeability Effects in Gas-Condensate Reservoir with a New Trapping Model. *SPE Reservoir Evaluation & Engineering* 3 (2); 171-178. SPE 62497-PA. https://doi.org/10.2118/62497-PA

Pusch, G., Lotsch, T., Muller, T., 1987. Investigation of the oil displacing efficiency of suitable polymer products in porous media, aspects of recovery mechanisms during polymer flooding. DGMK—Report: 295–296.

Puls, C., Clemens, T., Sledz, C., Kadnar, R., and Gumpenberger, T. 2016. Mechanical Degradation of Polymers during Injection, Reservoir Propagation and Production. – Field Test Results 8 TH Reservoir, Austria. Presented at the SPE 78th EAGE Conference and Exhibition, Vienna, Austria. SPE 180144-MS. https://doi.org/10.2118/180144-MS

Pye, D.J. 1964. Improved Secondary Recovery by Control of Water Mobility. *Journal of Petroleum Technology*. 16 (08): 911–916. SPE 845-P. http://dx.doi.org/10.2118/845-PA

Qi, P., Ehrenfried, D.H., Koh, H., and Balhoff, M.T., 2017. Reduction of Residual Oil Saturation in Sandstone Cores by the use of Viscoelastic Polymers. *SPE Journal*. 22 (02): 447. https://doi.org/10.2118/179689-PA

Qi, P., Lashgari, H., and Luo, H. 2018. Simulation of Viscoelastic Polymer flooding- From the Lab to the Field. Presented at SPE Annual Technical Conference and Exhibition, Dallas, Texas, 24-26 September. SPE 191498-MS. https://doi.org/10.2118/191498-MS

Ranjbar, M., Rupp, J., Pusch, G., and Meyn, R. 1992. Quantification and Optimization of Viscoelastic Effects of Polymer Solutions for Enhanced Oil Recovery. Presented at SPE IOR Symposium, Tulsa, Oklahoma, 22-24 April, SPE 24154-MS. https://doi.org/10.2118/24154-MS

Reichenback-Klinke, R., Stavland, A., Langlotz, B. and Wenzke, B. and Brodt, G. 2013. New Insights into the Mechanism of Mobility Reduction by Associative Type Copolymers. Presented at SPE Enhanced Oil Recovery Conference, Kuala Lampur, 2-4 July. SPE 165225-MS. https://doi.org/10.2118/165225-MS

Reichenbach-Klinke, R., Stavland, A., Strand, D., and Langlotz, B., and Brodt, G. 2016. Can Associative Polymers Reduce the Residual Oil Saturation? Presented at the SPE EOR Conference at Oil and Gas West Asia, Muscat, 21-23 March. SPE 179801-MS. https://doi.org/10.2118/179801-MS

Reis, T. and Wilson, H.J. 2013. Rolie-Poly Fluid Flowing through constriction: two distinct instabilities, *Journal of Non-Newtonian Fluid Mechanics.* 195: 77-87. http://dx.doi.org/10.1016/j.jnnfm.2013.01.002.

Renardy, M. 1994. Some Comments on the Surface- Tension Driven Breakup (or the lack of it) of Viscoelastic Jets. *Journal of Non-Newtonian Rheology.* 51(01):97-107. https://doi.org/10.1016/0377-0257(94)85005-4

Rivenq, R.C., Donche, A., and Nolk, C. 1992. Improved Scleroglucan for Polymer Flooding Under Harsh Reservoir Conditions. *SPE Reservoir Engineering.* 7 (01): 15-20. SPE-19635-PA. https://doi.org/10.2118/19635-PA

Rodd, L.E., Scott, T.P., and Cooper-White, J.J. 2005. Capillary Breakup Rheometry of Low-viscosity Elastic Fluid. *Applied Rheology.* 15 (1): 12-27. http://dx.doi:10.3933/ApplRheol-15-12-extract.

Rodriguez, S., Romero, C., Sargenti, M.L., Muller, A.J., Saez, A.E., and Odell, J.A. 1993. Flow of Polymer Solutions through Porous Media. *Journal of Non Newtonian Fluid Mechanics.* 49 (1): 63-85. https://doi.org/10.1016/0377-0257(93)85023-4

Rouse, P.E. 1953. A Theory of the Linear Viscoelastic Properties of Dilute Solutions of Coiling Polymers. *Journal of Chemistry Physics.* 21 (2): 1272. doi: 10.1063/1.1699180

Rubinstein, M. and Colby, R. H. 2003. Polymer Physics, 23. New York: Oxford University Press.

Salim Al- Sadi, F., Al- Amri, B.A, Al-Nofi, S.M., Wunnik, J.N.M., Al-Hardi, S.L., Shuaili, K., Cherukupalli, K., and Charkravarthi, R. 2012. Polymer flooding in a Large Field in South Oman – Initial Results and Future Plans. Presented at SPE West Asia EOR Conference, Muscat, 16-18 April. SPE 154665-MS. http://dx.doi.org/10.2118/154665-MS

Savins, J. G. 1969. Non-Newtonian Flow through Porous Media. *Industrial and Engineering Chemistry* 61 (10), 18-47. 10.1021/ie50718a005

Schneider, F.N. and Owens, W.W. 1982. Steady State Measurements of Relative Permeability of Polymer/Oil Systems. *SPE Journal.* 22 (1): 79-86. SPE 9408-PA.

Schulz, D.N. and Bock, J. 1991. Synthesis and fluid properties of associating polymer systems; *Journal of Macromolecular Science: Part-A*: Chemistry. 28 (11-12): 1235–1243. https://doi.org/10.1080/00222339108054096

Schummer, P. and Tebel, K.H. 1983. A New Elongational Rheometer for Polymer Solutions. *Journal of Non-Newtonian Fluid Mechanics.* 12 (3): 331-347. http://dx.doi.org/10.1016/0377-0257(83)85006-X.

Schunk, P.R. and Scriven, L.E. 1990. Constitutive Equation for Modeling Mixed Extension and Shear in Polymer Solution Processing. *Journal of Rheology.* 34: 1085. 10.1122/1.550075

Seright, R.S. 1983. The Effects of Mechanical Degradation and Viscoelastic Behavior on the Injectivity of Polyacrylamide Solutions. *SPE Journal*. 23 (3): 475-485. SPE 9297-PA. http://dx.doi.org/10.2118/9297-PA

Seright, R.S., Seheult, M., and Kelco, C.P. 2009. Injectivity Characteristic of EOR polymers. *SPE Reservoir Evaluation & Engineering*. 12 (05): 783-792. https://doi.org/10.2118/115142-PA

Seright, R. 2010. Potential for polymer flooding reservoirs with viscous oil. *SPE Reservoir Evaluation and Engineering*. 13(4). SPE 129899-PA. https://doi.org/10.2118/129899-PA

Seright, R.S., Fan, T., Wavrik, K., and Balaban, R.D.C. 2011a. New Insights into Polymer Rheology in Porous Media. *SPE Journal.* 16 (1): 35-42. SPE 129200-PA. https://doi.org/10.2118/129200-PA

Seright, R.S., Fan, T., Wavrik, K., Wan, H., and Favero, C. 2011b. Rheology of a New Sulfonic Associative Polymer in Porous Media. *SPE Reservoir Evaluation & Engineering Journal* 14 (06): 726-734. SPE 141355-PA. http://dx.doi.org/10.2118/141355-PA

Seright, R.S. 2011. Use of Polymers to Recover Viscous Oil from the Unconventional Reservoirs, Final Report. Contract No. DE-NT0006555 , US Department of Energy.

Seright, R.S. 2017. How Much Polymer should be Injected during a Polymer Flood? Review of Previous and Current Practices. *SPE J.* 22 (1): 1-18. SPE 179543-PA. https://doi.org/10.2118/179543-PA

Seright, R.S., Wang, D., Lerner, N., Nguyen A., Sabid, J., and Tochor, R. 2018. Can 25-cP Polymer Solution Efficiently Displace 1,600 cP Oil During Polymer Flooding? *SPE Journal.* SPE 190321-PA. https://doi.org/10.2118/190321-PA.

Sharma, V., Haward, S.J., Serdy, J., Keshavarz, B., Soderlund, A. Holmes, T.P., and McKinley, G.H. 2015. The Rheology of the aqueous solutions of ethyl hydroxyl-ethyl cellulose (EHEC) and its hydrophobically modified analogue (hmEHEC): Extensional Flow Response in the Capillary Breakup, Jetting (ROJER) and in a cross-slot extensional rheometer. *Soft Matter.* 11(16):3251-70. 10.1039/c4sm01661k.

Sheng, J. 2010. Modern Chemical Enhanced Oil Recovery: Theory and Practice. Gulf Professional Publishing.

Sheng, J.J., Leonhardt, B., and Azri, N. 2015. Status of Polymer-Flooding Technology. *Journal of Canadian Petroleum Technology.* 54 (02): 116-126. https://doi.org/10.2118/174541-PA

Silva, J.M., Machado, A.V., Moldenaers, P., and Maia, J.M. 2010. The Role of Interfacial Elasticity on the Rheological Behavior of Polymer Blends. Korea- Australia Rheology Journal. 22(1):21-29. http://hdl.handle.net/1822/13297

Silva, J.M., Machado, A.V., and Maia, J. M. 2007. Rheological Behavior of Compatibilized and Non-Compatibilized PA6/EPM blends, Rheological. Acta 46 (08): 1091 https://doi.org/10.1007/s00397-007-0201-z

Siskovic, N., Gregory, D. R., and Griskey, R. G. 1971. Viscoelastic Behavior of Molten Polymers in Porous Media. *American Institute of Chemical Engineer Journal.* 17 (2): 281− 285.

Skartsis, L., Khomami, B., and Kardos, J.L.1992. Polymeric Flow through Fibrous Media. *Journal of Rheology.* 36 (4): 589-620. http://dx.doi.org/10.1122/1.550365

Sousa, P.C., Vega, E.J., and Sousa, R.G., Montanero, J.M., Alves, M.A. 2016. Measurement of Relaxation Times in Extensional Flow of Weakly Viscoelastic Polymer Solutions. *Rheological Acta.* 56 (1): 11-20. https://doi.org/10.1007/s00397-016-0980-1

Smith, F.W. 1970. The behaviour of partially hydrolysed polyacrylamide solutions in porous media. *Journal of Petroleum Technology.* 22(02): 148-156. SPE 2422-PA. https://doi.org/10.2118/2422-PA

Sobti, A. and Wanchoo, R.K. 2014. Creeping Flow of Viscoelastic Fluid through a Packed Bed. *Industrial Engineering and Chemistry Research.* 53 (37): 14508-14518. 10.1021/ie502321a

Sorbie, K.S. and Roberts, L.J. 1984. A Model for Calculating the Polymer Injectivity Including the Mechanical Degradation. Presented at the SPE Improved Oil Recovery Symposium, Tulsa, Oklahoma. 15-18 April. SPE 12654-MS. https://doi.org/10.2118/12654-MS

Sorbie, K.S. 1991. Polymer Improved oil recovery; Blackie publisher. Glasgow and London.

Sochi. T. 2009. Pore scale Modelling of Viscoelastic Flows in the Porous Media Using the Bautisa Manero Fluid. *International Journal of Heat and Flow.* 30 (6): 1202-1217. https://doi.org/10.1016/j.ijheatfluidflow.2009.07.003

Sochi, T. 2010. Non-Newtonian Flow in Porous Media. *Polymer*. 51 (22): 5007-5023. http://dx.doi.org/10.1016/j.polymer.2010.07.047 .

Southwick, J.G. and Manke C.W. 1988. Molecular Degradation, Injectivity and Elastic Properties of Polymer solutions. *SPE Reservoir Engineering Journal.* 3 (04): 1193-1201. SPE 15652-PA. http://dx.doi.org/10.2118/15652-PA.

Standnes, D.C. and Skjevrak, I. 2014. Literature Review of Implemented Polymer Field Projects. *Journal of Petroleum Science and Technology*. 122: 761-775. https://doi.org/10.1016/j.petrol.2014.08.024

Stavland, A., Jonsbraten, H.C., Lohne, A., Moen, A., and Giske, N.A. 2010. Polymer flooding – Flow Properties in Porous Media versus Rheological Parameters. Presented at SPE EUROPEC/EAGE Annual Conference and Exhibition, Barcelona, 14-17 June, SPE 131103-MS. http://dx.doi.org/10.2118/131103-MS.

Stegemeier, G.L. 1974. Relationship of Trapped Oil Saturation to Petrophysical Properties of the Porous Media. Presented at Improved Oil Recovery Symposium, Tulsa, Oklahoma, 22-24 April. SPE 4754-MS. https://doi.org/10.2118/4754-MS

Stegemeier, G. 1977. Mechanisms of Entrapment and Mobilization of Oil in Porous Media. In Improved Oil Recovery by Surfactant and Polymer Flooding, 55–91. New York, New York: Academic Press.

Stolz, C., De Pablo, J.J., and Graham, M.D. 2006. Concentration Dependence of Shear and Extensional Rheology of Polymer Solutions: Brownian Dynamics Simulations. Journal of Rheology. 50 (02):137. https://doi.org/10.1122/1.2167468

Sun, W. and Li, K. 2014. Experimental Evaluation of Models for Calculating Shear rates of Polymer Solutions in Porous media. Presented at SPE Annual Technical Conference and Exhibition, Amsterdam, 27-29 October. SPE 170647-MS. https://doi.org/10.2118/170647-MS

Sylvester, N, D. and Rosen, S.L. 1970. Laminar Flow in the Entrance Region of the Cylindrical Tube. Part 2. Non-Newtonian Fluids. *American Institute of Chemical Engineers Journal.* 16 (6):967-972. https://doi.org/10.1002/aic.690160618

Taber, J. J. 1969. Dynamic and Static Forces Required to Remove Discontinuous Oil Phase from Porous Media Containing Both Oil and Water. *SPE Journal*. 9 (01): 3-12. SPE 2098-PA. https://doi.org/10.2118/2098-PA

Taber, J.J., Kirby, J.C., and Schroeder, F.U. 1973. Studies on the Displacement of Residual Oil: Viscosity and Permeability Effects. *AIChE symposium series* 69: 53.

Taber, J.J. 1981. Research on Enhanced Oil Recovery, Past, Present and Future, *Surface Phenomena in Enhanced Oil Recovery,* D.O. Shah (ed.), Plenum Press, New York City

Taha, S. 2010. Non-Newtonian flow in Porous media. *Journal of Polymer.* 51 (22): 5007-5023.

Tan, H. K.C., Tam, K.C., Tirattmadja, V., Jenkins, R.D., and Bassett, D.R. 2000. Extensional properties of model hydrophobically modified alkali-soluble associative (HASE) polymers solutions. *Journal of Non-Newtonian Fluid Mechanics.* 92 (2-3):167-185.
https://doi.org/10.1016/S0377-0257(00)00093-8

Tang, J.S. 1992. Inter well Tracer Tests to determine the Residual Oil Saturation to Water flood at the Judy Creek Bhl 'a' Pool. *Journal of Canadian Petroleum Technogy.* 31 (08). https://doi.org/10.2118/92-08-06

Tavassoli, S., Pope, G. A., and Sepehrnoori, K. 2014. Frontal Stability Analysis of Surfactant Floods. *SPE Journal.* 20 (03): 471- 482. SPE 169118-PA https://doi.org/10.2118/169118-PA

Tavassoli, S., Lu, J., Pope, G. A., Sepehrnoori, K. 2014. Investigation of the Critical Velocity Required for a Gravity-Stable Surfactant Flood. *SPE Journal.* 19 (5): 931-942. https://doi.org/10.2118/163624-PA

Taylor, K.C. and Nasr-el-din, H.A. 1995. Water soluble Hydrophobically Associating Polymers for Improved Oil Recovery: A Literature Review. Presented at SPE International symposium on the Oil Field Chemistry, San Antonio, Texas, California. 14-17 February. SPE 29008-MS. https://doi.org/10.2118/29008-MS

Taylor, K.C. and Nasr-El-Din, H.A. 1997. Water Soluble Hydrophobically Associating Polymers for Improved oil recovery: A Literature Review. *Journal of Petroleum Science and Engineering*. 19(3-4): 265–280. http://dx.doi.org/10.1016/S0920-4105(97)00048

Tiu, C., Zhou, J. Z. Q., Nicolae, G., Fang, T., Chhabra, R.P. 1997. Flow of Viscoelastic Polymer Solutions in Mixed Beds of Particles. *Canadian Journal of Chemical Engineering.* 75 (5): 843−850. https://doi.org/10.1002/cjce.5450750504

Trantham, J.C. and Moffitt, P.D. 1982. North Burbank Unit 1440-Acre Pilot Polymer Flood Project Design. Presented at SPE Enhanced Oil Recovery Symposium, Oklahoma, Tusla, 4-7 April, SPE 10717-MS. https://doi.org/10.2118/10717-MS

Tyseer, D.A. and Vetter, O.J. 1981. Chemical Characterization Problems of Water-Soluble Polymers. *Journal of Petroleum Technology.* 21 (6): 721-730. https://doi.org/10.2118/8977-PA.

Urbissinova, T.S., Trivedi, J.J. and Kuru, E. 2010. Effect of Elasticity during Viscoelastic Polymer Flooding: A Possible Mechanism of Increasing Sweep Efficiency. *Journal of Canadian Petroleum Technology.* 49(2): 49−56. SPE 133471-PA. http://dx.doi.org/10.2118/133471-PA.

Van den Ende, T.W. 2015. Extensional Viscosity aspect of HPAM in Porous Flow, An Experimental and Numerical Study, MS Thesis, Delft University of Technology, Delft, Netherland.

Veerabhadrappa S.K., Trivedi J.J., and Kuru E. 2013. Visual Confirmation of the elasticity dependence of unstable secondary polymer floods. *Industrial & Engineering Chemistry Research*. 52 (18): 6234-6241.

Vermolen, E.C.M., van Haasterecht, M.J.T., and Masalmeh, S.K. 2014. A Systematic Study of the Polymer Viscoelastic Effects on the Residual oil Saturation by Core Flooding. Presented at the SPE EOR conference, Muscat, March 31 – April 2. SPE 169681-MS. https://doi.org/10.2118/169681-MS

Viken, A.L., Skauge, T., and Spildo, K. 2016. Rheological properties of the hydrophobically

modified anionic polymer: Effect of varying salinity and amount of hydrophobic moieties. *Journal of Applied Polymer Science.* 133(23): 43530. http://dx.doi.org/10.1002/app.43520

Volpert, E., Selb, J., and Candau, F. 1998. Associating behavior of Polyacrylamide hydrophobically modified with dihexylacrylamide. *Polymer.* 39 (5): 1025-1033. https://doi.org/10.1016/S0032-3861(97)00393-5

Vorwerk, J. and Brunn, P. O. 1991. Porous Medium Flow of the Fluid A1: Effects of Shear and Elongation. *Journal of Non-Newtonian Fluid Mechanics.* 41 (1-2):119−131. https://doi.org/10.1016/0377-0257(91)87038-Y

Vossoughi, S. and Sayer, F.A. 1974. Pressure Drop for Flow of Polymer Solution in a Model Porous Medium. *Canadian Journal of Chemical Engineering*. 52 (5): 666—669. https://doi.org/10.1002/cjce.5450520521

Wang, D., Cheng, J., Yang, Q., Wenchao, G., and Qun, L. 2000. Viscous-Elastic Polymer Can Increase Microscale Displacement Efficiency in Cores. Presented at the 2000 SPE Annual Technical Conference and Exhibition, Dallas, 1-4 October. SPE 63227-MS. http://dx.doi.org/10.2118/63227-MS.

Wang, D., Xia, H., Liu, Z., and Yang, Q. 2001a. Study of the Mechanism of Polymer Solution with Visco-Elastic Behavior Increasing Microscopic Oil Displacement Efficiency and the Forming of Steady "Oil Thread" Flow Channels. Presented at the 2001 SPE Asia Pacific Oil and Gas Conference and Exhibition, Jakarta, 17–19 April, SPE 68723-MS.http://dx.doi.org/10.2118/68723-MS

Wang, D., Cheng, J., Xia, H., Li, Q., and Shi, J. 2001b. Viscous-Elastic Fluids Can Mobilize Oil Remaining after Water-Flood by Force Parallel to the Oil-Water Interface. Presented at the SPE Asia Pacific Improved Oil Recovery Conference, Kuala Lumpur, 8–9 October. SPE 72123-MS. http://dx.doi.org/10.2118/72123-MS

Wang, D., Han, P., Shao, Z., and Seright, R.S. 2006. Sweep Improvement Options for the Daqing Oil Field. Presented at the SPE/DOE Symposium on Improved Oil Recovery, Tulsa, 22–26 April. SPE 99441-MS. https://doi.org/10.2118/99441-MS

Wang, D.M., Wang, G, Wu, W. Xia, H., and Yin, H. 2007. The Influence of Viscoelasticity on Displacement Efficiency–from Micro to Macro Scale. Presented at SPE Annual Technical Conference and Exhibition, Anaheim, California, 11–14 November 2007. SPE 109016-MS. https://doi.org/10.2118/109016-MS

Wang, D., Seright, R. S., Shao, Z., and Wang, J. 2008. Key Aspects of Project Design for Polymer Flooding at the Daqing Oil Field. *SPE Reservoir Evaluation & Engineering.* 11 (6): 1117–1124. SPE 109682-PA. http://dx.doi.org/10.2118/109682-PA.

Wang, D., Xia, H., Yang, S., and Wang, G. 2010. The Influence of Visco-elasticity on Micro Forces and Displacement Efficiency in Pores, Cores and in the Field. Presented at the SPE EOR Conference at Oil and Gas West Asia, Muscat, 11–13 April. SPE 127453-MS. http://dx.doi.org/10.2118/127453-MS.

Wang, D., Wang, G., and Xia, H. 2011. Large Scale High Visco-Elastic Fluid Flooding in the Field Achieves High Recoveries. Presented at the SPE EOR Conference, Kuala Lumpur, 19–21 July. SPE 144294-MS. http://dx.doi.org/10.2118/144294-MS.

Wang, Z.B., Wang, Q., Ma, D.S. Ye, Y.Z., and Liu, Z. X. 2013. A New Method of Numerical Simulation for Viscoelastic polymer flooding. Presented at the SPE Reservoir Characterization and Simulation Conference, Abu Dhabi, 16-18 September, SPE 165972-MS. https://doi.org/10.2118/165972-MS.

Warner, H.R. 1972. Kinetic Theory and Rheology of Dilute Suspensions of Finitely Extendible Dumbbell. *Industrial Engineering Chemistry Fundamental.* 11 (3); 379-387. 10.1021/i160043a017

Wassmuth, F.R., Green, K., Arnold, W., and Cameron, N. 2009. Polymer flood Application to Improve Heavy oil Recovery at East Bodo. *Journal of Canadian Petroleum Technology*. 48 (02): 55-61. https://doi.org/10.2118/09-02-55

Wassmuth, F.R., Green, K., and Bai J. 2012. Associative Polymers Outperform Regular Polymers Displacing Heavy oil in Heterogeneous Systems. Presented at SPE Heavy oil conference, Calgary, Alberta, 12-14 June. SPE 157916-MS. https://doi.org/10.2118/157916-MS

Wei, B., Zeron, L.R., and Rodrigue, D. 2014. Oil Displacement Mechanisms of Viscoelastic Polymers in Enhanced Oil Recovery: A review. *Journal of Petroleum Exploration Production Technology*. 4(2): 113-121. https://doi.org/10.1007/s13202-013-0087-5.

Weiss, W.W. 1992. Performance Review of a Large Scale Polymer Flood. Presented at SPE Eight Symposium on the Enhanced Oil Recovery, Tulsa, Oklahoma, 22-24 April. SPE 24145-MS. https://doi.org/10.2118/24145-MS

Wever, D.A.Z., Picchioni, F., and Broekhuis, F. 2011. Polymers for enhanced oil recovery: A Paradigm for structure–property relationship in aqueous solution. *Progress in Polymer Science.* 36 (11): 1558–1628. 10.1016/j.progpolymsci.2011.05.006.

White, J. L. 1964. Dynamics of Viscoelastic Fluids, Melt Fracture, and the Rheology of Fiber Spinning. *Journal of Applied Polymer Science.* 8 (5): 2339−2357. https://doi.org/10.1002/app.1964.070080527

Wilton, R.R. and Torabi, F. 2013. Rheological Assessment of the Elasticity of Polymers for Enhanced Heavy oil recovery. Presented at SPE Heavy oil conference, Calgary, Alberta, 11-13 June. SPE165488-MS. http://dx.doi.org/10.2118/165488-MS.

Wissler, E. H. 1971. Viscoelastic Effects in the Flow of Non-Newtonian Fluids through a Porous Medium. *Industrial Engineering Chemistry Fundamentals.* 10 (3): 411-417. 10.1021/i160039a012

Xia, H., Wang, D., Wu, J., and Kong F. 2004. Elasticity of HPAM Solutions Increases Displacement Efficiency under Mixed Wettability Conditions. Presented at the SPE Asia Pacific Oil and Gas Conference and Exhibition, Perth, 18–20 October, SPE 88456-MS. http://dx.doi.org/10.2118/88456-MS.

Xia, H., Wang, D., Wang, G., Ma, W.G., Deng, H.W., and Liu, J. 2008. Mechanisms of the Effect of Micro forces on the Residual oil in the chemical Flooding. SPE Improved Oil Recovery Symposium, Tulsa, Oklahoma, 20-23 April. SPE 114335-MS. https://doi.org/10.2118/114335-MS

Xie, K., Lu, X., Li, Q., Jiang, W. and Yu, Q. 2016. Analysis of Reservoir Applicability of Hydrophobically Associating Polymer. *SPE Journal.* 21 (01):1-9.
SPE 174553-PA. https://doi.org/10.2118/174553-PA

Wu, W., Wang, D., and Jiang, H. 2007. Effect of the Visco-elasticity of Displacing Fluids on the Relationship of Capillary Number and Displacement Efficiency in Weak Oil-Wet Cores. Presented at the Asia Pacific Oil and Gas Conference and Exhibition, Jakarta, 30 October–1 November. SPE 109228-MS. http://dx.doi.org/10.2118/109228-MS.

Yesilata, B., Clasen, C., and McKinley, G.H. 2006. Non-Linear Shear and Extensional Flow Dynamics of Wormlike Micellar Solutions. *Journal of Non-Newtonian Fluid Mechanics.* 133: 73-90

Yin, H.J., Wang, D., and Zhong, H. 2006. Study of Flow Behavior of Viscoelastic Polymer Displacement in Micropore with Dead end. Presented at SPE Annual Technical Conference and Exhibition, San Antonio, Texas, USA, 24-27 September. SPE 101950-MS. https://doi.org/10.2118/101950-MS

Young, N.W.G., Williams, P.A., Meadows, J., and Allen, E. 1998. A Promising Hydrophobically Modified Guar gum for Completion Applications. Presented at the SPE Improved Oil Recovery Symposium, Tulsa, Oklahoma, 19-22 April. SPE 39700-MS. https://doi.org/10.2118/39700-MS

Yuan, M., 1981. A Rheological study of Polymer and microemulsion in porous media. MS thesis, UT Austin.

Zaitoun, A. and Kohler, N. 1987. The Role of Adsorption in Polymer Propagation through Reservoir Rocks. Presented at the SPE International Symposium on Oilfield Chemistry, San Antonio, Texas, 4–6 October. SPE 16274-MS. http://dx.doi.org/10.2118/16274-MS.

Zamani, N., Bondino, I., Kaufmann R., and Skauge, A. 2015. Effect of Porous Media Properties on the Onset of Polymer Extensional Viscosity. *Journal of Petroleum Science and Technology*. 133: 483-495. https://doi.org/10.1016/j.petrol.2015.06.025

Zechner, M., Clemens, T., Suri, A., and Sharma, M.M. 2015. Simulation of Polymer Injection under Fracturing Conditions—A Field Pilot in the Matzen Field, Austria. *SPE Reservoir Evaluation & Engineering.* 18 (2): 236–249. SPE 169043-PA. https://doi.org/10.2118/169043-PA

Zell, A., Gier, S., Salima, R., and Wagner, C. 2010. Is there a Relation Between the Relaxation Time and Measured in the CaBER Experiments and the First Normal Stress Coefficenct? *Journal of Non Newtonian Fluid Mechanics.* 165 (19-20): 1265-1274. https://doi.org/10.1016/j.jnnfm.2010.06.010

Zimm, B.H. 1956. Dynamics of Polymer Molecules in Dilute Solution: Viscoelasticity, Flow Birefringence and Dielectric Loss. *Journal of Chemical Physics.* 24 (02): 269-278.10.1063/1.1742462

Appendix [7]

Existing viscoelastic quantification methods relies on the core flooding experiments to predict the apparent viscosity of the enhanced oil recovery (EOR) polymer solutions in porous media. A novel method is developed that could predict their porous media behavior through bulk shear and extensional rheological measurements. In this appendix, the steps involved in the method development is detailed. It includes the polymer preparation, measurements of the filament diameter vs time data using capillary break-up extensional rheometer, obtaining the relevant extensional rheological parameters using appropriate theories, measuring shear rheological parameters, and determination of the downscaling factors. Relevant extensional parameters such as extensional relaxation time, maximum elongational viscosity at the critical Deborah number and strain hardening index are determined using upper convected Maxwell model, finite extensible non-linear elastic model, and power law model.

Step by step procedure

The steps involved in the method development are elaborated.

Polymer solution preparation

HPAM 3230, HPAM 3530, HPAM 3630 and pusher 700 polymers were obtained from SNF Floerger (USA). Hengfloc 63020 and Hengfloc 63026 were obtained from Henju Beijing (China). All the polymer solutions were prepared by adding polymer power in the brine solution and mixing at 200 rpm using a magnetic stirrer for 24 hours. The details about the polymer type, molecular weight, concentration and brine salinity are listed in Table 7.1.

Measuring the filament diameter with time

Extensional rheological measurements were performed on the prepared polymer solutions using capillary break up extensional rheometer (CaBER) to attain the filament diameter vs time data. Each polymer solutions taken in small quantity, was placed between the two circular plates with diameters of 6 mm. The movable top plate was separated from the stationary bottom plate, thereby forming a filament by imposing an instantaneous level of extensional strain on the fluid sample. 50 milli seconds was given as strike time for the separation of plates. The operational parameters are reported in Table 3.2. The fluid was squeezed together by capillary force after stretching. The

[7] A version of this appendix will be submitted to MethodsX.

midpoint diameter of the thinning fluid filament as a function of time monitored using the inbuilt laser micrometer is shown (Figures. S-7.1a to S-7.14a).

Determination of extensional rheological parameters

Pure extensional flow is generated by stretching the polymer samples. Filament drainage induced by the imposed step strain is governed by the balance between the driving capillary force and the resistive viscous and elastic force. The intermediate timescale of viscoelastic fluids that have been reported to be governed by the balance between elasticity and surface tension is represented by the exponential decline in filament diameter (Entov and Hinch 1997). The filament drainage (filament diameter with time) are used to get the maximum elongational viscosity at the critical deborah number ($\mu_{\max@De_{cr-0.66}}$), extensional relaxation time (τ_{ext}) and strain hardening index *(n_2)*

Determination of extensional relaxation time using Upper-Convected Maxwell (UCM) model

The UCM model is used to determine the τ_{ext} by regression. The linear data corresponding to the elastic region is extracted from the filament diameter versus time semi-logarithmic plot. The extracted data are then fitted with the UCM model using regression to match the exponential decline of filament diameter as given in Eq. (A.1). The surface tension of water (73 milli N/m) is used for all the solutions. τ_{ext} is determined using Figures A.1a to A.14a for all the polymer samples and the values are reported in Table 7.2.

$$D_{mid}(t) = D_o\left(\frac{G * D_o}{4 * \sigma}\right)^{\frac{1}{3}} e^{\left(\frac{-t}{3*\tau_{ext}}\right)} \quad \text{(A.1)}$$

where

$D_{mid}(t)$ is the mid-point diameter, mm;

D_o is the initial diameter of the sample, mm

G is the Elastic modulus, Pa

τ_{ext} is the extensional relaxation time, s

Determination of maximum elongational viscosity using finite extensible non-linear elastic (FENE) theory

The filament drainage, driven by the capillary force and resisted by the viscous and elastic force can be represented by the axial force balance. The axial force balance detailed in Anna and McKinley (2002), McKinley (2005) and used recently by Kim et al. (2010) is given by Eq. (A.2).

$$\frac{2\sigma}{D_{mid}} = 3\eta_{\varepsilon}\dot{\varepsilon} + \left(\tau_{zz} - \tau_{rr}\right) \tag{A.2}$$

where,

η_{ε} is the solvent viscosity, Pa.s

τ_{zz} is the first Normal stress, Pa

τ_{rr} is the second normal stress, Pa

$\dot{\varepsilon}$ is the strain rate, s^{-1}

The strain and strain rate is calculated using the Eqs. (A.3) and (A.4)

$$\varepsilon(t) = 2\ln\left(\frac{D_o}{D_{mid(t)}}\right) \tag{A.3}$$

$$\dot{\varepsilon}(t) = \frac{-2}{D_{mid(t)}}\left(\frac{dD_{mid(t)}}{dt}\right) \tag{A.4}$$

where,

ε is the Hencky strain, (dimensionless)

$\dot{\varepsilon}$ is the strain/elongation rate, (s^{-1})

The elongational viscosity is calculated by substituting Eq. (A.4) into Eq. (A.2). Since the filament flow is purely elongational, the stresses resisting the capillary action are extensional and viscosity calculated out of them represents the irrotational extensional viscosity. The details of these derivations can be found elsewhere (Anna and Mc Kinley 2002). The elongational viscosity is represented by Eq. (A.5)

$$\eta_{app}(e) = -\frac{(2x-1)\sigma}{\frac{dD_{mid}}{dt}} \tag{A.5}$$

where,

$\eta_{app}(e)$ is the apparent extensional viscosity, Pa.s

X is the correction factor for axial variation (0.7127)

Entov and Hinch (1997), using FENE theory derived that fluid relaxes at the rate 2/3rd of strain rate during filament drainage. Filament drainage is constant at the critical Deborah number of 0.66 and it represents the maximum elastic limit where the elongational viscosity tends to exhibit maxima (Kim et al. 2010; Clasen 2010). Maximum elongational viscosity that corresponds to the elastic limit around the critical Deborah number of 0.66 is obtained from the Figures A.1 b to A.14 b are represented as $\mu_{\max@De_{cr-0.66}}$ in Table 7.2. Critical strain rate is determined by dividing the critical Deborah number by τ_{ext}

Determination of strain hardening index using Power law model

During filament drainage, the fluids get strained that results in the increase of extensional viscosity with respect to strain. A viscoelastic polymer that thins in the shear field, thickens in the porous media and extensional field (Barnes 2010). The power law model is used to fit the extensional viscosity vs strain data around the critical Deborah number to calculate the average values of n_2 (Figures A.1c to A.14c).

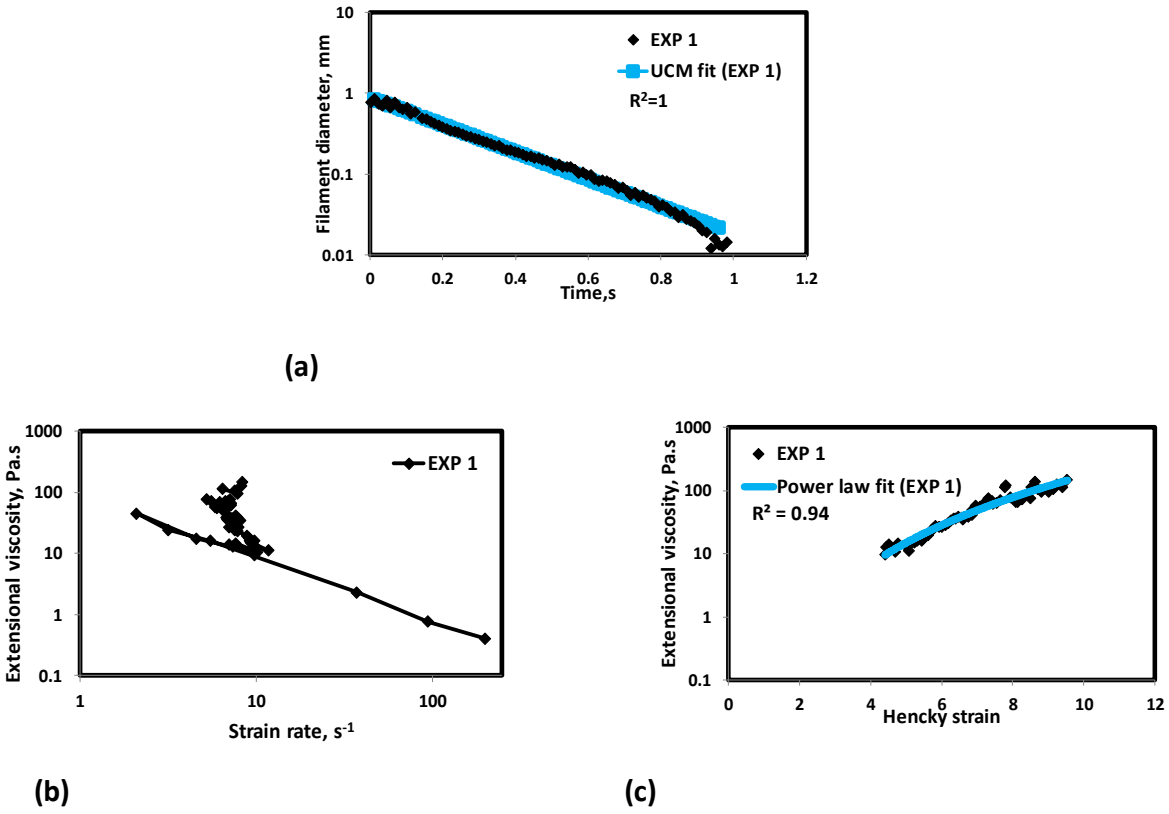

Figure A.1: *a) Filament diameter vs time plot for EXP 1 and the UCM fit to the linear elastic regimes for the determination of relaxation time b) Extensional viscosity as a function of generated strain rate plot showing the sharp rise in the extensional viscosity around the critical Deborah number c) Power law fit to the extensional viscosity vs Hencky strain values around the critical Deborah number for the determination of strain hardening index.*

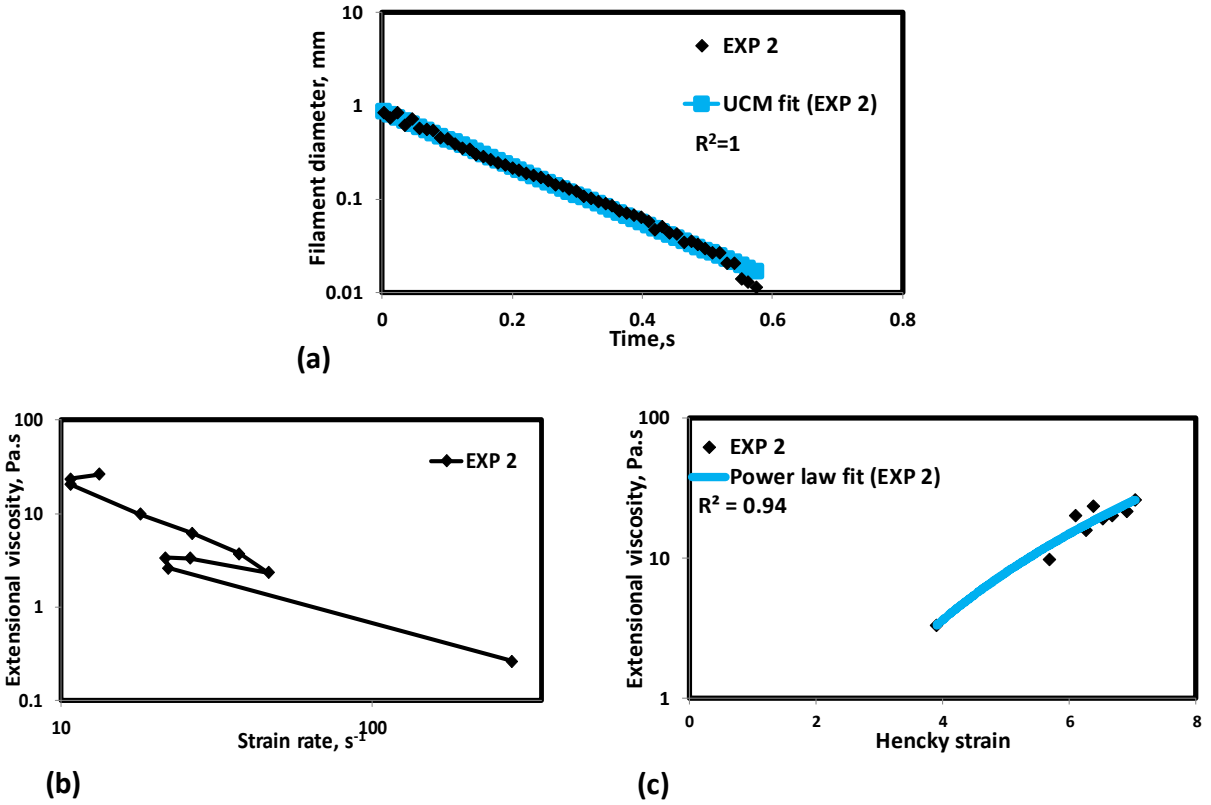

Figure A.2: *a) Filament diameter vs time plot for EXP 2 and the UCM fit to the linear elastic regimes for the determination of relaxation time b) Extensional viscosity as a function of generated strain rate plot showing the sharp rise in the extensional viscosity around the critical Deborah number c) Power law fit to the extensional viscosity vs Hencky strain values around the critical Deborah number for the determination of strain hardening index.*

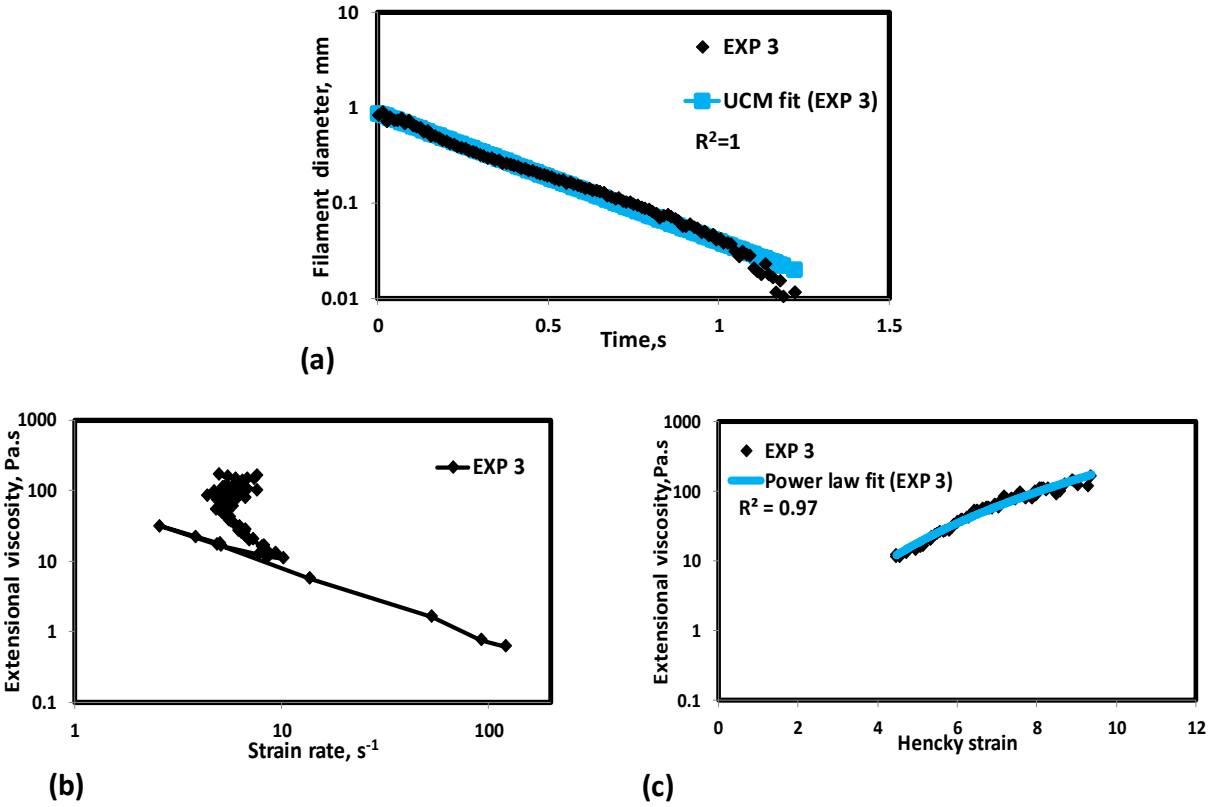

Figure A.3: *a) Filament diameter vs time plot for EXP 3 and the UCM fit to the linear elastic regimes for the determination of relaxation time b) Extensional viscosity as a function of generated strain rate plot showing the sharp rise in the extensional viscosity around the critical Deborah number c) Power law fit to the extensional viscosity vs Hencky strain values around the critical Deborah number for the determination of strain hardening index.*

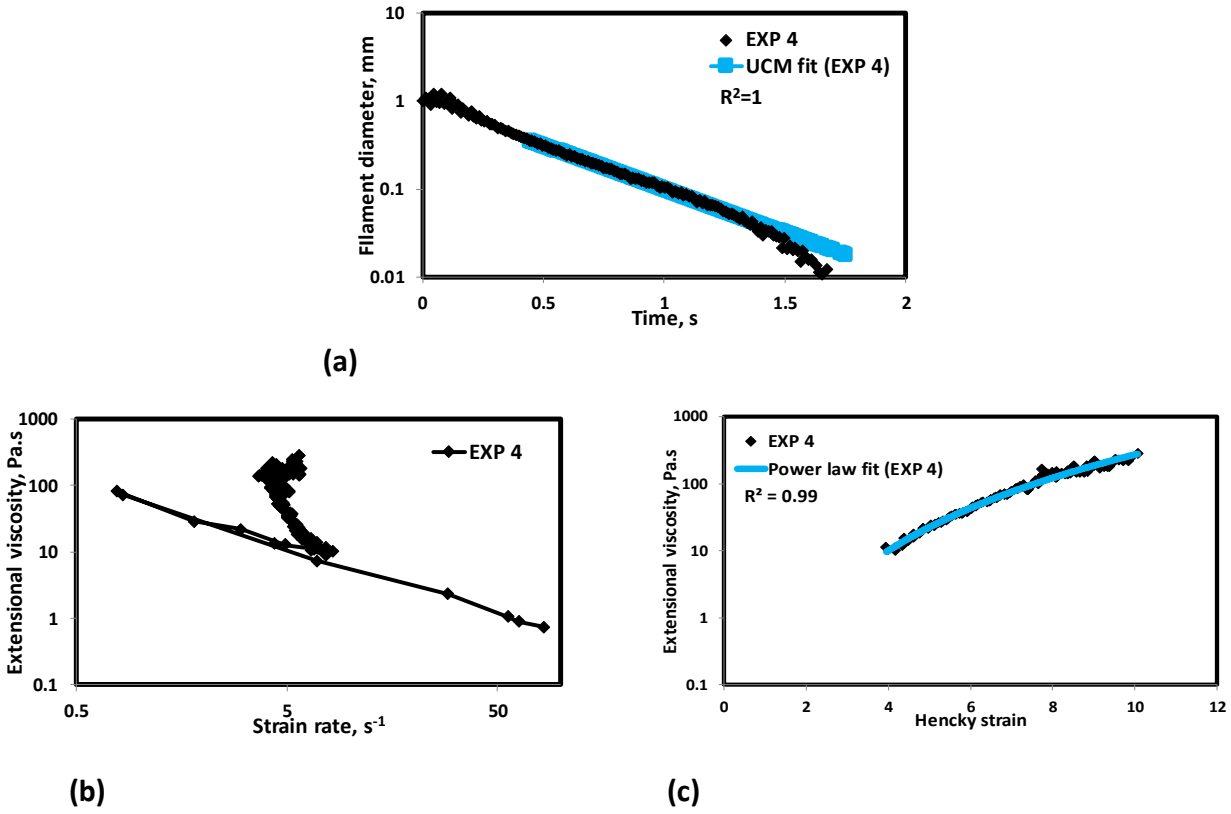

Figure A.4: *a) Filament diameter vs time plot for EXP 4 and the UCM fit to the linear elastic regimes for the determination of relaxation time b) Extensional viscosity as a function of generated strain rate plot showing the sharp rise in the extensional viscosity around the critical Deborah number c) Power law fit to the extensional viscosity vs Hencky strain values around the critical Deborah number for the determination of strain hardening index.*

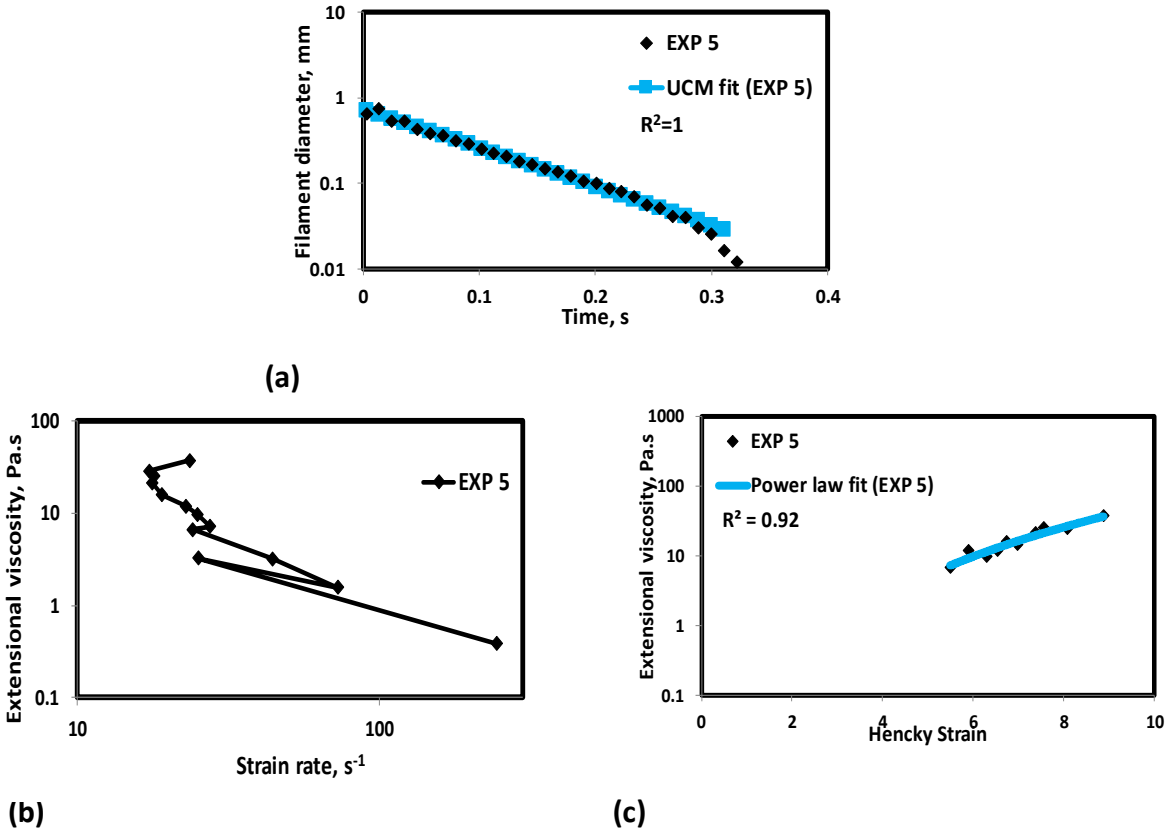

Figure A.5: *a) Filament diameter vs time plot for EXP 5 and the UCM fit to the linear elastic regimes for the determination of relaxation time b) Extensional viscosity as a function of generated strain rate plot showing the sharp rise in the extensional viscosity around the critical Deborah number c) Power law fit to the extensional viscosity vs Hencky strain values around the critical Deborah number for the determination of strain hardening index.*

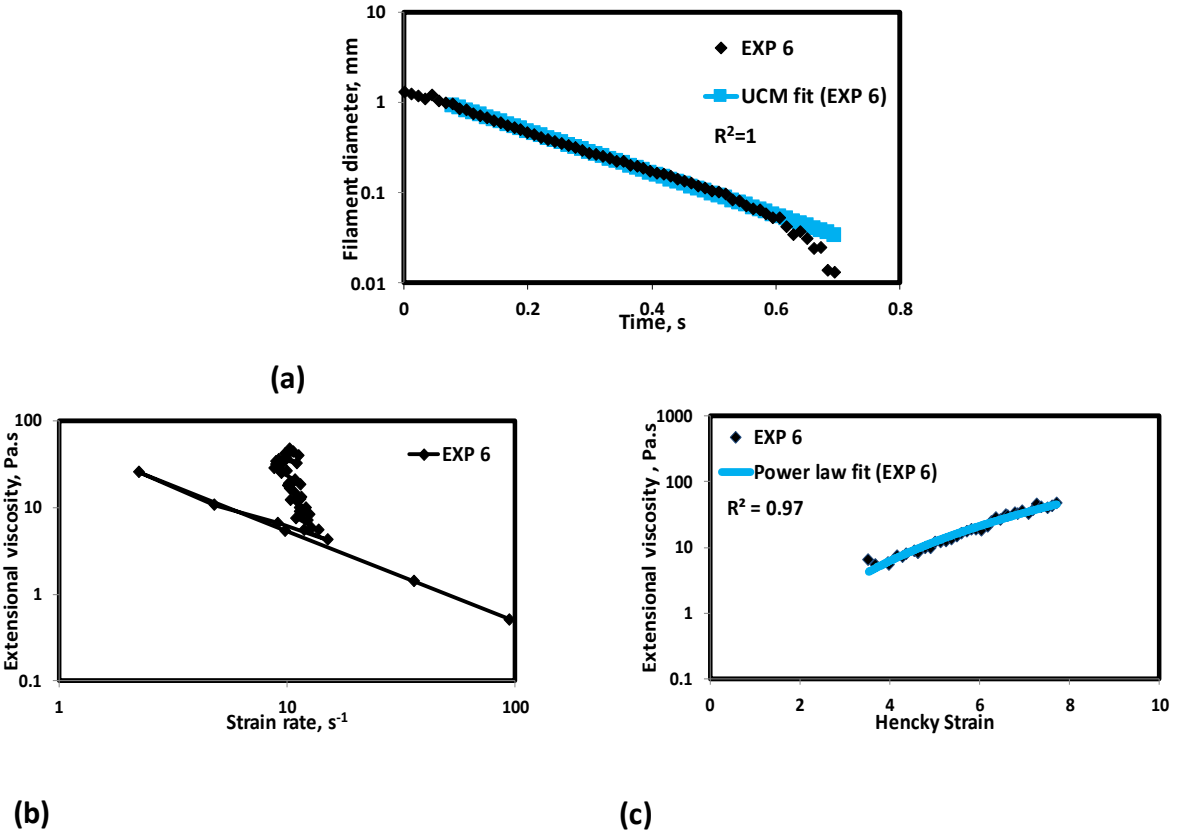

Figure A.6: *a) Filament diameter vs time plot for EXP 6 and the UCM fit to the linear elastic regimes for the determination of relaxation time b) Extensional viscosity as a function of generated strain rate plot showing the sharp rise in the extensional viscosity around the critical Deborah number c) Power law fit to the extensional viscosity vs Hencky strain values around the critical Deborah number for the determination of strain hardening index.*

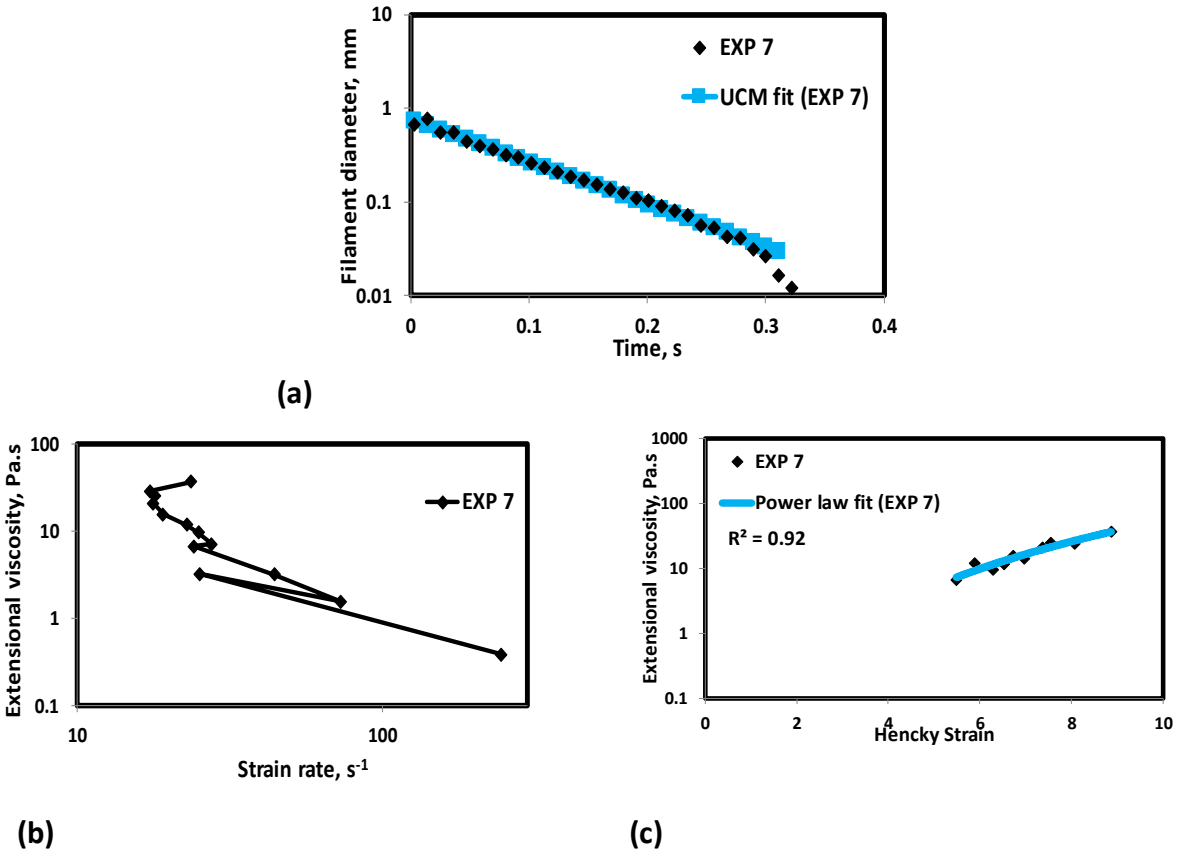

Figure A.7: *a) Filament diameter vs time plot for EXP 7 and the UCM fit to the linear elastic regimes for the determination of relaxation time b) Extensional viscosity as a function of generated strain rate plot showing the sharp rise in the extensional viscosity around the critical Deborah number c) Power law fit to the extensional viscosity vs Hencky strain values around the critical Deborah number for the determination of strain hardening index.*

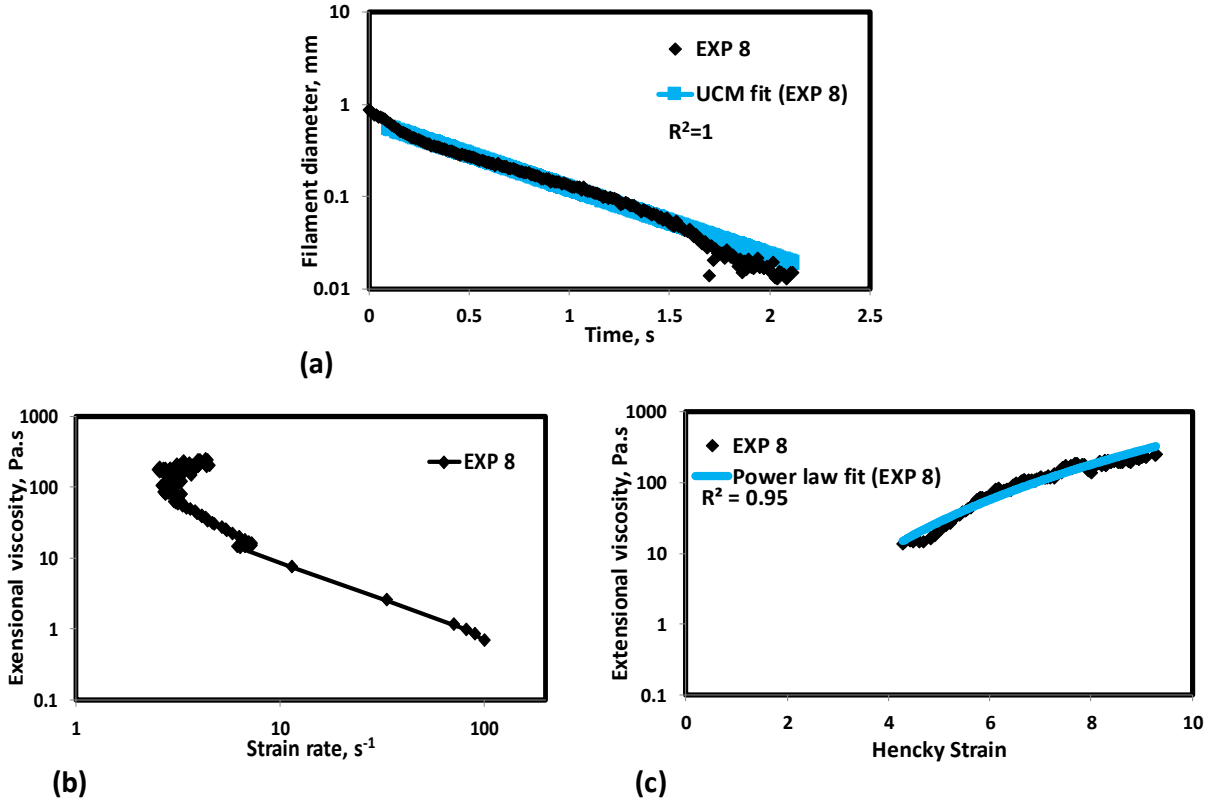

Figure A.8: *a) Filament diameter vs time plot for EXP 8 and the UCM fit to the linear elastic regimes for the determination of relaxation time (b): Extensional viscosity as a function of generated strain rate plot showing the sharp rise in the extensional viscosity around the critical Deborah number (c): Power law fit to the extensional viscosity vs Hencky strain values around the critical Deborah number for the determination of strain hardening index.*

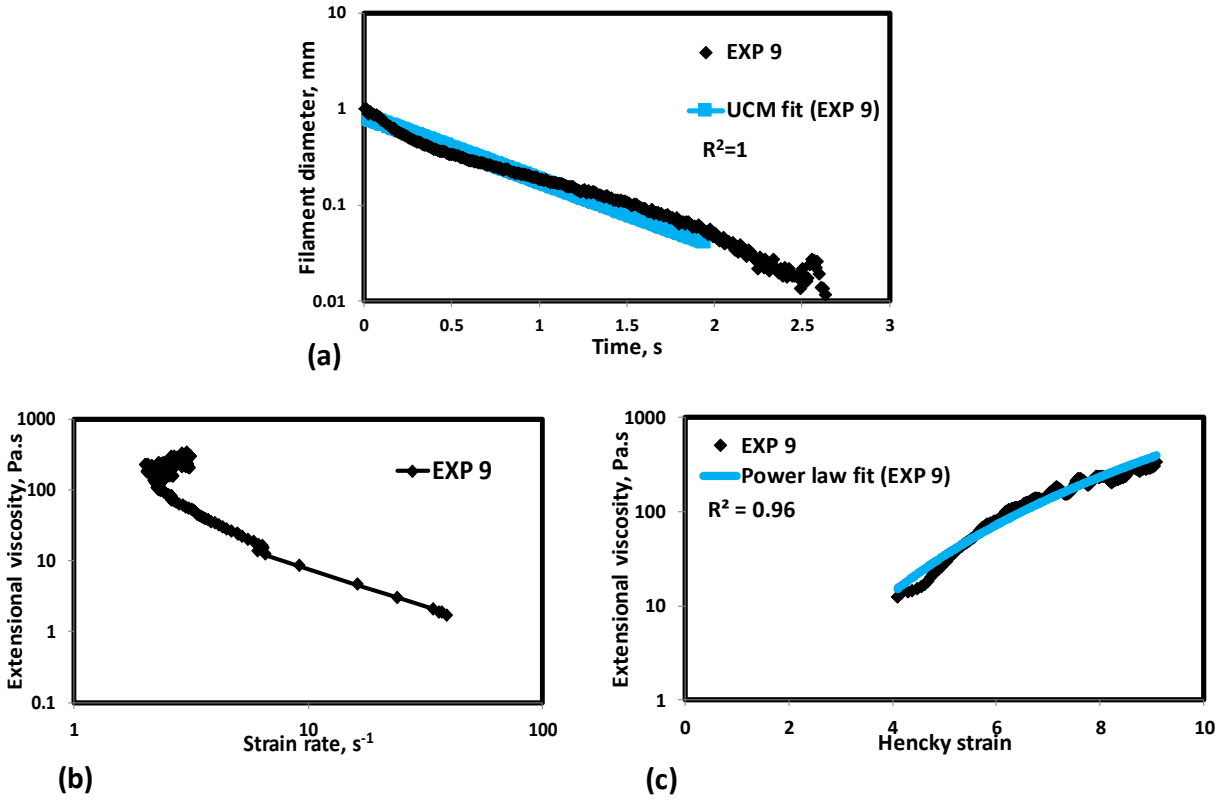

Figure A.9: *a) Filament diameter vs time plot for EXP 9 and the UCM fit to the linear elastic regimes for the determination of relaxation time (b): Extensional viscosity as a function of generated strain rate plot showing the sharp rise in the extensional viscosity around the critical Deborah number (c): Power law fit to the extensional viscosity vs Hencky strain values around the critical Deborah number for the determination of strain hardening index.*

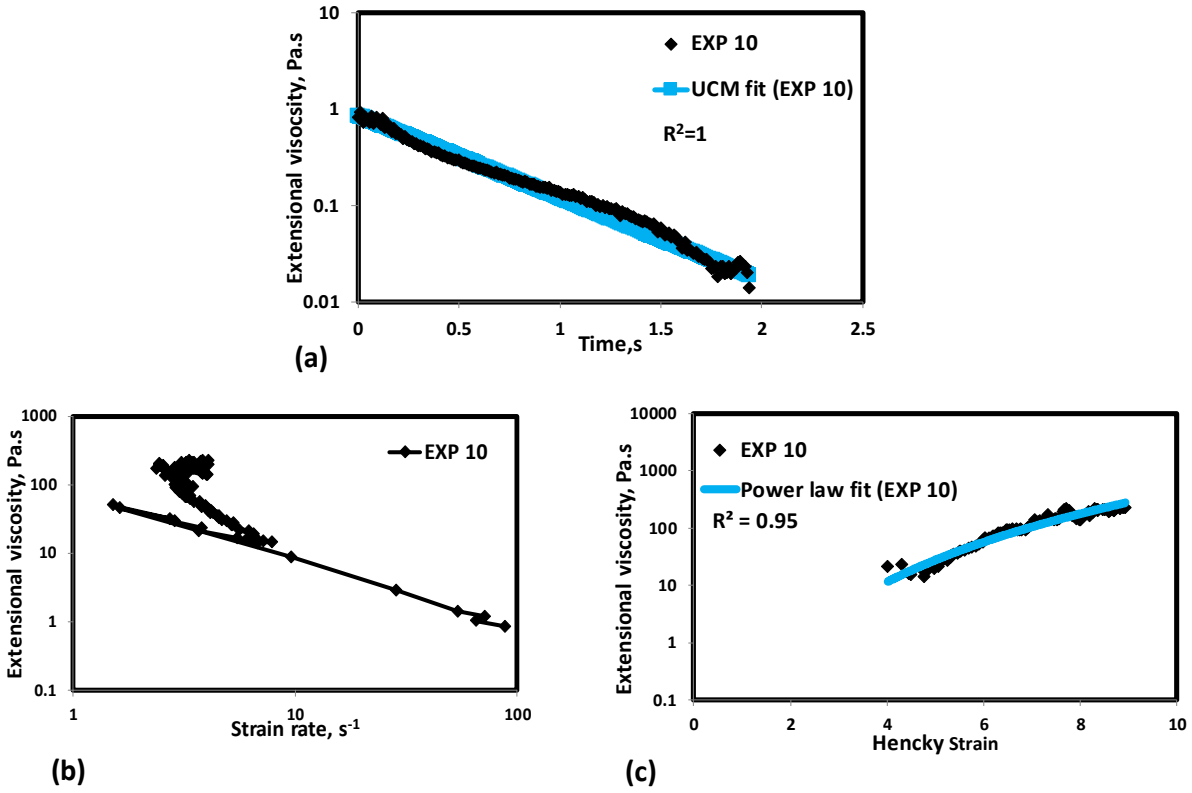

Figure A.10: *a) Filament diameter vs time plot for EXP 10 and the UCM fit to the linear elastic regimes for the determination of relaxation time (b): Extensional viscosity as a function of generated strain rate plot showing the sharp rise in the extensional viscosity around the critical Deborah number (c): Power law fit to the extensional viscosity vs Hencky strain values around the critical Deborah number for the determination of strain hardening index.*

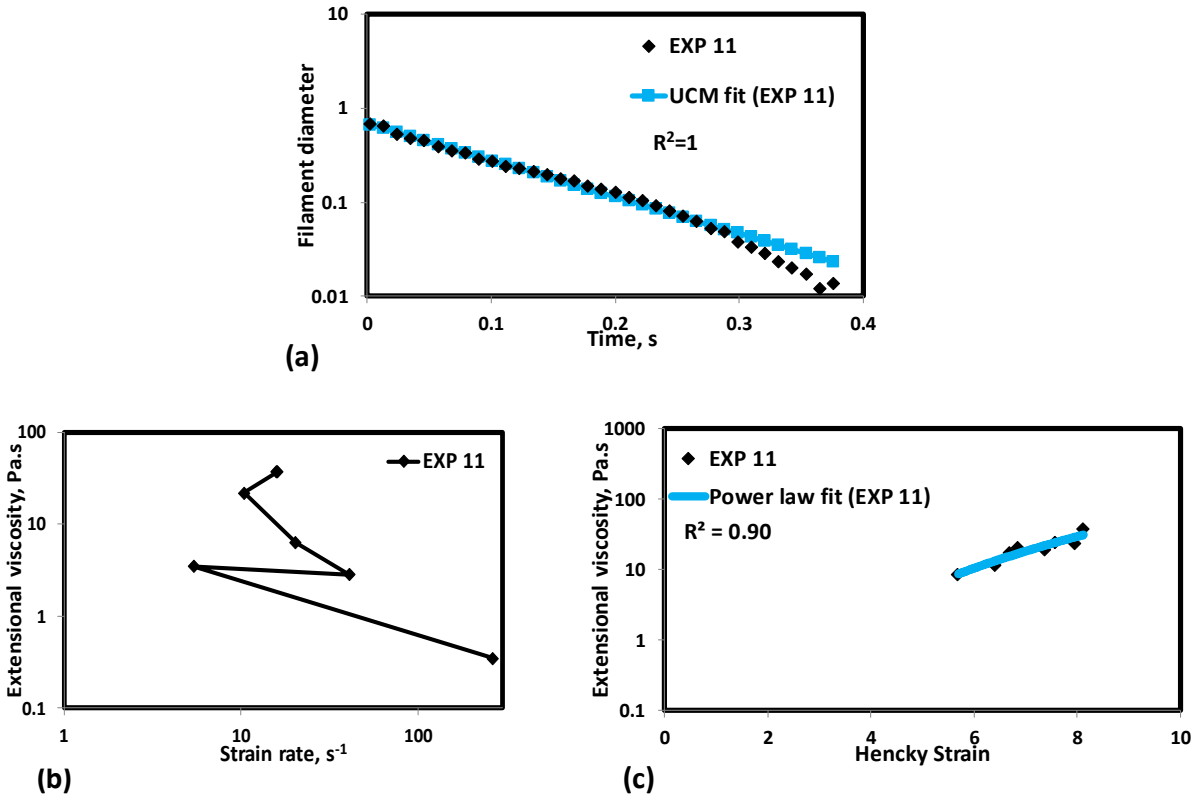

Figure A.11: *a) Filament diameter vs time plot for EXP 11 and the UCM fit to the linear elastic regimes for the determination of relaxation time (b): Extensional viscosity as a function of generated strain rate plot showing the sharp rise in the extensional viscosity around the critical Deborah number (c): Power law fit to the extensional viscosity vs Hencky strain values around the critical Deborah number for the determination of strain hardening index.*

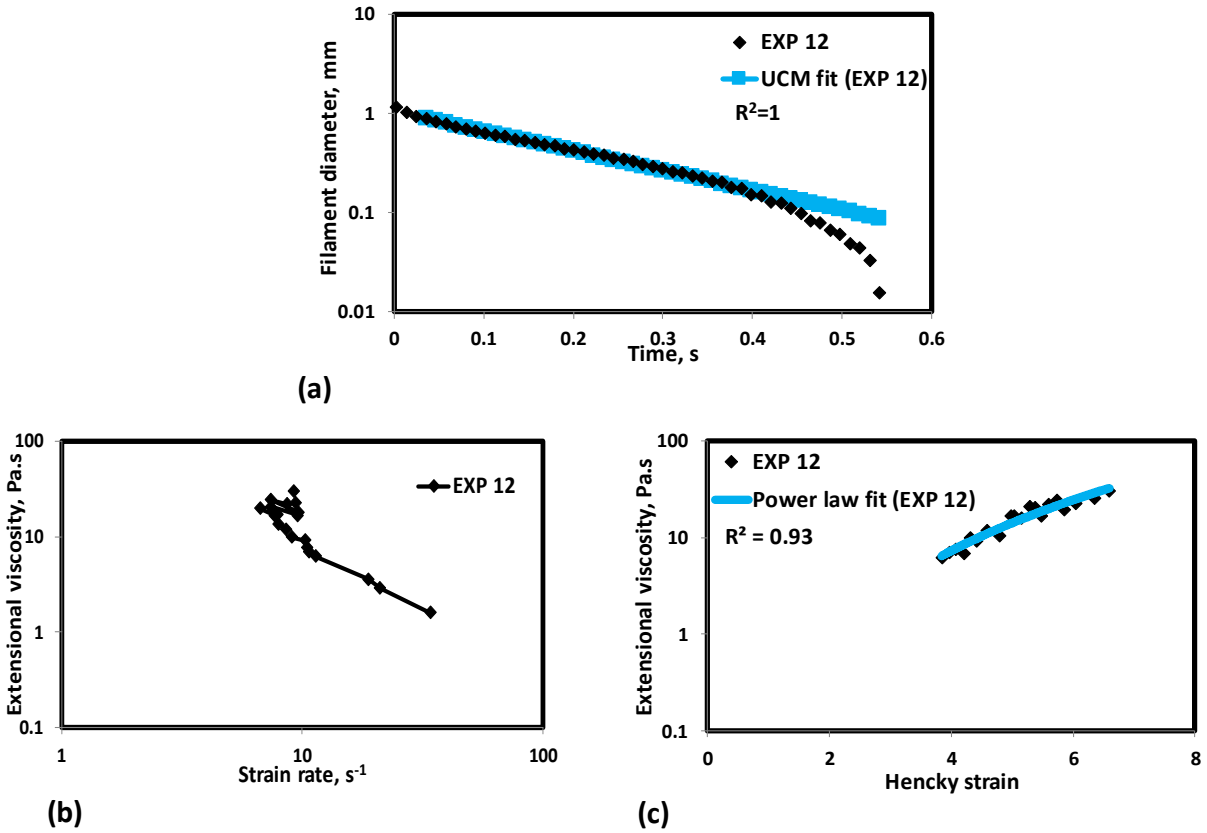

Figure A.12: *a) Filament diameter vs time plot for EXP 12 and the UCM fit to the linear elastic regimes for the determination of relaxation time (b): Extensional viscosity as a function of generated strain rate plot showing the sharp rise in the extensional viscosity around the critical Deborah number (c): Power law fit to the extensional viscosity vs Hencky strain values around the critical Deborah number for the determination of strain hardening index.*

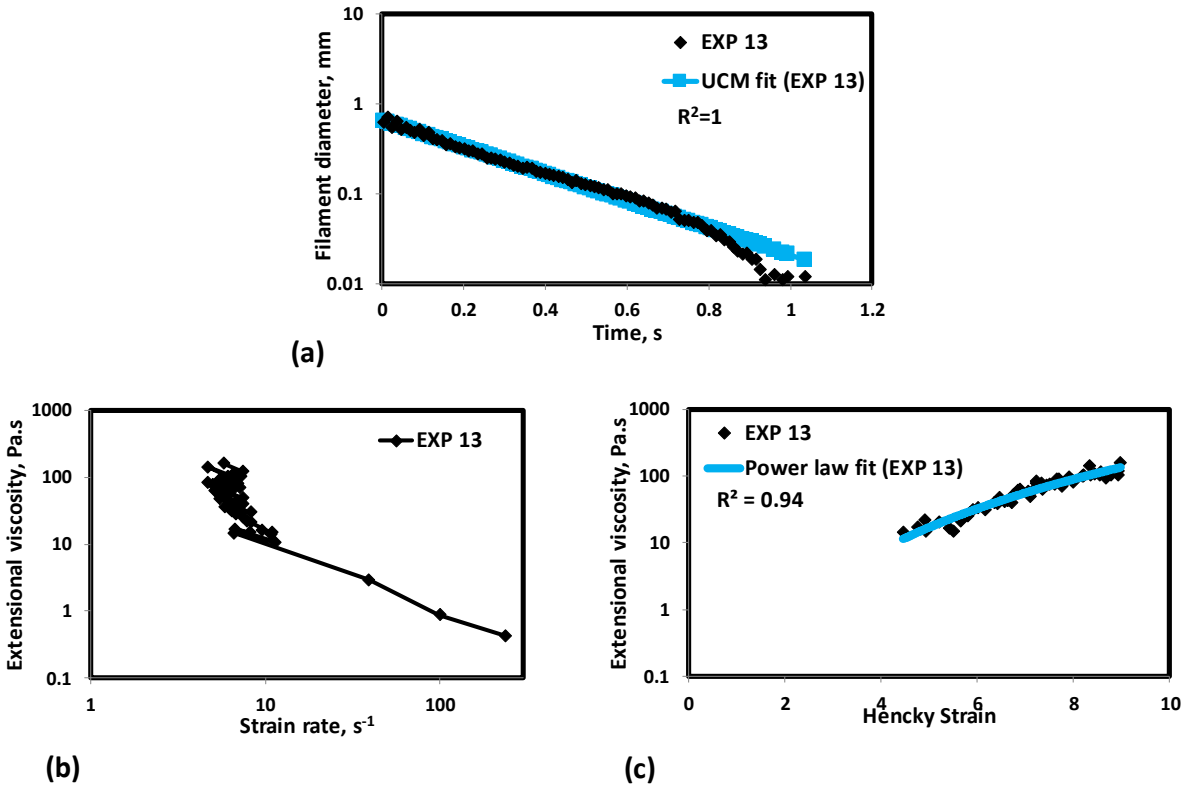

Figure A.13: *a) Filament diameter vs time plot for EXP 13 and the UCM fit to the linear elastic regimes for the determination of relaxation time (b): Extensional viscosity as a function of generated strain rate plot showing the sharp rise in the extensional viscosity around the critical Deborah number (c): Power law fit to the extensional viscosity vs Hencky strain values around the critical Deborah number for the determination of strain hardening index.*

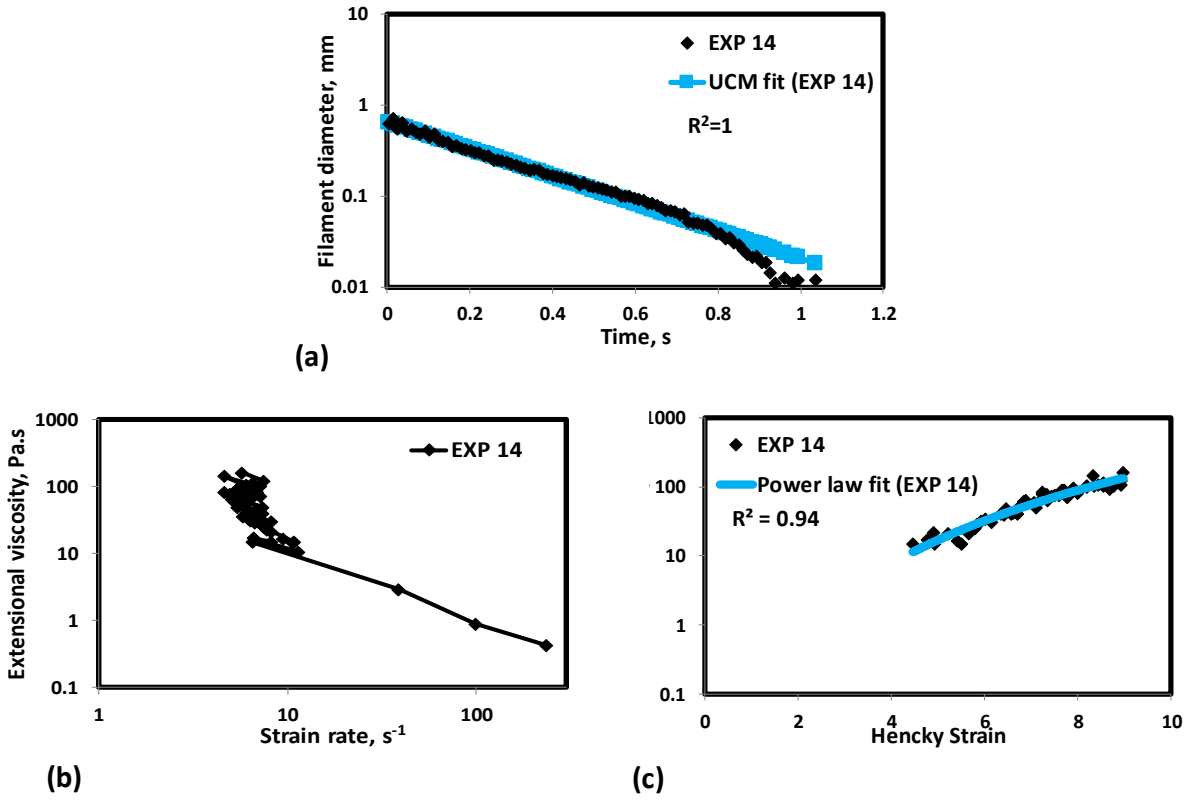

Figure A.14: *a) Filament diameter vs time plot for EXP 14 and the UCM fit to the linear elastic regimes for the determination of relaxation time (b): Extensional viscosity as a function of generated strain rate plot showing the sharp rise in the extensional viscosity around the critical Deborah number (c): Power law fit to the extensional viscosity vs Hencky strain values around the critical Deborah number for the determination of strain hardening index.*

Table A.1: *Measured Shear and Extensional Parameters to be used in AT-VEM*

Data set	Polymer	Mw (MDa)	Concentration (ppm)	Salinity (ppm)	μ_p^o, (cP)	μ_∞, (cP)	λ, (s)	n	τ_{ext} (s)	$\mu_{\max@De_{cr}=0.66}$ (cP)	n_2
1	HPAM 3630	18-20	1500	20040 (640 ppm Ca2+ ions)	13.7	1	0.221	0.755	0.086	147,000	3.520
2	HENGFLOC 63020	20	1500	20040 (640 ppm Ca2+ ions)	6.5	1	0.066	0.828	0.048	26,000	3.484
3	HENGFLOC 63020	20	1500	20040 (20 ppm Ca2+ ions)	18	1	0.175	0.72	0.107	165,000	3.586
4	HENGFLOC 63026	26	1500	20040 (20 ppm Ca2+ ions)	66	1	1.63	0.662	0.146	285,000	3.597
5	Pusher 700	8	1000	10000	8	1	0.057	0.75	0.032	37000	3.372
6	Pusher 700	8	1000	1000	36	1	0.158	0.6	0.0623	48,000	3.029
7	Pusher 700	8	1000	10000	8.4	1	0.057	0.72	0.032	37,000	3.372
8	HPAM 3630	18-20	850	20000	17	7	0.33	0.49	0.198	250,000	3.975
9	HPAM 3630	18-20	850	10000	21	8	0.33	0.42	0.216	340,000	4.092
10	HPAM 3630	18-20	600	10000	20	7.5	0.5	0.5	0.169	220,000	3.948
11	HPAM 3230	6-8	2500	25200	10	5.5	0.03	0.7	0.0371	37,000	3.602
12	HPAM 3530	16-17	200	0	9	1	0.3	0.58	0.073	30,000	2.989
13	HPAM 3630	18-20	500	21963	11	1	6.48	0.483	0.097	160,000	3.531
14	HPAM 3630	18-20	500	21963	11	1	6.48	0.483	0.097	160,000	3.531

Obtaining shear rheological parameters

The shear rheological parameters can be obtained using shear rheometer. For the experimental data used in the method development, the shear rheological parameters are listed in Table A.1. These parameters were obtained from corresponding literature. The Upper Newtonian viscosity (μ_p^o)

corresponds to the higher viscosity in the Newtonian regime at the low shear rate. Lower Newtonian viscosity (μ_∞) corresponds to the lower viscosity at higher shear rates. α is the constant and its value is equal to 2. Characteristic relaxation time (λ) is taken as the inverse of shear rate, at which the transition from the Newtonian to shear thinning regime occurs. Carreau model represented by the Eq. A.6 (Cannella et al. 1988) is used to determine the shear thinning index *(n)* using the non-linear regression.

$$\mu_{shear} = \mu_\infty + \left(\mu_p^o - \mu_\infty\right)\left[1 + \left(\lambda * \gamma\right)^\alpha\right]^{\frac{(n-1)}{\alpha}} \tag{A.6}$$

where,

μ_{shear} is the shear viscosity, cP

γ is the shear rate, s^{-1}

Coupling the shear and extensional parameters and determining the downscaling factors

Unified apparent viscosity model represented by Eq. (A.7) is the sum of shear and extensional viscosity (Delshad et al. 2008).

$$\mu_{app} = \mu_\infty + \left(\mu_p^o - \mu_\infty\right)\left[1 + \left(\lambda * \gamma\right)^\alpha\right]^{\frac{(n-1)}{\alpha}} + \mu_{\max} * \left[1 - \exp\left(-\left(\beta * \gamma * \tau_r\right)\right)\right]^{n_2 - 1} \tag{A.7}$$

where

μ_{app} is the apparent viscosity in the porous media

$\mu_{\max}$ is the maximum elongation viscosity (determined through flood experiments), cP

γ is the shear rate, s^{-1}

τ_r is the oscillatory relaxation time, s

n_2 is the strain hardening index, determined through core flood

β is the universal constant, 0.01.

The measured shear and extensional rheological parameters for all 14 set of experiments (represented in Table A.1) are used in Eq. (A.8) to predict apparent viscosity. The mismatch between the predicted and the observed values are minimized using non-linear regression method by downscaling the power factor to $\mu_{\max @ De_{cr-0.66}}$ and subtrahend of n_2. These downscaling factors

represent the scale down of pure elongation in the extensional field to the combination of shear and extension in the porous media. The average downscaling power factor of 0.35 to $\mu_{\max@De_{cr-0.66}}$ and subtrahend of 1.2 to n_2 is determined using non-linear regression. The apparent viscosity model, Azad-Trivedi Viscoelastic Model (AT-VEM), incorporating the measured shear and extensional rheological parameters, along with determined downscaling factor is represented by the Eq. A.8.

$$\mu_{app} = \mu_{\infty} + \left(\mu_p^o - \mu_{\infty}\right)\left[1 + \left(\lambda * \gamma\right)^{\alpha}\right]^{\frac{(n-1)}{\alpha}} + \mu_{\max@De_{cr-0.66}}^{0.35}\left[1 - \exp\left(-\left(\beta * \tau_{ext} * \gamma\right)^{n_2-1.2-1}\right)\right] \quad \text{(A.8)}$$

Predictability of AT-VEM

The predictability of AT-VEM and comparisons with UVM and Carreau Model for all 14-experimental data set (Magbagbeolo 2008; Yuan 1981; Mansour et al. 2014; Masuda et al. 1992; Seright et al. 2011a; Laoroongroj et al. 2014) are presented in Figures 7.3 to 7.16. The prediction of AT-VEM is comparable with UVM. The method can predict the viscoelastic onset and the shear thickening regime for varying range of reservoir permeability (200 mD to 37 D), porosity (0.22 to 0.395), brine salinity (0 ppm to 25200 ppm), concentration (200 ppm to 2500 ppm) and polymer molecular weight (6 mDa to 26 mDa) without the need of coreflooding experiments.